New Approaches to the Collection and Interpretation of High Sensitivity Temperature Logs for Detection of Groundwater Flow in Fractured Rock

by

Peeter Enn Pehme

A thesis
presented to the University of Waterloo
in fulfillment of the
thesis requirement for the degree of
Doctor of Philosophy
in
Earth Sciences

Waterloo, Ontario, Canada, 2012

AUTHOR'S DECLARATION

I hereby declare that I am the sole author of this thesis. This is a true copy of the thesis, including any required final revisions, as accepted by my examiners.

I understand that my thesis may be made electronically available to the public.

Abstract

The use of temperature logging for identifying water flow through fractures in sedimentary rock has declined since the 1960's and 70's primarily because of low sensor resolution and cross-connected flow along the borehole. Although sensor resolution has improved to the order of 10^{-3} C° for several decades, temperature logging has not experienced a notable increase in popularity. This thesis studies these and other fundamental limitations to the application of borehole temperature logging for identifying flow through fractured rock, and tests the hypothesis that the limitations can be overcome, presents new methods for accomplishing that goal, and increases the applicability of the technology.

Although some conventional open-hole testing (e.g. flow meters) rely on vertical cross-connected flow in the borehole annulus to identify transmissive fractures, the flow is recognized to both distort open-hole temperature logs and facilitate chemical cross contamination. Removable polyurethane coated nylon liners have recently been developed to seal boreholes and minimize cross-contamination. High sensitivity temperature logs collected in the stagnant water column of lined boreholes under different hydrogeologic conditions herein show the degree to which cross connected flow can mask important flow conduits and thereby distort the interpretation of which fractures control flow. Results from the lined holes consistently lead to identification of more hydraulically active fractures than the open-hole profiles and an improved qualitative ranking of their relative importance to flow consistent with contaminant distributions observed in rock core.

The identification of flow in fractures with temperature logs depends on the presence of a temperature contrast between the water and the rock matrix to create an aberration in the otherwise gradually varying profile. Atmospherically driven thermal disequilibrium commonly only extends several tens of meters from surface and dissipates with depth, making temperatures logs a variable assessment of flow that is depth limited to the heterothermic zone. The active line source (ALS) method, a series of temperature logs measured before and within a day after the water column of a lined borehole is placed into thermal disequilibrium with the broader rock mass with a heating cable, is shown to provide two advantages. First, the method eliminates the depth limitation allowing flow zones to be identified below the hetro-homothermic boundary and second, the qualitative assessment of ambient water flow in fractures is improved throughout the test interval. The identification of the flow

conduits is supported by the combined evidence from visual inspection of core, rock contamination profiles, acoustic televiewer logs and tests for hydraulic conductivity using straddle packers.

A new device, the thermal vector probe (TVP) is presented. It measures the temperature of the borehole fluid with four high sensitivity temperature sensors arranged in a tetrahedral pattern which is orientated using three directional magnetometers. Based on these, the total thermal gradient, its horizontal and vertical components as well as the direction and inclination are determined, typically at less than 0.01m intervals. Comparison of TVP data collected in lined boreholes under ambient conditions (thermal and hydraulic) as well during thermal recovery after ALS heating demonstrate the reproducibility of the results and superior characterization of thermal aberrations indicative of flow relative to single sensor temperature data. A detailed comparison of subdivisions in the thermal field to the vertical changes in the hydraulic gradient measured from three nearby high detail (12-14 port) multi-level installations demonstrates the interrelationship between hydraulic and thermal fields and thereby the potential benefit of the TVP in hydrogeologic investigations.

Developing confidence in the use of both the TVP and ALS techniques in lined holes relies on demonstrating the reproducibility of results, consistency with observations from other technologies, and numerical simulation. Comparisons of field data with highly detailed numerical simulations using the program SMOKER shows that the influence of water flow in a fracture around a lined borehole on the temperature patterns is complex and factors such as convection likely influence the shape of the thermal aberrations observed. Model results suggest that the temperature aberrations are related to the volumetric water flow, a distinct lower resolution limit exists (approximately 5.6×10^{-7} m^3/sec per metre across the fracture, m^2/s), and although flow above 10^{-4} m^2/s is readily detectable, prospects for quantification of higher flows are poor. Some field data indicate the numerically determined lower limit is conservative and the details of the limit require additional study.

The aspects of temperature logging historically limiting applicability for detecting and comparing flow through discrete or groups of fractures in rock are hereby better understood and consistently overcome. The high level of detail achieved in the data highlights the complexity of the system and offers opportunities for further refinement. The TVP and ALS technique applied in a lined borehole promise both new insights into, and potential for quantification of ambient groundwater flow through fractures in rock.

Acknowledgements

I would like to thank my supervisors Dr. John Cherry, Dr. Beth Parker and Dr. Tony Endres for their support and guidance throughout the process. Dr. David Rudolph and Dr. Giovanni Cascante for completing the committee, with the associated effort involved.

Many colleagues and collaborators have helped guide this work including numerous students, researchers and support folks at Waterloo University, the University of Guelph and in industry, especially: Ryan Kroeker, Jessi Meyer, Bob Engleton, Paul Johnson, Kristina Small, Dan Elliot, Darren Mortimer, Steve Borghese, Leanne Burns, James Plett, Dr. Emil Frind and many more. Detlef Blohm (IFG) has been a longtime supporter, with equipment, discussion and insight. Special thanks to Dr. John Molson for considerable time, extensive edits and numerous insights.

Funding for this work has been provided by Natural Sciences and Engineering Research Council of Canada to Dr. Parker and the University Consortium for Field Focused Groundwater Research. Field site access and cooperation was provided by Boeing, Hydrite Chemical, Syngenta Crop Protection and Guelph Tool Inc.

Dr. John Greenhouse was key to the start of this journey, mentored the path, and has always been a great friend and foil.
Last but certainly not least, Sandy, Jess, Becky & Nick!

Table of Contents

List of Figures

List of Tables

Chapter 1
Introduction

1.1 Hydrogeologic Investigations of Fractured Sedimentary Rock – A Broad Perspective

Characterizing groundwater flow through fractured sedimentary rock is a key concern as much of the world relies on the resource for its' drinking water supply (Berkowitz, 2002). The bulk of the water flow occurs in fractures or thin zones of high permeability (Quinn 2011). Investigations exploring water supplies generally focus on identifying major flow zones. However, when dealing with groundwater contamination in fractured rock, characterization of the smallest flow conduits becomes important because the slow ambient movement of water therein controls chemical diffusion initially into, and later out of, the rock matrix (Parker 1994). Hydrogeologic field investigations at contaminated sites are largely directed towards identifying flow zones, accurate sampling of contaminant distribution, developing a site specific conceptual model and often a numerical model for prediction of future contaminant distribution. Among the most important limitations of these predictions is the need for improved geophysical characterization of the rock mass and the groundwater flow through it (Berkowitz, 2002; Neuman, 2005).

Detection and measurement of groundwater flow in fractured rock is a particularly difficult problem and historically there has been no established technique to identify ambient flow (i.e. flow that would occur without the presence of a borehole). The conduits for flow can be inferred using borehole techniques that identify fractures such as rock core, caliper logs or acoustic televiewer (ATV) images; the potential for water movement is based on identifying available transmissivity (straddle packer tests, various flow-meter logs and open-hole temperature profiles); and evidence of prior flow can be identified by rock core chemistry. However, there remain inconsistencies between the inferred flow zones interpreted from these various techniques because each measures a different characteristic of the system, each with individual limitations and assumptions. For example, the group of techniques that identify potential flow paths cannot confirm how much if any groundwater flow occurs because these do not assess interconnectedness or the presence of a hydraulic gradient. Although drilling techniques can provide a rock core to visually inspect and in some cases evidence of flow identified, recovery can be poor in highly fractured zones and geologic logging of discontinuities is subjective, particularly when the flow zones relate to thin zones of inordinately high permeability (i.e. "vuggy layers"). Caliper logs measure borehole diameter but have finite limits to the aperture of a

discontinuity that can be detected and cannot differentiate fractures from voids. Similarly, although ATV logs provide both an improved, orientated resolution of borehole diameter as well as an acoustic image of the borehole wall, the differentiation of fractures from other irregularities (e.g. those caused by drilling) can be subjective and again resolution is limited (i.e. to a few mm). Although all these techniques provide an interpretation of fractures, none confirm current ambient groundwater flow.

Paillet (2000) and others have realized advances in measuring changes in vertical flow moving through open boreholes and thereby characterized flow from the hole into and out of the rock mass. However, devices that measure water movement in an open hole such as heat-pulse flow meters or impellers have limited ranges of operation. More critically, these techniques require a vertical hydraulic gradient to cause the flow through the borehole (or use pumping to create it), and since the interpretation involves measuring cross-connected flow, it provides little information from the perspective of resolving lateral flow under ambient conditions. Straddle packer tests (eg Quinn et al. 2011; Novakowski et al. 2005) measure the transmissivity of the formation over a set interval which combined with fracture frequency data provide a fundamental indicator of the potential for flow. These are generally either conducted over relatively broad (5-10m) spans and thereby lack resolution or when test interval spans are reduced, time consuming. In either case, these tests leave large portions of the borehole open which can distort the flow regime. A newer form of transmissivity testing, FLUTe profiling (Keller et al submitted), pressurizes the entire borehole and measures the ability of the rock mass to accept water as the hole is systematically sealed from the top down. This method shows promise of higher vertical resolution and improved implementation speed, but has not yet been fully assessed. These pressure and flow based tests all measure the ability for flow to occur, but not the degree to which it exists under ambient hydraulic conditions. Rock core chemistry techniques (Parker 1994) provide a highly detailed analysis of the historic flow of contaminated water but the results are not necessarily representative of current conditions and the application of the technique is limiting to within the extent of a contaminant plume. Together these mutually complimenting techniques provide a suite of tools for hydrogeologic investigation and support of numerical simulations of contaminated fractured rock sites referred to as the “discrete fracture network approach (DFN)” described by Parker et al. (2011).

The work herein reported involves the role of temperature logs, measuring the temperature of the borehole fluid, in the detection and characterization of groundwater flow through fractured

sedimentary rock. Temperature logs were the original method of inferring fracture flow, but have since (until recently) become of limited importance in these investigations.

1.2 Background - Evaluation of Temperature Logging

Although temperature profiles are reported to have been collected in water wells by James D. Forbes and William Thompson (aka Lord Kelvin) as early as the mid 1800's (Burchfield, 1975), the application of the technique for identifying flow in fractures is sparsely discussed in the hydrogeologic literature until the late 1960s. Trainer (1968) recognized that flow zones in dolomitic rocks of the Lockport formation (Niagara County, N.Y.) created abrupt offsets in temperature profiles of boreholes. Seasonal variations in surface temperatures propagating downward with cross-connected flow within boreholes provided the thermal disequilibrium that allowed flow zones to be interpreted, and Trainer laterally correlated these features over the span of a kilometer. Conway (1977) improved the identification of flow features by calculating the thermal gradient over a few metres which enhanced correlation between boreholes. Keys and Brown (1977) noted that lateral flow through fractures moving from an injection well creates discrete aberrations (peaks or troughs) in temperature profiles. Drogue (1985) superimposed seasonally varying thermal profiles from the same borehole to depict a cone of time-dependent variability the width of which decreases from surface and identified a characteristic boundary beyond which the temperature is stable and gradually increasing with depth. Drogue designated the shallow thermally variable portion of the profiles as "heterothermic", the deeper portions "homothermic", and identified the boundary between the two at approximately 25m in an example from Southern France.

The identification of flow based on discrete aberrations in temperature logs was subsequently used by many (e.g. Sillman & Robinson, 1989; Malard & Chapuis,1995; Bideau & Drogue,1993; Robinson et al,1993 and Ge,1998) but commonly their identification of the thermal aberrations suffered in the presence of vertically cross-connected flow along the borehole. Although fluid temperature logs are regularly collected in a typical geophysical logging suite through fractured rock, the reliance on the technique (based on the number of citations) has waned; the data has become of secondary value and is rarely emphasized in deference to several other techniques such as flow meters, fluid electrical conductivity (FEC) logging, and a variety of transmissivity measuring methods. In a review of the use of heat for groundwater insights Anderson (2005) cited over 200 references of which only seven focused on identification of flow in boreholes through fractured rock.

Pehme et at (2010, Chapter 2) attribute the declining reliance on temperature logging for providing identification of flow through fractures to two primary factors; historically poor resolution of temperature probes (until recently sensors could not resolve variations of less than 0.1C°), and the negative effects of borehole hydraulic cross-connection (e.g. Bidaux and Drogue, 1993; Robinson et al.,1993; and Genthon et al., 2005). The effects of borehole hydraulic cross connection are a ubiquitous problem influencing many forms of testing in open boreholes through fractured rock. For example, Price et al (1993) and Sterling et al (2005) demonstrated the impacts of hydraulic cross connection by showing substantial differences between ambient and cross connected hydrochemistry.

These fundamental limitations to the application of temperature profiles in fractured rock have now been overcome. The resolution of temperature probes used in borehole logging has improved to the order of 0.001 C° (e.g. Greenhouse and Pehme, 2002; Pehme et al, 2007a; Berthold and Börner, 2008), which greatly enhances the detection limits of flow from temperature logs. Methods for restricting the hydraulic cross-connection in boreholes with polyurethane coated nylon sleeves have been developed (Cherry et. al. 2007) and preliminary tests of temperature logs collected within these presented (Greenhouse and Pehme, 2002; Pehme et. al. 2007b).

1.3 Hypothesis

This thesis investigates the applicability of temperature logs for the identification and characterization of groundwater flow through discrete fractures or fracture zones in rock. It hypothesizes that:

"the fundamental limitations of temperature logging can be better understood such that procedures and interpretation techniques can be refined and new processes developed to improve detection and characterization of groundwater flow in fractured rock".

To determine how temperature techniques can be advanced, it is critical to better understand the existing limitations that have caused the technique to fall from favor. Sensor resolution is the first fundamental limitation, but this issue is in the control of manufacturers and has largely been resolved. Sensor resolution is herein addressed only as a byproduct of field tests and manufacturer's claims confirmed. This thesis concentrates on other fundamental limitations in the application of temperature logs and presents methods for overcoming those. It examines:

- the issue of cross-connected flow in an open borehole, the implications on interpretation of fracture flow from temperature logs (as well as other techniques) and what improvements are realized by data collection in a lined borehole where the influence of the borehole on flow distribution is removed;
- the thermal disequilibrium that is created by water flow through fractures and makes that flow detectable by way of temperature logs. The depth and resolution limitations imposed on the identification of flow by the need for thermal disequilibrium are examined and the adaption of the Active Line Source (ALS) as a method for creating and controlling it is presented;
- a new device is developed and tested; the thermal vector probe (TVP) is designed to measure the direction and magnitude of the temperature field in an effectively continuous manner along the length of the borehole. The TVP is used to examine the relationship between the hydrogeologic regime and the details of the temperature field;
- these advances: temperature logging in a lined borehole, creating thermal disequilibrium with the ALS and detailed measurement of the thermal field with the TVP, are simulated numerically to improve understanding of the implications of the physical properties of the system on the detection of flow with temperature techniques. Two key issues are examined in detail with numerical modeling; identifying and characterizing the implications of borehole convection due to temperature gradients; the variation of the thermal response with the magnitude of water flow through a fracture.

The results of these investigations and the implications on detection of water flow through fractured rock are summarized, recommendations for additional work presented, and conclusions drawn.

1.4 Thesis Structure and Components

The original design of this thesis was a series of modular peer reviewed manuscripts, with an introduction and overall summary consolidating the assembly into a single document. The technical chapters (2-5) address the key components of the study outlined:

1. General Introduction
2. Avoiding Cross-connected Flow with temperature logging in liner
3. Creating Thermal Disequilibrium – The Active Line Source Technique

4. Measuring a Thermal Vector – Temperature Vector Probe
5. Understanding Fracture Flow Effects on Temperature Logs – Modeling Results
6. Summary, Overall Conclusions and Recommendations for Additional Research

Other original works by the author that provide supplementary investigations supporting the primary effort of the thesis are included as Appendixes. These include a conference paper documenting the need for high data density and slow logging speed, the final report of an independent studies course on numerical modeling and a technical note to be submitted for publication describing a new method for processing hydrogeologic data from multilevel monitors. Minor amounts of text in the main document borrow from these appendices and are identified by italics.

At the time of submittal chapter (2) has been published in a referred journal (Pehme et. al. 2010). Other chapters (3, 4 and Appendix C) are prepared for journal submittal and peer review. Chapter 5 is intended to be divided into two components, "convection" and "response to flow", and refined prior to consideration for publication. Following the original intent, chapters 2 to 4 (inclusive) are presented in their complete form. Each includes abstract, figures, references and all supplemental material to be provided to the journal. To maintain modularity some duplication of references and figures occurs. Figure numbers have been altered to reflect both chapter and original individual document reference.

Chapter 2
Improved Resolution of Ambient Flow through Fractured Rock with Temperature Logs

P.E. Pehme, B.L. Parker, J.A. Cherry and J.P. Greenhouse

2.1 Overview

In contaminant hydrogeology, investigations at fractured rock sites are typically undertaken to improve understanding of the fracture networks and associated groundwater flow that govern past and/or future contaminant transport. Conventional hydrogeologic, geophysical and hydrophysical techniques used to develop a conceptual model are often implemented in open boreholes under conditions of cross-connected flow. A new approach using high-resolution temperature (±0.001ºC) profiles measured within static water columns of boreholes sealed using continuous, water-inflated, flexible liners (FLUTe™) identifies hydraulically active fractures under ambient (natural) groundwater flow conditions. The value of this approach is assessed by comparisons of temperature profiles from holes (100-200 m deep) with and without liners at four contaminated sites with distinctly different hydrogeologic conditions. The results from the lined holes consistently show many more hydraulically active fractures than the open-hole profiles, in which the influence of vertical flow through the borehole between a few fractures masks important intermediary flow zones. Temperature measurements in temporarily sealed boreholes not only improve the sensitivity and accuracy of identifying hydraulically active fractures under ambient conditions, but also offer new insights regarding previously unresolvable flow distributions in fractured rock systems while leaving the borehole available for other forms of testing and monitoring device installation.

2.2 Introduction

Fractured rock studies aimed at understanding contaminant transport have been in progress for many decades, prompted initially by proposals for creation of deep underground nuclear repositories and stimulated more recently by the prevalence of contaminants in bedrock aquifers at industrial sites. In the quest to achieve better understanding and predictions of contaminant behavior in bedrock, greatly improved characterization of groundwater flow in fracture networks is widely desired (e.g., NRC 1996; Berkowitz 2002; Sara 2003). In a recent summary of the state of knowledge concerning groundwater flow and solute migration in fractured rock, Neuman (2005) indicates the need not only

to identify dominant discrete fractures but also “the hundreds or thousands of fractures having a wide range of sizes”.

This paper focuses on the use of temperature measurements (i.e., temperature profiling) in boreholes sealed with removable liners to improve identification of fractures that are hydraulically active under ambient (non-cross-connected) conditions. Davis (1999) summarizes the early work of Humboldt and Arago in the mid 1800s using temperature profiles to describe groundwater flow, hot springs, and geothermal energy resources. Prensky (1992) summarizes the subsequent expansion of temperature measurements into other aspects of earth sciences and subsurface hydrogeology. Anderson (2005) provides a recent review of the use of heat and temperature measurements in groundwater science, indicating initial applications beginning in the 1960’s. Trainer (1968) was one of the first to use temperature profiles to investigate groundwater flow in bedrock fractures. He traced major laterally-continuous bedding plane fractures in a carbonate rock aquifer for several hundred metres by correlating inflections in open-hole temperature profiles. Drury (1984), Drogue (1985), Silliman and Robertson (1989), and Malard and Chapuis (1995), among others, provide field examples using open-hole temperature profiles to identify hydraulically active fractures. Bidaux and Drogue (1993) compared hydrochemical dilution profiles with temperature profiles at a fractured carbonate rock site and found temperature profiles worked well for the identification of high flow zones, but not low flow zones. These authors and also Robinson et al. (1993) identified two limitations to the usefulness of temperature profiles for identifying hydraulically active fractures: vertical flow in open boreholes, and inadequate temperature probe sensitivity. The limitation due to the low resolution of temperature measurements has since been overcome. Genthon et al. (2005) used thermistors in karst studies that resolved temperatures to 0.01 °C, concluding “high precision temperature logging is required since the details of the signal’s thermal variations could not have been detected with 0.1 °C precision”. Greenhouse and Pehme (2002) and Pehme et al. (2007a) used improved temperature probes to show repeatable borehole log variations of a few thousandths of a Celsius degree.

To avoid the adverse impacts of vertical flow in boreholes due to cross connection between fractures, temperature profiles have been measured in the static water columns inside water filled steel or PVC pipes (e.g., Keys and Brown 1978; Ferguson et al. 2003). Another approach involves permanently embedding sensors, most recently fibre optic temperature measurement in grout columns outside

boreholes casings (e.g., Henninges et al. 2005) sealed in the rock. However, these approaches are rare because dedicated boreholes are expensive and prevent boreholes use for other purposes. Fibre optic temperature measurements currently have limited resolution (Wisian et al. 1998) and embedding individual temperature probes in grout becomes prohibitively expensive when a large number of probes are required to produce the very detailed vertical resolution necessary for identifying fractures at numerous depths, which is our focus in this paper.

To obtain the most useful temperature profiles, avoiding flow within the open borehole caused by cross-connection is necessary so that measurements reflect the natural groundwater system (i.e., ambient flow). However, the practical means for accomplishing this has not previously been achieved. Consequently, temperature profiling has not become an essential or important technique in fractured rock hydrogeology despite the many examples presented over past decades. The approach used in the work present here avoids the borehole cross-connection effects typical of open holes in rock by way of an inexpensive, removable, flexible liner (FLUTeTM, www.flut.com) used for temporary borehole seals (Figure 2-1). Cherry et al. (2007) introduce the various forms of the FLUTe liner and provide a detailed discussion supporting the assumption that the liner creates a good seal. They provide three forms of evidence: visual (video data), multilevel head data, and a test by Bradbury et al. (2007) comparing hydraulic head data from a FLUTe multilevel installation with nearby buried pressure transducers. Once installed, these liners perform as continuous water-inflated packers, providing a static water column that takes on the ambient temperature distribution of the rock surrounding the borehole (Pehme et al. 2007a).

In this context, an "ambient" flow system has groundwater movement uninfluenced by the presence of the open borehole, and therefore the flow governing the temperature distribution should also control containment transport in the fracture network. For the temperature profile obtained from the static water column to be useful in identifying fractures where groundwater flow occurs, the water in the fractures must be in thermal disequilibrium with the surrounding rock; if not, the temperature profile represents the ambient geothermal gradient and is not useful in detailed fracture network studies.

Pehme et al. (2007a) conducted temperature profiling in two lined boreholes in a dolostone aquifer to measure thermal dissipation in response to heating the entire static water column inside the liner

(known as Active Line Source (ALS) Logging). Though their primary purpose for temperature profiling using heating was to determine the thermal conductivity of the rock, they note the method offers potential for identifying fractures with active groundwater flow. This paper is an assessment of this potential, whereby we examine high resolution temperature profiling inside both lined and open boreholes and assess the ability of this method to improve identification of hydraulically active fractures under ambient groundwater flow conditions without reliance on the ALS heat source.

Our goal is to extend the capability of temperature logging to discern many more hydraulically active fractures than currently possible using conventional temperature techniques with emphasis on ambient flow conditions. Within this process, we present the utility of (i) high-pass filtering to emphasize short wavelength variability that may be associated with fracture flow, referred to here as "variability logs"; and (ii) the comparison of the changes in temperature logs run at different times, referred to here as "change logs". We present data collected from a borehole drilled through a dolostone aquifer in Cambridge, Ontario, (UW1) as a detailed example of our approach and procedures in comparison to conventional temperature logging. For comparison, temperature profiling was completed in many of the same holes with the liners removed. In several of the lined holes, the profiling was done on multiple occasions spread over weeks or months to determine whether temporal variations provide additional evidence of active fractures. Temperature profiling and related measurements have been conducted in over 25 other lined holes in fractured sedimentary rock at four contaminated sites: two in Canada and two in the United States. Selected data from these other sites are introduced to show our conclusions are not unique to the Cambridge dolostone and illustrate a range of responses, including one example showing effects of a leaking liner. The details of the four boreholes discussed herein are provided in the supplementary text (Table S1). The boreholes selected to demonstrate the lined borehole method were also subjected to many other types of data acquisition including geological logging of continuous core, rock core contaminant analysis, other borehole geophysics, flow metering, straddle packer tests, and continuous hydraulic conductivity profiling. Select data from these other methods are used to establish hydrogeologic context for the temperature measurements and demonstrate the interpretations from temperature are consistent with and add value to other relevant data.

We present many types of data pertaining to fractures and the different meanings associated with the term "fracture" must be distinguished. Fracture can refer to the geometric discontinuities identified visually in rock core or televiewer borehole imaging. These discontinuities may or may not be hydraulically transmissive or interconnected with other discontinuities. Also, the presence of fractures can be inferred by hydraulic tests or induced flow activity in the absence of other types of information. In summary, identifying fractures having flow under ambient groundwater conditions is essential to understanding contaminant transport and these fractures are not necessarily those interpreted from hydraulic tests or by imaging open boreholes.

2.3 Cambridge Open-Hole Data and Interpretation

As a consequence of releases of the pesticide metolachlor in the 1970's, the Cambridge site has been the subject of extensive investigation, initially by consulting companies (e.g., Carter et al. 1995) and more recently by researchers at the University of Waterloo. Perrin et al. (2009) describe the hydrogeology of the general area and the site. The facility undergoing investigation is the only local site in Cambridge known to have handled metolachlor. UW1 was drilled at a location where a stratigraphic window in the overburden is believed to have allowed the contaminant to enter the dolostone (Carter et al. 1995). This facility has no history of TCE use; however, the property lies within an industrial area and releases are suspected to have occurred creating a TCE source for bedrock contamination 200-300 metres up gradient of UW1.

Figure 2-2 provides a suite of conventional open-hole data collected in borehole UW1 at the Cambridge site. This information is typical of what might be available for interpretation of flow and the planning of a multilevel monitoring system installation as part of a contaminated site investigation. Figure 2-2 includes the general stratigraphy (2a) intersected by UW1 as interpreted from continuous core, a natural gamma log (2c) collected from within the 150 m deep, 10 cm (4 inch) diameter open borehole, and a virtual caliper profile (2j) based on the average travel time calculated from a FAC40 (Advanced Logic Technologies, ALT) acoustic televiewer (ATV) log. The geologic sequence at UW1 is typical of Cambridge and the surrounding areas. The uppermost bedrock units are relatively flat-lying fractured dolostones of the Guelph and Lockport formations that overlie the Rochester shale. Based on the gamma log, the dolostone has relatively uniform, low clay content with the exception of the argillaceous "Eramosa" member, which forms the upper part of the Lockport

formation. The Eramosa is recognized regionally as a laterally extensive horizon, with a gamma signature readily distinguishable from other dolostone units above and below; in some parts of the region, it is considered to be an aquitard, but not in the study area. Groundwater flow in the dolostone aquifer occurs in fractures and is controlled by several pumping wells surrounding the site (the closest is approximately 900 m south). The pumping wells are open from just below the bedrock surface (approximately 15-30 mbgs) to depths between 60 and 100 mbgs. In a nearby multilevel installation, the hydraulic head near surface is higher than encountered at depth, inferring overall downward flow through the dolostone aquifer. The hydraulic head levels across the aquifer typically fluctuate by almost a metre over one week cycles due to municipal pumping in the area. Perrin et al. (2009) show evidence of karst features in the dolostone but conclude that although karst channels have local influence, they generally do not govern the ground water flow system and contaminant distributions in the Cambridge area.

Straddle packer tests were conducted at 2.2 m wide intervals through the length of UW1 (Figure 2-2b). All of the intervals tested are interpreted to have bulk hydraulic conductivity above the method detection limit of 10-8 m/s and several zones of elevated hydraulic conductivity exist throughout the borehole (e.g., 174, 189, 212, 226, 235, 249, 254, 272, and 278 masl). Numerous rock core samples (cylinders with 38 mm diameter and 40-70 mm length) cut from the larger core were tested in the lab for rock matrix permeability, and results consistently show hydraulic conductivity values much below the lower limit of the packer tests. Visual inspection of the larger core specimens suggests the effect of anisotropy is small. Comparing the results of rock core permeability tests against packer tests leads to the conclusion that either individual large aperture fractures or numerous smaller fractures with substantial combined hydraulic conductivity occur within many of the tested intervals, and therefore abundant potential for ambient ground water flow exists.

We use the irregularities in the borehole diameter, represented by the virtual caliper calculated from the ATV travel time (Figure 2-2j), as a convenient representation of geometric fractures for comparison with other open-hole data, acknowledging the pulse width of the probe limits the resolution of discontinuities on the borehole wall that are less than 3 mm (ALT 2002). While recognizing that the drilling process can increase the apparent fracture aperture at the borehole wall, given the competency of the dolostone and the scales at which the data herein are compared, any such

enlargement is likely inconsequential to this discussion. The ATV data show a higher fracture frequency above the zone at 235 masl than below. As well as identifying several large fractures, the ATV data indicate numerous smaller potential discontinuities of varying aperture. Other notable characteristics in the ATV data are a large void immediately below the bottom of the casing at 278.56 masl and the scarcity of irregularities between 174.5 and 192.5 masl. The size and frequency of the irregularities in the ATV data generally, but not always, correlate with zones of elevated hydraulic conductivity measured in packer tests. Obvious exceptions are the presence of two zones of hydraulic conductivity above 10-5 m/s (at 188 and 210 masl) within a portion of the borehole having relatively few and small fractures as well as other more severely fractured zones with lower hydraulic conductivity. Inconsistencies in the correlation between the ATV and packer tests are expected because the ATV does not distinguish between permeable and impermeable fractures, and cannot detect very small aperture fractures.

Variations in vertical flow in UW1 under open-hole conditions (Figure 2-2i) were measured on December 4 and 5, 2004, using a Mount Sopris model HFP2293 heat pulse probe. Measurements were made at 1 m intervals starting from the bottom and moving up, with the probe kept stationary at each test location. At each position, the instrument was allowed to stabilize prior to measurement and as many as four readings were taken to confirm repeatability of the results. The heat pulse flow meter data could not be interpreted above an elevation of 238 masl because the responses were either too irregular to differentiate a single pulse or entirely flat. Given the large downward gradients measured in two multilevel monitoring installations 8 to 10 m away (Perrin et al. 2009), the most plausible interpretation for the poor data quality is that the borehole is not stagnant above 238 masl but rather has high flow, dominantly downward and possibly with a horizontal component, beyond the measuring capability of the heat pulse probe. From 238 to 193 masl, the flow decreases through a transitional zone that is interpreted to have many fractures, the majority of which act as minor drains or outflow points along the borehole. Relatively low flow occurs below 193 masl with the exception of two tests just below 177 masl. This zone of low flow correlates with the portion of the borehole where the virtual caliper log indicates only a few fractures. Overall, the heat pulse flow meter data show strong downward flow entering the open borehole just below the casing with much of this water exiting at or near 238 masl.

The open borehole temperature logs at UW1 (Figure 2-2d) were collected in December of 2003 and again in January of 2004 with a BMP04 temperature probe manufactured by Instruments for Geophysics Corporation (IFG) of Brampton, Ontario. This probe measures the water temperature with an accuracy of 0.1 °C and resolution on the order of 0.001 C° (IFG 1993; Greenhouse and Pehme 2002; Pehme et al. 2007a, 2007b) with a time constant of approximately 1 s (Blohm 2007). The borehole water column was allowed to stabilize undisturbed for several days prior to collecting data to avoid thermal disturbance due to drilling, other geophysical logging, hydraulic testing, or in some cases, liner removal. The temperature was measured while downward logging at a nearly constant speed between 0.5 and 0.7 m/min and the system recording raw data at a rate of 2 Hz. The results were subsequently splined and re-sampled to convert the data set to a constant depth interval consistent with the nominal raw sampling distance (0.005 m for Figure 2-2d). To highlight small-scale irregularities and variability, common practice is to calculate a thermal gradient profile from the temperature data (Figure 2-2e, f), in this case as the difference in temperature over a vertical distance of 0.1 m, reported in units of °C/m.

The basic premise for the interpretation of a temperature profile is that below the near-surface, environmentally-influenced, heterothermic zone, the spatial variation of temperature in a relatively uniform medium such as solid rock should be a reflection of the very gradual regional geothermal gradient. The thermal conductivity of rock is typically 2.5 to 5 times that of water (Bejan 1993) and therefore, without annular flow, stagnant water in a borehole will not facilitate vertical heat conduction faster than the surrounding material. Furthermore, the only mechanism available to perturb the uniform geothermal gradient is the transport of heat by groundwater movement through flow pathways. Anderson (2005) summarizes many of the efforts at estimating broad scale recharge and discharge using heat as a tracer. In rock where the water movement is primarily in fractures, narrow aberrations (either positive or negative) in the temperature profile measured in a borehole, devoid of any cross-connection, are expected to be the result of water flow in fractures. Molson et al. (2007) use a numerical model to test the conceptualization of detailed temperature variations caused by flow in fractures as described above. In simulations of a fractured rock system where seasonal surface temperature variations typical of the Cambridge study area were invoked, they found numerous temperature variations of magnitudes similar to the measured temperature profiles presented in this paper for flow in a network of many interconnected hydraulically active fractures.

The only other mechanism that may cause thermal disequilibrium between the water in the borehole and the surrounding formation is convection, a potential occurrence when the temperature of the borehole environment increases with depth. Sammel (1968) addressed convection within a cased borehole and showed that within a 4-inch (10 cm) well at water temperatures of 10 to 15 °C, convection should be anticipated at critical temperature gradients of approximately 0.0035 to 0.0065 °C/m. Pehme et al. (2007c) show readings at the Cambridge site varied by less than one hundredth of a degree Celsius over a one week period where the gradients were less than 0.003 °C/m. The variability over the same period increased with the thermal gradient to approximately 0.035 °C where gradients were above 0.008 °C/m. No evidence indicates convection in the profiles presented or indicates it is a factor in these interpretations.

The gradient log (Figure 2-2), also referred to as the differential temperature, is a derivative of the temperature log commonly used to emphasize short wavelength events that could represent water movement (Keys 1989). However, when calculations are conducted over vertical spans that highlight small-scale features such as fracture flow, the result becomes bimodal and distorts the shape of a peak or trough anomaly. An alternative method for examining the variations within a temperature log that represent hydraulic flow through fractures while avoiding this distortion is to subject the data to a simple high-pass filter to produce what is referred to here as a "variability log". The raw data are smoothed with a box-car filter with a typical window length of 5 m. Subtraction of this smoothed "base log" from the original data creates the "variability log" that emphasizes features with length scales less than the filter window while suppressing broad features such as the geothermal gradient and the shallow environmental (seasonal) temperature variations, with minimal distortion of the shape of the small scale anomalies.

Figure 2-2 (g,h) shows the variability logs for the open-hole temperature data collected in UW1. The two open-hole temperature logs were collected approximately a month apart, and the data sets calculated from them (Figure 2-2e-h) show the same basic patterns indicating similar hydraulic conditions existed during (and immediately preceding) the two measurements. The water in a shallow fractured zone (285-290 masl) is warmer than the water deeper in the hole. Below the shallow zone, the temperature of the water in the borehole decreases only minimally, and almost linearly, with minor deviations to 238 masl coincident with the depth where flow meter measurements changed

from un-interpretable to interpretable. The flow meter results and the temperature profiles in the open hole are both consistent with the view that these open-hole data are dominated by downward flow above a fracture at 238 masl, which acts as a major hydraulic drain (sink), accepting much of the water flowing down the open borehole. The absence of variability above 238 masl suggests very little downward flow leaves the borehole at these depths despite the fracturing evident on the virtual caliper log. On the other hand, the variability may depend only on downward flow velocity below some threshold value (exceeded above 238 masl). From 238 to 200 masl, the temperature decreases steadily but with notably larger variability, implying flow out of the borehole into fractures. This variability is not coherent between the two temperature logs in its short-scale detail, but the decline in temperature and the level of variability correspond well to the progressively decreasing downward flow velocity indicated by the flow meter. Although the details of flow into individual fractures cannot be inferred, the decreasing downward flow velocities recorded by the flow meter in this section support the premise of outward flow of water into fractures, with the temperature variability possibly the result of minor flow complexities at the fracture entrance. The only distinct deep feature in the temperature data that is indicative of flow occurs at approximately 174 masl, near the top of the Rochester shale, where the ATV log indicates a series of fractures, the packer tests measure higher hydraulic conductivity, and slightly below where the heat pulse flow meter indicates downward flow increases over a short interval. Although the majority of the flow occurs higher in the borehole, some water movement is detected throughout the dolostone to the top of the Rochester shale.

In summary, although the heat pulse flow meter results and the temperature logs provide a mutually consistent interpretation of flow in the open borehole, there is little correlation between most of the features identified from these techniques and the numerous (geometric) fractures identified with the ATV or the high permeability tests measured with the straddle packer. Only the zone from 235 to 238 masl is distinguishable in all data sets, as the lower limit of high downward flow, and a zone of elevated hydraulic conductivity and several large aperture fractures. The data related to water flow show little indication of the high permeability zones or numerous distinct fractures above 238 masl. In general, these open-hole data do not provide a data-consistent basis for ranking the importance of sampling zones and designing a multilevel monitoring installation.

2.4 Cambridge Lined-Hole Data and Interpretation

After completion of the open-hole logging of UW1, a FLUTe Liner™ was installed to a depth of 135 m (171 masl) to prevent cross-connected flow. The liner was filled to achieve a head of approximately 3-5 m above the standing water level in the open borehole, thus inflating the sleeve so it presses against the borehole wall and seals the fractures. The borehole was then temperature logged several times over a two month period. Figure 2-3 displays a broader set of data collected in UW1 including open and lined temperature profiles alongside other geophysical logs, straddle packer testing, and rock core analyses to be discussed further later in this text. Figure 2-3(f) displays the three lined hole temperature logs collected on February 16, March 1, and April 12 of 2004, alongside the two open-hole logs from Figure 2-2d. Figure 3(i-k) shows the corresponding variability logs calculated from the respective temperature logs. The different scales used for the variability logs are set so as to display a similar level of apparent variability where the response in all three logs is similar and yet fractures are anticipated (190-220 masl).

The portions of the temperature profiles collected above 279 and below 187 masl inside the liner are similar to those collected in the open hole. However, with the vertical cross-connected flow restricted, the lined-hole temperatures between these elevations are cooler than their open-hole counterparts, and large, time-varying peaks in temperature at 235-240 and 253-259 masl clearly identify broad zones of ambient groundwater flow. The variability logs emphasize smaller scale anomalies within these broad peaks, which we believe identify individual fractures showing evidence of substantial ambient flow. To interpret these small scale variations relevant to groundwater flow, we look for irregularities that stand out on individual logs and are consistently present in some fashion on all three data sets (recognizing the actual shape of the anomaly may vary with time as discussed above). On that basis, in addition to the two major flow zones, and ignoring thermal irregularities in the vicinity of the casing, several smaller variations (for example at 226, 230, 250, 263, 272, and 282 masl) also meet these criteria. The features in the lined-hole temperature logs vary in character with time and often the variability logs are required to identify the most subtle features. The temperature variations in the 12/04/04 logs are on the order of 0.01 °C, and barely discernable on the original log. Nevertheless, these repeatable perturbations are strong evidence of groundwater flow effects at these depths.

All of the variability logs, both open- and lined-hole, show the temperature is highly uniform and steady below an elevation of 196 masl. Between 222 and 196 masl the temperature in the lined borehole continues to be relatively uniform and steady with only minor variations (e.g., at 210 masl) while in contrast, the open-hole temperature profile is irregular implying some flow. In this portion of the open-hole logs, the fractures are disproportionately emphasized as the temperature of the borehole fluid transitions from the deepest hydraulic outflow of consequence at 222 masl to near stagnant conditions below 196 masl.

Figure 2-4 contrasts the key characteristics of water flow interpreted from the temperature profiles collected in UW1 while both open and lined. Arrows of varying size are used to indicate the relative amounts of flow in the major zones and differentiate predominantly vertical flow along the axis from flow which is into or out of the open borehole, or across and around when lined. In the open-hole, downward flow originating from shallow fracture(s) near the water table at 284 masl dominates the upper part of the temperature profile. The linearly varying temperature with a low gradient is consistent with a large amount of water moving down the open borehole, gradually equilibrating with the formation. There are no indications of either additional sources or outflows until much, but not all, of the downward flow exits the borehole at 235 masl. The water that continues to flow downward below 235 masl is warmer than the formation and gradually reaches ambient temperatures at 200 masl. Over the interval from 235 to 200 masl, water is distributed to various small fractures as confirmed by the heat pulse flow meter results (Figure 2-3h). The temperature does not vary in time (is thermally stabile) and hydraulic activity below 200 masl is not otherwise indicated with the exception of a single inflection in the profile at 174 masl that implies some flow across the borehole.

The lined-hole temperature profiles provide a very different perspective. Over the interval between 284-235 masl, where the open-hole profile shows two flow zones, the lined hole shows at least seven (Figure 2-4). However, the importance of the differences goes beyond the number of flow zones. The lined-hole data (Figure 2-4) indicate the major flow is at 258 masl, but the strong vertical cross-connected flow makes this zone indistinguishable on the open-hole temperature profile. Although the flow zone at 258 masl is not as obvious in the April lined-hole data (Figure 2-4) compared to other open- and lined-hole data collected earlier in the year, it creates an irregularity on the variability log that is comparable to the other large flow zones in the borehole. The lined-hole temperature logs

allow for more flow zones to be identified on a consistent (repeatable) basis and a very different interpretation of the relative amounts of water movement in the zones that are identified or in some cases masked by vertical flow in the open hole.

2.5 Temporal Assessment of Temperature Profiles

Visual comparison of Figure 2-4 4a and b indicates major flow occurs under ambient conditions at 285, 255, and 235 masl. However, repetitive logging spaced by days to weeks or longer is required to identify additional flow zones. The change log procedure (Figure 2-5) was developed to improve representation of the temporal variations in temperature response. This involves assigning one logging event as the "reference" profile and, in a manner similar to the calculation of the variability log described above, smoothing it to create a "base" log representing the geothermal gradient and the environmental variations. The change log is then calculated by subtracting the base log from other logging events in the same borehole and normalizing the result by dividing by the time span (in days). The use of time to normalize the change is intended to improve comparison between boreholes at a site when logged on different days over periods of less than a month and has decreasing value when looking at long-term changes over several months or years. Logs collected prior to the base log are represented by negative time and later data sets by positive time, resulting in decreases in temperature over time being negative and increases positive. The long-term geothermal gradient and medium-term surface effects common to both logs are suppressed in the change log, accentuating the relatively short-term temporal variations in the borehole. Short-term changes in temperature reflect a redistribution of the groundwater temperature as a result of, for example, groundwater recharge events or changes in the flow system caused by municipal well pumping cycles. However, depending upon the time between the acquisition of the data sets, the change log may include some broader scale seasonal or environmental temperature variations.

Figure 2-5b shows the UW1 "change log" for the lined borehole. Superimposed on Figure 2-5b is the interpretation of the major flow zones previously presented in Figure 4, refined based on the change log. The qualitative assessment of the relative amount of flow as depicted by the size of the flow arrows is best rationalized in the temporal temperature variation represented by the change logs, as are the limits of "apparent major" and "apparent active" change. Notably, the flow zones dominating the February and March temperature profiles also manifest as aberrations in the comparatively

smooth temperature log collected in April, although they are considerably subdued and are best depicted in this case in the variability log, demonstrating the enhanced value of the combined use of variability and change logs.

Numerous other small scale irregularities in the change logs are present in the individual variability logs. For example, the small feature highlighted by purple asterisk on Figure 5 is apparent in all three independent data sets. The correlation of individual small scale features is best when the system is in the most disequilibrium, in this case, February and March. Where polarities reverse or features exist in two, but not three data sets, the most plausible explanation is that the details of groundwater flow have changed, possibly by variations in pumping or infiltration. Although many of these fine-scale features likely represent water flow with minimal flux, neither the size nor polarity are always consistent, and a better understanding of the details of the system would be required for these to be individually interpreted. Although the details vary, the temperature logs collected in six other boreholes at the Cambridge site under lined- and open-hole conditions have many of the same features and similar implications from the comparisons drawn from the UW1 data.

2.6 Applications at Other Sedimentary Rock Sites

Although the general nature of the differences in results between lined and open holes for three other sites where the techniques have been extensively applied (Guelph, ON; Simi, CA; and near Madison, WI) are similar to the differences observed at the Cambridge site, the temperature profiles from these other sites provide important additional insights. The hydrogeology of the Guelph site is similar to the Cambridge site including bedrock with the same geologic units, primarily dolostone. At the Simi and Madison sites, bedrock is mostly sandstone, flat lying at Madison and dipping about 30° at Simi. At the Cambridge site, municipal pumping wells are operating close to the study area, but at the other three sites pumping wells are comparatively distant from the holes. The Simi site is on a ridge and topography creates a strong downward hydraulic gradient to drive groundwater flow. Each of these sites provides very different hydrogeologic and/or geologic conditions than the Cambridge example. The decreasing temperature with depth throughout most of the Guelph and Madison boreholes and the variability through the entire length of the lined-hole logs in the three data sets suggests all are in a state of thermal disequilibrium to the depths drilled. Similar to the Cambridge site, the two most important aspects to examine for these other three sites are the number of hydraulically active

fractures apparent from open and lined holes and the differences in relative importance assigned to particular flow zones under cross-connected (open) and ambient (lined) conditions. Further discussion of the Guelph site follows, while data and details of the Simi and Madison sites (Figure 2-7S, and Figure 2-8S respectively) are provided as electronic supplementary information.

Figure 2-6 displays examples of open- and lined-hole temperature profiles from the Guelph site including arrows of varying size, representing relative amounts and direction of flow using a consistent color scheme (red for open-hole and blue for lined-hole) along with gamma logs. For the Guelph site, heat pulse flow meter data and a caliper log derived from the acoustic televiewer are also displayed (Figure 2-6). The open- and lined-hole temperature profiles from the Guelph site are similar in general characteristics to those from the Cambridge site, indicating overall consistency of the groundwater flow systems at the two locations. The open-hole temperature data collected in Guelph indicate water entering the borehole at approximately 325 masl, and although intermediate perturbations are present in the logs, the flow is dominantly downwards and exits at 261 masl. The open-hole variability logs are for the most part mutually consistent, but with poor correlation between the fractures identified in the ATV virtual caliper or the flow meter data and the open-hole temperature results. In contrast, although lined-hole temperature logs appear uniform below 320 masl, with a single bulge deep in the dolostone, the variability logs display numerous irregularities throughout the borehole that are highly coherent at amplitude levels of a centi-degree or less, indicating many fractures with flow exist. Peaks in the variability log (negative and positive) coincide with most geometric fracture zones identified from the ATV virtual caliper. The interpretation of the lined-hole data provides a total of ten major flow zones. These data suggest the main contributors to the temperature bulge (ambient ground water flow) are fractures at 263 and 267 masl, but only to a limited degree at 261 masl, the elevation at which the open-hole temperature data suggest the major outflow occurs. This example highlights the usefulness of the variability log in representing very small, yet repeatable irregularities that correlate well with other data sets. It also provides another instance where the most distinctive feature in the lined-hole temperature data profiles presents as one of several irregularities on the open-hole profile that would be unlikely to warrant particular attention in the form of additional testing or allocation of a port in a multi level installation.

The results from all four sites indicate the lined-hole temperature logs provide identification of hydraulically active fractures down to substantial depth at each site, ranging from 110 m at the Guelph site to 155 m at the California site. In all cases, both open- and lined-hole logs converge to a common temperature at the bottom of the borehole. Investigations of many contaminated sites on bedrock have most emphasis within a hundred metres of ground surface, suggesting the lined hole temperature method will likely have widespread usefulness. However, in this depth context, it is relevant to consider whether the four sites have provided a biased impression. For the lined-hole method to show active fractures, the temporal temperature variations occurring at the surface must be transmitted relatively deep into the bedrock fracture network. Each of the four sites considered in this paper has two conditions that are highly favorable for propagation of temperature disequilibrium: a vertical component to the general hydraulic gradient causing downward flow to the bottom of the domain of interest, nor has the overburden created a barrier to recharge by being excessively thick or having a low vertical hydraulic conductivity. At the Simi site, the overburden is thin or absent over much of the area; at the other sites the overburden is thin or lacking a substantial aquitard unit where moderate in thickness. If either of these two major factors were absent at any of the four study sites, the maximum depth of sensitivity of the lined-hole method may have been shallower, which could render the method less useful.

2.7 Additional Evidence for Numerous Hydraulically Active Fractures

In all of the cases presented, the temperature profiles inside lined holes show many more hydraulically active fractures than are indicated by open-hole logging. Other independent lines of field evidence, including rock core contaminant analysis, borehole hydraulic tests, and acoustic televiewer logging, support the concept of a large number of fracture pathways for groundwater flow. Parker et al. (1994, 1997) used analytical models and representative sandstone parameters from the literature to predict that with sufficient residence time, as a contaminant moves through the fractures of a sedimentary rock, chemical diffusion can cause a considerable amount of the contaminant mass to transfer from within fractures into the adjacent rock matrix. VanderKwaak and Sudicky (1996) confirmed the potential for the contaminant halo effect in fractured porous geologic media using a numerical model. Parker (2007) describes the most recent iteration of a methodology wherein analysis of closely spaced rock samples collected from continuous cored holes are used to create contaminant mass versus depth profiles, thereby inferring contaminant transport within fractures and

consequently active groundwater flow. Sterling et al. (2005) provide an example of such a profile from sandstone at the Simi site.

Rock core analyses were conducted for the volatile organic contaminant, TCE, and the pesticide, metolachlor, at the Cambridge site. Returning to Figure 2-3, the most hydraulically active fractures identified in UW1 based on temperature profiles are shown as blue shading alongside other geophysical logs, straddle packer testing, and the rock core analyses thereby providing the framework for examining all lines of evidence concerning fractures in this hole. The TCE and metolachlor profiles show that although the highest concentrations exist above 253 masl, numerous contaminant occurrences, particularly for TCE, are distributed across the thickness of the dolostone aquifer indicating that the fracture network is vertically interconnected (Perrin et al. 2009) and groundwater flow has occurred throughout the aquifer under ambient conditions. The straddle packer tests (Figure 2-3b) indicate measurable hydraulic conductivity exists in all intervals confirming that fractures exist from the top to the bottom of the dolostone. The ATV log also confirms that the fracture density varies with depth, but there are numerous fractures throughout most of this borehole (Figure 2-3m). Although neither the packer test nor the ATV results provide direct evidence of groundwater flow under ambient conditions, the presence of numerous fractures is consistent with the interpretation of many active flow zones from the lined-hole temperature logs and rock core profiles.

The degree of correlation of the hydraulically active fractures as identified by the lined-hole temperature profile, rock core contaminants, and implication of fractures identified from packer tests and the ATV log varies in different portions of the borehole. Above approximately 250 masl the flow zones as indicated by irregularities in temperature are at the same elevations as the peaks in the other three data sets and also match in relative size. The co-incidence between the major metolachlor and TCE contaminant concentration peaks in the rock core and the irregularities within the various forms of lined-hole temperature data in its raw (Figure 2-3f), processed (Figure 2-3g-k), and interpretation (shading) is generally very good. The variations and changes observed to dominate the lined-hole thermal profile at 254 and 270 masl coincide with the zones of highest contaminant concentrations. Although many of the lesser rock core peaks can also be related to aberrations in the thermal profiles, inconsistencies remain due to an inherent difference in the nature of the results from the two methods. From 222 masl (the limit of major change) to 250 masl, the temperature irregularities coincide with

the zones of high hydraulic conductivity and fractures in the ATV but relatively few rock core peaks exist, and below 222 masl the peaks identified in all four data sets match inconsistently. However, there is no reason to expect strong positive correlations between the four types of evidence for fracture occurrences because each of these techniques measures a different aspect of the system; the presence of an opening on an ATV log implies nothing about water movement, nor does water dissipation under pressure in a packer test confirm water flows under ambient conditions. In addition, the fracture network is three dimensional and therefore the borehole directly encounters only some of the fractures involved in contaminant migration near each hole. Although elevated contaminant levels in rock core analyses indicate migration pathways nearby, the actual groundwater flow may not intersect the borehole but instead be within a metre or so. The temperature profiling indicates the hydraulic activity at the moment of profiling; when done more than once, it indicates variation over a fixed, but relatively short, time interval. At the Cambridge site, the contaminants have been in the dolostone aquifer for at least two decades (Carter et al. 1995) while the number and pumping rates of municipal wells has varied. Therefore, the contaminant concentrations now found in the rock core represent the cumulative influence of diffusion into and then later out of the rock matrix blocks between fractures over decades; exact correlation between the degree of hydraulic activity in the fractures identified by temperature profiling and the strength of the contamination in the rock core is not a reasonable expectation. Lastly, the absence of a chemical peak infers little about water movement if the water is not contaminated.

Although the ATV caliper and straddle packer tests in UW1 indicate potential for flow below 200 masl and the TCE peaks confirm water movement has occurred, the temperature profiles are smooth and uniform over time implying little ambient flow. To create an aberration in the temperature profile, the water moving through the fracture must be at a sufficiently different temperature than the rock to cause a detectable change. Raw temperature logs vary temporally according to source (surface) temperature changes, the relative size and connection of flow paths, and the changes in driving forces (pumping in Cambridge). Although the variability logs improve the interpretation of the flow paths, the size of the variations also varies over time. As the degree of thermal disequilibrium between the water and the rock would decrease with depth, so also would the ability to resolve flowing fractures from temperature profiles. Importantly, the ALS technique (Pehme et al. 2007a, 2007b), presented as a method for estimating the thermal conductivity of the formation, artificially creates thermal

disequilibrium in the water column and has the potential to improve the detection of ambient flow at depth.

This study presents the hypothesis that variations in thermal energy, primarily originating at surface, can propagate through the overburden and be transported to substantial depth by groundwater flow in a fractured bedrock system before the temperature contrast is attenuated below the detectable limits of the field equipment. The temperature profiles provided are consistent with that hypothesis and no other alternative hypothesis has been identified to explain these field results. Although the lack of alternative explanations supports the hypothesis, it cannot be taken as definitive corroboration on its own. However, there is independent support from Molson et al (2007) wherein a numerical model of heat transport and groundwater flow in fractured rock examined the plausibility of this premise. The model includes density dependent groundwater flow through discrete, stochastically generated fracture networks coupled with thermal advection, conduction and retardation within the porous rock matrix. The model boundary conditions and media properties/parameters were selected to stylistically represent the setting and dolostone aquifer underlying the City of Guelph, ON and are also generally characteristic of the same aquifer in Cambridge ON. In the model natural heat energy pulses are generated based on seasonal air temperatures and applied as a thermal flux condition uniformly over the upper boundary surface. Molson et al. concluded that: "ground source thermal pulses can propagate deep into a fractured rock system and appear as weak thermal 'anomalies' within the fractures on the order of a few tenths or hundredths of degrees." Therefore, this modeling indicates that the use of high resolution temperature profiling to identify hydraulically active fractures, as we presented in this paper, is consistent with what is known based on the physics of heat transport in rock fracture networks.

In the assessment of lined-hole vs. open-hole temperature results, the lined-hole data clearly provide identification of substantially more active fractures under ambient flow conditions. However, the open-hole data can also give a misleading view of the ambient flow system in the fracture network. The peaks in contamination measured from the rock core data confirms fractures in the vicinity of 254 masl (Figure 2-3) are important for understanding contaminant migration. This same zone dominates the lined-hole temperature data yet is rendered relatively unremarkable in the open-hole temperature data by downward flow in the borehole.

In the examples provided, and in every borehole where we have compared open- and lined-hole data, the open-hole temperature logs differ distinctly from the lined-hole data above what would be interpreted from the open-hole results as the deepest major fracture. Below that point, the open-hole logs approach and eventually match the lined-hole profiles. This observation is consistent with the premise that the bottom of an open borehole typically acts like a cup, holding nearly stagnant water similar to the breached liner example (Figure 2-7S supporting information). A slightly deeper borehole could intersect another hydraulically conductive fracture, rendering the higher conduit inconsequential with regard to borehole flow, invisible to the open-hole temperature log, and leading to a different interpretation of which fractures control flow well above the limit of the borehole. In contrast, a lined-hole temperature log is independent of the intersection of deeper fractures and provides a superior representation of ambient conditions.

2.8 Conclusions and Implications

The high resolution temperature profiling in lined holes presented in this paper makes use of flexible liners that are relatively inexpensive, and are usually easy to install and remove. Used alone, the liners serve to prevent borehole cross connection, and therefore create the static water columns suitable for the temperature profiling described in this paper. At all four of the sedimentary rock sites presented the lined-hole temperature profiles indicate many more hydraulically active fractures and a different interpretation of which fractures facilitate the most flow than do the open-hole profiles. Larger numbers of active fractures indicated in the lined-holes are consistent with independent types of borehole information. The comparatively fewer number of active fractures detected in the open holes is most reasonably attributed to the masking effects of vertical flow resulting from hydraulic cross-connection between fractures.

The value of lined-hole temperature profiling is enhanced when profiling is done multiple times separated by days or weeks. The profile repetitions allow for application of the change log procedure and improve the potential for ranking the fractures in terms of degree of hydraulic activity. Open-hole temperature profiles usually identify two to five active fractures per hole regardless of hole depth. In conventional interpretations, these fractures are typically envisioned as the dominant conduits for groundwater flow; however, data collected from lined holes indicate they are commonly not the most hydraulically active fractures governing the ambient groundwater flow system. Therefore, at sites

where the goal of borehole measurements is to understand contaminant distributions and transport, a conceptual model for the fracture network based solely on open-hole data is prone to misrepresentation. Furthermore, such misrepresentations may result in the selection of the wrong intervals for monitoring when using wells or multilevel systems and erroneous fracture densities for discreet fracture models of groundwater flow and transport.

The temperature profiling method we have described currently has some limitations. First, in some unusual hydrogeologic circumstances, extreme hydraulic head variations over short intervals can cause inadequate sealing of the liner along parts of the hole. This loss of seal should be easily identified from the nature of the temperature profiles. Second, the method is not sufficiently sensitive to identify all hydraulically active fractures and therefore the number of fractures identified in a given hole should be regarded as a minimum. Various independent lines of evidence at each of the four sites suggest more, in some cases many more, hydraulically active fractures are present than we have highlighted in the lined-hole data. Attention is now being directed at improving detection limits and confidence in the interpretation of the smaller temperature variations as well as working towards a quantitative analysis using numerical models to calibrate against the field data. Third, the method is only effective if the temperature of the water in the fractures is in disequilibrium with the surrounding rock. Thermal disequilibrium at depth requires a combination of natural or man-made influences that create both a temperature differential (e.g., near surface heterothermic effects), and a driving force to move the water that is in thermal contrast through the fracture system, such as recharge or regional pumping. Although the ambient flow regime that drives the propagation of thermal disequilibrium will also be one of the dominant influences on contaminant transport, at sites where the maximum depth of interest is beyond the depth of thermal disequilibrium, the method is limited. However, the active line source (ALS) technique (Pehme et al. 2007a) offers potential to overcome this limitation.

2.9 Acknowledgements

Detlef Blohm, President of IFG, developed the temperature probe and made improvements as needs arose. Carl Keller, Chief Scientist at FLUTE, developed the flexible liner and provided assistance concerning liner use. The temperature profiles presented in the paper were obtained in concert with M.Sc. thesis research by Leanne Burns, James Plett, Chris Turner, Jonathan Kennel, Diane Austin, and Jessica Meyer. Personnel from Montgomery Watson Harza assisted at the California site.

Comments provided by Mary Anderson and three reviewers (Grant Ferguson, Gary Wealthall, and an anonymous individual) resulted in manuscript improvements. Funding support was provided by the Canada Foundation for Innovation and the Natural Sciences and Engineering Research Council of Canada via grants to Beth Parker and John Cherry, and the University Consortium for Field-Focused Groundwater Contamination Research.

2.10 Figures & Captions

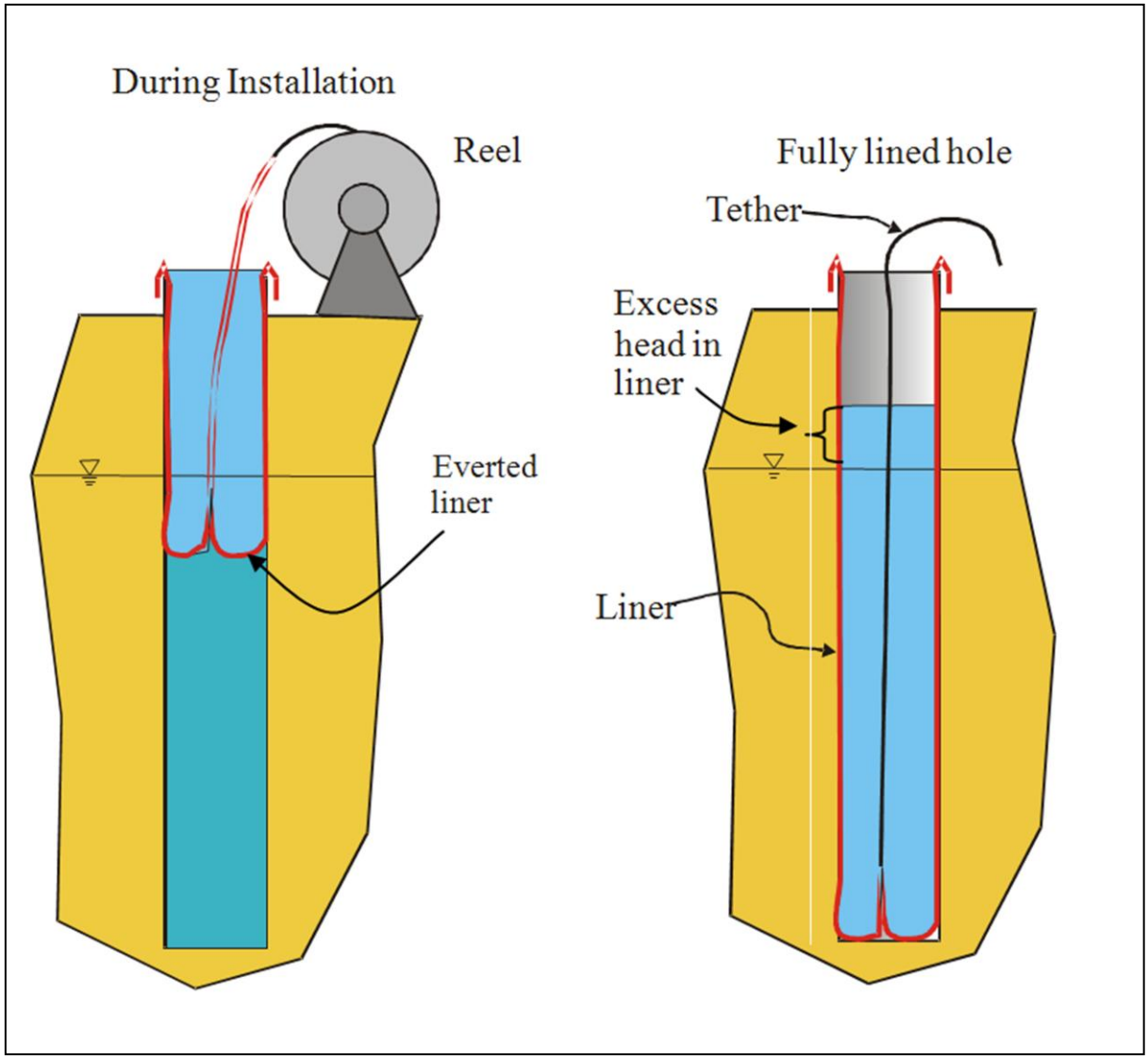

Figure 2-1 Schematic representation of the FLUTe liner installation (from Cherry et al. 2007).

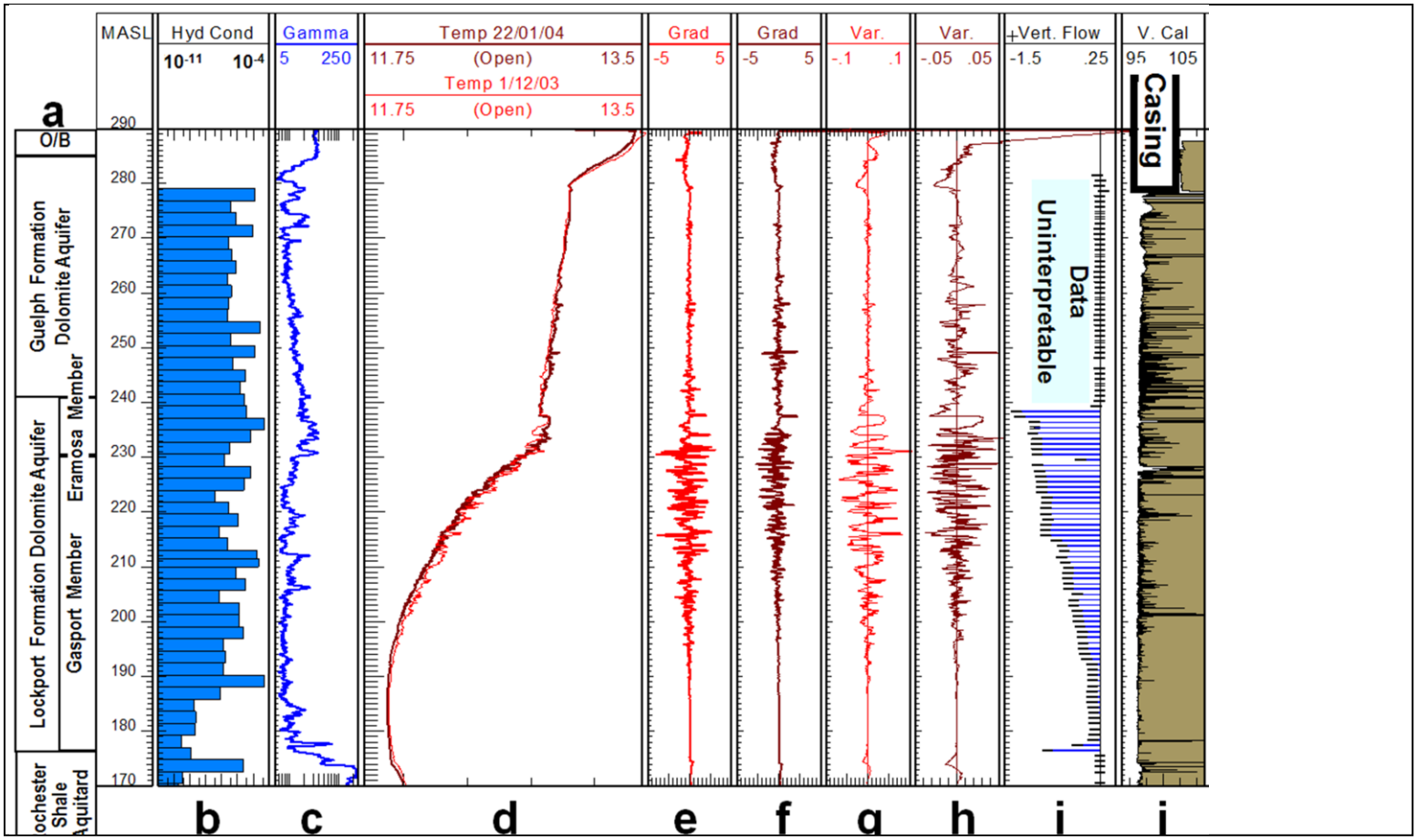

Figure 2-2: UW1 open-hole data.

Showing (a) the stratigraphic column (from Burns 2005), (b) hydraulic conductivity from straddle packer testing (m/s at a log scale), (c) gamma log (cps), (d) temperature logs collected in the open borehole on 1/12/2003 and 12/01/2004 (°C), (e&f) the thermal gradient (over 10 cm) of the 1/12/2003 and 22/01/2004 temperature logs, respectively (°C/m), (g&h) variability logs for 1/12/2003 and 22/01/2004, respectively (°C), (i) the stationary heat pulse flow meter tests (L/min), and (j) virtual caliper (mm) from travel time of acoustic televiewer data (FAC40 manufactured by ALT Limited).

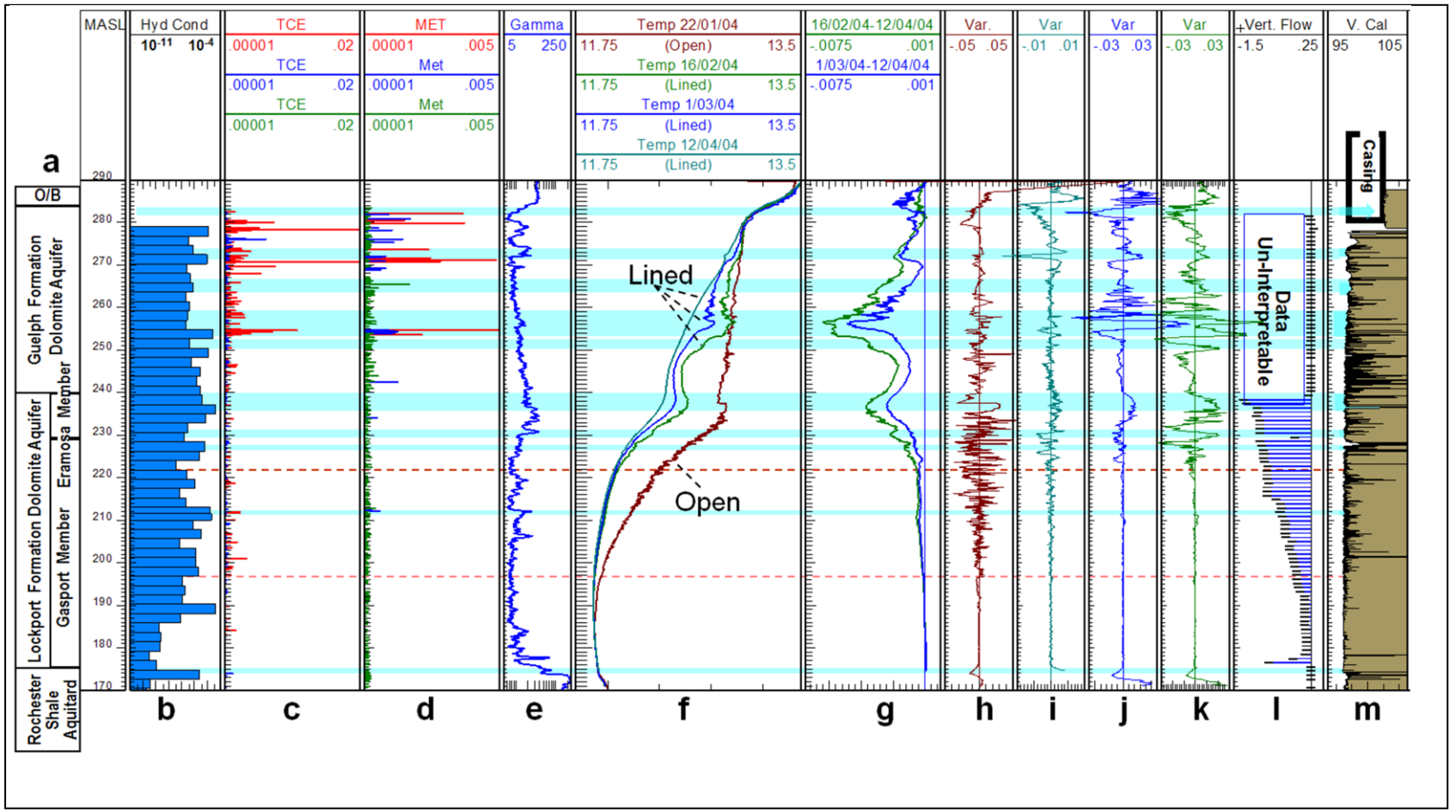

Figure 2-3 UW1 lined hole data.

Showing (a) the stratigraphic column, (b) hydraulic conductivity from packer testing (at a log scale), (c&d) TCE and Metolachlor rock core analysis ug/L (red, quantifiable; blue, low order quantification; and green, below detection limit), (e) gamma log (blue), (f) passive temperature logs collected in the lined boreholes from left to right on 12/04/2004, 1/03/2004, and 16/02/2004, and open boreholes on 1/12/2003 and 22/01/2004, (g) change logs from lined boreholes on 1/03/2004 (blue), 16/02/2004 (green), (h, I, j, & k) variability logs 22/01/2004, 12/04/2004, and 16/02/2004, (l) heat pulse flow meter, and (m) virtual caliper from travel time of acoustic televiewer data, with interpretation of flow zones (blue shading) and limits of temporal change in flow. (Columns a, b, c, and d from Burns 2005)

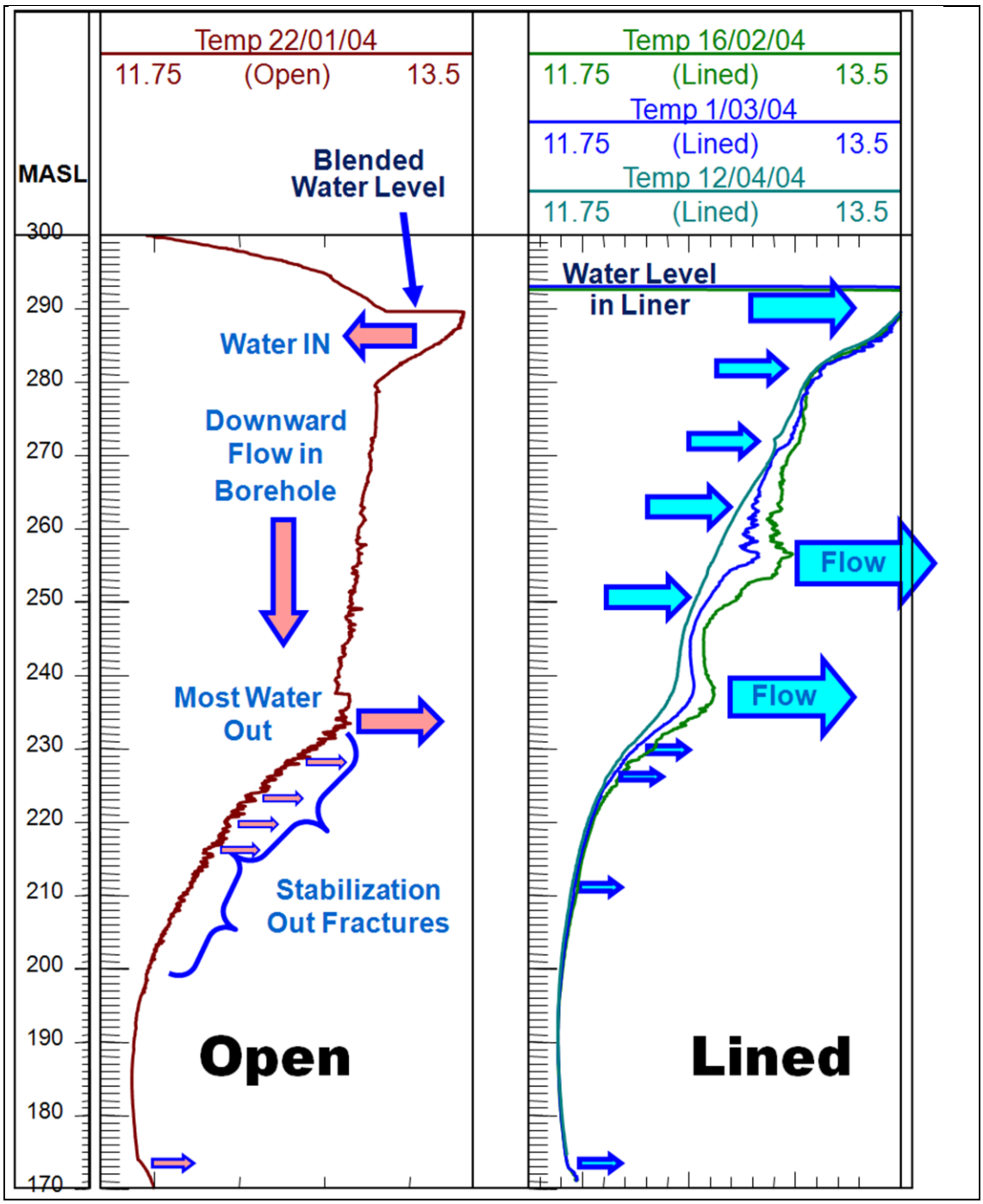

Figure 2-4 Comparison of basic interpretations of temperature logs collected in open and lined borehole UW1.

Blue arrows indicate major and minor flow zones. Red arrows are lower limits of shallow flow based on temperature variability.

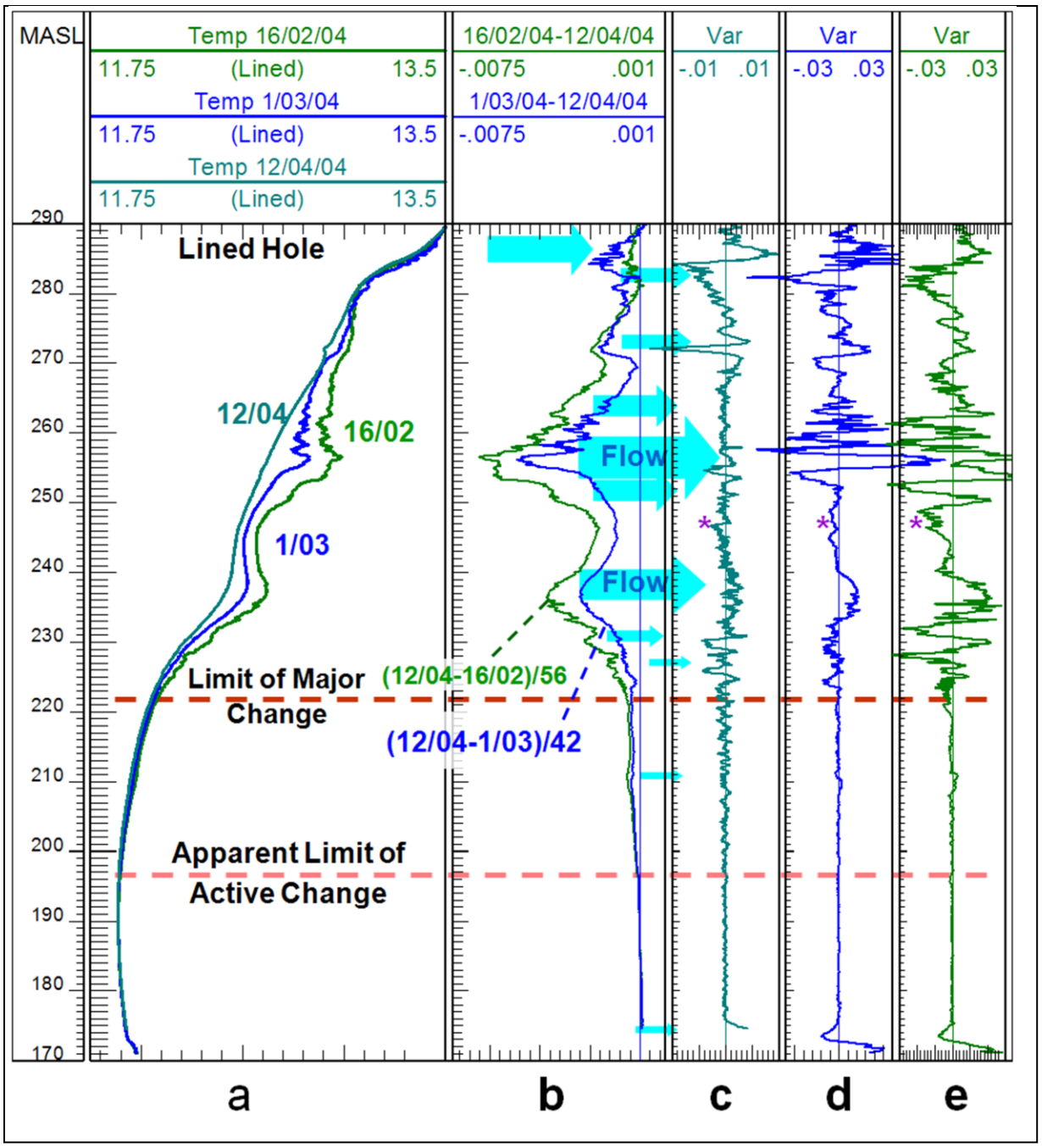

Figure 2-5 Repeated temperature logs in FLUTe lined borehole UW1.
Highlighting temporal changes: (a) lined-hole temperature logs, (b) change logs, and (c, d, & e) variability logs, with interpretation of key flow zones (blue arrows) and example of subtle anomalies (purple asterisk).

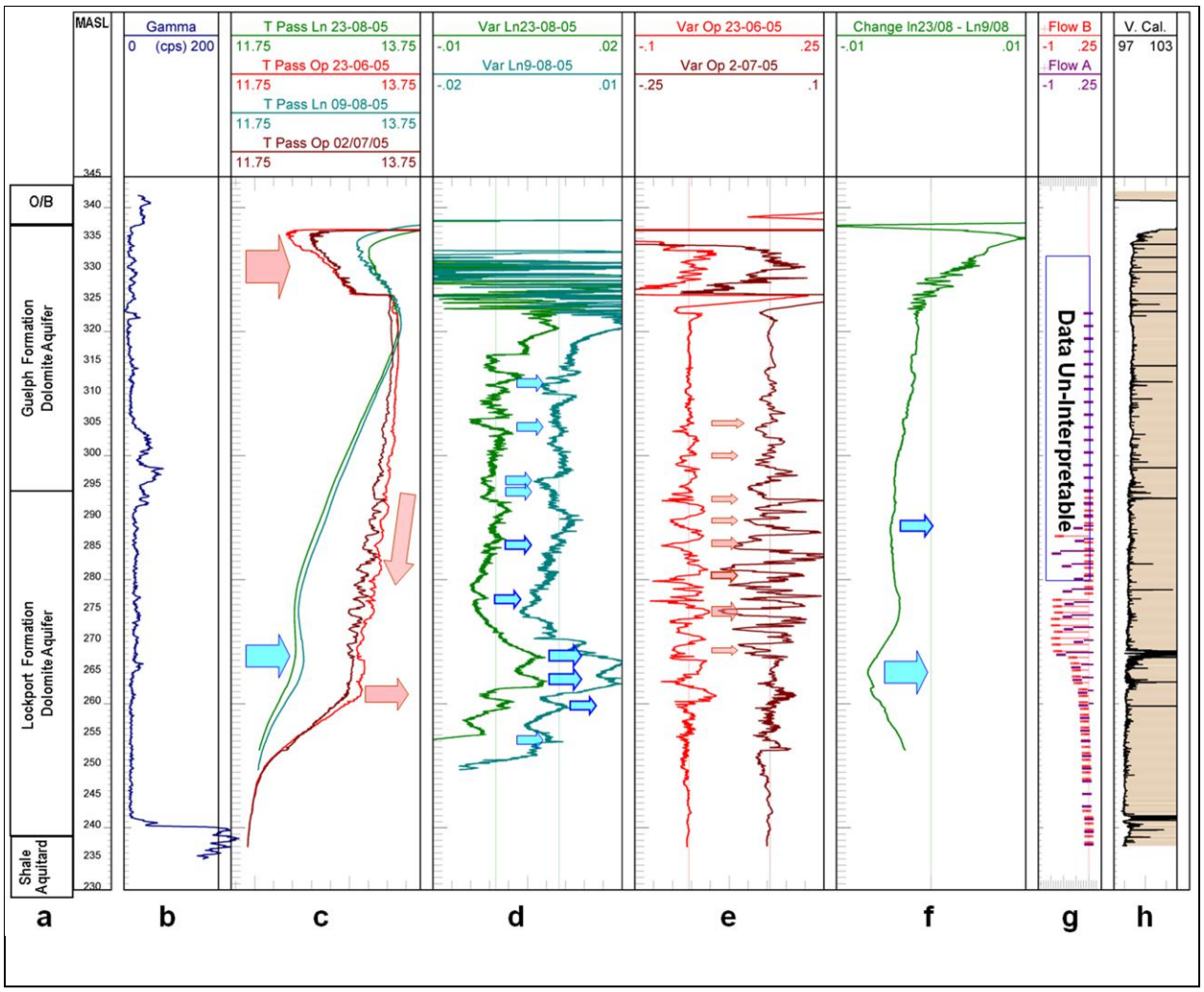

Figure 2-6: Data from MW24 (Guelph, ON):
a) Stratigraphy (ob=overburden, G1-4 Guelph formation subunits, LH=Lions Head, (from Perrin et al. 2009). Note that two naming conventions exist for the same stratigraphic sequences through portions of southern Ontario (i.e., the Amabel is equivalent to the Lockport Formation), dependant on location relative to the Algonquin geologic arch that separates the Appalachian and Michigan sedimentary basins. The geological community interprets the arch to be between the Cambridge and Guelph sites, and we have adopted the local conventions chosen by others (Coniglio 2007); b) gamma log; c) temperature profiles (open holes shades of red, lined hole blue); d) lined hole variability logs; e) open hole variability logs; f) change log; g) heat pulse flow meter flow; and h) virtual caliper from travel time of acoustic televiewer data. Arrows schematically represent zones of flow, amount (by size), and direction (orientation), and are referred to in the text (red for open hole and blue for lined hole).

2.11 Supporting Information

Additional Supporting Information may from the online version of this article.

Table 2-1S: Detailed characteristics of the boreholes discussed.

Site	Hole Dia. (cm)	Surface MASL	Approximate Depth to (m)		
			Ambient Water Level	Bottom of Casing	Bottom
Cambridge, ON	10	309.2	19	30.2	150
Guelph, ON	10	343.8	4	5.8	105
Simi, CA	20	~590	78	1.5	154
Madison, WI	10	281.4	16	21.3	152

2.11.1 Application at Other Sedimentary Rock Sites

Although the nature of the comparisons between the temperature profiles collected in lined and open holes at the sites in Simi, CA and near Madison, WI (Figure 2-7S and Figure 2-8S respectively) are similar to those observed at the Cambridge and Guelph sites, these sites provide additional insights. A color and symbol scheme consistent with the main text, including arrows of varying size, representing relative amounts and direction of flow as well as red for open-hole and blue for lined-hole temperature data are used in these figures.

The general characteristics of the temperature profiles from the Simi site (sandstone with mudstone interbeds; Williams et al. 2002) are much different than those from the Cambridge and Guelph dolostone. The topographically driven downward cross-connected flow in the open hole at the Simi site results in much of the open hole temperature profile appearing as a series of linear segments with gradually increasing values with depth and low variability (less than 0.1 °C). The uniform segments are separated by five abrupt temperature increases, or "steps". A reasonable interpretation of the open borehole data is that water enters the borehole at each of the steps and moves downward, gradually warming but in thermal disequilibrium with the formation until the next major flowing fracture is reached where the process repeats. The abruptness of the temperature changes implies individual fractures dominate water movement into the borehole. In contrast, using the size of the temperature variations as an indicator of the relative contribution of water, none of the variations within the FLUTe liner (Figure 2-7Sc, d) are as sharp as in the open-hole case, implying flow occurs over a series of fractures (a zone) rather than individual distinct discontinuities in the rock. Over the 55 m interval of hole at the Simi site, 22 flow zones are

indicated by the lined-hole profile, which is many more than can be identified based on the open borehole logs.

In late September, 2003 open- and lined-hole measurements were obtained in MP6 at the Wisconsin site. The process was repeated and a second set of open- and lined-hole data were collected in mid-December, 2003. Meyer et al. (2007) describe the hydrogeology of this study area and indicate the geologic units consist of Cambrian-Ordovicran inter-layered, nearly horizontal sandstone and siltstone with a dolostone unit. Groundwater flow is primarily horizontal in the sandstone beds with downward leakage towards the Mount Simon Formation, which is a regional aquifer. During the September episode, the liner had a leak as indicated by the inability to raise the water level inside the liner above the level in the formation. Comparison of the lined-hole temperature profiles (September vs. December) clearly shows the location of the leak; moreover, the lined- and open-hole profiles in September are identical above the level (roughly 212 masl) where the leak prevents liner seal, while below they appreciably diverge. The actual outflow must be slightly above the level where this divergence occurs because some head differential is needed to create liner seal below the leak. This differential occurs because overall the head in the formations decrease with depth (Meyer et al. 2007). This example demonstrates: (i) a temperature profile inside a liner can be used to determine the approximate depth of a liner leak, which is helpful in identifying the point where liner repair is needed, and (ii) useful temperature profile interpretation can be obtained from the sealed portion below the leak. This contrast between unsealed and lined-hole data in the same log supports the premise that a sealed hole provides a much different thermal perspective of the borehole.

The most distinct feature of the lined-hole temperature profile at the Wisconsin site is a major flow zone indicated at an elevation of 214 masl (Figure 2-7Sc). This is likely the zone of most active ambient groundwater flow at this borehole location, yet there is no indication of its existence based on inspection of the open-hole profiles. In addition to this major feature, nine other flow zones were denoted from the lined-hole profiles. Other lines of evidence at this site suggest many more flow zones in addition to those identified using the existing interpretation procedures. The sections of the open-hole temperature logs that have an irregular and highly variable response (e.g., 130 -150 m) are without general coherence between repeat logs and are therefore not interpreted as individual fractures, although some likely occur in this depth range.

The data from the Simi and Madison sites re-enforce the conclusions presented in the main text, in particular that the improved interpretation of lined temperature data is a general situation rather than

specific to Southern Ontario. These examples also show that the techniques have application in varying geologic and hydrogeologic settings.

2.11.2 Supplemental Figures

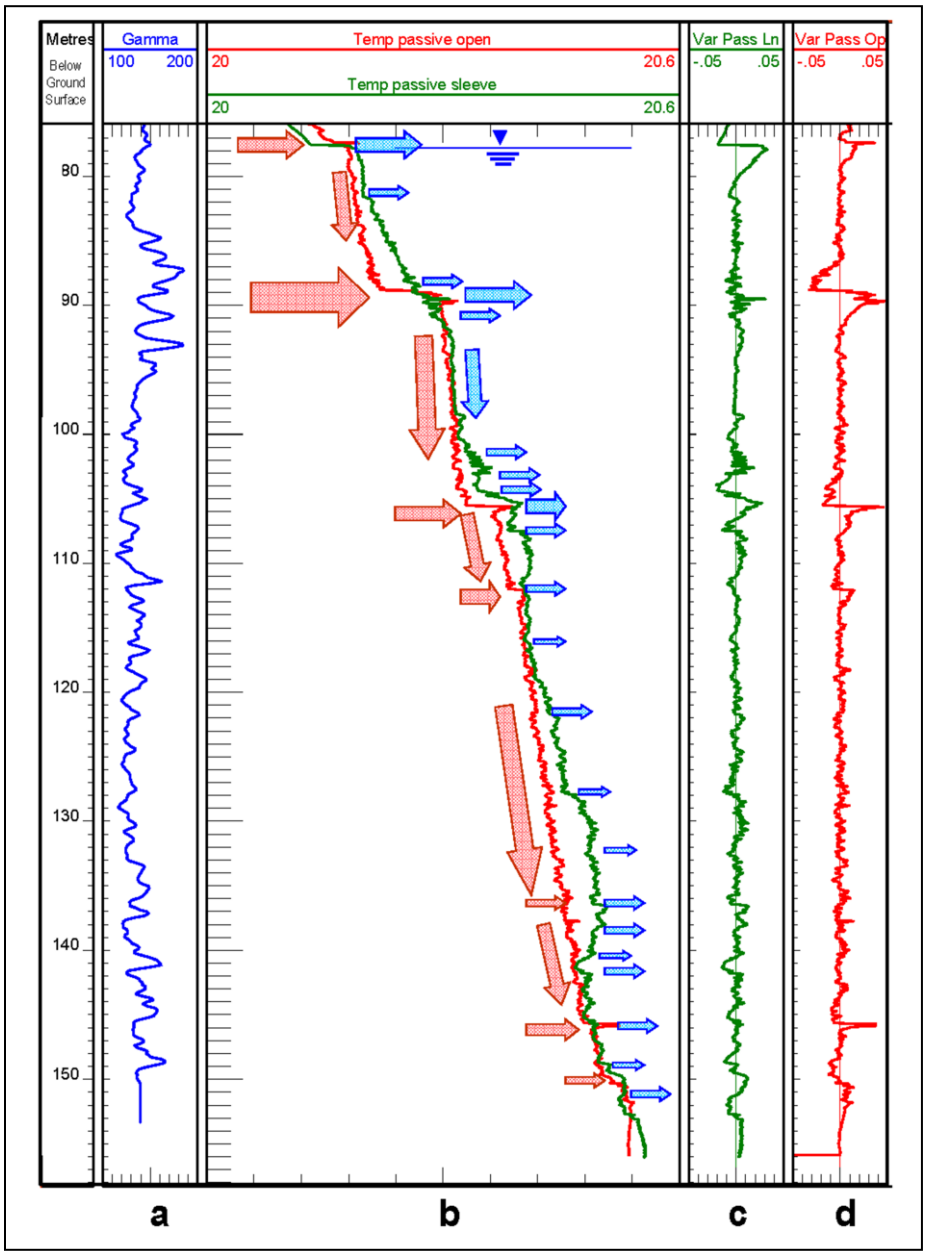

Figure 2-7S: Examples of temperature data from Simi, CA.
Data plotted relative to depth in metres from ground surface: (a) gamma log, (b) temperature profiles collected in open holes (red) and lined (blue) hole, and variability logs for lined- (c) and open- (d) hole conditions. Arrows schematically represent zones of flow, amount (by size), and direction (orientation), and are referred to in the text (red for open hole and blue for lined hole).

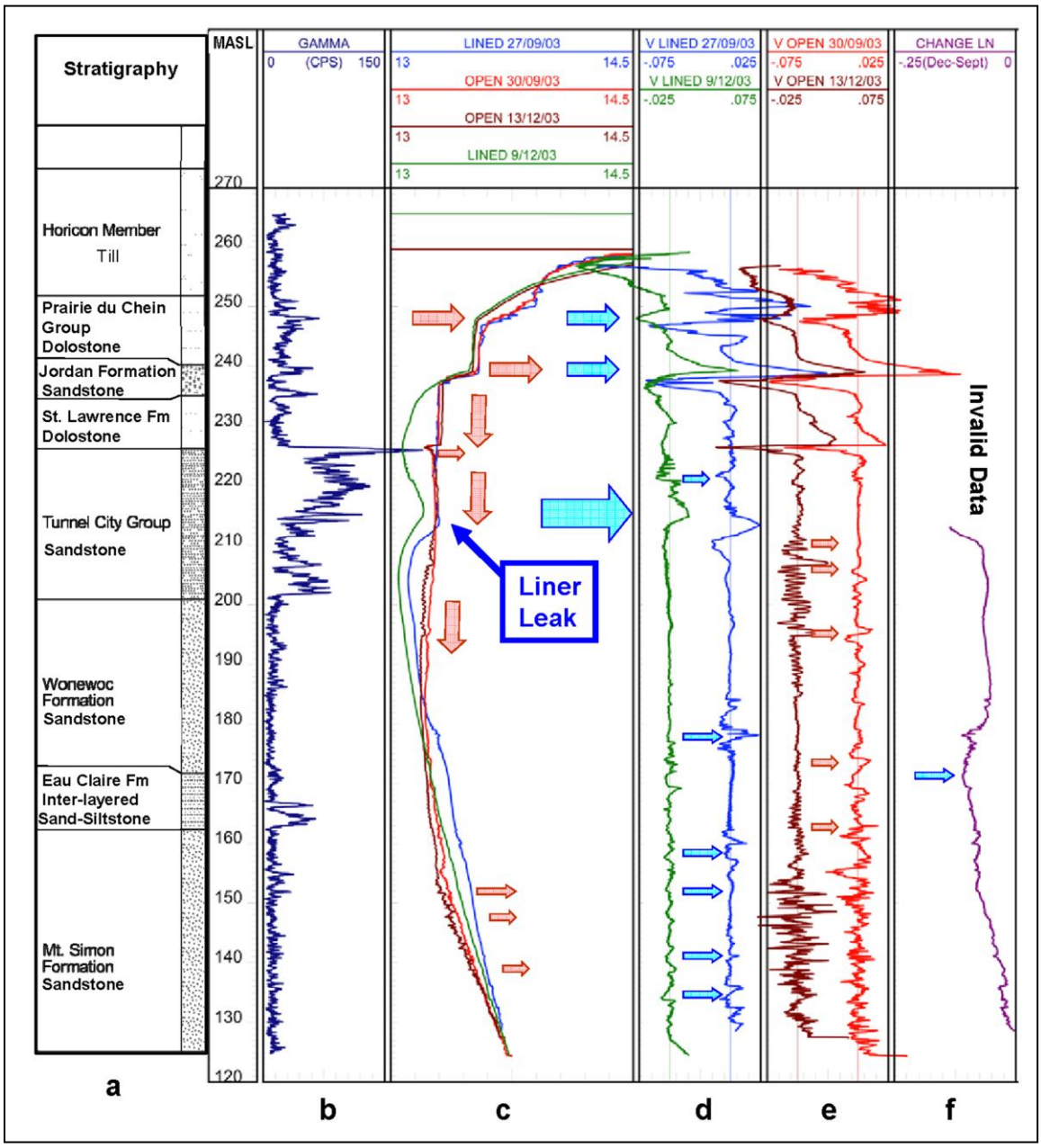

Figure 2-8: Examples of temperature data from Madison, WI.
Includes a, b & c) stratigraphy, hydrogeologic units (HG), and gamma log from Meyer et al. (2007), d) lined hole temperature logs from 27/09/2003 (red) and 9/12/2003 (purple), open hole temperature logs from 30/09/2003 (blue) and 13/12/2003 (teal), e) lined hole variability logs from 27/09/2003 (red) and 9/12/2003 (purple), f) open hole variability logs from 30/09/2003 (blue) and 13/12/2003 (teal), and g) lined hole change log. Arrows schematically represent zones of flow, amount (by size), and direction (orientation), and are referred to in the text (red for open hole and blue for lined hole).

Chapter 3
Enhanced detection of hydraulically active fractures by temperature profiling in lined heated bedrock boreholes

Peeter Pehme, B.L. Parker, J.A. Cherry, J.W. Molson and J.P. Greenhouse.

3.1 Overview

Borehole profiling using a temperature probe has become a more effective tool for identifying hydraulically active fractures in rock due to the combination of two advances: improved temperature sensors, with resolution on the order of 0.001^{o}C, and temperature profiling within water inflated flexible impermeable liners used to temporarily seal boreholes from hydraulic cross-connection. After inflation the open-hole cross-connection effects dissipate, so that both the groundwater flow regime and the temperature distribution return to the ambient (background) condition. This paper introduces a third advancement: the use of an electrical heating cable that quickly increases the temperature of the entire static water column within the lined hole placing the entire borehole and its immediate vicinity into thermal disequilibrium with the broader rock mass. After heating for 4-6 hours, the profiling is conducted several times over a period of a day to observe the temperature change returns to background. This procedure, referred to as the active line source (ALS) method, provides two advantages. First, there is no depth limit for detection of fractures with flow and second, both 2identification and qualitative comparison of the strength of the evidence for ambient groundwater flow in fractures is improved throughout the entire test interval. The advantages of the ALS method are shown by comparing results from two boreholes tested to depths of 90 and 120 m in a dolostone aquifer used for municipal water supply where most groundwater flow occurs in the fractures. Temperature logging in the lined holes shows many fractures in the heterothermic zone both with and without heating, but only the ALS method also shows many hydraulically active fractures deeper homothermic portion of the hole. The identification discrete groundwater flow at many depths is supported by additional evidence concerning fracture occurrence, including continuous core visual inspection, acoustic televiewer and tests for hydraulic conductivity using straddle packers as well as rock core VOC data, where available, showing deep penetration and many migration pathways. Confidence in the use of temperature profiles and the conceptual model is provided by numerical simulation and by demonstrating the reproducibility of the evolution of the temperature signal measured in the lined holes with and without heating. This approach for using temperature profiling in lined holes with heating is a practical advance in fractured rock hydrogeology because the liners are readily available, the equipment needed for heating is low cost and rugged, and the time needed to obtain the profiles is not excessive for most projects.

3.2 Introduction

In rock formations, most or essentially all groundwater flows in fractures. To gain insight into how contaminants behave in these environments, and to enable more accurate predictions of their arrival times at receptors, better characterization of groundwater flow in fracture networks is needed (e.g. National Research Council, 1996, Berkowitz, 2002; Sara, 2003). Many numerical models have been developed for simulating flow and contaminant transport in discrete-fracture networks in rock (FRAC3DVS, Therrien and Sudicky, 1994; FEFLOW, Trefry and Muffels, 2007; HEATFLOW, Molson and Frind, 2012); however, advances in acquisition of field data for fracture parameterization for such models has lagged far behind advances in numerical codes. In investigations of contaminated bedrock sites, data acquisition from boreholes is the primary approach to site characterization and many methods are used to identify fractures, including inspection of continuous core, borehole imaging (e.g. acoustic and optical televiewing), caliper logging, and hydraulic tests such as straddle packers (e.g. Quinn et al., 2011) and flexible liner profiling (Keller et. al. submitted). However, these cannot distinguish those fractures with active groundwater flow from those that have no flow under ambient conditions. In this paper in the context of active groundwater flow the term 'fracture' refers to any secondary permeability feature in the rock mass that acts as a preferential flow path relative to the low-permeability rock matrix including bedding parallel fractures, joints, styolites, isolation channels and any other geologic features with enhanced flow. There is an abundant literature concerning identifying zone with flow under forced gradient conditions, created when the hole being investigated is pumped and monitored or when one hole is pumped and responding holes are monitored. However, this paper concerns identification of fractures that have active, ambient groundwater flow which refers to flow in the rock uninfluenced by the borehole and not imposed by pumping or injection for the purposes of fracture identification. Therefore, there is a need for borehole methods that identify the fractures in which groundwater actively flows under ambient hydraulic conditions.

It has long been recognized that temperature profiles in open boreholes measured in rock offer insights about fractures with flow (e.g. Trainer, 1968; Bidaux and Drogue, 1993; Robinson et al.,1993); however, temperature has generally been used only minimally in fractured rock investigations at contaminated sites. Two recent advances provide impetus for temperature profiling to become much more important. The first is the greatly improved sensor resolution for temperature measurement (on the order of 0.001^{o}C) and the second concerns measurement of temperature profiles in holes sealed using impermeable flexible liners produced by FLUTe (http://www.flut.com) to prevent cross flow between fractures (i.e. hydraulic cross connection). Using these two advances for measuring temperature profiles under ambient flow conditions, Pehme et al. (2010) identificatied numerous hydraulically active fractures in boreholes in

dolostone and sandstone. The number of fractures identified by this method was much larger than the few identified when the holes were unsealed (i.e. open-hole conditions). Identification of all of the fractures in which active groundwater flow occurs is important in contaminated site investigations because the nature of contaminant plumes is very different between dense and sparse networks (Parker, 2007).

Keller et al., (in submittal) describe these liners and their installation in rock boreholes. The method of sealing boreholes using these liners is becoming common in contaminated site investigations to prevent cross contamination caused by flow into the hole from fractures at some levels and flow out of the hole from fractures at other depths as described by Sterling et al (2005). Although vertical cross connection in fractured rock holes has been recognized for decades and capitalized on for investigations in fractured rock, Pehme et al. (2010) showed that the open-hole conditions have been misleading with respect to identification of all hydraulically active fractures in the system and the improved sensitivity for identifying more active fractures when boreholes are sealed and sensitive temperature logging probe was used. The impervious flexible liners are urethane coated nylon formed into cylindrical tubes that are installed temporarily in the hole, with inflation by water, until a monitoring well is installed or the hole is subjected to hydraulic or other tests. As described by Pehme et al. (2010), typically several days after installation of the liner, the temperature distribution in the static water column inside the liner becomes stable at which time the hole is suitable for ambient temperature profiling to identify flow.

Although the use of high precision temperature probes in the static water columns of lined holes enables the identification of numerous hydraulically active fractures (Pehme et al., 2010), this approach has a depth limitation. Fractures are preferentially identified close to ground surface where groundwater flow transports heat perturbations from surface imparted by the atmosphere (i.e. surface temperature variations due to weather) and urban infrastructure. These surface-imparted temperature disequilibria are attenuated at depth due to thermal conduction in the rock mass. The maximum depth to which this thermal disequilibrium can be used to identify fractures varies considerably depending on both geology (ie. thickness and nature of overburden, degree of bedrock fracturing etc.) and hydrogeologic conditions (i.e degree of vertical and lateral flow, recharge vs. discharge etc.). However, there is commonly a need to identify active groundwater flow or contaminant migration at greater depths than the limits of thermal disequilibrium.

This paper describes a method aimed at eliminating the depth limitation for use of temperature profiling in lined holes to identify ambient flow through fractures. In this method, the static water column in the lined hole is heated continuously along the entire length of the hole to rapidly create strong thermal disequilibrium around the borehole and then temperature profiles are measured as the heat in the water

column dissipates. This method is referred to as the Active Line Source (ALS) method applied in lined boreholes. Greenhouse and Pehme (2002) introduced the ALS method applied in open (unlined) holes for fracture identification and Pehme et al. (2007) showed application of ALS in a lined hole to estimate thermal conductivity and drew attention to the possibility of identifying hydraulically active fractures using this techniques. Freifeld et al. (2008) adopted a similar heating process with fiber optic sensing to estimating rock thermal conductivity and thereby paleo-cooling. This paper provides the first detailed field examples of ALS in lined holes for fracture identification where many other methods were also used to acquire evidence of fractures. The results of ALS application in lined holes are compared to those from the same lined holes without ALS to demonstrate the added insights concerning occurrence of ambient flow in fractures.

The ALS method used in lined holes has been applied in more than 42 holes at 8 different sites in North America, primarily in dolostone and sandstone. The field results presented in this paper are from two holes, MW-25 located in Guelph, Ontario and UW-1 in Cambridge, Ontario. These two holes (both situated in a Silurian dolostone aquifer used for municipal water supplies), were selected as examples because the hydrogeologic characteristics of this aquifer have been described in detail by others. Perrin et al (2011) describe the general nature of the secondary permeability that includes fracture networks with solution channeling. Quinn et al (2011) present results of hydraulic tests using straddle packers to measure hydraulic conductivity and estimate fracture apertures using the cubic law. Keller et al (submitted) describe a flexible liner method for measuring hydraulic conductivity profiles in the dolostone aquifer. Pehme et al (2010) used UW-1 and MW24, which is 490m west of MW25, in a study of fractures identified by temperature profiling in lined versus unlined holes without the added heat.

MW-25 is the focus of this present study because the most comprehensive data sets using the ALS method in lined holes are from this hole. This hole, which is 104m deep, penetrates through the full thickness of the dolostone aquifer into the underlying shale. The thermal and hydraulic conditions in this hole have less complexity than holes under the influence of municipal pumping wells. MW-25 has a distinct downward decrease in temperature from top to bottom without any temperature reversals observed in some of the other holes and thus avoids any complications that could arise due to a potential for thermal convection where temperature increases with depth. UW-25 has no contaminants above drinking water limits and therefore when this hole is left open for tests requiring open hole conditions, such as open-hole temperature profiling, contaminant cross-connection is not a concern.

3.3 Conceptual Model and Hypothesis

Drogue (1985) introduced the terms ‘heterothermic zone’ to describe the shallow subsurface wherein atmospheric temporal temperature variability exists and ‘homothermic zone’ for the stable temperature zone at greater depth. The temporal differences in the upper portions of temperature profiles collected in various seasons progressively decrease deeper until a critical depth beyond which the thermal gradient is invariant and the rock is ‘homothermic’. Drogue (1985) identified the hetero-homothermic boundary at 25m depth in a limestone aquifer in Southern France. Figure 3-1 provides a conceptual description of these two zones for the case where overall temperature declines in the shallow subsurface. In the heterothermic zone, temperature profiles measured on any occasion typically have numerous depth-discrete peaks and troughs, often at several different wavelengths, with amplitudes attenuating with depth, overlapping and varying in time. This zone is in a continual state of thermal disequilibrium, adjusting to temperature variations at the surface related to weather and urban infrastructure. The nature of the downward propagation of shallow thermal variations as a tracer of recharge has been investigated by many (eg Taniguchi, 1993) and summarized by Anderson (2005). These studies generally use open boreholes, are coarsely sampled, and deal with broad change in temperature rather than the detailed variations of concern in fracture investigations. Below the heterothermic zone, the homothermic zone has an overall stable temperature and thermal profiles have a smooth shape primarily governed by the steady state transition from the mean annual surface temperature to the earth's geothermal gradient. In this conceptual model, fractures with active groundwater flow occur in both zones, however, the primary influence on the temperature profile in the heterothermic zone where thermal disequilibrium occurs is the effect of continual temperature variations at the surface. In the heterothermic zone, fractures with active groundwater flow are manifested in lined holes as distinct irregularities (peaks or troughs) in a temperature profile otherwise gradually varying with depth, referred to here as aberrations (Figure 3-1). The effective depth to the boundary between the heterothermic and homothermic zone depends on several factors including paleo temperatures, the thermal conductivity of the rock, the magnitude and spatial distribution of the surface temperature variations, groundwater flow rates in the fractures and the resolution of the temperature probe. Little is known about the depth to the boundary because, to determine the boundary, the holes must be lined, the effects of drilling or open-hole flow conditions dissipated, and a high resolution temperature probe utilized. These criteria have not been met at a large number of sites distributed around the globe. From our experience at eight locations, in North America, the depth is generally many tens of meters (i.e 30-50 mbgs or more), however that value also depends on the time scale chosen for comparison as well as the degree of uniformity set as the criteria for invariance, and in some pumped bedrock aquifers the boundary can be difficult to define or variable. The goal of the

ALS method is to improve the resolution of temperature logs for identification of flow throughout the borehole in both the heterothermic and homothermic zones.

The new method presented in this paper is based on the hypothesis that, when the hole is quickly heated along its entire length and then high resolution temperature profiles are measured while the heat is dissipating, (1) the hydraulically active fractures in the heterothermic zone show up more definitively than in the unheated profile and (2) fractures in the homothermic zone become more clearly evident relative to profiles done in the lined holes unheated. The basis for this hypothesis is the expectation that groundwater flow in the fractures will transport the applied heat away from the heated water column faster at the fractures than conduction will dissipate the heat where no fractures exist. Figure 3-2 illustrates this hypothesis, indicating that in the unheated (passive) case the amplitude of the aberrations at the fractures decrease in size though to the bottom of the heterothermic zone, beyond which flow through fractures is undetectable because there is no thermal disequilibrium. The disequilibrium created by heating the hole both makes flow detectable below the hetero-homothermic boundary in the cooling logs measured during thermal recovery and improves the qualitative relationship between flow and the size of the thermal aberrations throughout.

3.4 Numerical Simulations

To illustrate the conceptual model for thermal response during borehole heating and cooling, the numerical model Heatflow/Smoker (Molson et al., 2007; Molson and Frind 2012) was applied to a simple conceptual model. The model simulates three-dimensional groundwater flow and heat transport within a discretely-fractured porous medium using the finite element method. Water density and viscosity depend on temperature, and fractures are represented as two dimensional planar surfaces imbedded onto element surfaces. Figure 3-3 shows the finite element grid and the geometry of the single horizontal planar fracture and single vertical borehole within the 3-D array of elements for the test case. The fracture aperture is 1000 microns, the rock matrix porosity is 0.05 and the rock matrix hydraulic conductivity is 9.8×10^{-10} m/s, values which are representative for the dolostone aquifer under investigation (Burns, 2005). A thermal conductivity of 3.6 J/m/s/ºC (Appendix C - Table 6, Molson, 2006) is assigned to the rock matrix. Flow is assumed at steady-state. Further details of the model test conditions are provided in Figure 3-3.

The liner and heating cable in the hole are represented as shown in the insert of Figure 3-3, with the heated cable set on the up-gradient borehole wall. The impermeable liner, (3mm thick urethane-coated nylon) is represented in the model by the ring of small (1x1x2cm) elements of zero permeability and a

thermal conductivity equal to that of water (0.57 J/m/s/^{o}C) creating an impermeable boundary which transmits heat.

A field-observed hydraulic gradient of 0.0075 is imposed across the domain using fixed heads of 0.15 m and 0.0 m at the up-gradient and down-gradient boundaries, respectively. The initial temperature is a uniform 10 ^{o}C, which is imposed as a Dirichlet (Type 1) condition at the up-gradient (inflow) boundary. All other temperature boundaries are Neumann zero-gradient conditions. The conceptual model was run using a vertical 1D line-source heater placed at the borehole centre. An energy input rate of 20W/m was applied for 6 hours, then shut off. Model accuracy was tested by running a sensitivity analysis on element sizes, using conceptual testing (i.e. ensuring symmetric flow conditions within the fracture around the borehole, no flow within the borehole, and the ability to meet theoretical thermal decay rates), as well as calibration against field data.

Figure 3-4 illustrates the predicted temperature at the center borehole during heating and subsequent thermal recovery adjacent to the fracture and adjacent to the rock matrix 1.5 m below the fracture. The typical time-line for data collection in an ALS test, a "passive" log immediately before testing, an "active" log prior to the end of the 6 hr heating period, as well as three "cooling" logs (1/2, 6 and 12 hours) into the thermal recovery are each shaded. Both the short time lag between energizing the heater and the response at the center of the borehole as well as the temperature increase ('spike') immediately after the heater is turned off (Figure 3-4) are related to the distance between the heater and the measuring point. The time lag is attributed to the delay for the heat energy to conduct from the cable (line source) through the water to the centre of the hole. The spike at the end of the heating occurs because the rock continues to act as a heat source after power to the heater stops. However, the natural hydraulic gradient transports the stored heat energy towards the hole by advection rather than moving radially outwards through the rock by conduction with the thermal gradient as occurs during heating. These small scale, short duration effects vary according to the position of the cable in the hole and the groundwater flow direction. In the field, the cable has no centering device and therefore such small scale time lags and spikes must be considered in data interpretation, and are the primary reason for emphasis placed on the second and third cooling logs and thermal deviation logs for identifying flow.

In the simulation, energy from the heating cable generally raises the temperature in the borehole to 11°C, however the maximum temperature in the centre of the borehole at the fracture as the heater is turned off is 0.15 C° cooler. After 6 hours of heating, the simulated temperature profiles in the centre of the borehole during the cooling period show a strong aberration at and near the fracture but beyond 0.5 m above and below, the simulated response is uniform (Figure 3-4b). The transport of heat away from the

borehole column by the water moving through the fracture causes an accelerated decline in temperature (a negative aberration) in the three cooling profiles simulated. Although the magnitude of the signal is small, it is nevertheless two orders of magnitude larger than both the resolution of the temperature probe and the typical background variability of field data. The response has a minor asymmetric elongation upwards that suggests convection due to subtle density effects may be occurring. Although the model accounts for thermal convection within a porous medium, this is not a rigorous approach for a fluid-filled borehole, thus modifications to the existing model would be needed to investigate this further. Figure 3-4b indicates that to adequately resolve the profile shape over the vertical extent of the predicted aberration and to accurately determine the maximum deviation from the norm, the vertical spacing of temperature measurements in the field data must be on the order of 0.01 m or less.

3.5 Equipment and Method

3.5.1 Data Collection

The essential equipment used in the field includes five components: the temperature probe (the tool), a winch, heating cable, generator and computer. For the data presented in this paper, two temperature probes were used; early data were collected with a rented probe (a single sensor BMT-01 manufactured by IFG corporation, Brampton, Ontario, Canada), and the later results with a prototype probe. Both probes have a specified operating range of 0-50°C, sampling rate of 2Hz, a specified resolution of 10^{-4} C° (although our data supports 10^{-3} C°). Although the resolution of these probes is high, the absolute accuracy is subject to the calibration process which is more difficult to control. The data from the two probes were 'normalized' for the purposes of establishing a hetero-homothermic boundary by comparing the differences in response through approximately 10^4 readings in the lower (stable) portion of the borehole (MW25). The details of the original calibration and normalization are provided in the supplemental materials of this manuscript.

The heating cable is assembled by combining two rain gutter heaters (manufactured by “Wrap On” ™, model 14240, available at many major building supply outlets) in series (total resistance 17ohm) that, when powered at 220volts, produces 20W/m uniformly along its length. The heating cables used to acquire the data presented in this paper are readily available at low cost in many hardware stores in northern climates where they are sold for heating roof gutters to avoid ice problems. More recently this heating equipment has been replaced by a line heater providing more energy input. The heater is commercially available without need for custom design.

Data collected in MW25 is used for comparison of results with and without ALS testing. The hole was sealed with a Flute™ liner in a manner described by Keller et. al (submitted) and the water allowed to thermally stabilize before the ambient, lined-hole temperature (passive) logs were collected on August 9th and 23rd, 2005. The term "passive" is used to refer to any temperature log collected without prior heating. In the ALS procedure, the 'background' condition is considered to be as observed with the passive temperature profile preferably collected just before the beginning of the heating stage, usually the prior afternoon. The borehole is heated for as long as logistically practical (typically 4 to 6 hours), 4.1 hrs in the case of the ALS test started in MW25 on March 8th, 2006. The 'active log' is a temperature profile measured during the borehole heated stage just prior to the heater being turned off. The hole is typically logged three times during the cooling stage as the applied heat in and around the borehole dissipates and the system gradually cools towards background temperatures, as summarized in Table 1. The first cooling log (C1), is started within an hour after the heater is turned off, the second log (C2) is started 4-6 hours after the heating ceases (timed to start at approximately the same time into thermal recovery as the duration of heating) and the last cooling log (C3), is typically collected 18 hours after heating (early the following morning). Table 2 summarizes the details of the timing of the ALS data collection in MW25.

The logging rate used for the data collection is varied based on a compromise between resolution and the need to minimize both the time spent logging in the middle of the test and disturbance of the water column. Data were collected at the typically rate of 0.5-0.7m/min for the passive, C2 and C3 logs, and 1-1.5 m/min for the active and C1 logs when adequate time must be allowed for the effects of logging to dissipate prior to collection of subsequent data. It is worth noting that all background (passive) temperature logs (both open and lined hole) are collected at a nominal data interval of 0.005-0.007m. A critical factor in assessing the reliability of aberrations in temperature profiles is that the shape of features that span 10 to 20 cm are defined by many readings (14-20 when collected as specified) so depth resolution due to run speed is a critical factor.

3.5.2 Procedure for Identification of Flow from Temperature Logs

The industry standard method for accentuating small changes (both in terms of vertical extent and contrasting values) within a temperature log is a gradient log (C°/m) (e.g. Keys, 1989). The gradient is typically calculated as the change in temperature over a short distance (10cm is used in this case). The gradient presentation is well suited to highlighting small temperature changes in an open hole with cross-connected flow because water entering or leaving the borehole through fractures often manifests as steps in a temperature profile, however the process creates a bimodal pattern when applied to a unidirectional temperature aberration.

The identification of fractures showing active groundwater flow using temperature logs in lined holes is primarily based on an analysis of a processed version of the data referred to here as the 'thermal deviation log'. This procedure for processing temperature logs was previously termed the 'variability log' and described in detail by Pehme et al. (2010) but is renamed here to better associate it to the statistical process upon which it is based. To create a “thermal deviation log” the raw temperature profile is smoothed using a boxcar filter (typically with a window length of 5m) and the smoothed 'base log' is subtracted from the raw data. The resulting representation has been found to be more effective than using gradient temperature logs as described in the early literature (e.g. for interpreting lined-hole temperature logs). The thermal deviation log emphasizes log features, localized aberrations from the norm, with length scales less than the window, while suppressing larger scale features or trends such as the geothermal gradient and shallow seasonal variations, yet maintains the original shape of the temperature aberrations, which is critical to identifying those most likely to represent fractures with active groundwater flow and relative rates. The selection of specific small scale features on the thermal deviation log deemed to be fractures with active groundwater flow is, in the end, somewhat subjective particularly in the case of numerous indications of flow that are closely spaced. The degree of uncertainty is less when more than one thermal deviation log is available (i.e. when data are collected in the lined hole on more than one occasion, separated usually by several days or weeks). However, that comparison can be complicated if recharge events occur in the interim. Aberrations that are clearly evident in each of the individual logs at the same elevation are most unambiguously designated as active fractures.

3.6 Results and Discussion

3.6.1 MW-25 Characteristics Indicated by Non-Thermal Evidence

MW-25 was selected for detailed temperature studies, including open-hole and lined-hole unheated and heated profiling, as well as comparison of the temperature identification of active groundwater flow with many other lines of evidence concerning depth-discrete permeable fractures or geologic features. Figure 3-5 displays many of the non-thermal lines of evidence concerning fractures alongside the temperature profiles in the unlined and unheated lined hole. The hole is almost entirely comprised of dolostone with shale at the bottom and a slightly shaley zone (Eramosa formation) that at some locations hydrogeologically separates the aquifer into two stratigraphic units. The inspection of continuous rock core showed many fractures (Figure 3-5 column D). The longer interval (30.5-35mbgs) for which no fractures are shown are those where core was not recovered or was rubbly so that fracture identification was not possible as indicated by the RQD (column E). The acoustic televiewer log (ATV) also shows frequent fractures with at least one fracture in each 2 metre log interval (column G). Hydraulic tests with

straddle packers done as consecutive 1.5 m test intervals over the entire hole (Column H) in 2005 and a second time (2010) with 3.0 m test intervals were performed using the method reported by Quinn et al (in press) and show presence of permeable zones throughout the hole. If permeable fractures were not present, then the test results would have been orders of magnitude below what was measured. Therefore, based on the core log, ATV and packer test results there is evidence of numerous transmissive fractures. The next challenge is to determine which of these transmissive features also exhibit active flow under ambient (sealed hole) conditions.

The open-hole has downward vertical flow indicated by the heat-pulse flow meter (column J and K). Although the two closest municipal pumping wells are no longer used, the direction of flow remains almost entirely downward because the distant wells that continue to supply the City of Guelph (approximately $0.5 m^3/s$) draw water primarily from the lower part of the aquifer. There is a high transmissivity zone at the top of the rock just below the overburden where the rock is intensely fractured and weathered that supplies much of the water flowing downward in the borehole.

3.6.2 Temperature Profiles from MW25 Unheated

Understanding the merits of the ALS method in lined holes becomes evident when comparison is made with temperature profiling results from the hole in the unheated state both unlined and lined. Figure 3-5(columns L through S) shows unlined and lined unheated profiles for MW-25, with the March data adjusted using a linear normalization to the earlier probe. Both the unlined (open-hole) and lined hole profiles provide unique insights concerning the presence of hydraulically active fractures and the apparent depth to the bottom of the heterothermic zone. Although the presence of strong downward flow in the open hole can create disequilibrium and make some transmissive fractures below the hetero-homothermic boundary detectable, Pehme et al. (2010) show that many other more important transmissive fractures can go undetected in open-hole temperature profiling. The depth to the bottom of the heterothermic zone shown on Figure 3-5 is positioned where shallow zone temporal profile shapes in the lined hole become similar. Below this depth (37m), the three lined-hole profiles have the same overall shape. The exact positioning of the boundary between the heterothermic and homothermic zones is approximate but nevertheless a reasonable interpretation is between 35 and 40m depth. The details of choosing the hetero-homothermic boundary are in the supplemental text (section 3.12.1).

Figure 3-5 (column **a** and **b**) show the aberrations indicative of flow identified using the open-hole and lined-hole logs, respectively. These aberrations are based on interpretations of the thermal deviation logs described above. For the open-hole condition, there is only one log available for discerning flow but for the lined-hole there are three logs, August 9 and 23, 2005 and March 8, 2006. Each of the three

temperature logs in the lined-hole measure a different hydraulic condition, the March much more so than the other two. Reproducibility of a particular aberration, which is clearly larger than the resolution of the probe, suggests the consistent contribution of that feature to flow in the overall network, whereas intermittent occurrence suggests a transient flow or a temporary condition. Both columns show the largest and highest frequency of aberrations in the upper 25m. The open-hole temperature profile shows more aberrations in the homothermic and upper (above 85mbgs) portion of the homothermic zones than does the lined-hole profile. This is expected because this hole has downward cross-connected flow from the heterothermic zone into the homothermic zone, thereby creating the thermal aberrations in the homothermic zone. The high frequency of aberrations above 25m depth is generally consistent with the core log in the depth interval and the low frequency of picks in the lower third of the hole, particularly below 85mbgs inconsistent with the core. The thermal deviation logs calculated from the two lined-hole logs collected in August are mutually similar and exhibit a consistent pattern of small (0.001-0.002 C°) deviations above 92 mbgs without any distinct indications of strong water flow. The thermal deviation log from the March (2006) passive temperature exhibits many more and slightly larger changes in temperature than the earlier lined-hole logs, but with the exception of the aberrations at 54-60 mbgs, the few other distinct features bear no apparent coincidence with the zones of increased fracturing from the core and the ATV or any relationship to the zones of higher transmissivity indicated by the packer tests.

3.6.3 Temperature Profile from MW25 Lined and Heated

Figure 3-6 shows the results and interpretation of the ALS testing in MW25 alongside selected non-thermal data from the borehole. Comparison of the aberrations identified from the three types of temperature logs show substantially different results (Figure 3-6 columns **a** through **c** on the right hand side). The heated lined hole (ALS) profile has the most aberrations and the unheated lined hole has the least. The ALS profile shows no decrease in fracture occurrence in the bottom part of the hole as clearly does the unheated lined profile (**b**) and to a lesser degree the open hole as well (**a**). This is consistent with the expectation that in which heating increases resolution both in the heterothermic and homothermic zones and with the general understanding of the flow conditions in this dolostone aquifer in which much of the production of municipal wells is from the bottom most zone in the aquifer.

The identification of f aberrations resulting from flow were made using the C2 cooling log because it avoids the complications that can result from transient effects potentially present in the C1 log (see Figure 3-4) and has better resolution than provided by the C3 log where much of heat added has dissipated. Figure 3-7 shows the 62 to 73 mbgs depth interval at expanded scales so that an example of the detailed evidence for the aberrations can be examined. Column U shows the C2 log and beside it are the interpretation of flow(**c**), denoted in four colours, purple representing a relatively strong aberration

suggesting relatively large groundwater flux in the fracture, blue representing a less distinct aberration, with dark and light green representing the weakest form of aberration. These colour representations for flow are consistent with colours for flow shown in Figure 3-5 and Figure 3-6. For this 11m long interval, the ALS log provides 34 picks, the open-hole log 28 picks and the lined unheated log 14 abberations. The ATV log shows 11 fractures and the core log shows 18 fractures. The lesser number of fractures evident in the ATV log relative to the core log is expected because the ATV log cannot discern small or in-filled fractures due to breath of the acoustic pulse (ALT, 2002). The ALS shows flow where both the ATV and core logs do not show fractures are present; however, the straddle packer test results show that the hydraulic conductivity is also relatively large in theses intervals, much larger than the typical rock matrix hydraulic conductivity indicated for this dolostone by lab tests or intact core samples. Examination of core photos as well as both the amplitude image and the virtual caliper of the ATV indicate many fossiliferous, porous (vuggy) layers exist within this depth interval that would not be identified as fractures. It is also possible that a fracture close to, but not directly intersecting, the borehole could produce an aberration in the temperature profile but not be evident in the core. However, the proximity at which such influence could occur would dependent on the amount of flow and geometry relative to the borehole.

As expected the ALS log shows by far the most active fractures in the homothermic zone because, for the unheated lined hole the natural thermal disequilibrium is minimal and for the open-hole condition the cross-connection imposes an erratic (complex) thermal condition that obscures the less permeable fractures. However, in the heterothermic (9-37m depth) zone the difference in the number of active fractures indicated by the three types of logs is much less. The ALS log shows 107 aberrations, the unheated lined log shows 55 and the open-hole log shows 63. The greater number of picks shown by the ALS log is expected because the evidence for a pick is strongest of all in the C2 log where one can base judgment on comparison to the C1 and C3 logs. Figure 3-6 shows that some aberrations from the lined unheated logs do not show up in the ALS log or are a much smaller aberration in the heterothermic zone. This may indicate that not only does the ALS log identify more active fractures but it has better reliability. However, because the overburden is thin at this site facilitating atmospheric temperature variability and the shallow portion of the bedrock is hydrogeologically dynamic, this statement of reliability cannot be confirmed by these data alone. Overall the interpretation of the ALS test indicates many more layers with active flow, provides better differentiation of the relative size of the aberrations through both the hetero and homothermic zones, and exhibits better consistency with non-thermal data throughout the aquifer than do either the open or lined unheated temperature logs.

3.6.4 Reproducibility, Sensitivity and Consistency

There are currently no independent techniques that measure ambient (non- cross-connected) flow in the fractures; therefore, there is no way to prove that the picks for fractures with active groundwater flow actually have this flow and consequently indirect evidence must be used. Important aspects of the indirect evidence are that the reproducibility of the detailed characteristics of the temperature profiles must be established, and that profiles behave in accordance with reasonable expectations for the thermal system as well as being congruent with complementary data sets. The aberrations are based only on interpretation of the details evident on the thermal deviation logs. Reproducibility was examined in MW25 by profiling in the unheated lined hole on three occasions as discussed previously. Figure 3-8A shows that the two August 2005 profiles (9^{th} and 23^{rd}) expressed as the standard deviation of the raw temperature log as determined over successive 1m intervals (i.e. 200 temperature readings) and also as the average absolute temperature deviation (within 1 m sliding windows) along the borehole length. The emphasis here is on the data below about 30m, primarily the homothermic zone where the best reproducibility is expected because transient temperature variations should be minimal. The details of repeatability within the homothermic zone are shown in the expanded window Figure 3-8A' which spans $5x10^{-3}$ C° and shows the logs from August 9^{th} and 23^{rd} are essentially identical when viewed from either statistical perspective. With the exception of a few minor increases in the values, the baseline average absolute thermal deviation is $2x10^{-4}$ C°. Where minor increases occur they are very repeatable (nearly identical) between the two profiles even though the peak average absolute deviation is below 10^{-3} C°. The standard deviations within the 1m intervals for both profiles exhibit a consistent uniform near linear decline with depth(R^2 =0.92), from 0.005 at 30m depth to 0.0005 C° at 90m depth. Although the temperature also decreases with depth, that decline is not linear and therefore the decrease in standard deviation is more likely related to depth than temperature. Overall the two profiles collected in August are near duplicates, which provides confidence in the reproducibility of both the instrumentation and measurement method, as well as confirm that, with few consistent exceptions which likely result from deep flow zones, the level of variation is primarily a function of depth in the homothermic zone.

Although it is expected that the standard deviation of the temperature will decrease with depth in the lined unheated case, there is no depth dependency expected for the standard deviation of a lined heated profile. When heating the standard deviation should be independent of depth because the imposed thermal disequilibrium is uniform along the hole length and the dolostone aquifer is known to have strong lateral groundwater flow throughout the full aquifer thickness determined from testing during municipal well pumping. This lack of temperature to depth dependency is shown in Figure 3-8B which displays the four logs (P,C1,C2, C3) as standard deviations in both full and expanded scale. There is no decrease in

standard deviation with depth in the C1 data. Although a minor decline in the standard deviation occurs with depth in the C2 data, the size and frequency of variations in the standard deviation is consistent throughout the homothermic zone. By the time of the C3 log, the depth dependency has increased, nearly approaching that of the passive log but with slightly larger variations in standard deviation at those depths that had the highest variations in the C2 data. These statistical presentations confirm that ALS test largely overcomes the relationship between depth and the size of variations in temperature logs and results behave in a manner consistent with the conceptual model presented.

In another examination of reproducibility, the UW-1 borehole, located in the town of Cambridge and approximately 16km south west of MW25 was used to measure six cooling logs in the lined heated hole. Figure 3-9A shows the geological and hydrogeologic characterization of the hole and the temperature profile focusing on the lower portion of the borehole, below 55m depth, where relatively few hydraulically active fractures were identified using lined unheated profiles (Pehme et. al, 2010). Figure 9B shows the temperature of the borehole as continuously monitored at 35mbgs during heating and initial thermal recovery and intervals during which the lower portion of the borehole was logged (circles). A higher output heater cable was used above 49m depth because the experiment was concurrently used for testing cable response. The six cooling thermal deviation profiles are shown (columns M-R), each displayed at a different temperature scale to achieve visual consistency. The temperature scales range 0.12, 0.06, 0.05,0.023, 0.007 and 0.0035 C° for cooling logs C1 through C6, respectively as in columns R through M respectively. Except for the first cooling log, which has transient effects and the last cooling log for which the resolution of the sensor (~0.001C°) is evident because the span (0.0035 C°) is close to the resolution, the profiles are nearly identical. This is evidence of excellent reproducibility because each of the profiles is an independent data set.

Figure 3-9B (column S) shows the 64 flow zones between the depths of 55-120m in UW1. The occurrence of fractures with flow distributed along the entire hole is generally consistent with the ATV log, the core log (not shown) and the hydraulic tests done using straddle packers. The hydraulic tests show no general trend with depth and the magnitude of the lowest values indicates presence of permeable fractures. As was MW25 in Guelph, UW1 is located in an area of Cambridge where the wells draw water from the entire vertical thickness of the dolostone aquifer (Perrin et. al. 2011). As is the case with MW25 the fracture picks from the lined heated hole profiles show intervals in the hole where neither the ATV or core logs show fractures, but the hydraulic tests using straddle packers indicate permeability. Therefore the temperature logs are consistent with independent evidence of hydraulic features along the length of this hole.

Another line of evidence concerning the presence of fractures with groundwater flow is the contaminant distribution in UW1 determined from measurements of contaminant concentrations of TCE and Metolachlor on numerous depth discrete samples by Burns (2006). Pehme et al. 2010 showed these results of TCE and metolochlor analysis from UW1 alongside temperature logging results. These analyses show measureable TCE throughout the thickness of the aquifer that proves evidence of interconnected hydraulically active fractures throughout the length of the borehole. The frequency of rock core contamination can only be explained if closely spaced hydraulically active interconnected fractures exist throughout the hole because the contaminant diffusion hallows are relatively small in the low permeability blocks of rock between fractures and contamination is pervasive throughout the aquifer (eg. Parker et. al 1994, 1997).

3.7 Limitations and Improvements

For optimal use of the ALS method described in this paper, it is essential that the borehole be lined and that a tight seal is created to prevent vertical flow between the liner and the borehole wall. Liners are currently available to conveniently seal holes of diameters greater than 3.5 inches. Although liners are typically easy to install, some hydrogeologic conditions such as where the permeability is low towards the bottom of the borehole, complete installation can take a long time. Complete eversion is desired or else one loses the opportunity to ALS test the bottom section, a distance equal to twice the length of the un-everted liner. Small leaks in the liner can cause a decrease in ALS log resolution or create misleading results. However, where the hydraulic gradient is downward, typically only the portion of the data set above the leak is compromised. Liner leakage is usually easy to determine with periodic measurements water column height within the liner and recent advances in the FLUTe liner design have increased reliability substantially. In holes where there is an upward hydraulic gradient between one depth and another, there is potential for the liner seal across a section of the borehole to be ineffective if the head differential imposed by the standing water column inside the liner is inadequate for this particular zone. In such cases, the lack of seal will not be detected as liner leakage the condition can be difficult to discern with a single thermistor probe as used in this paper; however, multi sensor probes that measure thermal gradients (Pehme et. al., Chapter 5) are capable of identifying this condition.

The heated lined-hole method described in this paper has been applied successfully in bedrock borehole, diameters between 4 and 12 inches. Resolution is expected to decrease with increasing borehole diameter as the distance between the sensor and the fracture facilitating flow becomes larger; however, good results were obtained from a 12 inch hole.

At present, this method of detecting and judging the amount of ambient flow in individual hydraulically active fractures is still qualitative in that there is no basis for quantifying the flow. Relative flow intensity is estimated (e.g. weakest, intermediate and strongest) in each hole from the relative size of the aberration, however there currently is no basis for calculating groundwater velocity or flux. There also exists a need to better understanding of potential effects of heat induced convection in the water column inside the liner that may occur due to temperature gradients and at what value they become significant.

3.8 Conclusions

This study shows that high resolution temperature profiling in lined holes immediately after heating the entire hole provides much more information about fractures with ambient groundwater flow than does profiling in the hole lined but without heating. Most importantly, the heating provides identifications of ambient flow throughout the borehole length, not just within the heterothermic zone, so there is less bias and more complete identification of hydraulically active fracture. In the two holes focused on in this study, the heating method identified many fractures throughout the 100m thick dolostone aquifer, whereas without heating, active fractures were identified primarily in the heterothermic zone. Secondly, the identifications of flow using the heating method do not depend on depth and therefore, the relative amplitudes of the thermal deviations are expected to be, in most cases, a qualitative indication of the amount of groundwater flow in each zone. More research is needed for quantification of groundwater flux and/or velocity.

Considering that the three options for temperature profiling are available namely open-hole, lined-hole and lined, heated hole (ALS), it is most commonly appropriate to only do the ALS test because it provides the most sensitive results along the entire length of the borehole. In contaminated areas, it is desirable to limit the length of time that the hole is allowed remain open so that cross contamination is minimized and profiling in the open hole should generally be avoided.

The ALS method is practical for use in many fractured rock investigations because liners can easily be installed in holes of greater than 3.5 inches diameter. The fracture identifications obtained from using the lined ALS method pertain to the groundwater system under conditions not influenced by the presence of the hole (i.e. ambient conditions) and these identifications are of those relevant for analysis of contaminant transport. In contrast the conventional non-thermal open-hole approaches for identifying hydraulically active fractures such as borehole flow metering, full-hole applied salinity dilution and also open-hole temperature profiling are governed by the flow conditions induced by borehole cross connections between fractures. These open-hole methods consistently identify much fewer fractures than the ALS technique in lined holes. The lined-hole ALS method commonly identifies fractures where ATV

image logs show no features indicative of fractures because the ATV logs are not capable of identifying the smallest aperture fractures due to beam width. In some cases even the core show no indication of open fractures (i.e. no break in the rock core). This discrepancy between the rock core and the lined hole ALS profile is attributed to the occurrence of thin seams of secondary porosity (vuggy layers) identified in core and fractures with active flow near but not actually intersecting the borehole. The results presented in this paper are a step in continual improvement for advanced temperature logging for high resolution characterization of groundwater flow in discrete fractures and conduits in bedrock systems.

3.9 Acknowledgments

Detlef Blohm, president of IFG, developed the temperature probe and made improvements as needs arose. Assistance in the field involving installation and removal of the the FLUTe liners was provided by Bob Ingleton, Paul Johnson and Ryan Kroeker. Funding support was provided by Natural Sciences and Engineering Research Council of Canada and the University Consortium for Field Focused Groundwater Research. Field site access and cooperation was obtained from Syngenta Crop Protection and Guelph Tool Inc.

3.10 TABLES:

Table 3-1: Details of data collection steps in the ALS process

Stage		Details	Purpose/Comments
1	Background	Ambient temperature of the fluid column in the borehole is measured prior to the addition of heat. **P**- a "passive" log is collected at a slow rate of decent (0.5-0.7 m/min)	Provides base against which to assess: amount of heat added target values of thermal recovery basis for confirming overall borehole thermal stability (see C3) optimally completed the afternoon prior to heating
2	Heating	Energy is introduced with a line heater (typically at 15-20 W/m for 4-6 hrs) uniformly down borehole **A** – "Active" log is collected (1.5-2 m/min) which measures temperature prior to turning off the heater	Used to estimate amount of heat added: data tends to be noisy, presumed to be primarily caused by small changes in the distance between the heat source and sensor(s) power depends on heater(s) used and voltage applied timed to end near end of heating cycle
3	Recovery	**C1** – Log collected during cooling, starting approx. ½ hour after heater turned off (1-1.5 m/min)	Heater may be removed depending on logistical considerations provides indication of the early stages of cooling most variable of the recovery logs
		C2 – Cooling log started at approximately the same length of time after the heater is turned off as total heating (i.e. usually ~5½-6½ hrs after end of heating), (0.8-1m/min)	Designated as start of "late" time good indicator of flow zones theoretical start of linear decay (Beck et. al. 1971, Pehme et al 2007a), used to estimate thermal conductivity
		C3 – logged the next day (approx. 24hrs after the start of heating) at 0.5-0.7 m/min	Well into late stage recovery used in estimation of thermal conductivity compared against P log to access recovery process and overall thermal stability

Table 3-2Details of temperature logs collected during ALS process in MW25.

Log	Date & Time (March, 2006)	Time from reference (s-from heat on/off)
Passive (P)	6th	
Heating	8th, 8:30 - 12:40	
Active (A)	8th, 10:30	7200 - heat on
Cooling 1 (C1)	8th, 13:15	2100 - heat off
Cooling 2 (C2)	8th, 16:00	12,000 - heat off
Cooling 3 (C3)	9th, 09:15	74,100 - heat off

3.11 Chapter 3 Figures

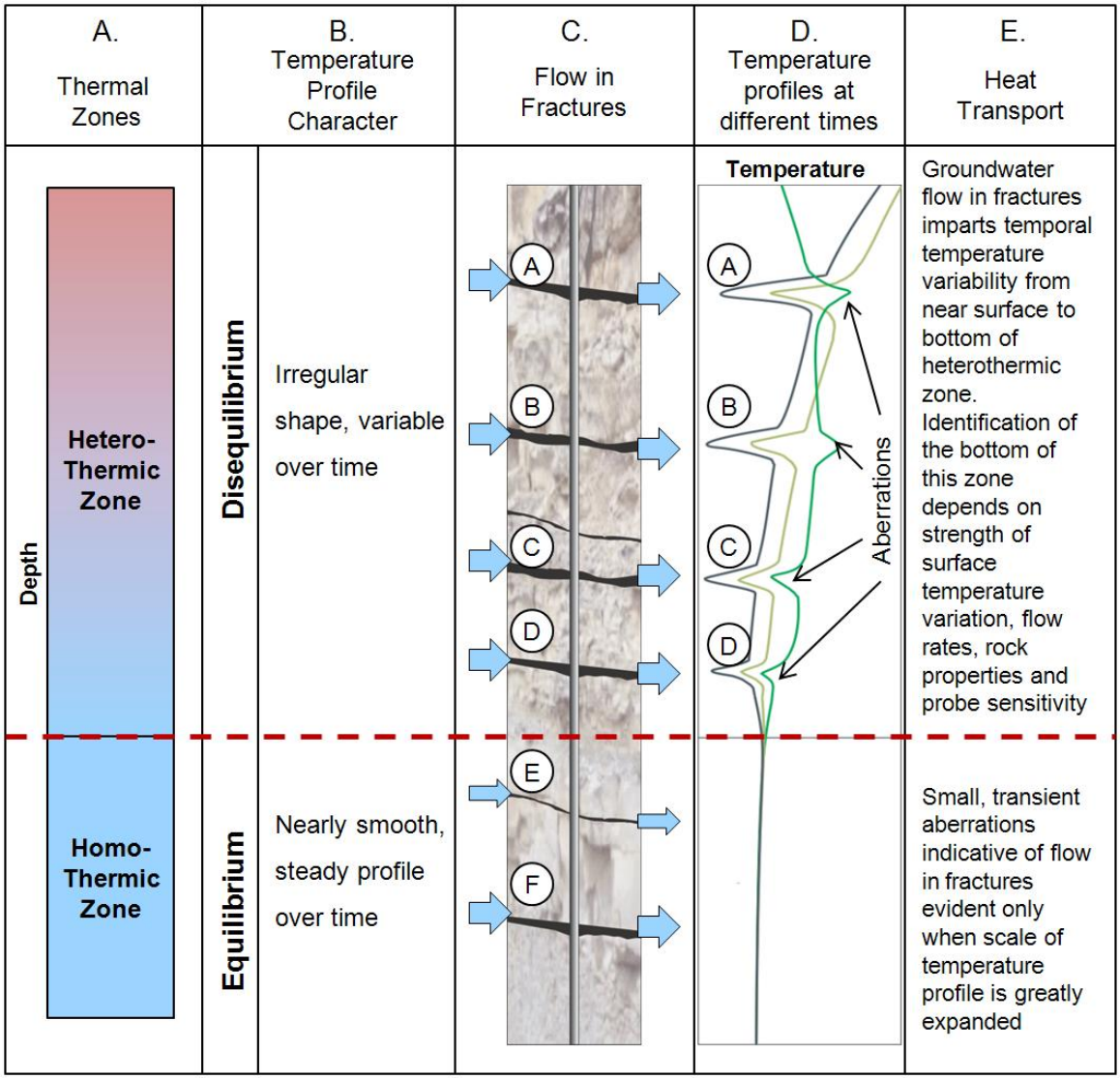

Figure 3-1: Terminology and characteristics of thermal zones and temperature profiles in the static water column of a lined hole resulting from heat transport by groundwater under ambient conditions.

The transient aberrations displayed on temperature profiles (column D) are used to identify fractures with active groundwater flow for the case where shallow temperature is generally higher than in the deeper zone. An aberration is a feature on the temperature log attributed to groundwater flow

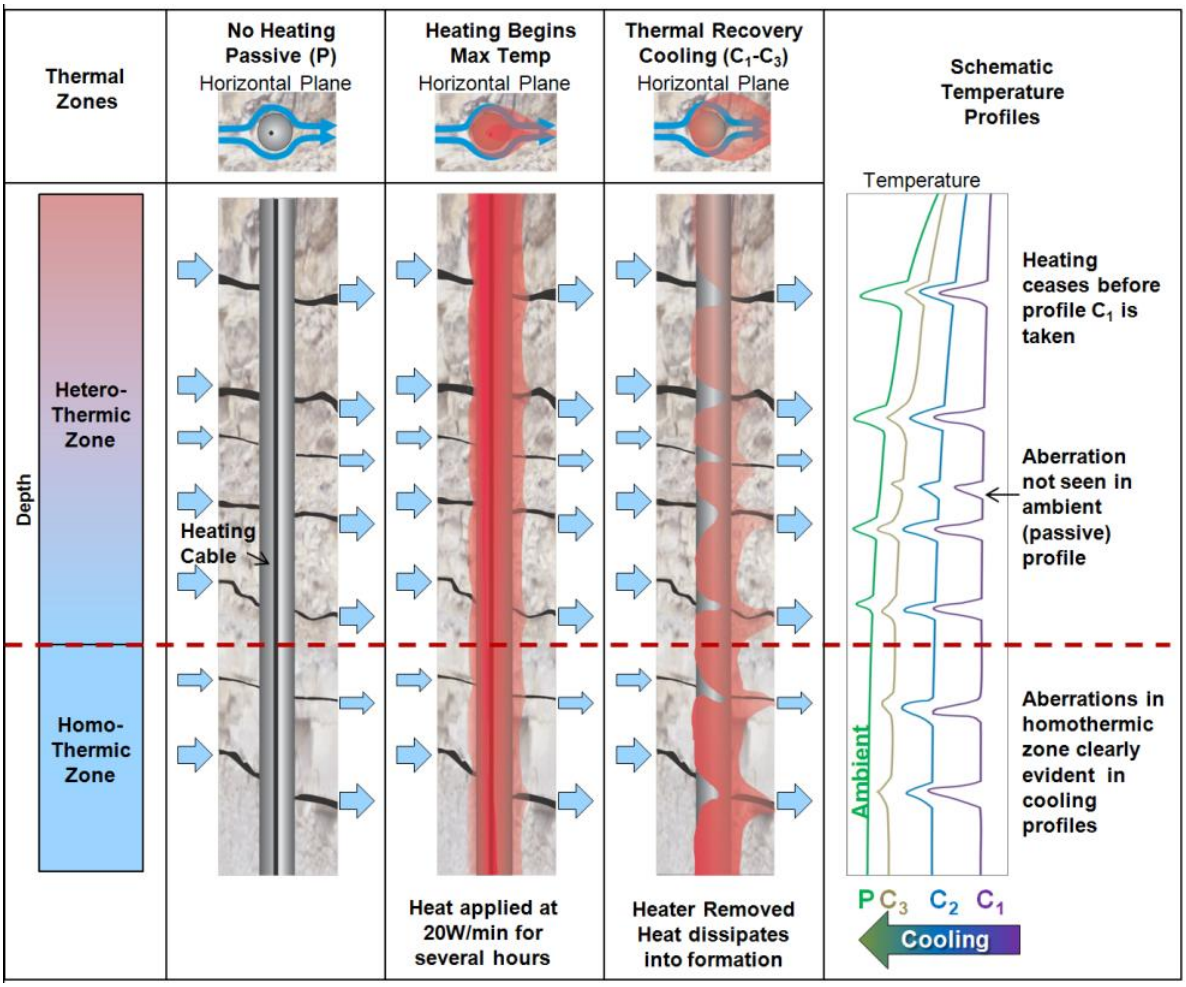

Figure 3-2: Conceptual model for identification of fractures with active groundwater flow using the ALS method.

Heater cable heats entire hole (4-6 hours) and is then turned off and the system gradually returns towards background thermal condition. Temperature profiles are collected are typically collected three times while the heat is dissipated (C1, C2 and C3). The passive temperature log identifies fractures only in the heterothermic zone but the cooling logs can identify fractures throughout the entire borehole depth and in all cases as negative inflections from the base level.

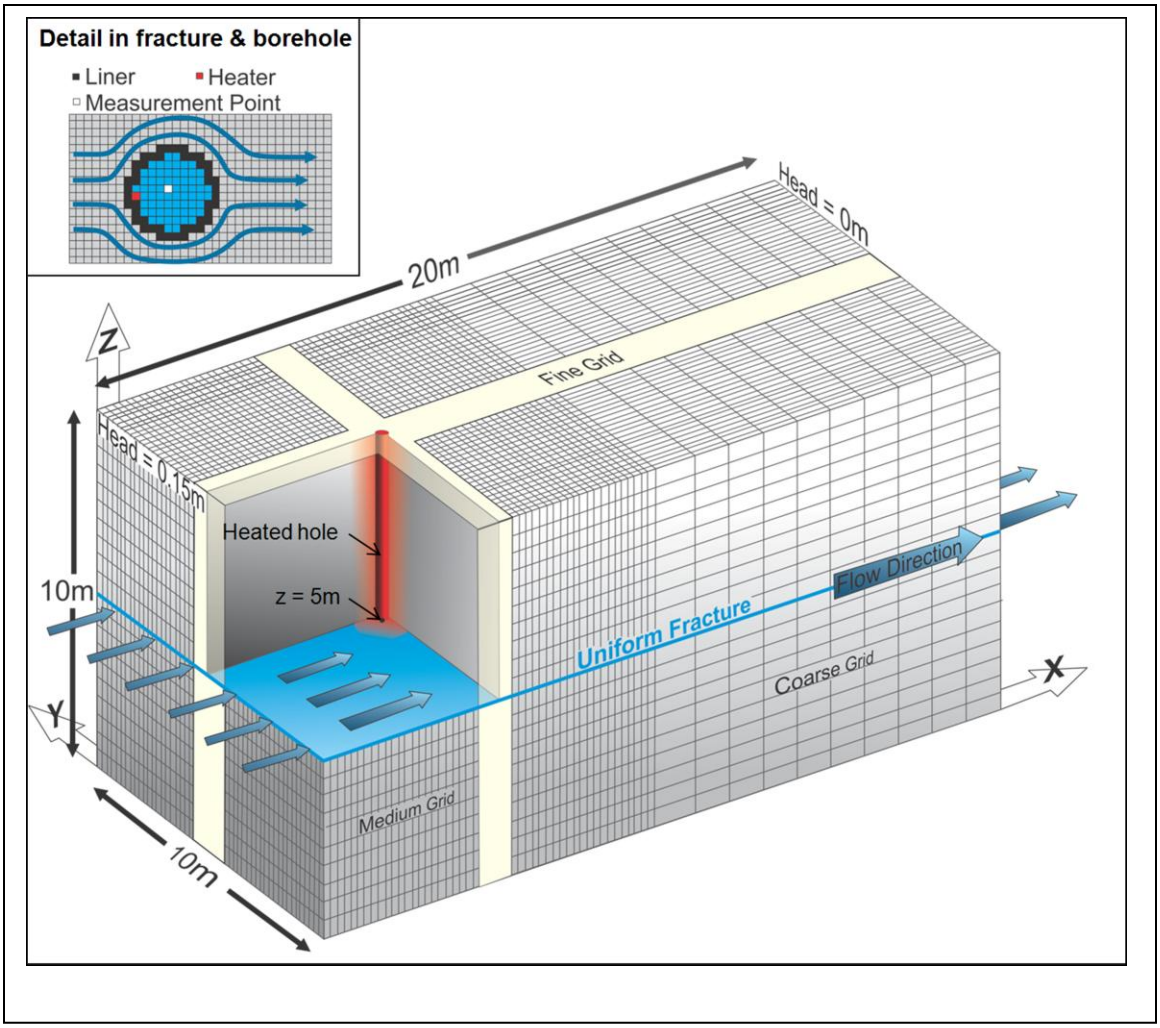

Figure 3-3: Model domain and the numerical grid.
The hole is heated uniformly for a 6 hours along its depth and active groundwater flow occurs only in the fracture. The domain is discertized with 1x1x2cm elements in and around the borehole. Heater is set on the up-gradient side of the borehole. Figure 4 shows model results at the measurement point.

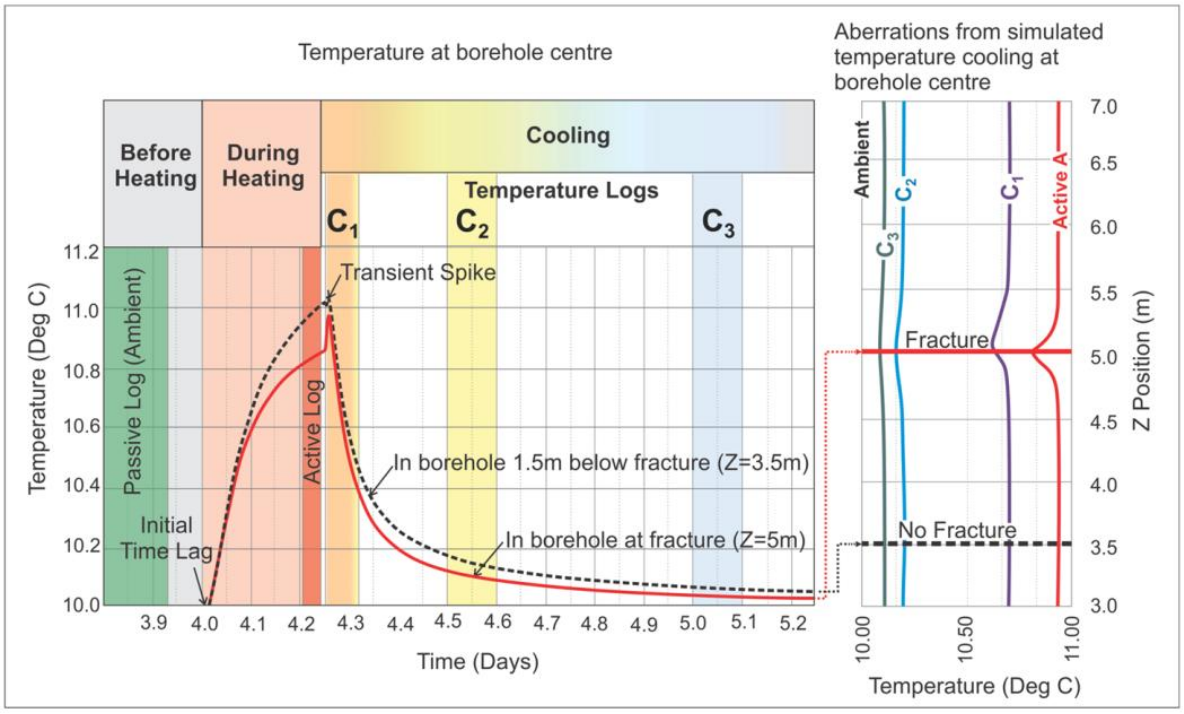

Figure 3-4: Temperature at the borehole centre (at fracture and 1.5m below) from numerical models heating and cooling associated with a single fracture.
Typical periods of data collection are shaded. Following heating the hole, temperature profiling, is done on three occasions, referred to as cooling logs (C1, C2, C3). Aberrations become less apparent as temperature decreases successively with each log with the water in the lined hole returning towards the background (passive) condition. The active profile is obtained just before heating ceases

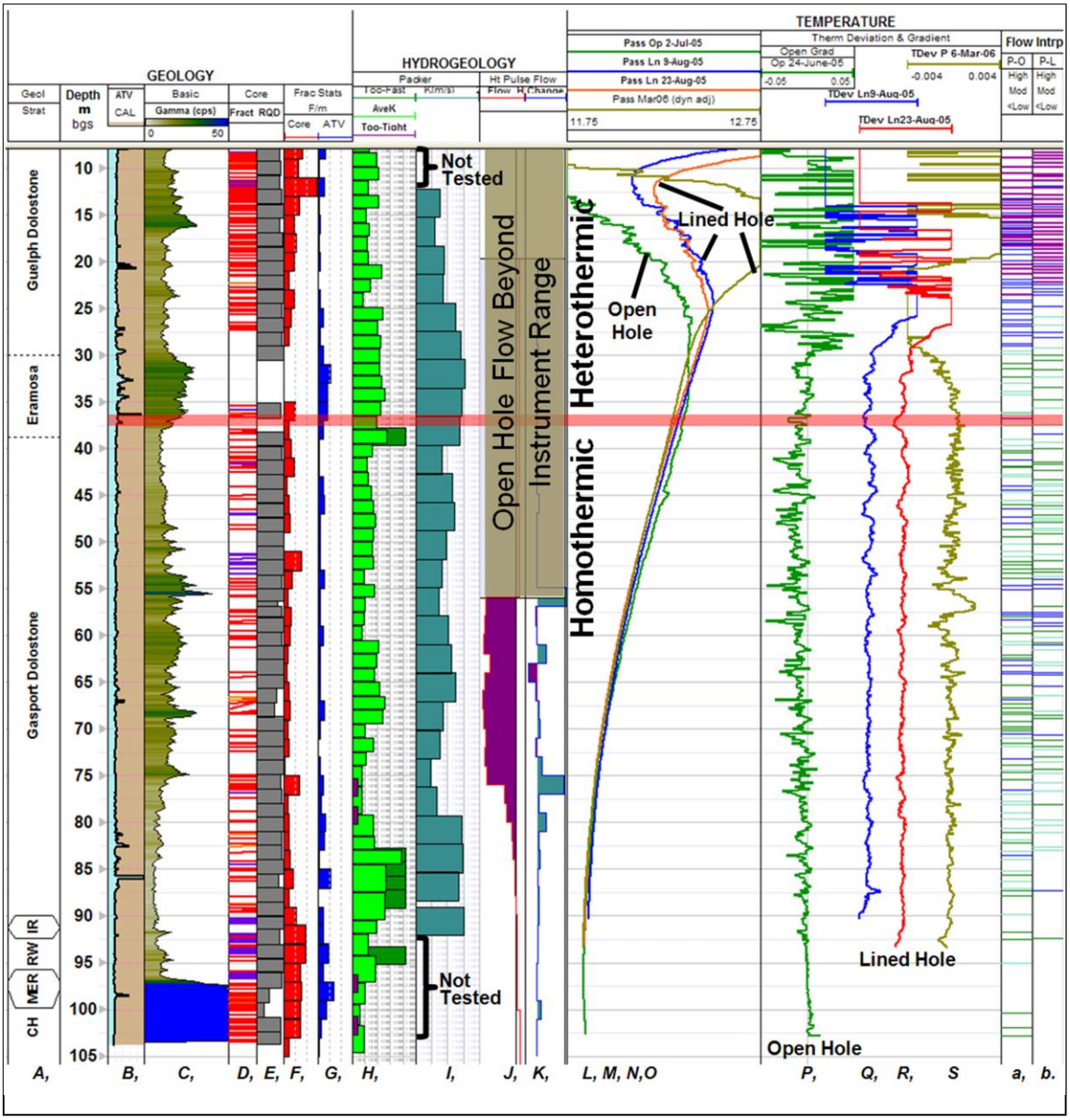

Figure 3-5: UW25 Comparison of selected data set with repeated passive temperature logs; Highlighting thermal uniformity below hetero-homothermic boundary and the few flow zones in comparison to core and straddle packer testing.

A- Stratigraphy, B- ATV travel time as virtual caliper, C- Shaded gamma log (0-70cps), D- Core fractures, E- Rock quality description (RQD, 0-100), F- Fractures/m 0-15 (core), G-Fractures/m 0-15 (ATV amplitude), H,I-Straddle packer tests 1.5m interval (hydraulic conductivity 10^{-8}-10^{-4} m/sec, log scale), H-Straddle packer tests 3m interval (hydraulic conductivity 10^{-7}-10^{-3} m/sec, log scale),J-Flow (heat-pulse -0.7-1l/min), K-Incremental change in flow, L-O open hole temperature 2/7/05, Lined Temperature L-9/8/05, M-23/8/05, N-6/3/06 (normalized to earlier probe response) (all temperature logs 11.75-12.75 C°, P- gradient open hole temperature (L) -0.05 to 0.05 C° , Q-Thermal Deviation (M), R- Thermal Deviation (N), S-Thermal Deviation (O). (Q,R&S range = -0.04 to 0.04 C°). a-Interpreted Flow Open Hole (O), b- Interpreted Flow Lined Hole (P,Q&R) (Qualitative flow interpretation Very High, High, Moderate, **Low** and Some).

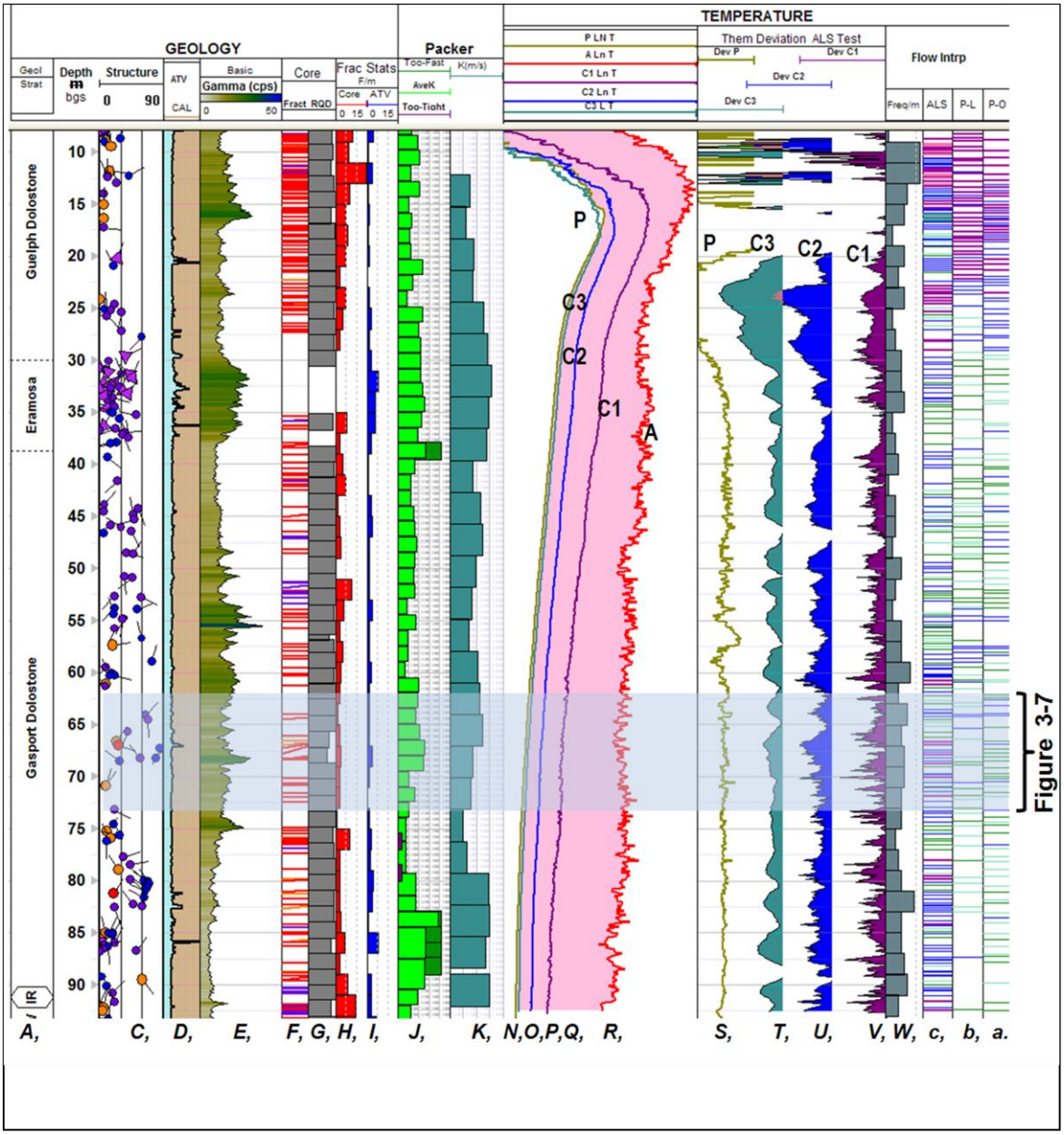

Figure 3-6: UW25 ALS Data and Thermal Deviation C1-C3 temperature used to identify many more flow zones in the lower half of the borehole consistent with other data indicative of potential flow.

A- Stratigraphy, C-Interpreted discontinuities from ATV amplitude, D-ATV travel time as virtual caliper (95-108mm), E-shaded gamma log (0-50cps), F-Core fractures, G-rock quality description (RQD, 0-100), H-Fractures/m (core), I-Fractures/m (ATV amplitude), J- Straddle packer tests 1.5m interval (hydraulic conductivity 10^{-8}-10^{-4} m/sec, log scale), K-Straddle packer tests 3m interval (hydraulic conductivity 10^{-7}-10^{-3} m/sec, log scale), N-6/3/06 Passive Temperature, O,P,Q- Cooling Logs C3,C2,C1, R-Active Temperature during heating (all Temperature logs 8.80-11.80 C°), S-Thermal Deviation (N,-0.004-0.004), T- Thermal Deviation (O,-0.015-0.002), U- Thermal Deviation (P,-0.025-0.005), V-Thermal Deviation (Q,-0.1-0.015). a- Interpreted Flow ALS-Lined Hole (combined C1,C2), b- Interpreted Flow Open Hole (Figure 5), c- Interpreted Flow Lined Hole (N), (Qualitative flow interpretation **Very High**, **High**, Moderate, **Low** and Some). W- Flow zones/m ALS interpretation (a) **Labeling sequence is consistent with Figure 3-7**.

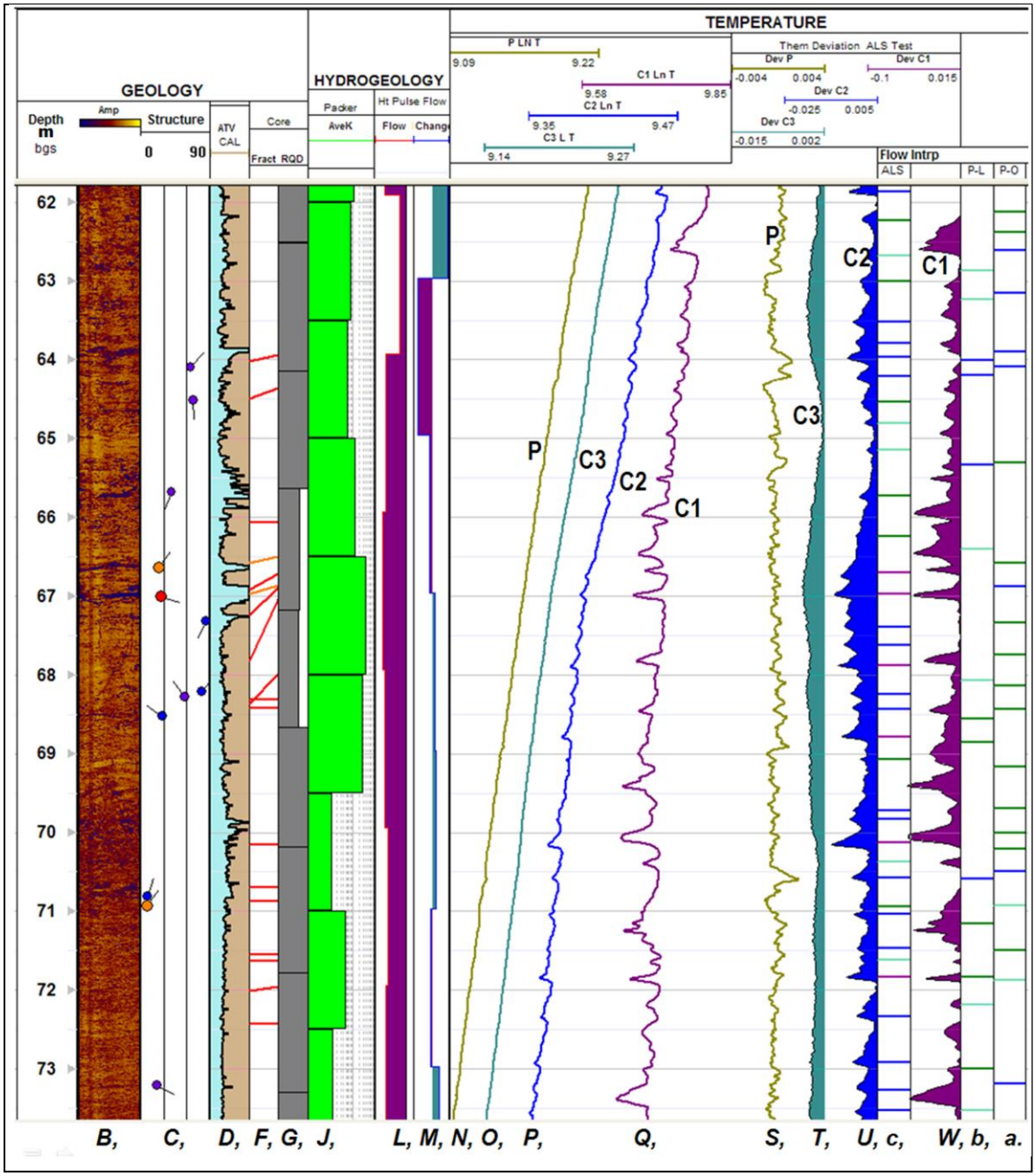

Figure 3-7: Detailed comparison of UW25 ALS profiles with other data sets highlighting negative aberrations in C1 and C2 profiles indicative of flow.

Note fracture frequency histograms are removed and passive temperature data from 2005 added. Scales have been optimized for this depth interval where appropriate. Columns as in Figure 6 with addition of B-ATV amplitude as color scale, L-Flow (heat-pulse -0.7—0.4l/min), M –incremental change in flow (-0.14-0.14l/min),.

Note: Virtual Caliper (D) at 99-101mm, (J) at 10^{-5}-10^{-8} cm/s, (L) -0.7 to -0.4 l/min, (M) -0.14 to 0.12 l/min. *Qualitative flow interpretation* **Very High**, **High**, Moderate, Low and Some

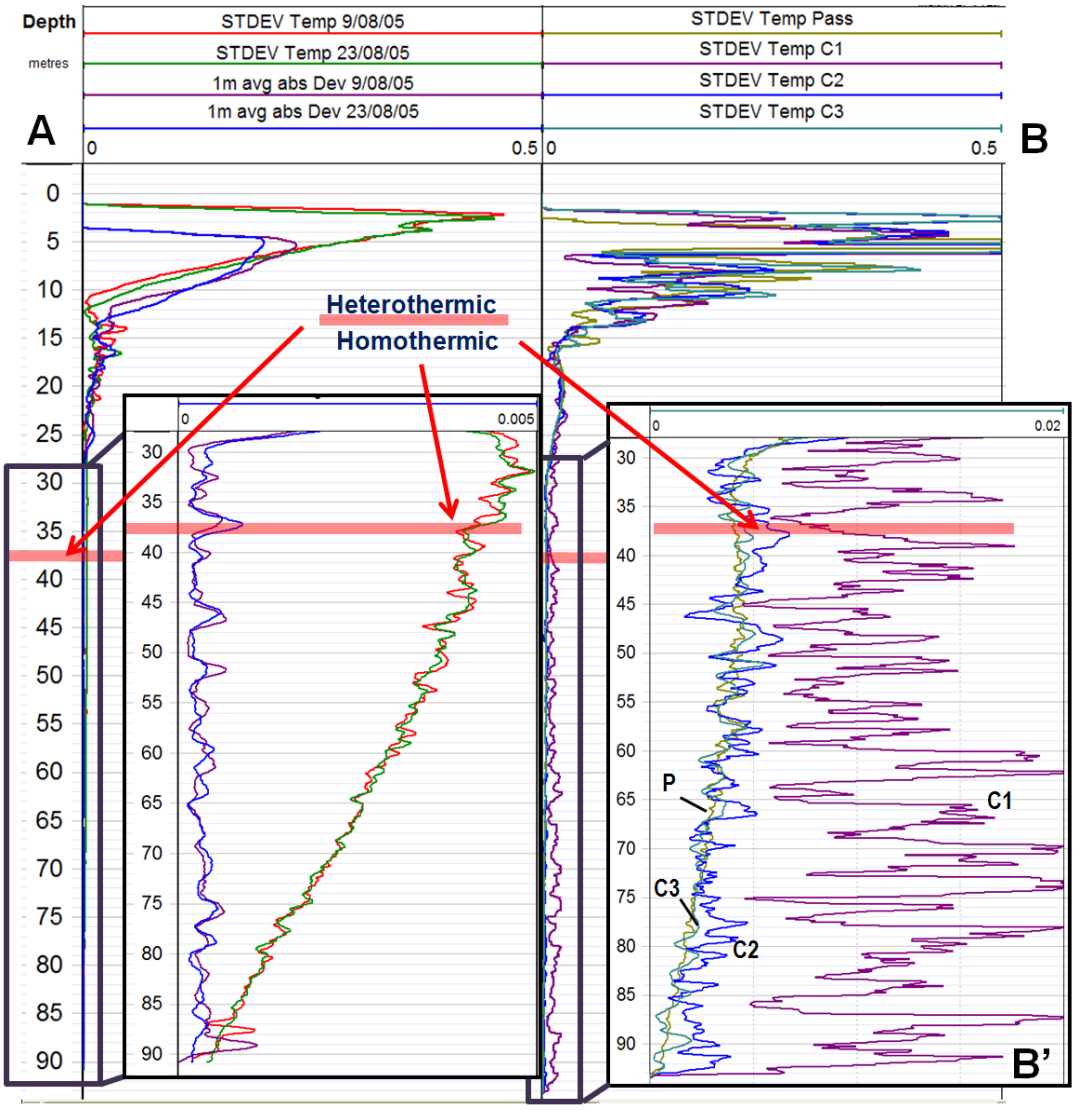

Figure 3-8 A: UW25 Detailed Examination of absolute and standard deviation of repeated passive temperature logs in homothermic zone, note standard deviation declines linearly with depth. B:UW25 ALS Standard Deviation emphasizing C1 and C2 are independent of depth. A-Purple(9/08/05) and Blue(23/08/05) Standard Deviation of Temperature (1m moving window) Red(9/08/05) and Green(23/08/05) - Average absolute variability (1m moving window), original data interval 0.005m. (**A-** Complete borehole, **A'**- expanded in depth and temperature *).*
B-, Standard Deviation of Temp (1m moving window) Average absolute variability (1m moving window), original data interval 0.005m. **B-** complete log, **B'-** expanded in depth and temperature

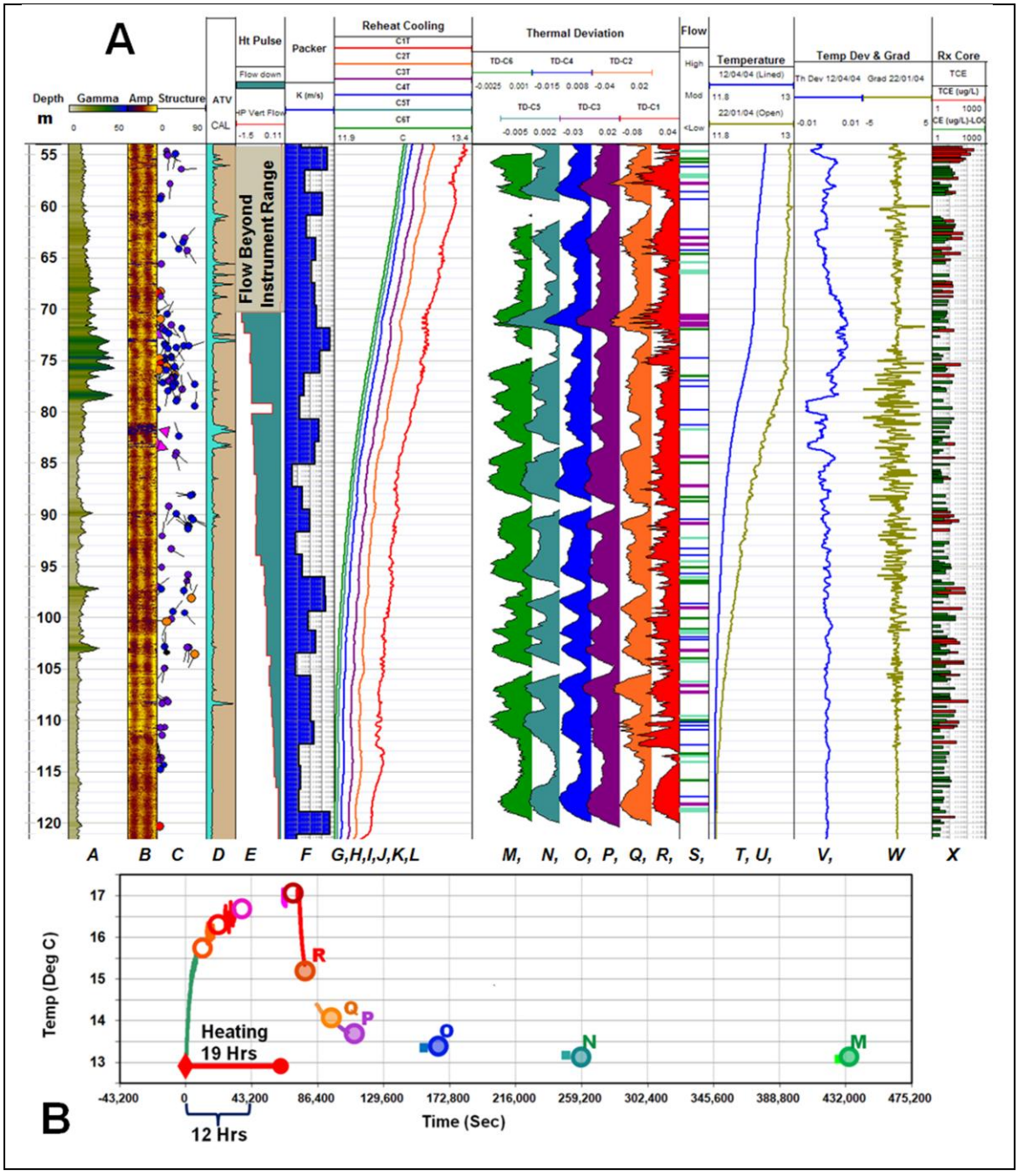

Figure 3-9 A- UW1 ALS Data and Thermal Deviation C1-C6 temperature confirming repeatability of temperature deviations even when range is small.

UW1 ALS Data and Thermal Deviation C1-C6 temperature A shaded gamma log (0-70cps),B- ATV amplitude (colour scale), C-Interpreted discontinuities from ATV amplitude, D-ATV travel time as virtual caliper, E- Flow (heat-pulse -1.5-0.11l/min), F- Straddle packer tests (transmissivity 2x10-8-2x10-4cm/sec, log scale), G,H,I,J,K,L – Cooling Logs C6,C5, C4,C3,C2,C1 (all temperature logs 11.80-13.80 C°) M,N,O,P,Q,R-Thermal Deviation (C6-C1), S- Interpreted Flow ALS Lined Hole (M-R, Qualitative interpretation Very High, High, Moderate, Low and Some). T-Passive Temperature Lined-hole 12/04/04, U- Temperature Open-hole 22/01/04, V- Thermal Deviation (T), W-Temperature Gradient (U), X-TCE Rock Core(1-1000ug/l log scale) .

3.12 SUPPLEMENTAL MATERIAL

3.12.1 Supplementary 1- Temperature data normalization between probes and the heterothermic-homothermic boundary

The sensors used in the thermal probes rely on measuring the variations in electrical resistivity in a small wire that result from changes in its temperature. Although the system can be designed to be electronically stable and detect minute changes in resistivity and hence relative temperatures, the proper calibration to absolute temperature at a similar accuracy is a challenge. Although, the variation of resistivity with temperature is stable and gradual, the relationship is neither consistent between sensors nor is it entirely linear. In the calibration process (Blhom, 2011) the sensor is monitored continuously while immersed in a water bath that is slowly cooled from 50°C to 0°C. Reference temperatures are measured at 5C° intervals and the two data sets subsequently related using a best-fit, 3rd order polynomial. Errors are introduced in the absolute accuracy of the resistivity-temperature calibration by factors such as sensor reference separation, convection, differential cooling and the entire process is dependent on the accuracy and time constant of the reference probe. However, the calibration spans more than 10^4 times the resolution of the sensors providing a high degree of relative accuracy and the stability of the electronics is proven experimentally as described in the main text.

The data collected in March 2006 with a second (new) sensor were normalized to the original sensor used in August 2005 by plotting the difference between the profiles against the March data (Figure 3-10). The lower 50 meters of the borehole (approximately 10^4 readings) exhibited a linear relationship with an $R^2 = 0.97$. The normalized March passive (background) data are used for the purposes of assessing and describing the temporal temperature variations and the characteristics of the transition from heterothermic to homothermic conditions. In all other comparisons and discussions the March data are dealt with in their original form. It is noteworthy that it is the high level of sensitivity achieved that necessitates normalization, and such differences would be only marginally detected with older generation sensors.

The suite of passive logs, August (2) and March (1 normalized), are shown in Figure 3-11, as well as the change logs (using the process described by Pehme et al (2010)) using the August 9th, 2005 smoothed profile as the reference and an open hole heat-pulse flow-meter data set (collected May 25th, 2005). The change logs are shown both normalized by time (an expanded depth scale is used to emphasize change below 25 metres) and the total change (below 10m).

Based on the change logs, the temporal variability of the borehole is divided into three distinct depth ranges: 1) above 25mbgs, the temperature changes are large with several potential subdivisions based on major changes or inflections in the profiles, 2) from 25 to 37.5m mbgs there is low but distinct time dependent temperature variability, and 3) below 37.5mbgs the short term (14 day) change is relatively constant with depth, varying by approximately 10^{-4} C°, a level consistent with the resolution of the sensor and the comparatively short time span period used to "time-normalize" the change. The seasonal (Aug-March) change is also below the reported sensor resolution throughout the entire depth range (50m). Since overall (absolute temperature) normalization was completed using the Aug 23 data and the change is calculated against the August 9th profile, this validates the normalization process used between sensors. It is worth noting that the August to March change below 37 mbgs appears relatively uniform because a 290 day time span was used to time-normalize the change which suppresses short term variability (in comparison to the August 23 change log). It is notable that a broad parabolic pattern occurs between 40 and 90mbgs with the largest temporal change occurring at 56 mbgs, coincident with the boundary between where the open-hole heat-pulse flow meter could not measure because of too much cross-connected flow above and measurable flow below. This same depth corresponds to a fracture, a geologic change and a minor increase in transmissivity based on packer tests. Based on temperature change the limit of the heterothermic zone is designated as 37.5 mbgs although the majority of the temporal variability is above 25 mbgs and the intervening zone is transitional.

3.12.2 Supplementary 2- Standard Deviation vs Temperature – Passive Temperature MW25 Guelph

Sokal and Rohlf (1981) describe a linear relationship between the mean and the standard deviation as a defining characteristic of a Poisson-distributed, data set that would be asymmetrically distributed about a specific value. By definition, the temperature in the homothermic zone is stable over time and independent of the driving forces of heterothermic variability. Therefore, to better understand the mechanisms influencing the response it is useful to resolve whether the systematic decrease in standard deviation is related to position in the geologic sequence, (i.e. distance from the driver of thermal disequilibrium) or the temperature. Figure 3-12 is a plot of the standard deviation within sequential 1m windows as a function of the average temperature within that window for the three passive lined logs below 30 mbgs. The March data is shown without normalization of the data against the older probe and therefore shown in at a different scale in the insert. The July and August data display a repeatable linear relationship (R^2 = 0.92 and 0.94 for the 9/8/05, 23/8/05 data, respectively) above approximately 11.95°C and a standard deviation of approximately 2.5×10^{-3} C°). The same trend

is apparent in the March data although that log is more variable (has higher deviation and a lower R^2 value, R^2= 0.62) due to the affects of water movement (see main text). Below 11.95℃ the standard deviation declines at a progressively increasing rate as the temperature decreases and below approximately 11.8℃ (a standard deviation of 0.001C°) the two are independent. It is likely that both the distance from the driver of disequilibrium (the heterothermic zone) and temperature are factors near the transition to heterothermic conditions but that the resolution of the probe is becoming an increasingly large component of the variation in readings as temperatures reach the local lower limit of the plot. Additional testing at different background temperatures and with the trend reversed (i.e. temperature increasing with depth) is required to further resolve the relationship between probe variability and changing temperatures.

3.12.3 *Supplementary 3 Absolute Deviation & Standard Deviation vs Temperature – ALS Cooling Logs Temperature MW25 Guelph*

To provide comparable data for the ALS (C1,C2, C3 and passive) logs to the August passive data previously discussed, the average absolute deviation of one metre intervals is plotted against depth in Figure 3-13 and the standard deviation against temperature in Figure 3-14. Figure 3-13 shows that the average deviation is several times larger than the March passive data case and there is no decline in deviation with depth in C1 or C2. The C3 data is transitional; at some depths (e.g. 43-53 and below 80 mbgs) similar in pattern to C2 and at others depth (e.g. 52-58 and 69-78 mbgs) aligned with the passive log.

Figure 3-14 shows all four data sets P, C1,C2 and C3 together as well as P,C1 and C2 in expanded version as an insert. The figure confirms that the comparatively large variations in the C1 are independent of the actual temperature and that there is a gradual trend towards the uniformity of the passive data as the borehole undergoes thermal recovery. Although overall the standard deviation values have decreased to below 0.005C° for C2 and a slight decline in values occur at lower temperatures, the values are both variable and do not exhibit a strong trend. The overall pattern of the C3 standard deviations against temperature is similar to the passive log (described above), however with larger irregularities. The implication for this case is that, by the following day, most, but not all, the effects of heating the borehole have dissipated.

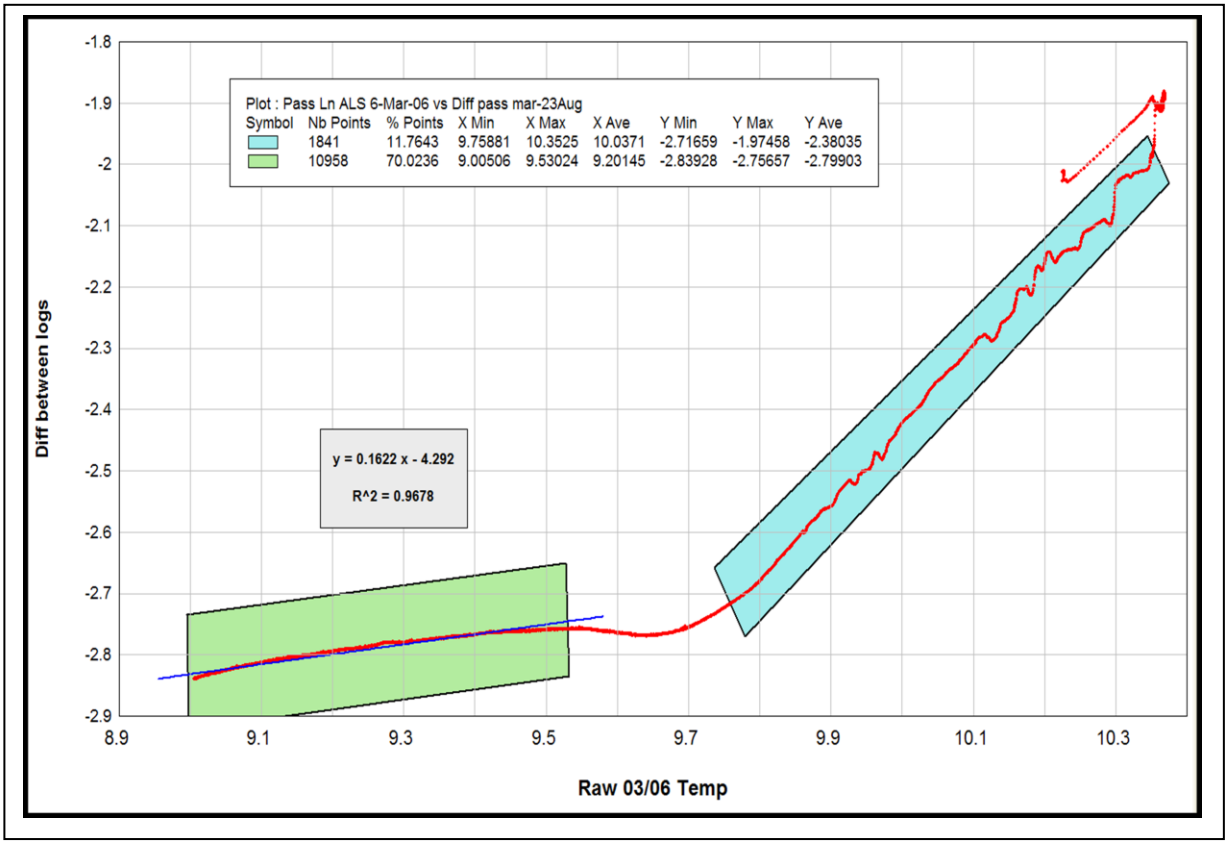

Figure 3-10: The difference between March and Aug 23 logs plotted against March data.
Linear regression in lower portion (55m) used for to normalize March log to August.

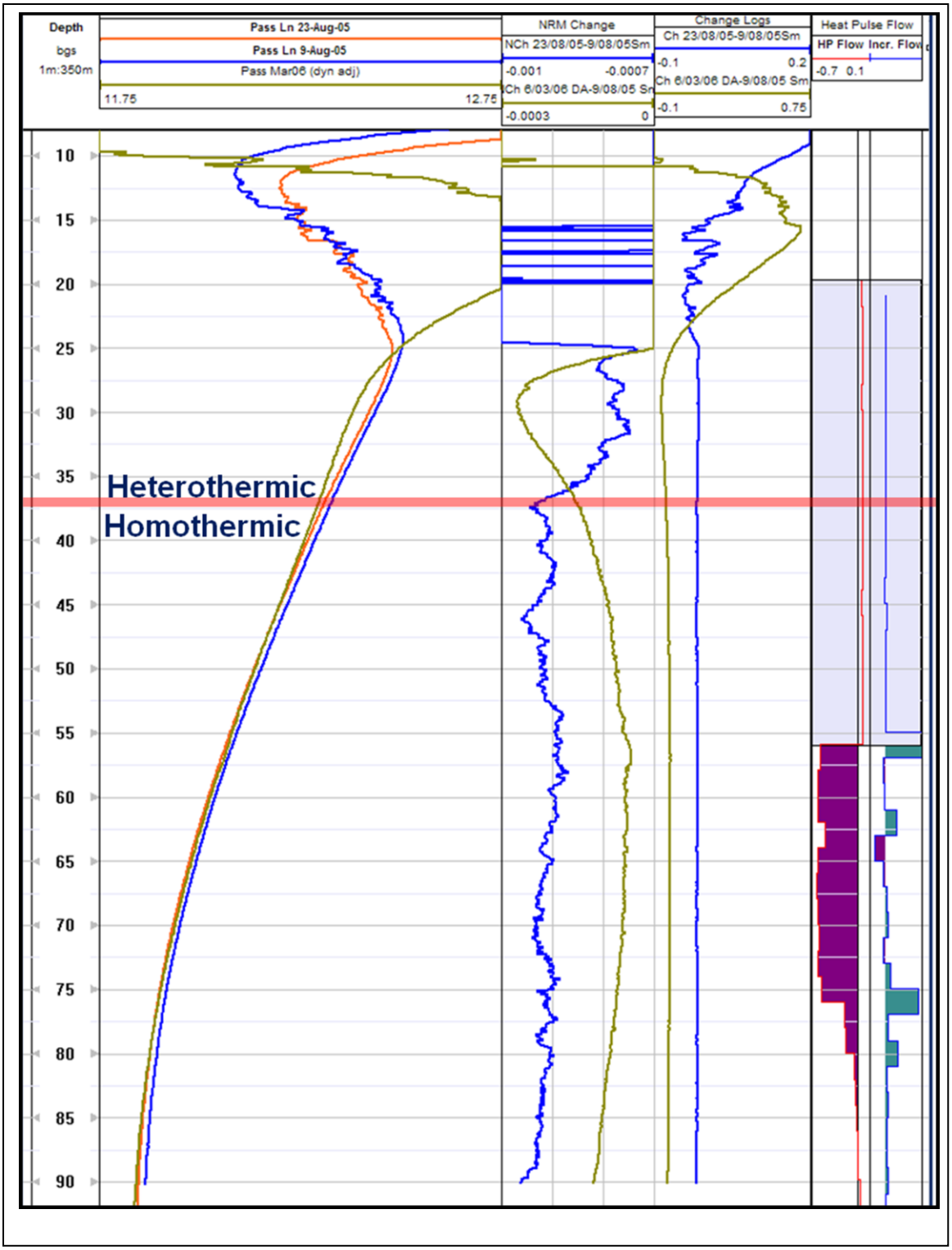

Figure 3-11: Normalization of TVP probe (March data) to older probe.
Change logs shown normalized by time (days) and without. Effective heterothermic limit is 37m. Note: some change occurs throughout borehole. The March change is an arc maximizing at the same flow feature where heat-pulse becomes measurable.

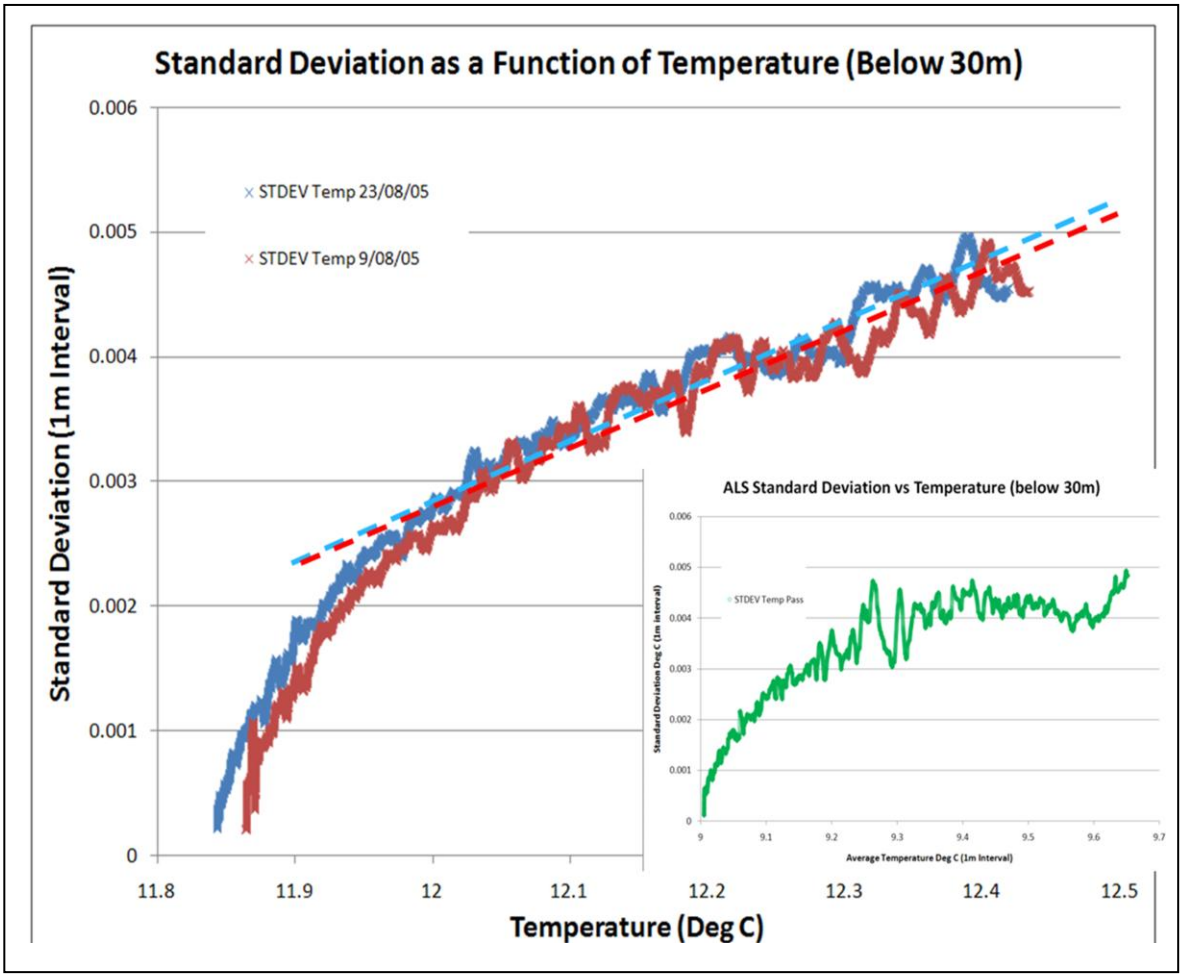

Figure 3-12UW25 Standard Deviation of Passive Temp (1m moving window) vs Temperature Logs,

Original data interval 0.005m. Red- 23/8/05, Blue- 23/8/05, Green- 8/03/06 (average temperature X-axis without normalization.

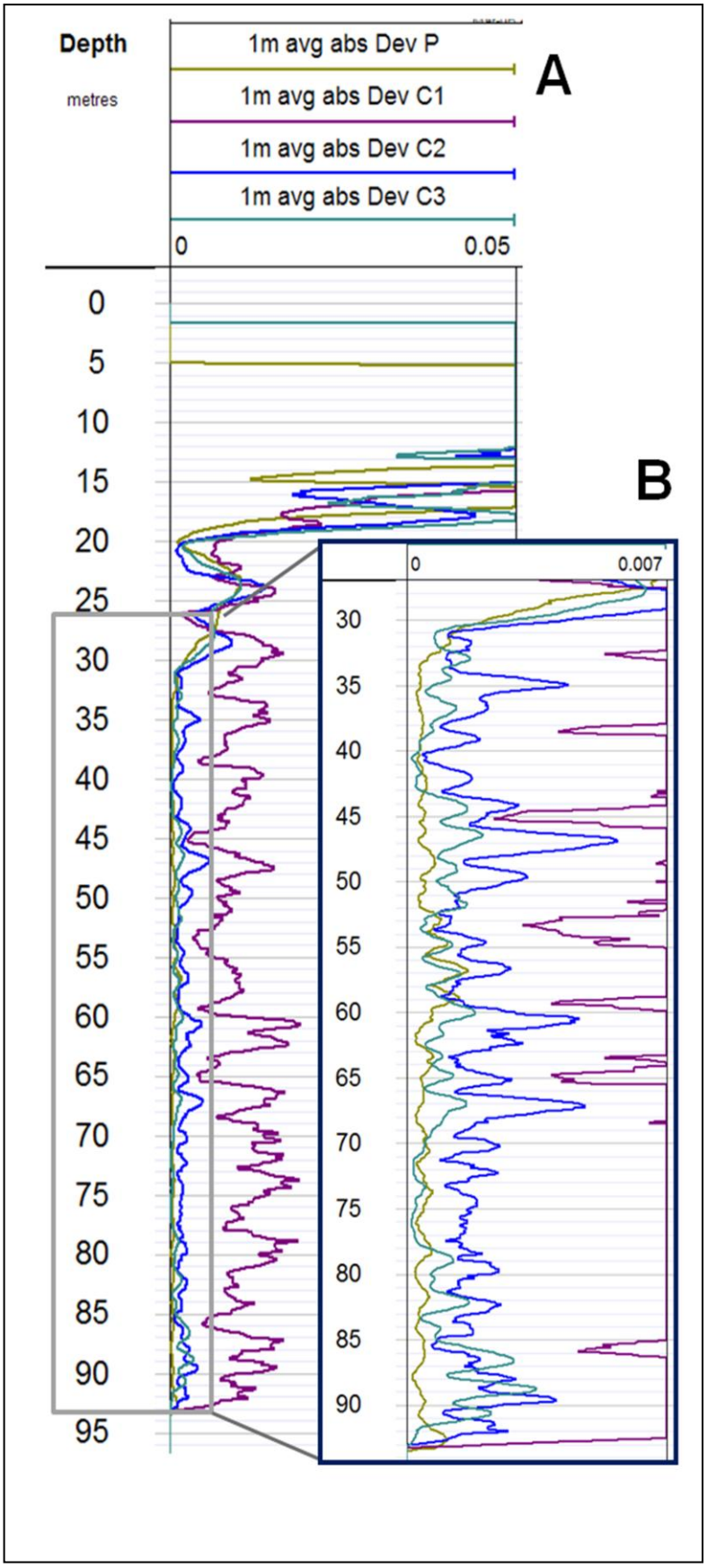

Figure 3-13: UW25 ALS recovery data and Passive Temperature Log. Average absolute deviation (1m moving window, original data interval 0.005m. A- complete borehole, B-expanded in depth and temperature

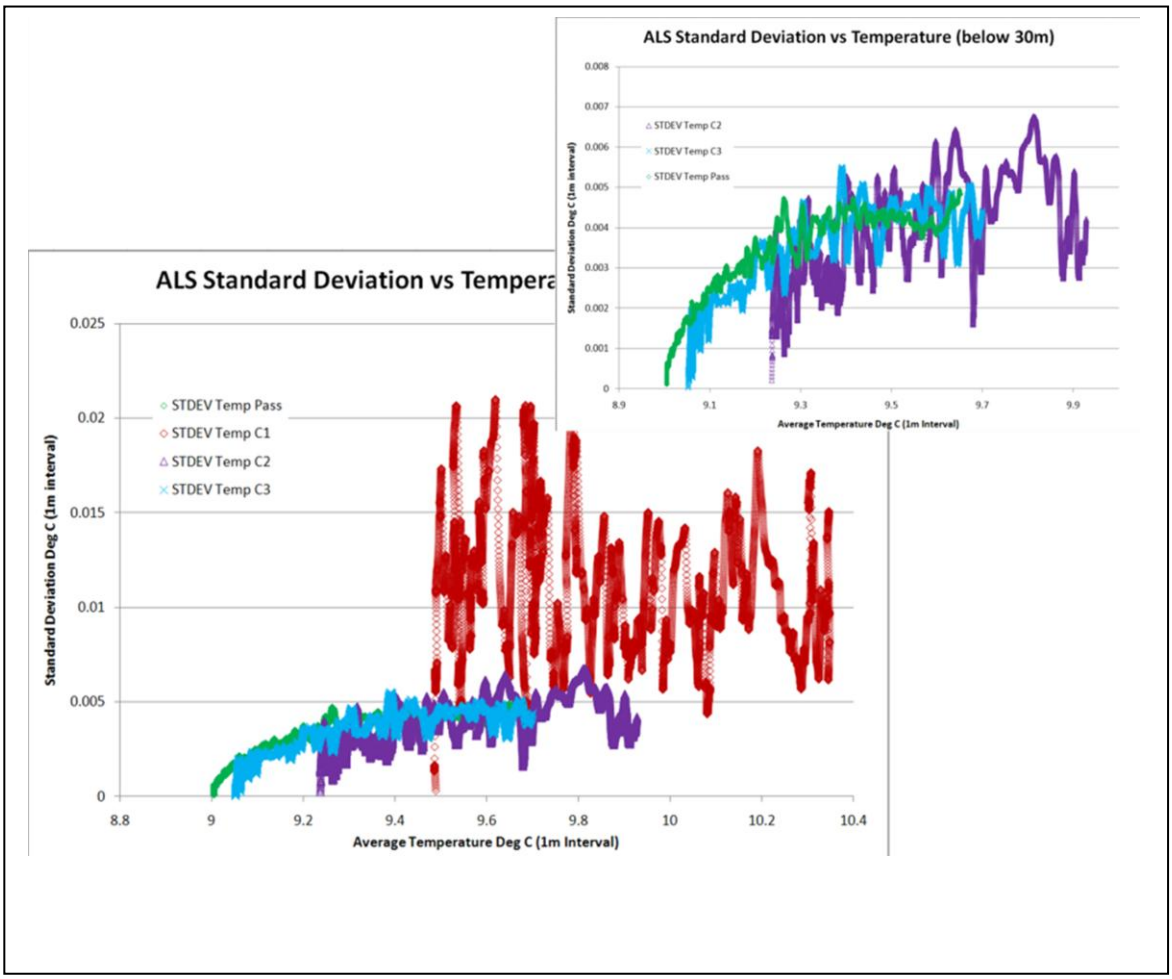

Figure 3-14: UW25 ALS Data Standard Dev against Temperature.
Data shown at expanded scale to emphasize temporal return to ambient distribution during thermal recovery. Standard deviation of temperature calculated over 1m moving window.

Chapter 4
An Oriented Temperature Measurement Probe for Characterizing Groundwater Flow Around Lined Boreholes in Fractured – Temperature Vector Probe

Peeter Pehme, D. Blohm, B.L. Parker, and J.A. Cherry

4.1 Overview

Two recent developments in the use of temperature logging have increased its applicability to characterizing flow through fractured rock. The sealing of boreholes in using water-filled, flexible impermeable liners prevents vertical cross connection between fractures intersecting the hole and establishes a static water column inside the liner which after time develops a temperature stratification that mimics that in the surrounding formation. Measurement of the temperature profile of the lined-hole, water column (using a high sensitivity single-point probe achieving resolution on the order of 0.001 C°) has been shown to be capable of identifying fractures with active flow under ambient groundwater conditions (without cross connecting flow along the borehole). Detection of flow in fractures has been shown to be further improved with the use of a heater to create thermal disequilibrium in the active line source (ALS) technique and eliminate normal depth limitations in the process. This paper describes a significant advancement in temperature profiling through the use of a temperature vector probe (TVP). The TVP measures the temperature of the water column in the lined hole using four high sensitivity sensors arranged in a tetrahedral pattern oriented using three directional magnetometers. Based on these data, the horizontal and vertical components of the thermal field, as well as the direction of temperature gradient are determined, typically at depth intervals of less than 0.01 m along the length of the hole. The performance of this probe was assessed by trials in over 30 lined boreholes; this paper presents results from two holes through a fractured dolostone aquifer in Guelph, Ontario. No other devices exist for measuring flow magnitude and direction under the ambient flow condition created by lined holes. The performance of the TVP is assessed by examining the reproducibility of the temperature measurements through an ALS test, and by the consistency of the results relative to other types of larger-scale information from the study area. Temperature profiles were measured in lined holes under both ambient thermal conditions and subject to ALS heating of the entire length of the holes to demonstrate performance and reproducibility. The hydraulic gradient in three-dimensional space was measured at three locations using depth discrete, multilevel monitoring systems in other holes to independently estimate the

various groundwater flow directions. The characteristics of the hydraulic and thermal regimes are compared to assess response to changes in flow in a fractured rock system. When used in the lined holes, the level of detail provided by this multi-sensor probe is much greater than that provided by a single-sensor probe; and this detail strongly supports inferences concerning the relative magnitude and direction of the flow. The thermal field in the water column at depths where fractures with flow intersect the borehole are more complex than indicated by single-sensor probes, and in some zones there is evidence of thermal convection. The results of this study indicate that our multi-dimensional temperature probe offers superior temperature profiling results compared to a conventional single-sensor, thereby substantially enhancing the characterization of groundwater flow in fractured rock.

4.2 Introduction

Understanding and predicting contaminant migration and fate in fractured rock requires use of numerical models (e.g. Fractran, Sudicky and McClaren 1992; Therrien and Sudicky, 1996) that represent flow and transport in networks of numerous discrete interconnected fractures. For these numerical methods to be most useful in replicating field sites, it is necessary that the characteristics of the groundwater movement: the number and frequency of conduits (fractures and other highly permeable seems), direction of flow, the groundwater flux and/or velocity be determined to design and constrain the models. Borehole temperature measurements have been used in fractured rock investigations since the early 1900's; however, only recently has temperature profiling become an important method for fracture investigations due to three technological advances and improved understanding of the interaction between groundwater flow through rock and temperature variations:

> The sensitivity of temperature probes now achieve resolution in the order of 0.001C°,
> The effects of borehole cross-connection can be avoided by sealing the boreholes using flexible impervious fabric liners (i.e. FLUTe™ liners, Cherry et al. 2007), and
> The depth limitation created by the need for natural thermal dis-equilbrium water and the rock for detection of flow have been overcome with the active line source (ALS) technique (Pehme et al, chapter 3).

The use of thermistors that resolve temperature variations in the order of a thousandth C° in fractured rock is documented by Berthold, S and F. Börner (2008) as well as Greenhouse and Pehme (2002). Pehme et al (2010) reported on the combined use of a high sensitivity temperature probe in lined holes. The liner is filled with water to a level a few metres above the highest formation head so that the water pressure forces the liner tightly against the borehole wall to create a seal. Once sealed, the water column is essentially static and equilibrates to the temperature distribution of the formation

around the borehole. Pehme et al. (2010) show that the temperature profiles measured in the static water column identify many more fractures than profiles obtained without the liners because in the open hole there is typically cross connected flow as water moves between fractures at different pressure vertically through the borehole. The cross-connected flow between shallow and deep fractures facilitated by the presence of the hole masks the temperature variations that would normally occur at intermediate fractures that can have large flow under ambient hydraulic conditions. Ambient flow refers to the flow system that exists without any cross-connecting influence of the hole, which is generally the flow condition of most relevance when considering the transport and fate of contaminants.

Subsequently, Pehme et al. (Chapter 3) discussed the depth restrictions imposed on the usefulness of temperature logs for detecting flow because of the reliance on heterothermic conditions to affect a detectable temperature variation at fractures. Further they show that limitation can be overcome by forcing a controlled thermal dis-equilibrium with the active line source (ALS) in a lined borehole. The interpretation of repeated high sensitivity temperature profiles before, during and after heating (during thermal recovery) in an ALS test extends the application of temperature into the homothermic zone, and thereby further increases the number of flow zones identified as well as improves the qualitative comparison of the amount of flow in each feature.

This paper presents a new advance for high sensitivity temperature profiling in fractured rock boreholes referred to herein as the temperature vector probe (TVP). This probe can be used in boreholes with and without liners; however, as shown by Pehme et al (2010) for the single sensor temperature sonde, the analysis when the TVP is employed in lined holes has greater potential for identifying fractures with flow relevant to contaminant transport and is the current focus. The purpose of this paper is to describe the probe design and provide field evidence in lined boreholes under both ambient conditions and subjected to an ALS test to show its capability to measure the magnitude and orientation of the temperature field continuously along the length of a borehole. The probe has an array of orientated high sensitivity temperature sensors to provide insights into the temperature field not available from single point probes and thereby can be used to infer the characteristics of horizontal and vertical groundwater flow in the formation around the borehole without cross-connection effects.

The methods for data processing and deployment of the device have been refined for over a decade through use in over thirty boreholes across North America and Europe. This paper focuses on data obtained from boreholes in a fractured dolostone aquifer in Guelph, Ontario, used for municipal water

supply. In this assessment of the performance of the TVP, it is not possible to compare the results concerning groundwater flow directions and flow magnitude to other types of measurements of these parameters because no other method exists to determine these under ambient flow conditions in a lined borehole. Methods for detecting flow around open or locally sealed holes exist such as dilution for groundwater flux in a packer isolated intervals (Halevy, et. al, 1967). Similarly, the *GeoFlow*® (Kerfoot, 1992) limits vertical flow and uses glass beads to control the increase in groundwater velocity as it enters the borehole in a system that measures the travel time of a heat pulse with multiple thermal sensors to interpret the horizontal component of flow and direction. Both these systems leave the remainder of the borehole open and interconnected, which may influence flow in the overall rock mass and create flow conditions that are so different from ambient that comparisons would be unfounded.

Because there are no other borehole devices that provide a basis against which to compare the measurement of the thermal field and inferences made about the characteristics of ambient groundwater flow, the performance assessment of the TVP probe is based on other approaches such as reproducibility and the consistency of the characteristics of the thermal field as determined by the TVP in the context of hydrogeologic data (the relevance of the results). Reproducibility is demonstrated by comparing the recovery of the thermal field towards its original state after complete disarray is created by ALS heating using data from one hole (MW25) at the Guelph test site as an example. The characteristics of the thermal field through an ALS test are examined at both a borehole and individual fracture scale at MW25 with comparison against other borehole data typically used for hydrogeologic site characterization to demonstrate consistency. The details of the thermal field measured by the TVP from another borehole (MW77) at the Guelph site are compared to the distribution of the hydraulic pressure (head) measured in high detail multilevel installations in three adjacent boreholes and the inferred flow direction to demonstrate broad consistency with the hydraulic conditions in the study area.

4.3 Temperature Vector Probe

4.3.1 Probe Design and Parameter Estimates

The thermal vector is determined based on the simultaneous measurement of temperature at the four corners of an inverted tetrahedron pattern, and the orientation of the probe relative to the earth's magnetic field using three orthogonal magnetometers (M_X, M_Y and M_Z). For reference the sensor that leads the group is designated T1 and the three coplanar sensors T2, T3 and T4 in a counter clockwise

manner looking up the borehole (Figure 4-1). T2, T3 and T4 are equally-spaced at 34.72mm apart and T1 is 34.72mm proud of the plane created by the others.

The parameters measured and those subsequently calculated are summarized in Table 1 and shown schematically in Figure 4-2a and Figure 4-2b. An orthogonal thermal coordinate system T_X, T_Y and T_Z, is defined relative to the four sensors (Table 4-1, Figure 4-2a). The magnetometers are not necessarily aligned with the thermistors, therefore the horizontal angle between the thermal coordinates and the magnetic coordinates (ie between T_Y and M_Y) are determined experimentally. In near vertical (most) boreholes the offset angle is used to orientate T_H to magnetic north and then finally corrected for the local magnetic declination relative to true north. The components of the thermal field for a vertical borehole are calculated using basic vector algebra. Calculation of the components in an inclined hole requires additional information of the borehole tilt and azimuth (typically available from acoustic or optical televiewer data) and a triple matrix rotation (provided in the supplementary material in the electronic version of the manuscript).

A cage is designed to protect sensors while minimizing disturbances of water column during data acquisition. Greenhouse and Pehme (2002), Pehme et al (2010) and Pehme et al (Chapter 2 and 3) have demonstrated the Instruments for Geophysics (IFG) design of individual sensors to be sensitive to variations in temperature in the order of a thousandth of a Celsius degree, have variability of a few ten thousandths of a degree and to be stable over time (see supplementary electronic material for details). The time constant of the probe depends on a variety of design factors, the most important of these is the sensors and how these are exposed to the borehole fluid. Although it is difficult to measure the actual time constant when it is extremely low, IFG specifies the time constant to be less than 1 second (D. Blohm, 2007).

4.3.2 Vector Orientation

An early prototype of the probe used an optical gyro to measure rotation (in milli degrees per second) from a target established on surface. That design had the advantage of being independent of interference from steel casing and metallic minerals within the rock. However, data reduction was labor intensive and errors due to vibrations or interruptions accumulated over the duration of a log which occasionally necessitated re-logging of boreholes when closure upon returning to surface was poor.

Most of the environments where this device has been deployed are of sedimentary origin with few metallic minerals, and therefore orientated (fluxgate) magnetometers can be used to reference

measurements to the terrestrial magnetic field. Directional magnetometers are a standard technique for orientation borehole probes such as acoustic and optical televiewers (e.g. ALT, 2009; ALT, 2012) and orientation probes (eg. 2DVA-1000, Mount Sopris, 2012). The probes rely on ratios of the components of the magnetic field and are therefore relatively independent of diurnal variations in the earth's magnetic field. The magnetometers are orientated relative to the sensors by establishing artificial temperature gradients with respect to magnetic north while systematically rotating the probe in both clockwise and counterclockwise directions and result in an estimated accuracy in the orientation of ±5 degrees. Although reliance on magnetometers sacrifices the ability to collect orientation data in steel-cased boreholes, the quality of orientated data does not rely on continuous logging, nor does it deteriorate with the length of time data is collected. Further, magnetometers facilitate stationary monitoring and raw data to be subdivided into smaller files when needed because continuous data collection is no longer needed to ensure accurate orientation of the probe.

4.3.3 Quality Control Considerations and Sensor Calibration

The accuracy and quality of the results are based on the ability to measure the thermal gradient within a small diameter borehole. As a result of the mechanical and electronic design, each individual sensor has the precision to detect temperature changes in the order of 0.001C° however, for the probe to work as intended the calibration of the four thermistors relative to each other is critical. The second issue is the measurement of the orientation (rotation) of the probe. Although these two considerations are independent, both must be adequately understood and controlled to calculate a reliable thermal vector.

As is the case with a single thermistor temperature probe, it is not as critical that the TVP probe provides an accurate temperature of the borehole fluid, but that all four sensors precisely and similarly respond to very small variations in the borehole fluid temperature such that spatial changes in temperature are measured to a high level of certainty. Therefore correction factors are required for three of the four sensors. The manufacturer calibrates individual sensors of the TVP probe by establishing a second order polynomial correction against a standard laboratory temperature probe in a bath as the water temperature is varied from slightly above 0°C to 50°C. Although this process yields excellent relative resolution, the absolute measurements are dependent on the accuracy of the standard, (approximately 0.1°C) and the uniformity of the water temperature within the bath.

A secondary calibration is required to standardize the response between the four sensors. Several variations of thermal baths were attempted in a variety of insulated and non-insulated containers in several configurations and over varying time periods. However, because of the sensitivity of the

sensors, in each case individual temperature responses gradually and continuously vary, presumably due to thermal gradients and convection within the baths in response to slight temperature changes in the laboratory environment. Nor did vigorous mixing of the water within the containers to eliminate the lateral variability provide adequately stable temperature measurements and a satisfactory calibration. Because the design of the sensors provide the desired high sensitivity, laboratory calibration of the probe continues to be a challenge and we have yet to contemplate a practical (inexpensive) method that provides an adequately stable thermal environment in the lab.

However, based on the premise that deep in the homothermic zone is a stable and uniform thermal environment, calibration was achieved by turning to borehole measurements. Temperature logging is conducted within a borehole liner which eliminates vertical cross-connected movement of water along the annulus of the holes as a potential source for thermal fluctuations. Identification of portions of the borehole where the temperature of all the sensors is constant over several metres was used to provide calibration points for T2, T3 and T4 against T1 at a particular temperature based on the assumption that neither a vertical gradient exists locally or that there is any localized thermal disequilibrium resulting from flow. However that process provides only a single offset correction which can vary slightly as different temperatures are measured through the borehole. Subsequently the procedure has been modified to use all the readings through the homothermic portion of the borehole, preferably where temperatures are broadly declining with depth to avoid potential for convection. The process defines separate linear relationships for T2, T3 and T4 that corrects each to T1 over a range of temperatures applicable to a specific borehole. Although the current process includes some data at fractures where the response is not uniform, the large number of measurements (typically more than 10,000 for each sensor) negates the influence on the relationship and R^2 fit values are generally greater than 0.995. Further details of the process are provided in electronic version of this manuscript. It is important to note that periodic recalibration is needed and in the event of a repair of any of the thermistors or the electronics a complete new set of calibrations should be undertaken.

4.4 Results

Figure 4-3 shows a schematic representation of the anticipated response of the TVP to a simple case of warm water moving through a fracture and around a lined borehole in a comparatively cooler matrix. Each of the thermistors responds slightly differently to the disruption in the thermal field created by the water (heat source). As a result the horizontal component of thermal gradient (vector) would have a single peak with a maximum at the elevation of the fracture. The vertical gradient

would vary from a negative extreme immediately above the fracture to a positive peak immediately below and the inclination of the total field would correspondingly reverse polarity at the fracture. The horizontal direction of the gradient is arbitrarily shown to become northward from a southerly orientation while in practice in the sections of the borehole where the horizontal gradient is low the direction is poorly defined and tends to be variable. Figure 4-3 is a highly simplified hypothetical response, the thermal field becomes more variable for example due to overlapping effects of adjacent fractures, induced thermal disequilibrium in the ALS process or convection the patterns and gradients would also increase in complexity.

As there is no broadly accepted device to measure ambient thermal variations or flow around a borehole, we are unable to provide a basis for independent corroboration of the TVP probe results. Therefore, as an initial assessment of the performance of the probe, three criteria within two categories are considered:

Consistency of results with other data and site conditions:

- Are the trends and changes in thermal patterns consistent with other data at both the borehole and individual fracture scale, and
- Are the results consistent with the hydrogeologic regime in the area of the borehole?

Reproducibility:

- If the thermal regime is forced into disarray does it return to the original state?

4.4.1 The Thermal Field as Measured by the TVP

Figure 4-4 shows an example of a TVP data set with select other data from MW25, a 103.7m deep, 10cm diameter regional background borehole drilled through the Lockport formation dolomite below approximately 4m of overburden at a G360 research site in Guelph, Ontario. Except for the Eramosa subunit, a discontinuous aquiclude, the Lockport formation is generally considered an aquifer, and had been pumped as a regional water supply (from approximately 70-90mbgs) prior to contamination by trichloethelene (TCE). The details of MW25 and local geology are provided by Pehme et al (2010). The borehole had been lined with an impermeable polyurethane (FLUTe) liner the summer prior to collection of a passive (unheated) TVP data set on March 6, 2006. In addition to TVP data, Figure 4-4 includes the interpretation of discontinuities and a virtual caliper both from an acoustic televiewer log, a shaded gamma profile and a schematic of discontinuities identified from the core. A part of the liner extends un-everted up into the bottom of the hole limiting the TVP log to a maximum

depth of approximately 90m. The TVP data shown from the March logging of MW25 includes the T1, calibrated CT2, CT3 and CT4 profiles, as well as the horizontal, vertical and total vectors, the horizontal direction of the thermal vector and the inclination of the total thermal vector off the horizontal. In addition, column "L" is a T1 thermal deviation profile, wherein a smoothed temperature (with a 5 metre running average) is subtracted from the original data to highlight small scale variations within a broadly changing thermal gradient as per Pehme et al (2010).

Pehme et al (Chapter 3) identified the boundary between the heterothermic and homothermic zone to be at approximately 37 metres, near the bottom of the Eramosa subunit, based on a comparison of passive temperature logs collected in the lined borehole in March 2006 and two other lined hole temperature data sets collected in August of 2005. A distinct change in the horizontal component of the thermal vector and its direction, from approximately westward (270 degrees) to southward (180 degrees) occurs at the hetero-homothermic boundary. Note, the depth of the boundary had been previously indepently interpreted based on single sensor data and the coincidence is supportive evidence of the validity of the TVP measurements.

The TVP data are used to subdivide the interval logged into 27 thermal sub-units (dashed lines Figure 4-4) as distinguished by distinct changes in the character, magnitude or direction of the thermal vector. In most cases the boundaries of the subunits coincide with a geologic change (based on the gamma log) although occasionally more than one geologic layer is included within a thermal subunit. The results imply a cause and effect relationship between the geologic layering and the temperature field. However the correlation does not indicate whether the affect is direct or if another control, i.e. groundwater flow is an intermediate control such that geology and structure dictate flow which is reflected in the details of the temperature field.

To examine the detailed response on the TVP, a portion of the data in Figure 4-4 data from within the homothermic zone are expanded in Figure 4-5 and within the shallow highly dynamic heterothermic zone in Figure 4-6. Deep in the borehole, Figure 4-5(76.25 to 77.50mbgs), the response of the sensors is relatively uniform within the expanded temperature range (0.020C°; 9.050 to 9.070°C). The T4 temperature level is approximately 0.002C° higher than the other three sensors indicating a horizontal gradient of approximately 0.062 C°/m eastward. There is a possibility that the offset is created by miss-calibration of the sensors. However, detailed examination of the profiles confirms that elsewhere in the borehole one or another sensor is higher or all have the same temperature. In addition, where offsets begin and end multiple sensors change over short intervals rather than as gradual drifts over

the span of the hole, both observations supporting the conclusion the gradient is likely real and not a artifact of miss-calibration.

Aberrations in the temperature profiles occur at 76.42mbgs (coinciding with several fractures identified in the core) and at 77.22mbgs (0.08m above a steeply dipping fracture). In neither case is an obvious fracture identified in the ATV amplitude image, which, based on a qualitative assessment is interpreted to be of low resolution due to rock flour accumulating on the borehole wall. However the travel-time of the ATV pulse measures several increases in the borehole diameter which could result from fractures or voids behind the mud cake[1]. A smaller fracture identified in the core at 76.90mbgs also coincides with an increase in borehole diameter, but has no corresponding temperature aberration. Both of the positive aberrations identified in the temperature profile span approximately 0.1m and each is sampled by 5-8 measurements. Both are therefore considered properly sampled and neither are spurious irregularities in the TVP response. Lateral water movement is the only reasonable heat source to which to attribute the increase in sharp temperature across such a narrow band. At each feature, the warmer portion of the hole is on the north side (presumably indicating southerly flow in the fracture), rather than the broader gradient wherein temperature increases in the easterly direction. The upper aberration is dominantly a vertical variation in temperature and the lower aberration is most distinct in the horizontal gradient. The thermal deviation profiles (L) highlight the comparison between the strong signal at the fractures relative to the low level of noise (less than 10^{-3} C°) above, below and between the aberrations.

In Figure 4-6 the temperature range depicted is from 8.900 to 10.500 °C within the shallow highly dynamic heterothermic zone. Although all four sensors are variable, the largest variations occur at fractures identified in the ATV data and the core logs. However, the temperature sensors do not respond uniformly, with one or another sensor indicating temperature increasing with depth while the others show decreasing values (e.g. 8.55-8.7m) and aberrations span as much as 0.15m. Overall, the vector components (gradients) within this portion of the borehole are variable and although these respond at fractures where flow could occur the individual components are of limited usefulness for detailed analysis in the shallow high flow zone. Overall, the temperature is rising with depth in this portion of the borehole creating a thermal gradient conducive to convection and that density driven water movement may be occurring in the borehole and contributing to the patterns observed. By

[1] Note a thin layer of mud cake on the borehole wall is not anticipated to influence the TVP data because the borehole is lined, unless however the mud extends into the fracture and restricts water movement beyond the liner.

removing the overall temperature gradient, the thermal deviation column (L) highlights a series of reoccurring negative "saw-tooth" patterned aberrations with a sharp lower end and extended upper limit in three of the four sensors implying the water in the fracture is cooler than the matrix. The T2 sensor has an upward offset of approximately 0.1m causing a distortion in the thermal field implying that convective may be occurring[2].

4.4.2 Application of the Active Line-Source

To assess the consistency of the response, the results from an active line-source (ALS) test (Pehme et al., Chapter 3) within MW25 are examined. The full length of the borehole was heated using an active line source for (4.12hr) at a rate of 20W/m and repeatedly logged with the TVP before, during heating (active log) and for three cooling data sets (starting a 0.6hr, 3.3hrs and 20.6hrs after the heater was turned off) as the system recovered from the controlled thermal dis-equilibrium. Pehme et. al. (Chapter 3) provides a detailed analysis of the process and interpretation of these results based on the response of a single (T1) sensor. Figure 4-7 shows the TVP data from the process superimposed on the thermal subunits interpreted from the passive dataset and discussed above. Other non-thermal data are provided for comparison as in Figure 4-4 and the heterothermic portion of the hole is shaded for reference.

The active temperature profiles collected during heating (columns J,O and T) are comparatively variable relative to the other profiles, likely as a result of the changing proximity of TVP to the heater cable during logging, resulting in a highly irregular direction for the large horizontal T vector (T^H). Although the magnitude of T^H decreases with time (data sets C1 and C2) and many discrete irregularities can be identified, thermal sub zones as described above only begin to develop in T^H_{C2} data. The horizontal direction of the thermal vector is regular in both C1 and C2 uniformly indicating higher temperatures towards 300° relative to true north at the top of the hole, gradually rotating to 340° at the bottom. The uniformity of the direction is interpreted to indicate the side of the borehole where the heater was located and the rock is preferentially warmed.

By the time the C3 data are collected, the direction of T_H has returned to that which existed before heating throughout most of the hole with the exception of the interval between 37 and 68mbgs. The horizontal gradients of the passive dT^H_P and dT^H_{C3} are similar with one or the other slightly higher or lower, but most importantly the changes in the relative magnitude of the gradients occur where the

[2] Convection and TVP response are discussed in detail within Chapter 5.

direction changes and both tend to vary at the thermal subunits established from the original passive TVP data. Note again the hetero-homothermic boundary with a change in the character of the response with the horizontal directions of C3 and passive the same above the boundary and uniformly separated by 45 degrees below. In C3 the data shows an overall systematic return from the thermal disequilibrium imposed back towards the original passive condition in both direction and gradient though most of the borehole. The thermal subunits originally identified from the passive data coincide with distinct changes in the characteristics of the C3 temperature vector and some additional subdivisions can be identified. The slight difference in base temperatures (F vs. G) indicates some residual energy from heating persists in the system consistent with the subtle differences between passive and C3 data sets described.

Figure 4-8 shows the temperature profiles and the horizontal components of the thermal gradient data at proportionally expanded scales in the depth range of 70.1 to 72.5mbgs. Note the base temperatures for individual data sets (passive, active and three cooling) vary according to the ALS process and different scales are used as appropriate to facilitate comparison. The interval includes six fractures identified in the core, two of which were confirmed in the ATV interpretation. These data are over 30m below the hetero-homothermic boundary and, as described above on a borehole scale. Based on the degree of variability in the response, the individual thermistors exhibit a systematic return towards uniformity over time progressing from C1, C2 and C3 as the affect of heating dissipates. In the C2 data set the T3 sensor has the highest and most uniform response as it is interpreted to be closest to the heated side of the borehole. T2 and T4 measure similar relatively lower temperatures, are both irregular, and are interpreted to be on the opposite side of the borehole from the heater. T1, at the center of the borehole, is relatively uniform, at an intermediate temperature with six distinct negative inflections (aberrations). The C1 data set exhibits similar characteristics with larger variability and aberrations but less differentiation between the actual temperatures measured by individual sensors. In this portion of the borehole much of the heat energy has dissipated and the C3 data set provides little differentiation[3] of flow. In the ALS process (Chapter 3) potential flow zones are identified based on preferential cooling identified primarily in C2 and C3 data. The majority of the flow zones, highlighted in Figure 4-8, based on the C2-T1 profile, are in the proximity of (consistently 0.1-0.2m below) fractures observed in the core. Although the individual C1 temperature profiles are more complex than the C2 data, corresponding aberrations can be also identified in the earlier temperature

[3] The numerical sensitivity analysis (Appendix B) concludes heating the borehole for longer periods improves resolution and the 4hrs used in this case was inadequate to create an optimum C3 response.

profiles. Discrepancies exist in depth alignment between different forms of data which, although inconsequential at the scale of the complete hole, become important for detailed examination of individual features. In both the C1 and C2 data sets, the zones of preferential cooling are neither uniform within either the circumference of the borehole and are vertically asymmetric about the low point in the profiles, all having a characteristic steep lower slope and an extended gradual upper side (i.e., a "saw-tooth" pattern most obvious in the T1 profiles). The patterns in these variations suggest that other factors such as localized convection are influencing the response. Since distinct negative aberrations do not exist in the T2, T3 or T4 data sets, having either not formed or formed and dissipated, there is little information available from the C2 or C3 horizontal gradients.

In this case, the C1 data provides clearer differentiation, although based on T1 alone only four of the six aberrations could be identified. In some cases there is a slight depth offset between data sets or possibly a time dependent shift and subdivision of aberrations. The C1 horizontal gradient exhibits peaks at each of the aberrations and suggests the differentiation of an additional aberration at 71mbgs that does not manifest in the T1 profile of the data set. In this portion of the borehole the identification of flow zones is improved by considering both C1 and C2 data sets with no additional insights achieved from the C3 or passive data.

4.4.3 Characterizing Flow using Thermal Vectors

Figure 4-9 shows the variation of hydraulic head over time in three 10cm diameter boreholes (23, 74 and 75) in an area of the Guelph research site (see inset) southwest of MW25. Each borehole extends to approximately 40mbgs within the Lockport formation dolostone, terminating near the top of the Eramosa subunit (described above). Each of the boreholes has a FLUTe multi level monitor system (Cherry et. al 2007) installed with 15 or 16 measuring ports (details provided in Table 2), with a pressure transducer (Solinst/Geokon 4500H, Georgetown, Ontario, Canada) monitoring the water pressure. The transducers have a manufacture specified accuracy of +-2%, but eight transducers (between the three installations, italicized and shaded in Table 2) were nonfunctional. The transducers were sampled at 1 hr intervals for 55 days starting on 15 October, 2008. The design of the monitoring intervals were based on synthesis of rock core chemistry, a suite of open and lined-hole geophysical logs including: ATV, temperature, gamma, conductivity, neutron, density and heat pulse flowmeter data as well as straddle packer testing.

In Figure 4-9 the time varying pressure head at each elevation are combined and displayed as Time-Elevation-Head (TEH) cross-sections (Appendix C) with colour shading ranging from blue (334.7m) to pale pink (338.4m). The upper measurement intervals in all three installations monitor a zone of

highly fractured rock at the bedrock surface. In MW-23 and MW-74, the pressures observed in the upper two sampling intervals are 0.5-1.0m higher than observed in any of the other intervals monitored and highly variable pressures in response to rain events. The comparatively high and variable pressure values observed are likely due to the proximity of the 4m deep East-West trending drainage ditch which crosses the area and provides a direct conduit for surface water to reach the bedrock surface. Further from the ditch at MW75, underneath the compacted gravel parking lot, the highly fractured surface of the rock is at relatively low pressure and although some subtle increases in pressure occur with precipitation, these are not as strong as at the boreholes closer to the ditch. In addition, at all three locations there is evidence of propagation of the pressure pulse through to the bottom of the sections in some cases confirming vertical hydraulic connection.

All three TEH sections display alternating layers of higher and lower head with depth, although the contrast in pressure values varies between locations with MW23 the most muted of the three. Using MW-75 as a base, three layers of continuously lower pressure are identified (arbitrarily labeled A, B and C for correlation purposes). Over the first 30 days, the overall head in the sections is slightly lower than later in the data set and A appears thicker, implying that possibly the hydraulic layer should be subdivided into an additional layer (labeled as A'). The labels are shown at consistent elevations on the MW74 and MW23 sections and the arrows indicate the interpreted vertical offset in the correlation of layers. Although the degree of variability is muted in MW23, A and B are identifiable with minor vertical offset in all three sections. A' manifests as a separate layer at MW-74, but is not indistinct at MW23 (note however the optimum transducer for detecting the layer was not functioning in ML11). The upper low-pressure layer (C) at MW75 corresponds to the near-surface zone at MW74 and MW23 interpreted to be at high pressure as a result of the drainage ditch (discussed above).

Based the correlation of vertical head variations at the three borehole locations, the sections were vertically subdivided into eight layers of similar pressure (head) with approximate boundaries shown in Figure 4-10(A). The TEH sections were all re-sampled at a arbitrarily select time (e.g. 20 days) to estimate the head at the corners of triangle created by MW23, MW74 and MW75 (shaded in Figure 4-9) at 18 elevations (at representative elevations for seven of the eight layers of similar head, and with additional samplings to refine changes at layer boundaries). The re-sampling of the sections yields 18 vertically distributed data subsets, each with three head values (one at each of the boreholes) for which the average hydraulic gradient (magnitude and direction) across the triangle was

calculated[4]. The results of this process are shown overlain on the TEH section of MW75, Figure 4-10(A), as a series of vertically distributed arrows. Each of the arrows (see key) shows the calculated direction of flow (the down-gradient direction) and the relative magnitude of the average hydraulic gradient across the triangle at that elevation. Together the vertical series of eighteen arrows are a depiction of the average hydraulic regime across at the triangle at a point in time. The process was repeated at other times to assess any temporal variations in the hydraulic patterns, and although minor differences in the shallow hydraulic regime occur. no large variation with time was observed under ambient flow conditions.

The results of this process, Figure 4-10(A), indicate the largest hydraulic gradients to exist in the fracture zone near the bedrock surface. Low horizontal gradients tend to occur in zones of relatively higher pressure (332.5-338.5masl and 314-320masl) and higher horizontal gradients exist where pressures are lower (332.5-225masl, 323-327masl and 309-312masl). The flow direction is generally distinctly towards the SSE from surface to an elevation of 312masl with the exception of the interval between approximately 321 and 324.5masl which has a southward flow. In the deepest low pressure hydraulic unit the gradient indicates flow towards the NW over the entire 55 day period.

Figure 4-10(B) shows a TVP temperature data set measured (May 12, 2004) in MW77, a lined borehole located at the edge of the space defined by the three monitoring locations (MW74, MW75 and MW23). The components of the thermal vector are displayed as: horizontal (C), vertical (D) and total (E) gradients, the horizontal direction (F) and the inclination off the horizontal (G). Horizontal lines are superimposed on Figure 4-10(B-G) as guides to extrapolation of major and minor changes in one or more characteristics of the thermal vector to the hydraulic conditions. Although many more thermal boundaries can be defined than hydraulic units described above, each of the hydraulic boundaries coincides with a change in the character of thermal field. There is scatter in the direction of thermal gradient; however, overall the predominant direction is towards the SSE from 334.0-321.0 masl. The direction is poorly defined from 321.0-317.0 masl below which the direction is 280° (NW) and 0° (N). The major changes in the direction of the temperature field correspond to the general direction as the hydraulic gradient. The portion of the rock between 314 and 321masl where pressures are relatively high (and hydraulic gradients are low) coincides with a low, near horizontal thermal gradient with portions having poorly defined direction. This zone is relatively uniform in the

[4] Following procedures for a 3 point hydraulic gradient estimate available in a standard hydrogeologic text (eg. Freeze and Cherry, 1979).

hydraulic representation, partially because of lack of data, however clear and distinct subdivisions exist in the thermal patterns.

Although the highest thermal gradients in the rock (334.0-335.5masl) also coincide with the highest hydraulic gradients (largest arrows), a direct relationship between hydraulic and thermal gradients is not consistently observed. For example, the thermal gradient between 328.5 and 332.4masl is relatively high (0.3-0.4C°/m) in comparison to between 322-326.4mbgs (0.15-0.2 C°/m), but the deeper portion of the rock has a higher hydraulic gradient than the shallow one. However, within these intervals the changes in the hydraulic conditions coincide well with changes in the thermal field. These patterns are consistent with the premise that changes in the thermal patterns are dependent on water movement and are controlled by many of the same rock properties that control flow such as fracturing, porosity and permeability, but that the temperature patterns are also subject to other driving forces (eg near surface temperature variations).

4.5 Summary

The purpose of employing the TVP is to gain insight into ambient groundwater flow by way of understanding the influence of water movement on the behavior of the thermal field within the rock. The IFG sensor design provides the sensitivity required to measure systematic variations within the 3 dimensional components of the thermal field under passive conditions and in response to induced thermal disequilibrium to interpret the characteristics of ambient flow through fracture and flow zones within the rock mass. Since there is no other device available to characterize the thermal field or the ambient flow in the rock mass at the detail achieved with the interpretation of the TVP, there is no method to independently confirm the interpretation and we rely the broader consistency of the results to assess performance. This assessment is further complicated because the entire system is temporally dynamic and although it may be reasonable to assume that broad patterns are relatively stable in time and space, that may not apply at a detailed scale.

The data presented demonstrate internal consistency. The details of the ambient thermal field once measured are forced into disarray with ALS heating and the field shown to return to that originally measured. The example presented here is typical of the process and in scores of ALS tests the only cases that have deviated from the original on return from thermal equilibrium are when nearby wells have been pumped and the flow regime changed within the period of ALS testing or borehole liners have leaked.

When the details of the thermal field are compared to the hydraulic regime as measured by triangulating between nearby multilevel installations the changes in the thermal field are consistent with variations in both hydraulic pressure and gradients. However the multi-level installations have lower spatial resolution and depths of hydraulic boundaries are not as well defined as the changes in the thermal patterns. The details of the temperature field requires thermal disequilibrium to exist and is dependent on other factors in addition to flow, and therefore the thermal field as it returns to equilibrium can be complex and may not have a simple direct dependence on flow. The TVP data improves differentiation of the borehole into thermal subunits not evident in single sensor temperature logs, without the distortion caused by the process of calculating thermal deviation. Thermal subunits are defined based on variations in the characteristics (either or both orientation and magnitude) of the thermal vector. Although often associated with geologic boundaries, the thermal units can also occur independently and in preliminary comparisons coincide with major pressure boundaries akin to hydrogeologic units described by Meyer et. al. (2008). Although relative changes are almost always evident, the accuracy of the directional analysis is dependent on both a good seal with the liner to restrict vertical flow along the borehole and proper calibration of the response of the four sensors against each other. Repeated measurements at different ambient temperatures and over time has shown that the calibration can vary over a broad range of temperatures, however at any one location the range of temperatures measured is generally limited and a linear relationship between sensors provides an adequate correction.

4.6 Conclusions

The findings show that the TVP responds in an expected, consistent and reproducible manner; based on all results to date we conclude that the device can be used to measure the characteristics of the thermal field. The highly detailed temperature data collected indicate that the thermal field within the borehole can be more complex than would be appreciated from a single sensor probe, particularly when disequilibrium is created with the ALS technique. Within that complexity is potential for new insights into ambient flow in the surrounding rock. However because the temperature patterns vary with other factors, the relationship is not a simple one, yet relating flow to the simple presence or absence of a hydraulic gradient is also an oversimplification that ignores aperture and interconnectedness. The patterns in the thermal response are consistent over extended portions of the borehole and often have clear, well defined boundaries which are honored by the high data density. The patterns in the thermal field as measured by the TVP at MW77 reflect changes in the groundwater flow regime as indicated by variations in hydraulic gradients. This data frequency cannot be achieved with the most densely instrumented multi-level installation and therefore the TVP

data has great promise in planning those installations and refining the interpretation of the data gathered from them. The successful completion of this first stage confirms additional work is warranted to improve field techniques, increase the data base of examples under other conditions and refine the understanding of the processes through quantitative analysis of models and systematic comparison variations in the thermal vector with hydrogeologic conditions. With better understanding of the processes involved, the TVP shows promise of additional insights and improved characterization of ambient groundwater flow in fractured rock particularly when combined with the ALS.

4.7 Tables:

Table 4-1: Terms, Components and Symbols

Measured:		
T_1, T_2,T_3,T_4	°C	single point temperature sensors
M_x, M_Y, M_Z	nT	orthogonally orientated magnetic field. M_x, M_Y on plane of T_2,T_3,T_4, M_Z vertically upwards
Defined:		
C		center point of plane and equidistant from T_2,T_3,T_4 , origin of all reference systems
T_X,T_Y,T_Z	°C	orthogonal thermal axis, T_Y from C in direction of T_3 - T_2 T_X from C in direction of T_4 – C T_Z from C downwards from of C-T_1
T-M correction	deg	angle between M_Y and T_Y on plane of T_2,T_3,T_4
Calculated:		
T_C	°C	temperature on plane and at center of T_2,T_3,T_4
dT_h	C°/m	Horizontal temperature gradient
dT_v	C°/m	Vertical temperature gradient
ϕ		Angle between dT_h and Tx
dT	C°/m	Total temperature gradient
ang dT_h , α	deg	clockwise 0° to 360° (north)
ang dT	deg	(off Horizontal) -90° (upward) to 90° (downward)

Table 4-2: Details of Monitoring Ports, *Note: nonoperational transducers are italicized and shaded.*

Monitoring Interval	MW23		MW74		MW75	
	Midpoint	Length	Midpoint	Length	Midpoint	Length
ML1	336.17	1.52	335.78	1.52	336.19	1.52
ML2	334.04	1.52	333.49	1.83	333.90	1.83
ML3	332.06	1.22	*331.20*	*0.91*	332.07	0.61
ML4	329.32	1.83	*329.83*	*1.22*	331.00	0.91
ML5	327.03	1.52	328.00	1.22	329.48	0.91
ML6	324.59	1.52	*326.33*	*0.91*	*327.35*	*1.52*
ML7	322.76	1.52	325.11	0.91	*325.22*	*1.52*
ML8	320.93	1.52	322.97	0.91	323.84	0.61
ML9	319.26	1.22	321.14	0.91	322.32	1.22
ML10	316.98	0.91	319.01	0.91	*320.64*	*0.91*
ML11	*314.38*	*1.83*	317.18	0.91	319.12	0.91
ML12	312.25	1.22	315.81	0.61	*317.29*	*1.52*
ML13	310.57	1.52	314.44	0.91	315.00	1.22
ML14	308.75	0.91	312.31	1.52	313.02	1.52
ML15	304.39	6.58	310.02	1.22	310.59	1.52
ML16	*NA*	*NA*	308.34	1.52	308.60	1.22

4.8 Figures:

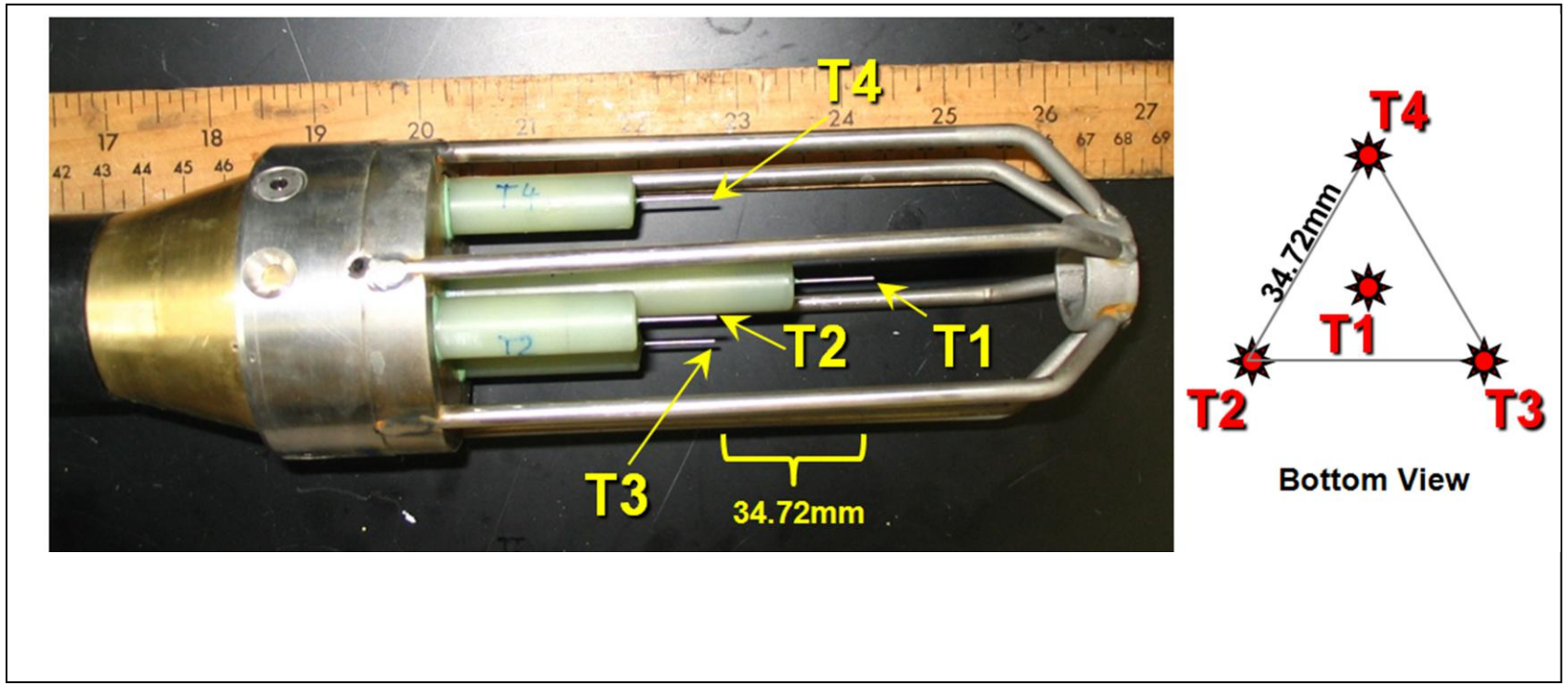

Figure 4-1: Temperature Vector Probe (TVP) head, with 4 thermistors and protective cage, bottom view shows distribution of thermistors as viewed from below.

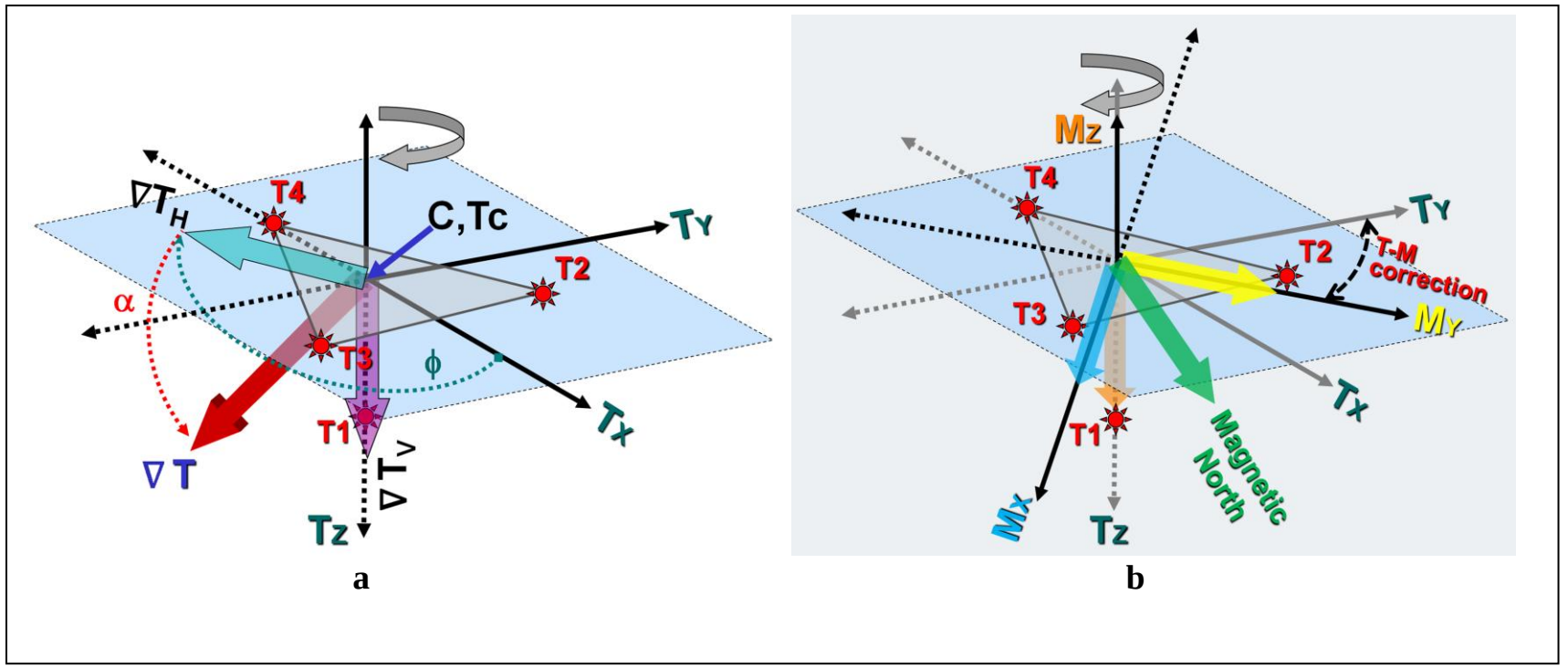

Figure 4-2a,b: Schematic of Temperature Vector components calculated and determining orientation relative to the geomagnetic field (vertical hole*).*

The horizontal (∇TH) and vertical (∇TV) components of the thermal field are calculated based on temperature sensors T1,T2,T3 and T4 relative to thermal cartesian coordinate system (Tx,TY and Tz) and from these the total field vector (∇T), the angle of ∇TH relative to Tx (ϕ) and the angle of ∇T relative to the horizontal Tx-TY plane (α). Note increasing temperature with depth is positive. b) The orientation of the axis Tx, TY and Tz are related to magnetic north based on orthogonally orientated directional magnetic sensors and the probe specific temperature-magnetic coordinate offset correction. Note in a vertical hole only Mx and MY are considered, in an angled hole all three components are considered and the orientation of the hole must be independently measured.

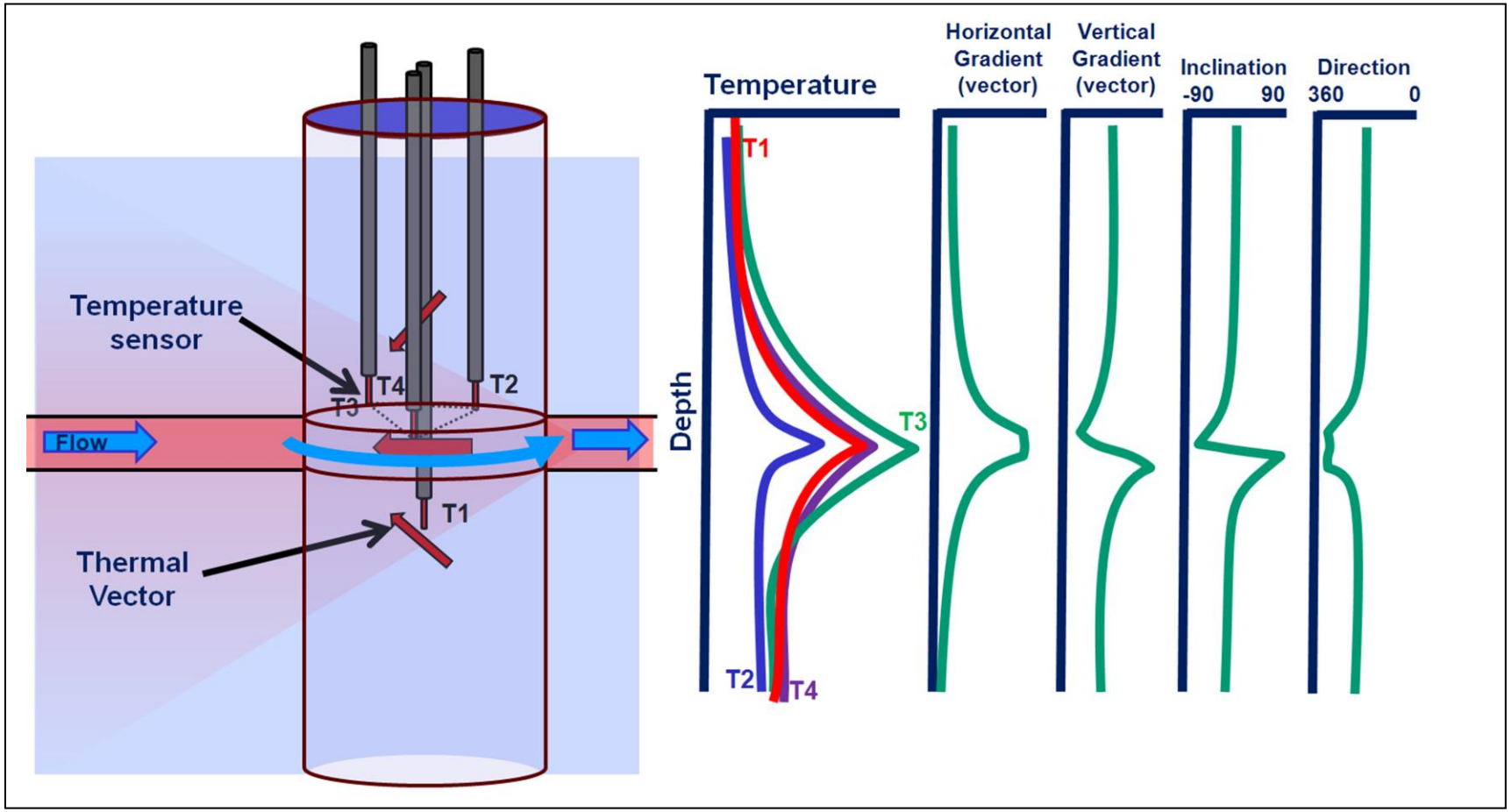

Figure 4-3: Schematic TVP response to simple case of water in fracture warmer than rock matrix.
Four sensors simultaneously measure the temperature of the borehole fluid. If water flowing through the fracture is in thermal disequilibrium with the rock matrix (in this case warmer) it creates an aberration in the thermal field (ie a change in the magnitude and direction of the horizontal, and vertical gradients (vector components of the field).

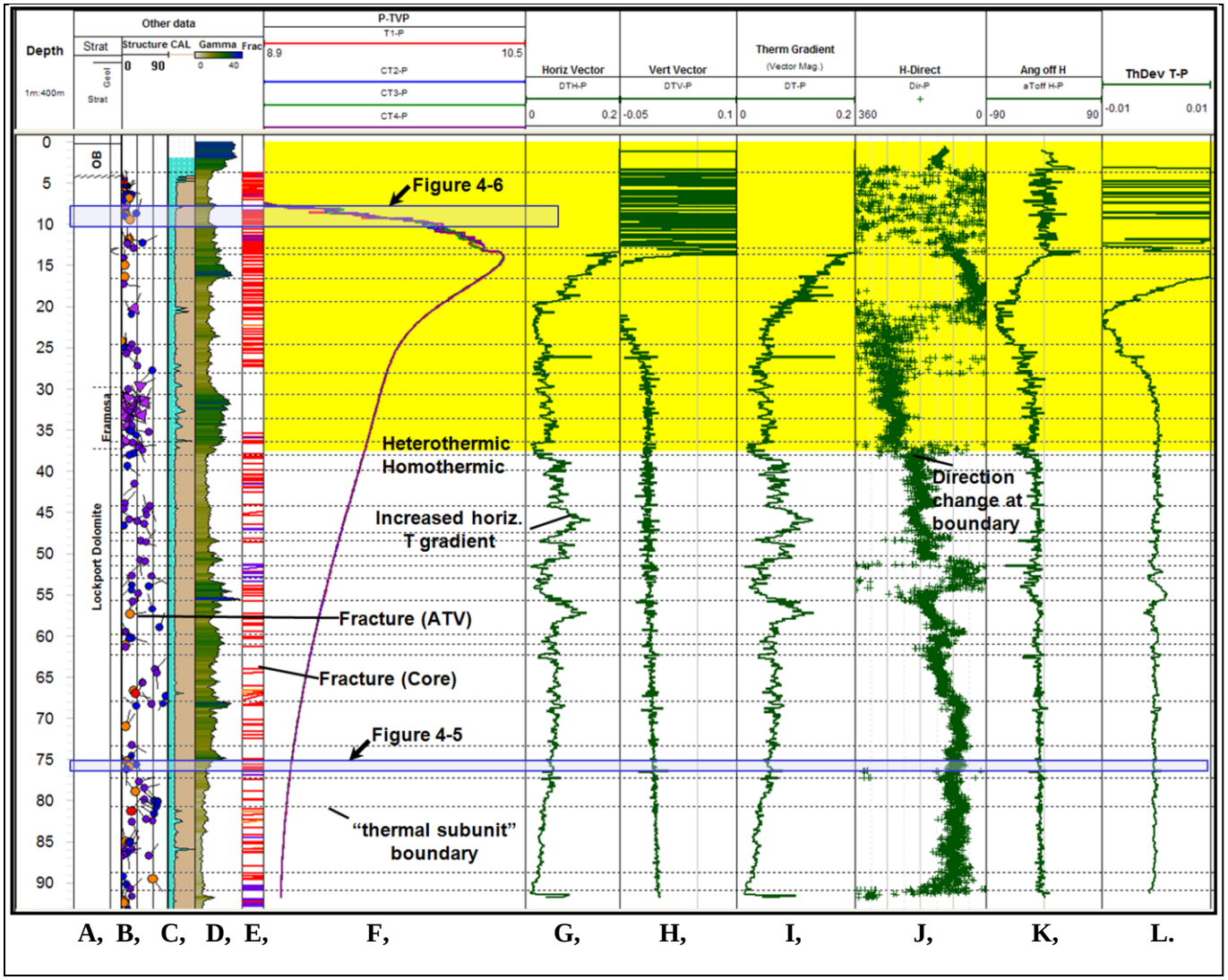

Figure 4-4:Comparison of the variation of the temperature vector components against depth under ambient conditions in MW25 with geologic and structural data. Thermal subunits defined by broad changes in the direction and magnitude of the components of the thermal vector coincide with changes in geology (gamma) and degree of fracturing (ATV and core). A-Stratigraphy, B-ATV interpretation as tadpoles (mauve triangles, red-orange, purple and blue circles represent progressively smaller aperture less distinct decreasing discontinuities, C-ATV travel time as virtual caliper, D-shaded gamma log (0-70cps), E-Core fractures, F-Lined Passive Temperature (T1-red, corrected CT2-blue, CT3-green, CT4-purple; range 8.900-10.500 ° C), G-Horizontal thermal vector (C°/m), H-Vertical thermal vector (C°/m), I-Total thermal gradient (vector magnitude) (C°/m), J-Direction of horizontal thermal vector relative to True North (deg), K-Inclination of total thermal vector off horizontal (deg, positive upwards), L- Thermal Deviation (F-T1), -0.01 to 0.01 C°), dashed horizontal lines –boundaries between thermal subunits interpreted based on G-L, blue rectangles expanded in Figure 4bi,3bii.

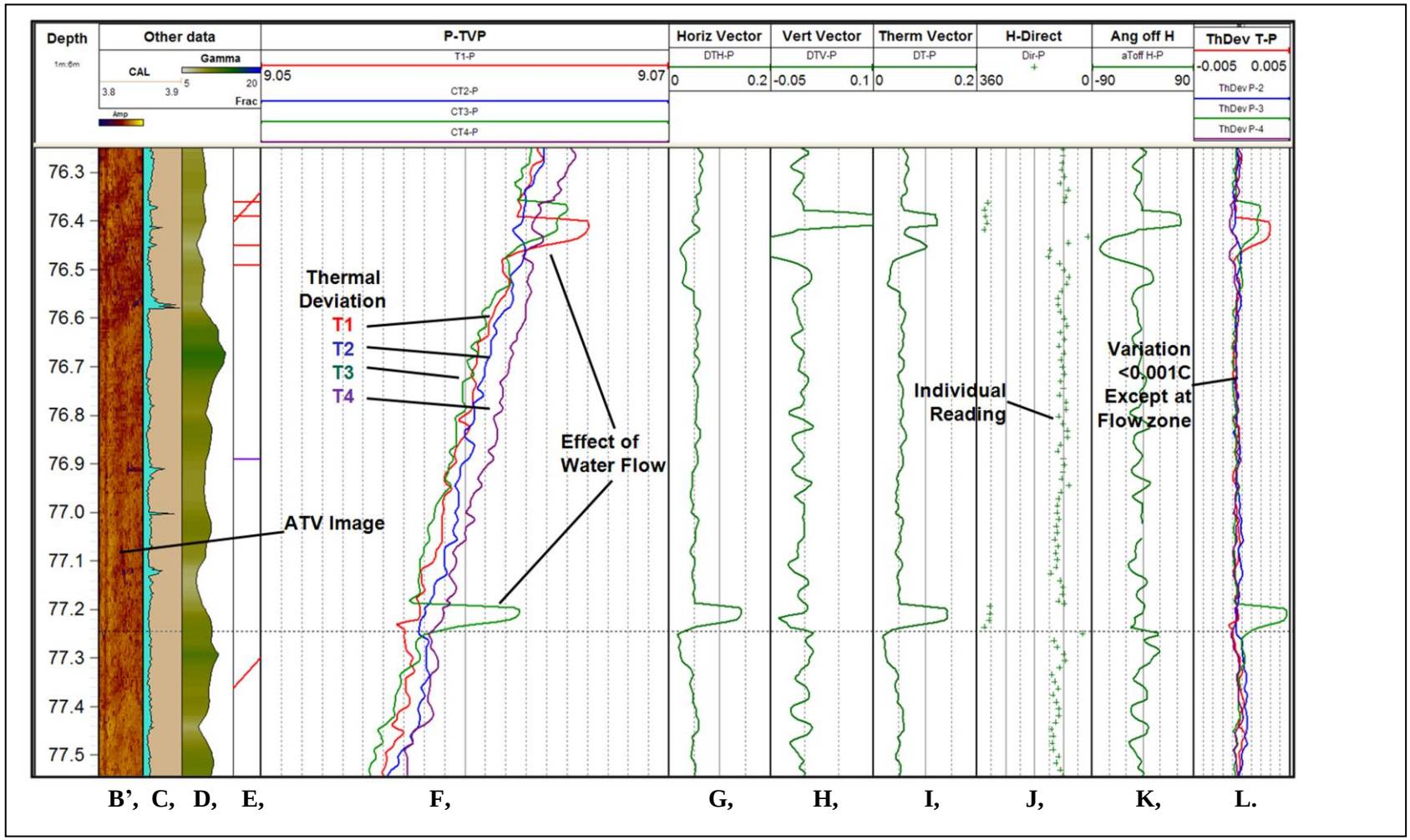

Figure 4-5: Detailed comparison of the variation of the temperature vector components in homothermic zone (Figure 4-4: 76.3-77.5mbgs). Flow at 76.4 and 77.2 mbgs are detected as temperature changes in one or two sensors, but over multiple readings and at levels 4-5 times larger than background variability in the individual readings confirming the aberrations are not related to detector variability. Although the general direction is the same, the thermal vector is inclined at 76.4mbgs and horizontal at 77.2mbgs implying changes in flow direction. B'-ATV amplitude image, C-K as per Figure 4a (except F range 9.050-9.070 ° C), L-Thermal deviation (T1-red, corrected T2-blue, T3-green, T4-purple; range -0.005 to 0.005 C°).

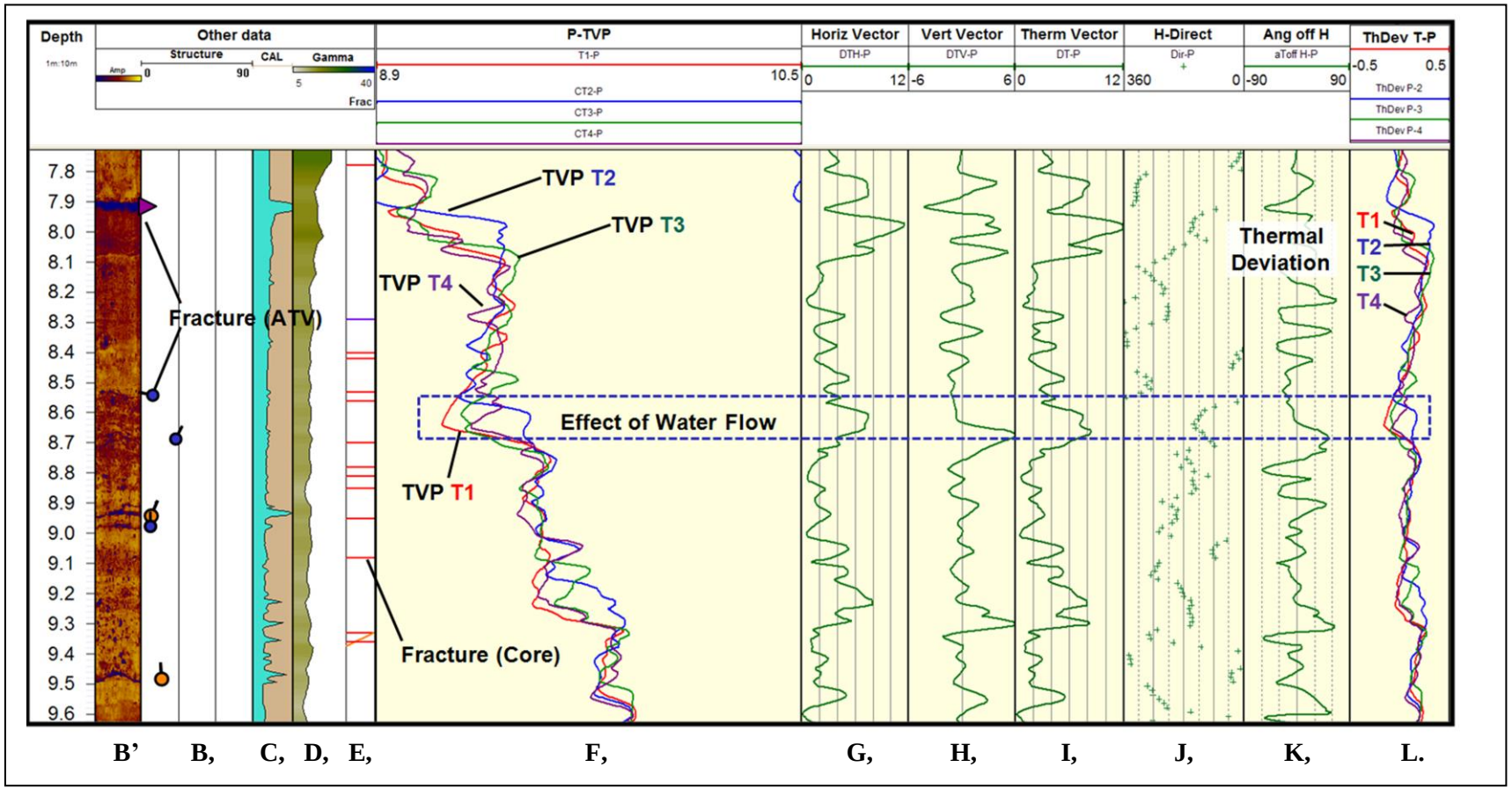

Figure 4-6: Detailed comparison of TVP measurements in heterothermic zone (Figure 4-4: 7.8-9.6mbgs) with geologic and structural data. Note the complex variability in the measurements of individual sensors within the thermally dynamic zone, the coherence when examined as thermal deviation and correlation with fractures observed in core and ATV data. Asymmetry of temperature profiles and offsetting peaks and troughs imply convection may be occurring. ***B-L as per Figure 4a,4bi, Scales compressed due to variability in heterothermic zone.***

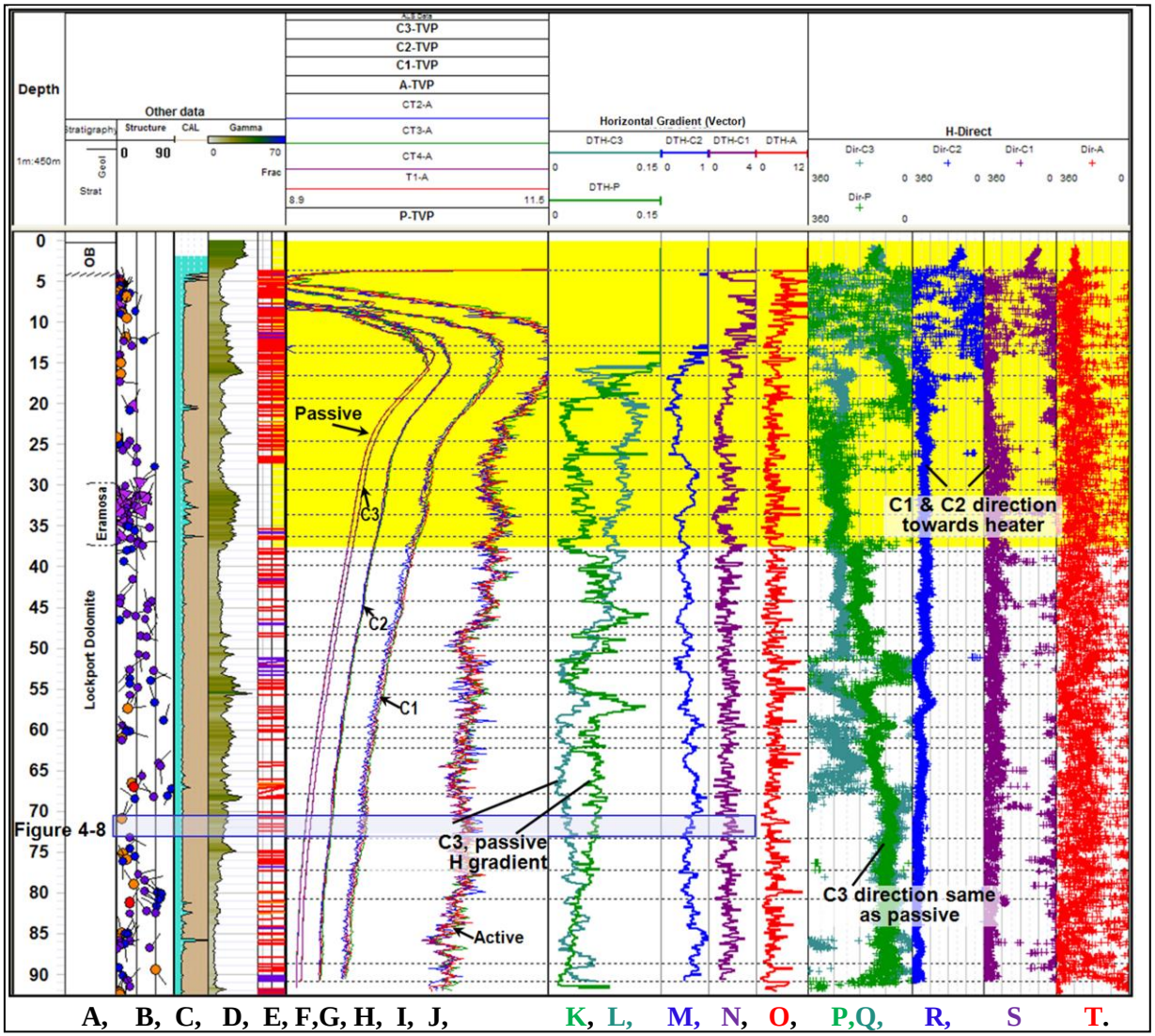

Figure 4-7: Disruption of the temperature field during active line source (ALS) test and recovery towards ambient condition as measured by the TVP in MW25. The heating process (active data) places the thermal field into disarray. As the borehole gradually cools towards ambient temperatures, the cooling logs (C1,C2 and C3) show the thermal field direction shifting from being orientated towards the heater towards the passive data (prior to heating) thereby confirming the original measurement of the thermal field. Note the character of the thermal vector during ALS recovery varies at the thermal subunits originally identified from passive data confirming the consistency of the identification. *A-* Stratigraphy, B-ATV interpretation as tadpoles (mauve triangles, red-orange, purple and blue circles represent progressively smaller aperture less distinct decreasing discontinuities, C-ATV travel time as virtual caliper, D-shaded gamma log (0-70cps), E-Core fractures, F-Lined Passive Temperature, G, H,I -Cooling 3,2,1 temperature data, J-Active temperature data (for F-J:T1-red, corrected CT2-blue, CT3-green, CT4-purple; range 8.900-11.500 ° C), K-O, -Horizontal thermal vector (C°/m), P-T -Direction of horizontal thermal vector relative to True North (deg),(for K-T: green passive, red-active, purple- C1, blue C2, teal-C3, dashed horizontal lines –boundaries between thermal subunits interpreted as in Figure 4, yellow shade heterothermic zone, blue rectangle expanded in Figure 5b.

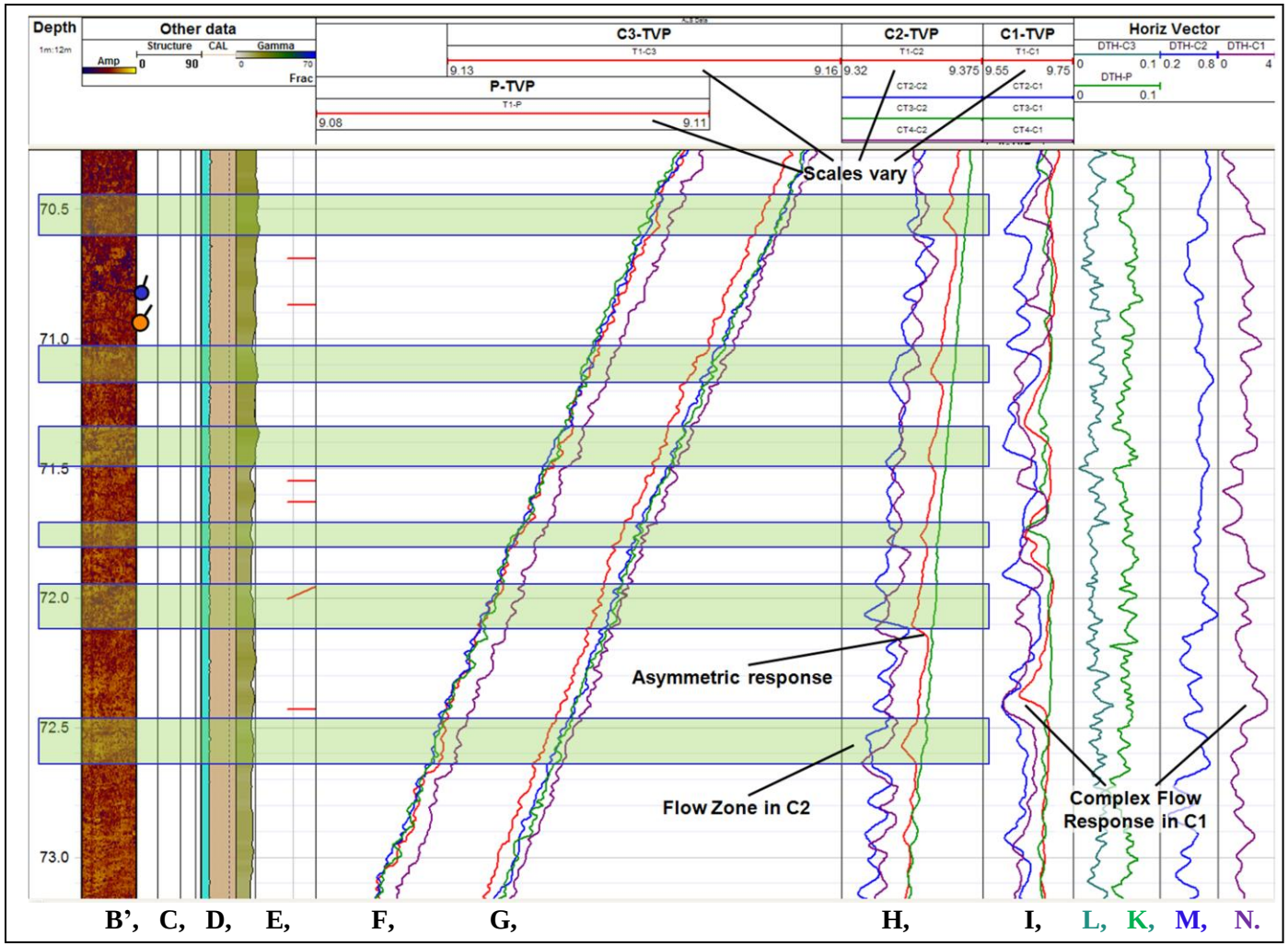

Figure 4-8: Expanded portion of Figure 4-7 (70.2-73.2mbgs) showing the detailed evolution of individual flow features through the thermal recovery process. C1 data are highly variable and although large variations occur, the individual thermistor response varies considerably. Although an overall minor gradient still exists in C2, T1 provides the clearest indication of flow zones, T3 is dominated by the heat in the rock (warmest) and without variations, while both T2 and T4 are relatively irregular as these are furthest from residual heat in the rock (coolest). A consistent offset between the interpreted and core fractures implies minor depth misalignment and asymmetry response may be an indicator of convection. C3 is similar to the passive data confirming the return to ambient conditions. B'-ATV amplitude image, C-N as per Figure 5a (except temperature ranges vary F= 9.060-9.110°C, G= 9.130-9.160°C, H= 9.320-9.375°C, I= 9.550-9.750°C), boxes highlight potential flow zones discussed in text.

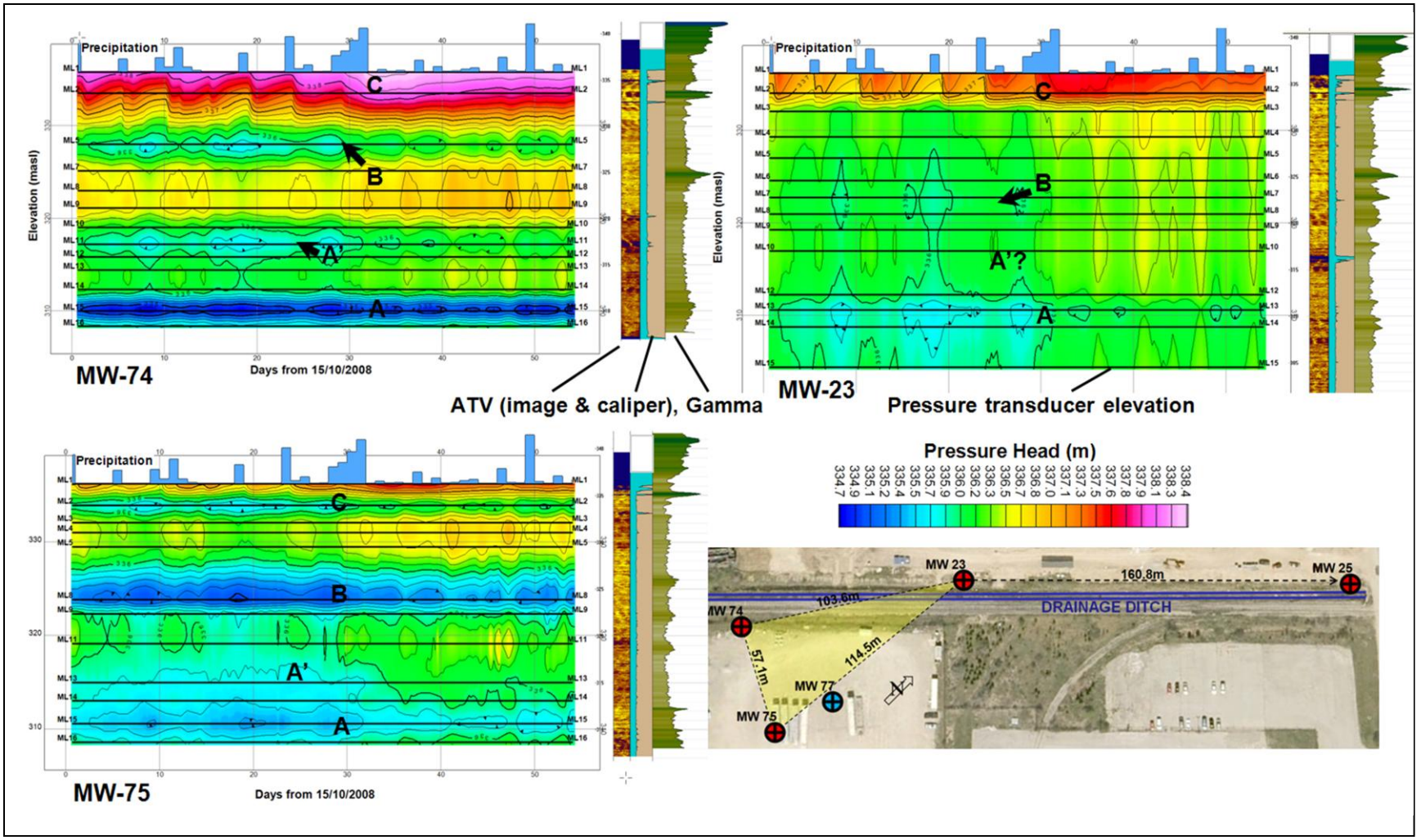

Figure 4-9: Time-Elevation Head Sections: MW23, MW74 & MW75 from Guelph test site showing the pressure stratification at the Guelph site. Zones of higher and lower pressure can be correlated between three boreholes.

ATV amplitude and travel time (as caliper) and gamma log and location map provided for reference. Center of operating transducer intervals shown as lines across each section. A, B and C are elevations of low pressure patterns (based on MW75) extrapolated between sections and arrows indicate vertical offset of the corresponding low pressure layer in MW74 and MW75. For details of TEH sections refer to Appendix C.

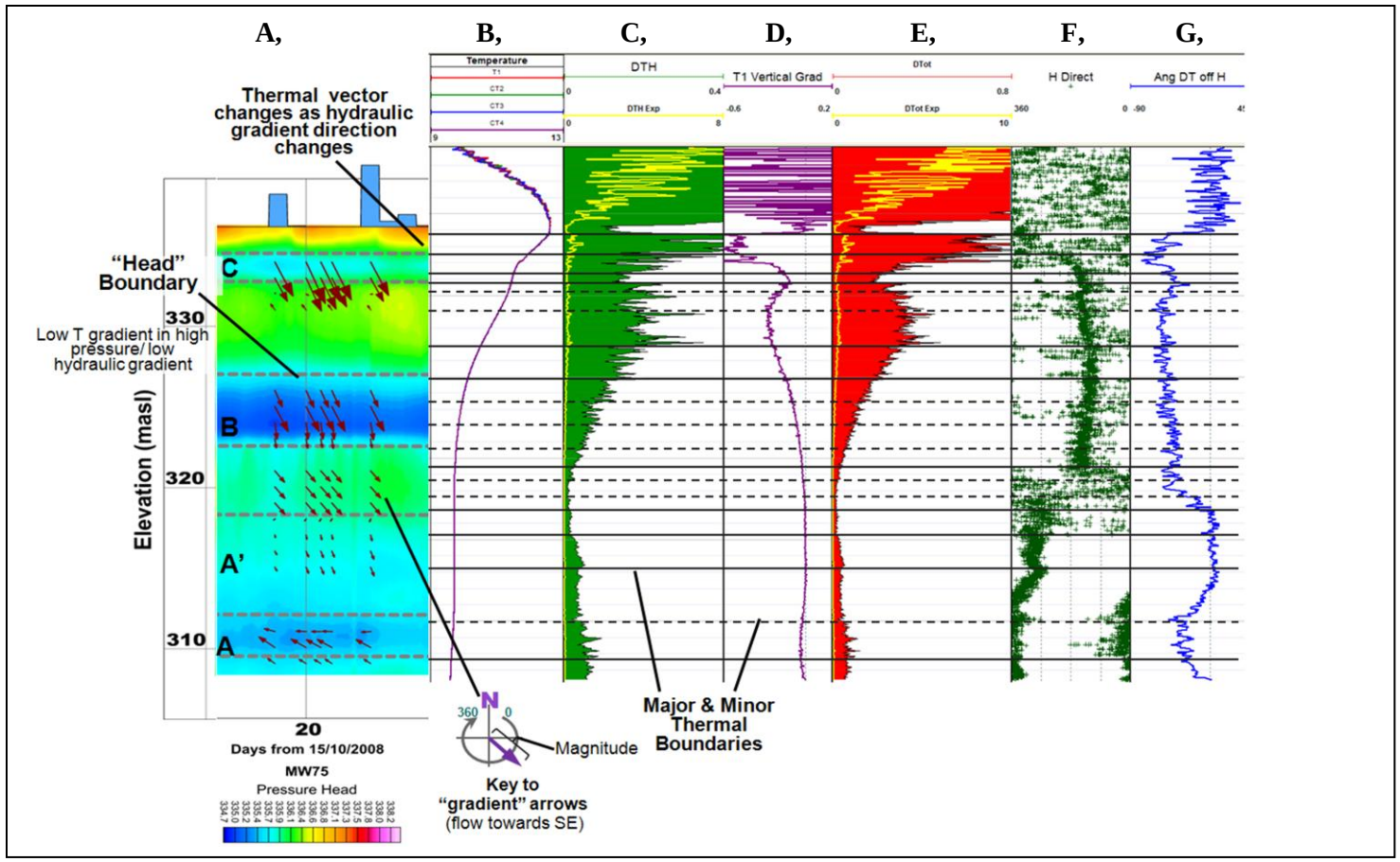

Figure 4-10: Comparison of MW77 ambient TVP thermal vector components against local pressure head stratification (MW75) and horizontal hydraulic gradients.

The variations in the magnitude and direction of the hydraulic gradients (calculated by triangulation between borehole MW74, MW75 and MW23, Figure 6) and inferred groundwater flow coincide with the thermal subunits as determined by the changes in the thermal vector confirming relationship between the thermal field as measured by the TVP and hydro-stratigraphic variations. A-TEH section (Figure 6) with average hydraulic gradient as flow magnitude and direction (see Key), B-passive temperature data (T1-red, corrected CT2-green, CT3-blue, CT4-purple; range 9.000-13.000 ° C) C- Horizontal thermal vector, at 0-0.4 C°/m (green) and 0-8C°/m (yellow), D- Vertical Thermal Gradient C°/m, E- Total Thermal Vector at 0-0.8 C°/m (red) and 0-10 C°/m (yellow), F-Direction of horizontal thermal vector relative to True North (deg), G-Inclination of total thermal vector off horizontal (deg, positive upwards. Solid & dashed horizontal lines –boundaries between thermal subunits interpreted from TVP data. Hydraulic vector key (length of arrow represents horizontal hydraulic gradient calculated from TEH sections (Figure 6) and orientation of arrow flow direction).

4.9 SUPPLIMENTAL MATERIAL

4.9.1 Calculations of thermal Vector

Assuming a planer thermal field, T_C is the temperature equidistant coplanar from T2, T3 and T4 which is the average of the three readings (4-1).

$$T_C = \frac{(T_2 + T_3 + T_4)}{3} \qquad (4\text{-}1)$$

The horizontal and vertical components of the temperature field (T_H and T_V) are eq 4-2 and eq 4-3 respectively and the magnitude of the thermal vector T_T the vector sum of the two (4-4), where d_{ij} represents the distance between sensors i and j).

$$T_H = \sqrt{\left(\frac{(T_4 - T_3)}{d_{43}}\right)^2 + \left(\frac{T_2 - \frac{(T_4 + T_3)}{2}}{\sqrt{d_{24}^2 - \left(\frac{d_{43}}{2}\right)^2}}\right)^2} \qquad (4\text{-}2)$$

$$T_V = \frac{(\Delta T_1)_{over 3.5cm}}{d_{1C}} \qquad (4\text{-}3)$$

$$T_T = \sqrt{T_H^2 + T_V^2} \qquad (4\text{-}4)$$

The inclination angle of T_T is determined with Equation 4-5 and Equation 4-6 calculates the angle between T_H and the T_Y axis.

$$\arccos(\alpha) = \frac{(T_1 - T_{T_C})}{d_{1C}} \qquad (4\text{-}5)$$

$$\arctan(\phi) = \sqrt{T_H^2 + T_V^2} \qquad (4\text{-}6)$$

Using matrix rotation for and angled borehole: :

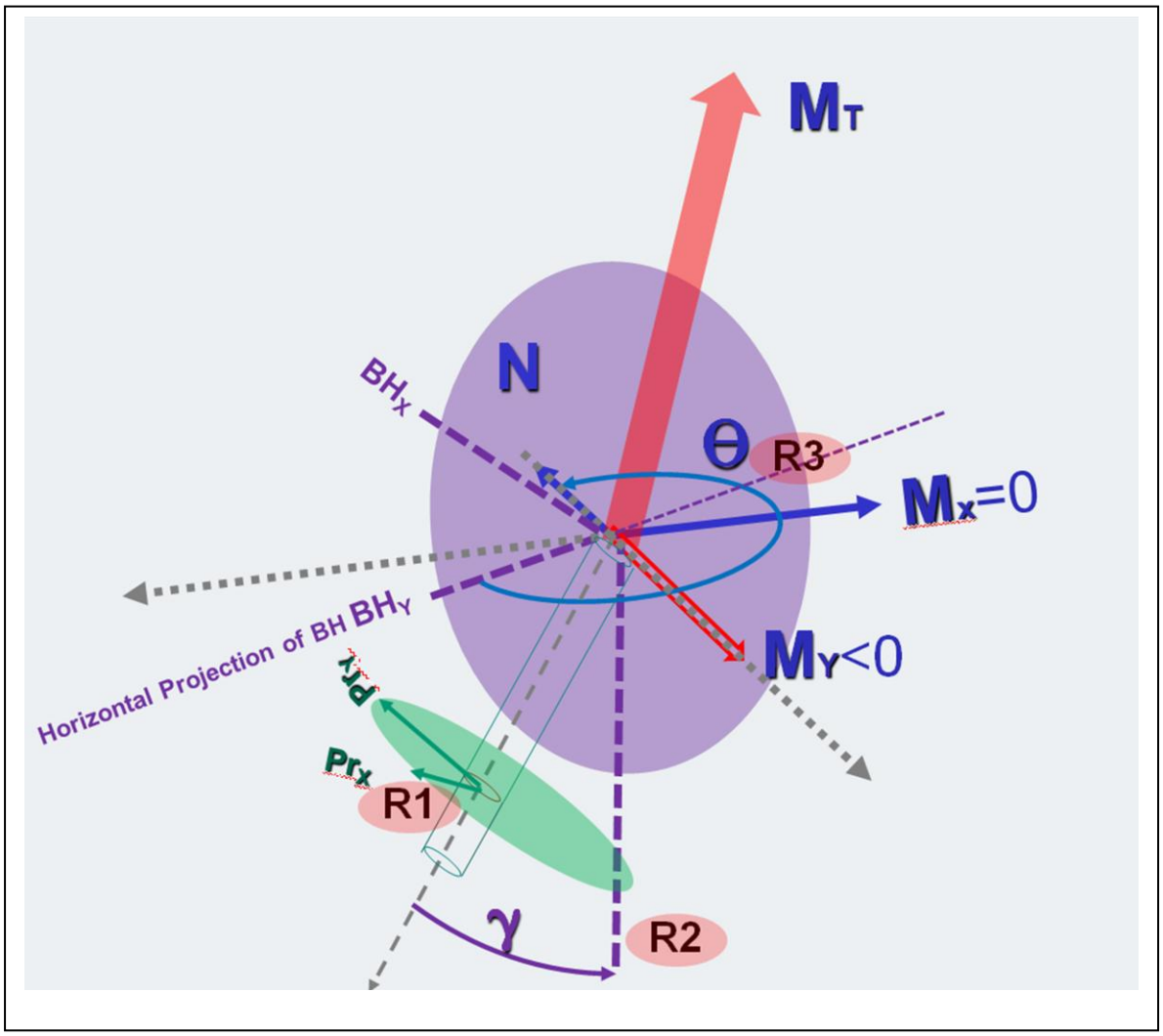

Figure 4-11: Magnetic field components of inclined borehole.

\Where:

m_X, m_Y, m_Z	Measured magnetic field
${}^{Pr}m_X$, ${}^{Pr}m_Y$, ${}^{Pr}m_Z$	Magnetic field components on plane of probe (Y= high side)
α	Rotation of probe off high side
${}^{BH}m_X$, ${}^{BH}m_Y$, ${}^{BH}m_Z$	Magnetic field components rotated to plane of vertical borehole
γ	Borehole inclination off vertical
Θ	Borehole deviation off North
M_X, M_Y, M_Z	Earth's magnetic field, $+M_Y$ = North, $M_Y<0$, $M_X=0$

Rotation		
R1	$\begin{bmatrix} m_x \\ m_y \\ m_z \end{bmatrix} \begin{bmatrix} \cos\alpha & -\sin\alpha & 0 \\ \sin\alpha & \cos\alpha & 0 \\ 0 & 0 & 1 \end{bmatrix} = \begin{bmatrix} {}^{Pr}m_X \\ {}^{Pr}m_Y \\ {}^{Pr}m_Z \end{bmatrix}$	Rotation on plane of probe aligning to ${}^{Pr}m_Y$ as highside
R2	$\begin{bmatrix} {}^{Pr}m_X \\ {}^{Pr}m_Y \\ {}^{Pr}m_Z \end{bmatrix} \begin{bmatrix} 1 & 0 & 0 \\ 0 & \cos\gamma & \sin\gamma \\ 0 & -\sin\gamma & \cos\gamma \end{bmatrix} = \begin{bmatrix} {}^{BH}m_X \\ {}^{BH}m_Y \\ {}^{BH}m_Z \end{bmatrix}$	Rotation on plane of Borehole (Incl)
R3	$\begin{bmatrix} {}^{BH}m_X \\ {}^{BH}m_Y \\ {}^{BH}m_Z \end{bmatrix} \begin{bmatrix} \cos\theta & -\sin\theta & 0 \\ \sin\theta & \cos\theta & 0 \\ 0 & 0 & 1 \end{bmatrix} = \begin{bmatrix} M_X \\ M_Y \\ M_Z \end{bmatrix}$	Rotation on plane of Surface (Decl)

$[m]\,[{}^{Pr}rt]\,[{}^{incl}rt]\,[{}^{dcl}rt] = [M]$
$\begin{bmatrix} m_x \\ m_y \\ m_z \end{bmatrix} \begin{bmatrix} \cos\alpha & -\sin\alpha & 0 \\ \sin\alpha & \cos\alpha & 0 \\ 0 & 0 & 1 \end{bmatrix} \begin{bmatrix} 1 & 0 & 0 \\ 0 & \cos\gamma & \sin\gamma \\ 0 & -\sin\gamma & \cos\gamma \end{bmatrix} \begin{bmatrix} \cos\theta & -\sin\theta & 0 \\ \sin\theta & \cos\theta & 0 \\ 0 & 0 & 1 \end{bmatrix} = \begin{bmatrix} M_X \\ M_Y \\ M_Z \end{bmatrix}$

$M_X = m_X (\cos\alpha \cos\Theta - \sin\alpha \cos\gamma \sin\Theta) - m_Y (\cos\alpha \sin\Theta + \sin\alpha \cos\gamma \cos\Theta) - m_Z \sin\alpha \sin\gamma$

$M_Y = m_X (\sin\alpha \cos\Theta + \cos\alpha \cos\gamma \sin\Theta) + m_Y (\cos\alpha \cos\gamma \cos\Theta - \sin\alpha \sin\Theta) + m_Z \cos\alpha \sin\gamma$

$M_Z = m_X (-\sin\gamma \sin\Theta) - m_Y \sin\gamma \cos\Theta + m_Z \cos\gamma$

$M_X = 0$

$$\alpha = \operatorname{atan}\left[\frac{(m_X \cos\Theta - m_Y \sin\Theta)}{(m_X \cos\gamma \sin\Theta + m_Y \cos\gamma \cos\Theta + m_Z \sin\gamma)}\right]$$

Restricted by

$M_Y = m_X (\sin\alpha \cos\Theta + \cos\alpha \cos\gamma \sin\Theta) + m_Y (\cos\alpha \cos\gamma \cos\Theta - \sin\alpha \sin\Theta) + m_Z \cos\alpha \sin\gamma < 0$

In the northern hemisphere

4.9.2 Individual temperature sensor response

Figure 4-12: MW 25 example of raw data collected against time shows variability in sensor response while stationary in a lined borehole.shows a section of a raw TVP log through a portion of UW25, the borehole described in detail in the main text. The portion of the data where the probe is stationary consists of 120 individual readings with each sensor. Standard statistical parameters for each sensor are provided in Table 4-3: Statistics of stationary data (Figure S1) 140.8-142.8 min. These data show that individual sensors have a maximum standard deviation of 0.0003 C° and the maximum span of readings of 0.0015 C°.

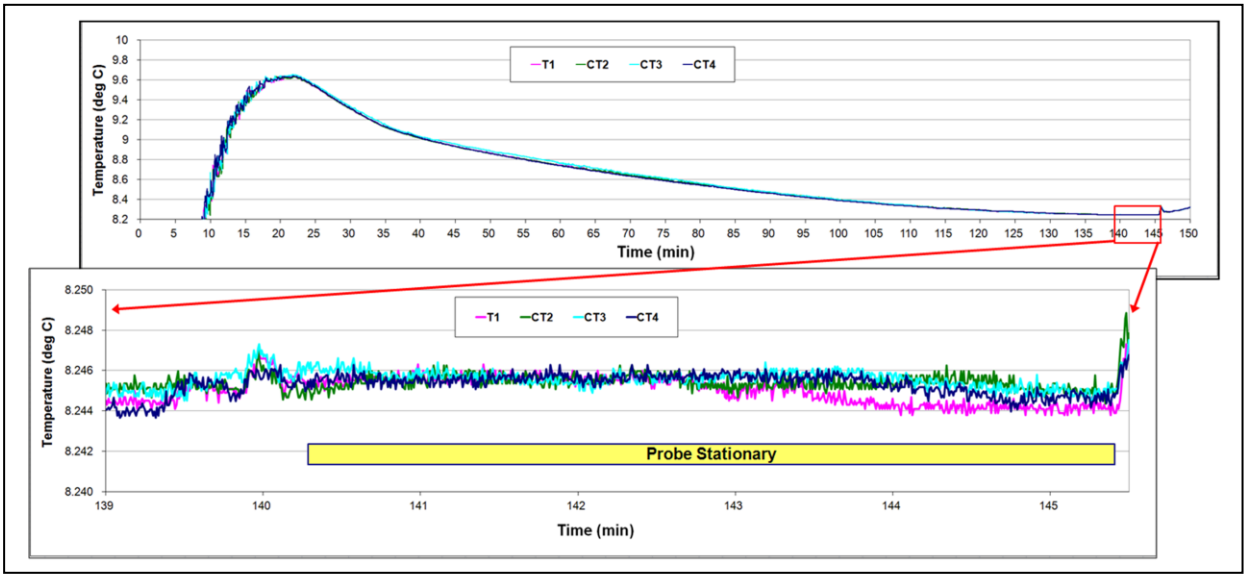

Figure 4-12: MW 25 example of raw data collected against time shows variability in sensor response while stationary in a lined borehole.

Table 4-3: Statistics of stationary data (Figure S1) 140.8-142.8 min

(all values °C)	T1	T2	T3	T3
Mean	8.24561	8.24965	8.07311	8.21924
Stand Dev	0.00022	0.00028	0.00025	0.00023
Max	8.24630	8.25030	8.07390	8.21990
Min	8.24500	8.24890	8.07240	8.21870
Range	0.00130	0.00140	0.00150	0.00120
Offset		-0.00404	0.17250	0.02637

Chapter 5
Understanding Fracture Flow Effects on Temperature Logs – Modeling Results

5.1 Introduction

Over the past half decade, several advances in high sensitivity temperature logging have been made including the use of liners to limit borehole cross-connection, the active line source (ALS) techniques to create and monitor controlled thermal disequilibrium, the temperature vector probe (TVP), as well as data processing methods developed to present and analyse the results. Applied to fractured sedimentary rock, these new methodologies have indicated that many more potential flow zones may exist than otherwise suggested from previous work. The highly detailed examination of thermal processes has provided improved resolution and new insights, yet the details of the processes are shown to be more complex than originally assumed and new questions have arisen. However, because other technologies are not yet available to validate the details of ambient flow through fractured rock, and because of the high sensitivity required which makes laboratory simulation of the process a financial impracticality, validation and interpretation of the results are an ongoing challenge.

Numerical modelling of the processes, albeit subject to the limitations of fundamental inherent assumptions, offers a method of validating the ALS and TVP techniques as well as potentially resolving new questions raised by the fieldwork. Pehme undertook a numerical study of the basic thermal processes associated with the ALS technique ((Appendix B; J. Molson, supervisor/collaborator and E.O. Frind, editor) as part of the doctoral course requirements. This chapter expands[5] on two key elements of Appendix B that have particular importance in the interpretation of field data presented in chapters two to four and implications on the progression of the analysis of the results in a quantitative interpretation of hydrogeologic conditions.

5.1.1 Modelling Heat

Although the importance of temperature on physical and geochemical processes in hydrogeology has been recognized and incorporated into various models (e.g., Molson et. al. 1992, Su et al. 2006, and many

[5] *To differentiate the original text in this chapter from the work in Appendix B the latter is identified in quotations and italicized as well as referencing figures where applicable, some parallelism remains and similarity of limited text will occur where common subject matter is discussed*

more), most previous work deals with issues of large scale transport in porous (un-fractured) media. Few (e.g., Bataillé et. al, 2006) have worked within rock environments and little work in the hydrogeologic literature[6] deals with individual fractures and at the scale attempted here. Appendix B identifies a notable exception with implications herein:

"As part of their investigation of convection in a borehole, Berthold and Börner (2008) used a finite element code (COMSOL Multiphysics v3.3) to simulate detailed water movement and thermal variations, comparing their results to laboratory and field data. The authors chose to deal with the simulations in a 2D space; citing "computing time reasons" as the justification for avoiding a 3D simulation. However their treatment of the problem is fundamentally flawed in that by assuming a 2D representation, the borehole becomes a vertical plate of water thus reducing both the friction and the heat transfer to the rock and consequently increasing the tendency for convection. In the absence of flow, the situation would have symmetry in radial coordinates, but not in a Cartesian representation, thus their 2D representation was inappropriate. Intuitively one would then expect convection to appear as a vertically extended doughnut shape rather than the sphere Berthold and Börner show. In spite of these simplifications they predict convection cells to be of approximately the same vertical dimensions as the variations herein observed and noted in our field data."

Appendix B employs the numerical model Heatflow/Smoker (Molson et al, 2007; Molson and Frind 2012). Smoker is designed to simulate water movement through discrete fractures and in the surrounding matrix while accounting for fluid density variations as a result of temperature changes. The rock mass (and overlying overburden) is represented using 3D deformable elements and fractures are treated as 2D planar surfaces imbedded onto the element surfaces. The code derives a solution for the nonlinear transient coupled system defined by a set of flow and heat transport equations (Molson and Frind, 2012).

The modelling exercises described in Appendix B simulate the field procedures and the measurements made through the ALS process on a single lined borehole intersecting a planer horizontal fracture with uniform (controlled) flow. The system is allowed to stabilize (at 10°C) for 4 days, the borehole is then heated with a "line heater" for 6 hours and the system is allowed to return to thermal equilibrium. The process is repeated while varying individual or simple combinations of physical and geometric parameters and the effects on the transient temperature distribution are analyzed by interpreting the model data sets. By systematically increasing and decreasing individual parameters, the sensitivity of the system and the ALS technique to each parameter were ranked. The physical properties of the model were set to simulate conditions within a fractured dolomite (i.e. the Guelph and Cambridge field sites), but the range of parameters encompassed other sites (California and Wisconsin) as well.

[6] Although literature searches have included journals dealing with the petroleum, nuclear waste and hydrothermal issues, these were not exhaustive and there is potential that additional research exists.

The rectangular model domain has x, y and z dimensions of 20, 10 and 10 metres, respectively, and a horizontal fracture (1 mm aperture) is placed at z=5 metres (Figure 3-3). A 10 cm diameter vertical borehole is simulated at x=5, y=5 by creating a "cylinder" of elements with a porosity of 1, and thermal characteristics of water. A critical aspect of the model is that the well, fracture and surrounding vicinity (a square column, 0.4 x 0.4 x 1m of 1x1x2 cm elements) is finely discretized to accurately represent the detailed flow and temperature variations that might occur. The liner is simulated by assuming the outer elements of the borehole are impermeable (using a hydraulic conductivity of $1x10^{-55}$ m/s). The complete details of dimensions and discretization of the model are provided in Appendix B.

The results of systematically varying individual parameters of the simple single fracture model are described in Appendix B. The predicted variations in the thermal decay are assessed both from the temperature in the center of the borehole at the fracture intersection and at a reference point in the borehole adjacent to the unfractured matrix (1.5 m below the fracture) as each parameter is varied and compared against a "base case" (Figure 5-1 and Figure 3-4). The response predicted by the model is related to field work by noting the temperature values at those times in the decay process at which field data (cooling logs 1, 2 and 3) are typically collected. The difference between the measurement at the fracture and reference point is used to create an effective "relative cooling", which is plotted against the log time used to divide the thermal recovery into early, intermediate and late times. The logarithmic rate of the decline in late time[7] provides a robust systematic assessment of how the influence of the water moving through the fracture varies as the tested parameters change, e.g Figure 5-2 for the base case.

5.1.2 Conclusions Drawn from Sensitivity Analysis

The model parameters tested were ranked based on their influence on the late time rate of decline (Figure 5-3) and Appendix B presents 21 conclusions from the sensitivity study and 8 recommendations critical to field work.

Several of the conclusions are relatively straightforward but of critical importance[8] to future work:

[7] "Late Time" begins at the time at which the system had undergone thermal decay (as measured from the end of heating) as it was originally heated; if the hole is heated for 6 hours late time begins 6 hrs after the heater is turned off.

[8] Original numbering in Appendix B are provided e.g. (14)

1. The ALS process can be effectively and consistently divided into four stages: heating, early, intermediate, and late cooling. Although all four provide insights into the processes, the thermal behaviour of the system is most consistent during late cooling. (2)
2. The observed temperature is directly related to the energy introduced and inversely as a function of the dissipation of that energy, primarily depending on the thermal conductivity of the rock and the amount of water moving through the fracture. Within the range of parameters modelled herein, the relative cooling provides a simplified presentation of the complex relationship such that the amount of cooling is in some manner a function of the flow. (17)
3. Based on the tabulated and graphical comparison of the influence of the various model parameters on the characteristics of the log-log decline of relative cooling, it is apparent that background temperature, borehole diameter, rock thermal conductivity and location of the heater can all have as much or more influence on the log-log rate of decline in relative cooling than does the velocity of water moving in the fracture. Quantitative analysis of water movement will not be resolved as a simple function of the rate of decay on either a log-linear or log-log scale because too many variables exist that could influence the response. (18)

Two of the 21 conclusions have particular impact on both the qualitative and (future) quantitative interpretation of flow in fractured rock from application of ALS and TVP techniques and are further investigated with additional modelling herein:

4. The model indicates that convection may be occurring in the borehole in the vicinity of the fracture. However, it also appears that the stratification of hot over cool water above the fracture is a stabilizing influence restricting the upward limit of the convection cell. (10)
5. Although there appears to be a linear relationship between the relative cooling and the log of the water velocity, when the velocity is changed by varying the fracture aperture, the data no longer fits that relationship, indicating that total flux (m^3/s) rather than velocity is likely the quantifiable parameter. (20)

The issues of convection and fracture flow are discussed in the subsequent sections. Each is presented individually with: i) an introduction to establish context and to identify specific questions to be answered, ii) discussion outlining the results of additional modelling, field data and data processing completed and iii) specific conclusions are drawn.

5.2 Data and Discussion

5.2.1 Convection

The issue of thermal convection in boreholes was dealt with in larger diameter boreholes by Gretner (1967) and small diameters by Sammel (1968). From Pehme et al. (2007):

Sammel (1968) addressed the prospect of convection within an open borehole and showed that we should anticipate critical convection to begin at gradients of approximately 0.0035 to 0.0065 °C/m for a 4 inch diameter hole.

Sammel used data collected in two piezometer nests within shallow alluvial sediment deposits, each with a shallow (3m) and a deep (12-15m) well. He used differences in the temperature profiles in adjacent wells as evidence for convection and based on temporal thermal variations. He concluded that "in northern temperate latitudes water columns within 9 to 12 m of land surface in many wells will be thermally unstable during much of the year", and "temperature in thermally unstable water-filled holes may depart significantly from temperatures in the surrounding rock". His field data did not "clearly define the relationship between critical thermal gradients and theoretical critical gradients, but they suggest that the theoretical critical values are close to and probably higher than the actual ones".

We note that although Sammel's equipment was capable of measurements within 0.001°C it had a time constant of approximately 3 minutes which hampered his ability to measure temporal variations. Much of his and Gretener's (1967) work in larger diameter wells rely on the temperature variations over time as evidence for convection and neither gave any consideration to thermal variations being caused by water moving past the borehole.

Gretner (1967), Sammel(1968), Bőrner & Berthold (2007) and Cermak et al. (2008) all rely on forms of the characteristic Rayleigh number $\boldsymbol{Ra_t}$ (Equation 5-1) from Hales (1937) which describes the tendency of the system to convect based on thermal gradient $\boldsymbol{\nabla T}$ and a characteristic dimension $\boldsymbol{r}$. From Bőrner & Berthold, (2007):

$$\boldsymbol{Ra_t = \frac{\beta g \nabla T}{D_t \eta} r^4} \qquad \textbf{Equation 5-1}$$

with $\boldsymbol{\beta}$ the thermal expansion coefficient, ∇ T the thermal gradient, $\boldsymbol{D_t}$ the thermal diffusivity, η viscosity, and for which Gershuni and Zhukhovitskii (1976) indicate $\boldsymbol{r}$ is the radius of a vertical channel with circular cross section. When $\boldsymbol{Ra_t}$ exceeds the critical value $\boldsymbol{Ra_c}$ convection begins. Equation 5-2 is the $\boldsymbol{Ra_c}$ for a column where $\tilde{\lambda}$ is the ratio of the thermal conductivities of the fluid and the surrounding material.

$$\boldsymbol{Ra_{c\,(column)} = \frac{96}{5(1+7\tilde{\lambda})}\left[3(33+103\tilde{\lambda}) - \sqrt{3\left(2567+14794\lambda+\widetilde{26927}\tilde{\lambda}^2\right)}\right]} \qquad \textbf{Equation 5-2}$$

Detailed representations of the Smoker model simulations for the base case at medium and highly expanded scales (Figure 5-4) shows asymmetric temperature patterns exist within the borehole. In this example, the heater was set on the up-gradient side of the borehole and the thermal distribution shown is at a C2 condition. T1 would be read along the center of the borehole and the dashed circle represents the cylinder sampled by T2, T3 and T4. Figure 5-4A shows that the rock adjacent to the heater has been preferentially warmed during heating and supplies source of heat during decay that dominates the thermal gradient through the borehole above and below the influence of the water moving through the fracture. The expanded view along the flow direction Figure 5-4B indicates an upward extension of heat on the up-gradient, heater side and a downward extension on the down-gradient side away from heater. The response is asymmetric extending within the borehole from 4.84-5.34 (0.50m) on the up-gradient side and from 4.66-5.34 (0.68m) down gradient (using the 10.137 C colour change). The pattern across the Y plane is illustrated in Figure 5-4C and shows a nearly symmetrical distribution of temperature with the lowest values (a trough) on the outer cylinder sampled to be slightly below the plane of the fracture. Considerable variation is predicted between the Y=5m and either borehole wall side indicating that a two-dimensional representation in the X-Z plane would not apply.

Although the model accounts for density and viscosity changes as a function of temperature which are the driving forces for upward movement of water when temperature increases with depth, there is no provision for friction along the borehole wall which would act to stabilize flow, therefore, Smoker does not rigorously account for convection. The consistent occurrence of more irregularities in logs where the temperature increases with depth rather than when it declines supports the conclusion that convection is occurring in some cases. However, unlike Bőrner & Berthold (2008) who assume that convection accounts for essentially all of the variability observed in a temperature log, the field data previously shown and the Smoker model suggest flow through fractures remains the critical cause of inflections in temperature profiles. The issue warrants a more thorough consideration as it could have important consequences in fine-tuning the depth and interpretation of temperature anomalies. Specifically, the questions arising are:

- Does evidence of convection exist in the field data?

If it does,

- What is the form (shape) of the convection cells?
- What are the implications on identifying flow features (aberrations in temperature profiles)?
- How do key changes in conditions influence the details of the interpretation?

5.2.1.1 Conceptualizing Convection Cells

In many conceptual models (e.g. Bőrner & Berthold, 2008; Cermak et al. 2008), convection is depicted as some form of circular two-dimensional flow (Figure 5-5A). Their justification for simplifying numerical models to two dimensions is scant, the latter case referring to the arguments of Frick and Clever (1982) for convection between two parallel walls. Adopting Cermak et al.'s (2008) convention that warm water rises and extrapolating the distribution of temperature to what would be observed with the TVP probe in the presence of circular convection, some of the outside sensors (T2, T3 or T4) should measure a downward flow of cool water, while other outside sensors measure an indication of the warmer water rising, and T1 should be intermediate with a near linear increase with depth. Bőrner & Berthold depict convection as a series of vertically stacked quasi-circular cells with flow alternatively rotating in opposite directions. Cermak et al.'s (2008) models predict the circular pattern can become distorted with portions vertically overlapping and in some cases two cells shift to being beside each other. Cermak et al. acknowledge that implicit in the acceptance of this circular two-dimensional representation is that convection in a borehole acts in the same fashion as in a vertical slot with a vertical thermal gradient but do not address the consequences of that simplification.

Because the process is controlled by a balance of buoyancy when warm water rises into cooler water against frictional forces along the borehole walls, an alternative conceptual model for two adjacent convection cells is that the flow is cylindrical or "donut" shaped, with water either rising or declining in the center of the borehole and moving in the opposite direction along the borehole wall (Figure 5-5B). In this conceptual model, symmetry would be radial, not 2 dimensionally cardinal. In the anticipated TVP response, since the driver is the warm water from below (and assuming water moves up the middle), T1 would measure a local increase in temperature higher than the other three sensors and T2,T3 and T4 would all have similar negative deflections in their temperature profiles. If the flow direction reversed, then T1 is expected to be cooler than the other three sensors. In either case, the presumption in predicting the response of the TVP to borehole convection is that the sensors are accurately calibrated and the diameter of the probe relative to that of the borehole is such that both upward and downward flow are encountered by the sensors.

5.2.1.2 Evidence for Convection in Field Data

Figure 5-6A shows a 2 metre portion of TVP response in an ALS test in a 250m deep lined borehole (C6) at the Santa Susana Field Laboratory (SSFL) near Chatsworth CA. C6 is a 0.127 m (5 inch) lined borehole drilled through an inter-layered sequence of fractured sandstones and shales that generally dip at approximately 30 degrees (refer to Sterling et al. (2005), for a complete description of the geology of the

site). This borehole is chosen as an example because there is an overall increase in temperature with depth which promotes convection. Since the hole is lined, no vertical hydraulic gradient exists. However, the borehole is in a local depression with topography elevated by 15-20m on three sides, which combined with the overall geologic dip and large daily air temperature variations typical of a southern California mountain top, may create complex thermal patterns at depth.

Because of the length of the borehole and logistical limitations, the equipment and schedule of the ALS test were modified; C6 was heated for 10.5 hrs (at 14 W/m), the first and second cooling logs were started 14 hrs and 21 hrs after the heater was turned off, respectively. The first cooling log is collected after the beginning of "late time" on the thermal decay plot (Figure 1) and therefore will herein be designated as C2 and the second thermal recovery data set will be designated C3 to maintain consistency between labelling and timing.

The borehole intersected a large deep flow zone at 237mbgs; however, this discussion will focus on an intermediate-depth zone (~90 mbgs) as a typical example of results. Figure 5-6A includes the response from the four sensors of the TVP probe, as well as the vertical temperature gradient (over a 0.034 m span), the thermal deviation[9] of T1 and $\boldsymbol{Ra_t}$ based on the T1 response for the passive, and the first and second (C2 and C3) data sets. Differences between $\boldsymbol{Ra_t}$ and $\boldsymbol{Ra_c}$ are shaded (green) to highlight the depths at which the borehole temperature gradient is conducive to convection. The limits of the temperature plots for the passive and cooling logs differ to reflect the overall temperature shift during thermal decay, but in all cases the range (maximum-minimum) is the same so that the sizes of variations can be directly compared.

A linear calibration of the individual sensors was based on cross-plots of the T2, T3 and T4 sensors against the T1 data set from 20 mbgs to the bottom of the borehole using the passive logs. The comparison between the TC (average of T2, T3 and T4)[10] and T1 each smoothed over 5 m is used as an assessment of the appropriateness of the calibration to the C2 and C3 data sets. The difference between the two for the C2 and C3 data sets is less than 0.001C^{o} suggesting the calibration is reliable or that if error exists, it is randomly distributed between T2, T3 and T4. The probe uses magnetometers to determine direction; that data were also used to vertically adjust and align the temperature sensor

[9] A temperature log minus a smoothed version of itself (over 5 m); refer to Section 2.3 for details on calculations

[10] Refer to Chapter 5 for details of the Thermal Vector Probe (TVP) measurements and calculated parameters.

responses along the length of the borehole based on minor variations in the total magnetic field. Depth adjustments were less than 0.1m in either direction (upwards near the top and downwards towards the bottom) and in all cases both systematic and gradual. The consistency of the thermistor calibration and an estimated vertical alignment of sensor data to within 0.02m affords a highly detailed discussion of thermal patterns within the borehole.

Addition of heat in the ALS process creates "controlled disequilibrium" and the conceptual basis for the interpretation is that groundwater flow preferentially cools the borehole creating negative aberrations in the cooling logs. Figure 6B shows the data from Figure 5-6A with the estimated depth of the larger flow zones indicated as lines across the figure divided into three groups: red are distinct negative aberrations on the profiles of both C2 and C3 data, green are large aberrations in the C2 and minor ones in C3, blue are large in C3 but less distinct in C2. In all cases of green and blue, some form of minor aberration also occurs in the data set that wasn't used as the primary identifier for the pick. The passive data has not been used to identify flow zones because of the uncertainty of whether a positive or negative aberration from the norm represents flow. Over this portion of the borehole the C2 data exhibit the largest temperature aberrations while the C3 data indicate many more, but these are uniform in character. In both data sets the aberrations tend to be sharp at the bottom and elongated upwards. Examples of the three designations (red, blue and green) are discussed in detail below.

Based on the anticipated response of the TVP, convection is indicated at several intervals, particularly in the passive data. Zones where convection is implied by contrary (positive and negative) aberrations of different sensors at the same depth are shaded. Adopting a conservative approach, only those intervals are highlighted where the maximum individual sensor responses are different by more than approximately 0.01ºC, i.e. an order of magnitude larger than the sensor resolution. Given that warm water rises and cooler water descends, and assuming that the probe has not rotated[11] over the interval, the motion is described by:

- the colour of the shading,
- the direction and colour of the circular arrow, and
- the location of the arrow relative to the center of the column.

[11] Non rotation is assumed so that the character of convection can be readily colour coded on the figure. The assumption is inconsequential to the applicability of this analysis because the discussion deals with size and character only. An analysis of the implications to flow in the rock mass would require proper orientation in space, which is possible as the probe measures rotation with directional magnetometers.

The colour of shading indicates which sensor is warmest (thereby where water is moving upward) and the thickness of the convection cell. The colour of the arrow indicates which sensor is coolest (water moving downward). Adopting the convention that T2 (blue) is on left side of the column, the lateral position of the arrow indicates the general location of the cell relative to the center of the borehole. The direction of the motion through the center of the borehole is based on whether the T1 response is most similar to the cooler or warmer response, or independent of both. A single arrow is consistent with the circular conceptual model of convection and two arrows indicate the cylindrical model applies. Where two arrows occur, the center of the borehole (T1) is either: warmer (red arrows) with water moving up the middle, or cooler (blue or purple arrows) and downward movement in the center. There are many more occurrences of circular motion implied than cylindrical. However in very few cases does the data indicate that the circular cell is centered in the borehole, most often the pattern is offset to one of the sides of the borehole and highly asymmetrical. The implication is that although the convective water motion is most often circular, the pattern is distorted and could not be represented in only two dimensions.

In general, using the arbitrary threshold of differences greater than 0.01C°, there are many more convection cells indicated in the passive data than in either the C2 or C3 results. This could result from either or both the length of time available for convection cells to form in a passive state or the dominance of the horizontal over the vertical thermal gradient during thermal recovery. Many, but not all, of the implied convection cells are associated with either a spike in Ra/Rc and in several cases, particularly in the C2 and C3 data, a Ra/Rc spike occurs without any indication of convection. Where there is coincidence of a Ra/Rc spike and an interpretation of a convection cell, the spike tends to occur at the base. Although the lack of correlation between Ra/Rc spikes calculated from T1 and convection is consistent with the circular model, basing Ra on any of the other individual sensors would not improve the comparison. The broader implication is that the critical Raleigh number as calculated from a single sensor is not a reliable indicator of convection and likely an oversimplification of a complex balance of forces.

Figure 5-6C shows expanded views of portions of Figure 5-6B for examination of distinct examples of the three classes of aberrations identified and identified as green, blue or red lines. At 90.31mbgs there exists a flow zone (green) identified by a large aberration in C2 with a minor response in C3. There is a 4-6 cm offset in the elevation of the base of the feature as measured by the different sensors in the C2 data. The C2 RA/Rc indicates convection should exist and the offset of the profiles suggest convection (a distorted circular type) below the flow conduit. Based on three of the four sensors increasing in

temperature in the passive data, the anomaly appears as a positive aberration under ambient conditions[12]. The flow feature forms the boundary between two convection cells in the passive data, the lower has the characteristics of a cylindrical pattern and the upper that of a circular form. At 90.12mbgs a distinct aberration in C3 data indicates flow (blue) yet there is little change in the character in any of the C2 data, presumably sufficient time has not elapsed to create the aberration. The flow feature exists close to the apex of an aberration in the passive data, but with characteristics of distorted circular convection. A similar flow zone exists at 90.95mbgs, however in this case there is the possibility that convection (distorted circular) is also occurring in the C3 data. This feature corresponds to a weak convection cell in the passive data but with generally a negative (cooler) aberration in the profiles at 90.92mbgs.

The clearest example of an aberration that is distinct in all data sets (red) occurs at 91.18mbgs. The patterns are irregular and distorted in both C2 and C3 with secondary inflections in individual profiles which imply that the thermal aberrations could be created by 2 fractures in close proximity. Both the C2 and C3 data exhibit separation of individual sensor responses, but only the C2 data meets the threshold for assigning a convection cell. A distinct circular convection cell exists above this flow feature in the passive data. Although it is not entirely clear because of the pattern of the individual responses in the passive data, it is likely that this feature flowed cooler than the surrounding rock under ambient conditions.

Although the C2 and C3 aberrations examined above are relatively distinct, even where the differences between the sensor responses did not meet the arbitrary criteria chosen for designation of convection there are indications of some potential for water movement within the borehole. The detailed images of the C2 and C3 data in Figure 5-6C show that the base of an individual aberration as measured by any of the thermistors can vary in elevation by as much as 5-6 cm in this portion of the borehole creating a potential error in the interpretation of the depth of the flow features. A critical issue identified by the sensitivity analysis (Appendix B) was the effects of the location of the heater relative to the flow direction and the center of the borehole: i.e whether heating is up-gradient or down-gradient of the center of the borehole, or at a 90º angle towards the side (side-gradient). These offsets are of interest both from the perspective of the accuracy of identifying the elevation of the flow feature for detailed comparisons with other data such

[12] The arrival of relatively warmer water at a fracture under ambient thermal and flow conditions in an environment where temperature generally increases with depth would imply upward flow, but in this case because the borehole is in depression, the surrounding rock may be at higher temperature at the same elevation, flow could be horizontal or even somewhat downward.

as core logs and televiewer images, but also for assessment of whether the Smoker model can simulate such detail.

Figure 5-7 shows the modelled C2 profiles for the base flow case along the center of the borehole and at the four cardinal coordinates (on the measurement cylinder of the probe) for the three heater locations. In each case the profiles are shown both as would be measured and as thermal deviation in the same fashion as the field data presented above. In Figure 5-7 the largest aberration is created when the heater is up gradient, approximately 0.05 C° in comparison to approximately 0.04 and 0.03 C° for the heater down and side–gradient, respectively. The up-gradient heater creates a larger difference in temperatures around the borehole (approximately 0.02 C°) depending on where the sensor measures the profile. The vertical span is similar in all three cases, slightly broader than the span of the largest C2 aberrations observed in Figure 5-6B. As observed in the field data, in all cases the aberrations are slightly elongated upwards, more so when the heater is up-gradient, although the degree of distortion depends on the location of the sensor. The offset in the elevation of the base values of the individual profiles varies from .012 m with the heater up-gradient to 0.08m with the heater down or side-gradient. In all cases the base of the central (T1) profile provides the most accurate depth estimate. The depths of the base values of the surrounding profiles span the fracture with most occurrences above the fracture. The sensor closest to the heater is always the highest in elevation implying that the location of the heater and not flow will have most influence on the direction of flow within a convection cell.

Although the exact details of the model response do not duplicate the field data, the general characteristics are similar. Given the differences in the parameters between the site and the model and that the probe samples the circumference of the measurement cylinder at three points which are not necessarily optimally located, the general similarity in response strongly supports confidence in the use of the model to improve understanding of the field situation. We cannot proportion the influence of the location of the heater, the water movement through the fracture and other characteristics on the patterns observed and the detection by the TVP probe. To better understand the predicted change in convection patterns, two other variables, borehole diameter and flow velocity through the fracture are briefly examined.

Figure 5-8 shows an expanded view of a 0.20 m diameter borehole, with the heater up-gradient and all other parameters as in the base case at C2 time. Since the measurement cylinder is fixed it includes a smaller portion of the borehole, and the base values are more difficult to identify because of the breath of the aberration. The vertical extent of the aberration is approximately a metre, and highly skewed upwards. The base values of all of the sensors would be above the fracture, T1 by 0.05m, and the range of

elevations for the bases of the other sensors is predicted to span approximately 0.20 m. Consistent with the formulation of Hales (1937) and the work of others (e.g. Sammel, 1968) the model indicates the influence of convection will increase dramatically with borehole diameter. The Smoker simulations imply the individual responses of the sensors are vertically elongated and details may be more difficult to differentiate in data collected within a larger diameter borehole.

In a relatively extreme example, Figure 5-9 shows the predicted influence of increasing the velocity of the water flow through the fracture to 0.45 m/s by increasing the aperture of the fracture from the base case from 0.001 to 0.01m. Similar to the effect of increasing borehole diameter, the span of the aberration increases to approximately 1m and the up-gradient side measurements of the profile become strongly skewed upwards and on the down-gradient side slightly downwards. The base of the aberrations could vary in depth by 0.10 m, but in this case the base of the T1 sensor response would coincide with the depth of the fracture. Although both the increase in the borehole diameter and the increase in water velocity (flow) increase the breadth of the aberration, the differences in the characteristics of the base values indicate that the change in diameter borehole has a larger influence on the potential for convection.

5.2.1.3 Convection: Summary and Conclusions

It is important to re-iterate that this application of "Smoker" for characterizing convection is intended as a guide and not an exact duplication of field results. Neither the details of the code nor the adaptations employed to represent the scenario (such as the assumption of 100 percent porosity in the borehole) allow a claim of rigorous representation of the processes simulated. The TVP sensors do not extend to the borehole walls and therefore interpretations of thermal patterns across the borehole and water movement are based on measurements of only four locations along the 4 cm diameter central cylinder and are an inherently limited sampling of the field conditions. However, Smoker does provide a three-dimensional characterization that is generally a good match with the field data (with respect to temperature patterns, dimensions and rates of thermal decay). In addition, there are practical limitations to collecting such highly detailed temperature data (i.e. the probe may not be centered, the protective cage will create eddies disturbing the measurement, and the difficulties in calibration) that will add inherent variability to field data. Therefore, some discrepancies are to be expected between the simulations and the data, and yet it is reasonable to consider the Smoker results a good representation of the thermal and hydraulic processes.

The model predicts increased effects of convection with increased borehole diameter, consistent with the analysis of Sammel (1968) and others. However, a more detailed application of theoretical principles to field data, for example use of the indicator Ra/Rc (from T1) as an indicator of the location or size of convection cells is inconsistent. In most cases the patterns of convection in the field data are characteristic

of a distorted circular convection although several cylindrical patterns were also identified within the limited portion of the borehole presented in detail.

There is much less indication of convection within the ALS process than in the passive data as overall horizontal rather than vertical thermal gradients dominate after heating. Figure 5-10 shows the general characteristics of the convection model suggested from the field data and supported by the Smoker model. It is likely that convection will occur but that it is not arbitrary, that there is a driver where flow through fractures preferentially cools creating a large gradient below the fracture. Although the upper side of the aberration creates a balancing force that isn't as strong, witness the upward elongation of the aberrations in the field data which is duplicated by the modelling. The data and model supports the conceptual model of a complex distorted combination of circular and cylindrical movement. The field data shows that to be the case at some locations but at others the patterns are inconsistent and simple shifts of the ALS data align results well, implying that although the elevation of the thermal aberration may change slightly across the section of the borehole, a convection cell may not exist.

Although in most cases where an indication of a flow zone exists it can to some degree be identified in both C2 and C3 data, in many cases the aberration was distinctly stronger in one or other data set. When an aberration is present in C2 and weak in C3, it is reasonable to assume the effect has dissipated. When the aberration is indistinct in C2 and clear in C3, it is likely that the response is in intermediate time and has not yet fully formed; more investigation is required to better understand these processes. However, the process is in overall thermal decay and a normalization procedure will be required to accurately compare the C2 and C3 responses.

The presence of strong circular convection does not necessarily create an aberration in the T1 response at the fractures of the passive logs, in all cases if an aberration distinctly formed in a cooling log it will be clearly seen in the T1 profile. The size and alignment of the base of the negative aberrations (i.e. at the troughs) vary with the location of the heater, water velocity and the borehole diameter. In most cases convection creates an upward shift of the ALS effect that can span 10-20 cm. The T1 profile consistently provides the best estimate of the actual location of the fracture, but in larger diameter holes, there will be a tendency to interpret the fracture to exist above the actual depth, potentially by as much as 5-10 cm.

Although the predominance of circular convection patterns is consistent with the Cermak et al.'s (2008) two-dimensional representation of a borehole as a slot, the TVP data show the distortion exists in three dimensions in both passive and ALS data sets, a conclusion supported by the Smoker simulations. This analysis indicates that the system presents a highly complex four-dimensional problem in the simplest

case. Clearly neither cardinal nor rotational symmetry apply and simplifying the condition into a two-dimensional model is inappropriate. In an ALS-driven disequilibrium, symmetry is further compromised because the location of the heater will be controlled by the inclination of the hole and the flow direction is unlikely to be uniform throughout, adding additional complexity. The response of all four sensors from both C2 and C3 data sets should be considered in the ALS analysis. Although additional work and more comprehensive models are required to better understand the relationship between the ALS response and flow, the existence of a cause and effect is supported and holds promise for the application of the ALS to quantify flow.

5.2.2 Influence of Groundwater Flow

5.2.2.1 Background

The sensitivity analysis (Appendix B) includes tests wherein the hydraulic gradient is varied to control the movement of water through the fracture with the heater both up and down-gradient (positions A and C). A strong linear relationship (R^2s = 0.999) between the relative cooling (temperature 1.5m below – temperature at the fracture) and the water velocity at a log scale was implied based on an initial three tests. However, calculating additional points to expand the data set and duplication of existing ones (the same velocity but based on a different fracture apertures) resulted in a poor fit to the original relationship (Figure B34). Appendix B concluded that the change in the relative cooling observed was not a simple relationship with velocity and speculated that the controlling factor may instead be groundwater flow (the volumetric rate of water) passing the lined borehole. This section expands on the initial models completed in the sensitivity analysis and addresses the questions:

- Although relative cooling has a trend with velocity does flow provide a more systematic and reliable variation?

If so:

- How does the relative cooling vary with flow?
- What are the implications for quantifying flow from temperature logs?

Molson and Frind (2012) relate velocity (v,ms^{-1}) to the hydraulic gradient (∇h) with the relationship wherein 2b is the full fracture aperture (m), ρ is the water density (1000 kgm^{-3}) and g the gravitational

acceleration (9.8 ms^{-2}). The viscosity of water, μ (kg/m/s) varies with temperature according to Equation 5-4 (Molson and Frind, 2012).[13]

Equation 5-3 $$\boldsymbol{v = \frac{-(2b)^2}{12\mu}\, \rho g \nabla h}$$

Equation 5-4 $$\boldsymbol{\mu(T) = 0.001787 * e^{(3.073\times10^{-2}T + 1.303\times10^{-4}T^2)}}$$

5.2.2.2 Data and Results

Twelve additional model simulations (designated D39, D50 through D60) were conducted with varying hydraulic gradients (∇h), fracture aperture (2b) and heater locations (A or C) to explore the relationship between the degree of cooling and flow rate through the fracture. Table 5-2 summarizes the results for these and previous models. Flow rate (m^2/s) is based on the volume of water passing through a fracture per metre transverse width, based on the velocity established by Equation 3. The relative cooling (°C) is tabulated according to the heater location (A or C) and the time from the initiation of the model (4.5 d, 5 d or 5.25 d) representing ALS cooling logs C2, C3 and a potential later C4 respectively. In all cases heating occurred from 4 d to 4.25 d with the 20 W/m heater. All other base case parameters were left unchanged. Note, only with the flow at its lowest rate does the relative cooling approach the limit of detection with the IFG probe.

Figure 5-11 shows the relative temperature drop (during cooling) against log(flow rate) with the heater up-gradient[14] (A) and Figure 5-12 shows the same relationship with the heater down-gradient (C). Both Figure 5-11 and Figure 5-12 show the relationship between relative cooling and log(flow rate) to be linear over well-defined phases with distinct changes between each. Both very obvious and also subtle differences exist between these phases. When the same flow rate is obtained ((log(flow rate) = -3.5) with different velocity-aperture parameters and with the heater at A), there is some minor scatter of points at 4.5 d but the difference is essentially undetectable at this scale for 5 d and 5.25 d. The cooling is based on the central value at the fracture (X,Y,Z = 5.00m), which, as discussed above, may be slightly different

[13] Other researchers (e.g. Berthold and Börner, 2008) use alternative equations to estimate μ which can lead to a 35% difference in velocity values using Equation 5-3. See Appendix B section for additional discussion.

[14] To minimize confusion within discussion that includes both hydraulic and thermal gradients, the terms up-gradient and down-gradient are reserved for the direction of the hydraulic gradient only (i.e. down-gradient is towards the positive X direction in the model) and "flow" refers to water movement exclusively. Thermal or temperature gradients are explicitly referred to as such.

from the base value of the aberration. Whether the subtle differences between the repeated points are a result of convection or modeling error is beyond the scope of this effort and for this discussion inconsequential.

Table 5-1 summarizes the individual slopes of the line segments identified on Figure 5-11 and Figure 5-12 as well as the associated inflection points. The lines in both figures intersect the x-axis at approximately the same points (log(flow)= -6.16 (A) and -6.4 (C)), indicating that the lower limit for the creation of a temperature anomaly with the ALS technique is at a flow rate of approximately $5.6x10^{-7}$ m^2/s (~0.05 m^2/d). Above this limit, the relative cooling increases under what will be referred to herein as "low flow" conditions. When the heater is up-gradient (A) the slope of the line is approximately 1.8 times greater (1.80 - 4.25d, 1.75 - 5.0, 5.25d) than when the heater is down-gradient (C).

At the other extreme, when rates of water movement through the fracture are within the "high flow" regime, the relative cooling varies little with increased flow. With the heater up-gradient (A), the amount of cooling does not change when flow is above the threshold of 7.94×10^{-5} m^2/s at any of the times plotted. With the heater at C, a (slight) increase (~10^{-3} C°/log(m^2/s)) occurs at both 5d and 5.25d under high flow conditions. However earlier, at 4.5d the sensitivity of relative cooling to flow is approximately 4 times greater. The transition zone from low to high flow regimes, labelled as "intermediate flow", is not gradual, but is also linear when the heater is up-gradient. The intermediate flow regime is of very short duration and not well defined when the heater is down-gradient (C); whether the transition is linear or a simple inflection cannot be resolved from this set of models. The existence of inflection points in the relative cooling vs. flow relationship implies critical conditions (thresholds) occur, related to either or both geometry and flow which control the slope of the line.

5.2.2.3 Discussion

It is important to understand the process that creates the subdivision into linear segments in Figure 5-11 and Figure 5-12. Figure 5-9 shows that as the velocity of the water in the fracture increases, the vertical extent of the aberration expands, potentially influencing the reference value for the relative cooling. Examination of the individual model results shows the background is relatively uniform relative to flow and the linear sections are a function of the temperature variation at the fracture only and not a combination of varying conditions at both the fracture and the reference point.

To examine the nuances of what occurs during the linear sections of the flow-relative cooling graphs, Figure 5-13 presents a matrix of enlarged views of the borehole at 4.51d, 5.01d and 5.51d with flow rates at the middle of each linear segment when the heater was up-gradient (A) and Figure 5-14 is a comparable

matrix where the heater was down gradient (C). In the low flow case (top row) of Figure 5-13 the rock above and below the fracture on the up-gradient side is warmer than the down-gradient side (Figure 5-9) and a halo of warm water exists as heat is conducted against groundwater flow and a broad plume of elevated temperature extends on the down gradient side of the borehole. The heat transfer is inversely related to temperature gradient and the cooling effect at the borehole wall is therefore low. As flow increases, the breath of the warm water "halo" decreases, increasing the thermal gradient at the borehole wall and the effective cooling on the up-gradient side while on the down-gradient side of the borehole the thermal gradient remains relatively uniform. When the flow is increased above 2.51×10^{-5} m^2/s (second row) the both temperature along the up-gradient borehole wall becomes uniform, as does the heat transfer into the water on that side of the borehole. As intermediate flow increases the temperature gradients along the up-gradient side remain uniform while the plume of warm water on the down- gradient side cools, progressively increasing thermal gradients and consequently heat transfer. Eventually in the final stage, as flow further increases, there is no indication of any down-gradient "plume" of heat, implying the rate of energy transfer to the water is uniform around the borehole and no longer varies with increasing flow rate, consistent with the observation of a horizontal line in the high flow regime above a critical threshold in Figure 5-11.

When the heater is down-gradient, the heat energy is stored in the rock on the down-gradient side of the borehole. Figure 5-14 shows in the low-flow case, only a minimal backward extension of the temperature plume occurs against the hydraulic gradient creating a relatively high and near uniform heat flow rate, while both the temperature change and heat transfer along the down-gradient side of the borehole is low. As flow increases, the thermal gradient becomes uniform along progressively more of the circumference of the borehole until ultimately only a gradual increase in heat transfer occurs along the down-gradient side of the borehole with increasing flow. The implications of these observations are similar to those from the case when the heater is up-gradient, suggesting that the slope of the line is a function of an interaction between the rate of heat transfer as controlled by the temperature gradient across the borehole wall and the portion of the circumference across which that energy transfer is uniform (i.e. where the gradient no longer changes with increased flow). The rate of water flow controls whether the cooling along the surface of the borehole wall extends radially outward or if heat is "washed" down gradient. The systematic increase in the portion of the circumference where heat transfer is constant relative to the changing gradients, results in the log linear function of relative cooling against flow through the fracture.

As flow increases beyond specific thresholds, the characters of the heat transfer along the up-gradient side of the borehole remains uniform and only those portions of the borehole that continue to vary control the rate of increase in relative cooling. When the heater was up-gradient there were three stages; low flow -

with a gradual (albeit different) gradient on all sides of the borehole, intermediate flow – with the gradient changes occurring primarily on the down-gradient side of the borehole and, high flow with a uniform gradient around the entire borehole. When the heater was on the down-gradient side, the thermal gradient on the up-gradient side of the borehole is always uniform which makes the low flow condition (the heater at C) analogous to the intermediate flow situation when the heater was up-gradient (at A). This is consistent with the observation that the slope of the low flow segment with the heater at C is similar to the intermediate flow condition rather than the low flow condition when the heater was up-gradient (Table 5-1) and that in all cases the transition to the high flow condition occurs at approximately the same flow rate. Attributing the character of the cooling-flow relationship to changing exposure of the liner is consistent with the observations made from the model.

If the location of the heater relative to the direction of water movement is known, flow could be estimated based on the relative cooling observed at any time over the late cooling period by referring to a set to type curves. Multiple estimates from several logs collected at different times would improve confidence in that estimate. However, once a "high flow" condition is reached, the models indicate that accuracy will decrease dramatically such that the prediction would be a "greater than" value if the heater is up-gradient of flow. However, the characteristics of the relative cooling vs. flow curves apply to the specific conditions (background temp, borehole diameter etc) that were maintained constant in this phase of the modelling process. The borehole diameter, the thermal conductivity of the rock and the amount of heat transferred to the system would also play an important factor in the slopes of the linear sections as the available area for heat transfer would increase and thermal gradients vary. Figure 5-15 and Figure 5-16 show additional points to the low flow condition (when the heater has been up-gradient) for cases of varying rock thermal conductivity and heating time increased to 12 hours respectively.

Figure 5-15 shows the slope of the rate of change will increase by a factors of approximately 28 to 45 percent (varying over time) if the thermal conductivity decreases to 2.4W/m2/C. A repeated simulation with thermal conductivity increased to 4.8 W/m2/C confirms a comparable decrease in predicted slope of the relationship. Figure 5-16 compares the change in cooling with log time were heat is added for 12 hours, again showing an increase in the slope of the relationship between cooling and flow within the "low flow" condition. The systematic decay in late time suggests similar trends are a reasonable expectation when other parameters are varied, and additional modeling is required to establish those trends, (see conclusions below).

An important common characteristic of Figure 5-11, Figure 5-12, Figure 5-14 and Figure 5-16 is that the Smoker model predicts that below approximately 5.6×10^{-7} m^3/sec (0.05 m^3/day), there is no difference in

temperature at the fracture relative to the rock mass and, therefore, flow cannot be detected with the ALS technique. Figure 5-17 shows the combination of velocity and fracture aperture conditions wherein the flow is detectable (green) and those where it is not (red) based on the specified threshold and Equation 5-3. The practical consideration is that a transition zone would likely exist above the theoretical detection limit where the confidence is reduced (red shading extending slightly above the threshold line). Although the consistency of the detection limit as parameters are varied implies this depiction of a threshold based on the model results is a convenient summary of the limitation of the ALS technique, however comparison against other analysis of the SSFL site indicates possible inconsistencies. Early work with a two-dimensional hydraulic model (Fractran) at the site is based on both published work (e.g. Sterling et al., 2005) and 33 packer tests distributed between two boreholes (Sterling, 1999). The data were used to develop a conceptual model in which the fracture frequency is 0.9 per metre, the mode of the fracture aperture and velocity histograms are 125 microns and 5 km/yr, respectively. Based on the threshold established above, most of these flow zones would be undetectable with the ALS technique. Yet analysis of the ALS data collected at the site in all six boreholes tested identifies numerous zones of ambient flow based on thermal aberrations (with magnitudes well above the instrument's threshold limit and confirmed in multiple data sets), many more so than the number of individual fractures identified by any other technique. If the analysis of the field data is accepted and more flow zones exist, either the detection limit as modelled in Smoker or the conceptual model developed from Fractran, or both, are inaccurate. However, attributing the inconsistency to a simple incongruence between the models belies the issue that each analysis is based on many individual assumptions embedded in the fundamental equations that may not apply in this case. In addition, it is unlikely that a process that progresses from combining the number of fractures identified from core, with hydraulic transmissivity from a small number of packer tests to establish hydraulic apertures limited and a two dimensional Fractran model to estimate velocity that is consistent with a detection limit from simplified single fracture model of temperature. The site conceptual model relies on proper identification of flow zones and accurate estimates of transmissivity from straddle packer tests, for which the techniques used to establish values are undergoing continuous improvement (e.g. Quinn et al 2011). These tests rely on several field related factors (such as well development) and theoretical assumptions, for example discussion persists in the literature (eg. Brush and Thomson, 2003) regarding the details of the Navier-Stokes flow equations and the most appropriate assignment of values to the aperture of a fracture. Approaching the discrepancy from the other perspective, work is needed to better model the ALS process in a lined borehole with a more robust simulation of the conditions. Such inconsistencies are acknowledged and will require resolution, but identification of the potential cause(s) is also beyond this application of the model and presents another opportunity for future investigation.

5.2.2.4 FLOW: Summary and Conclusions:

The additional sensitivity analysis with the Smoker model confirms that the temperature change at the fracture in the ALS process is a log-linear response to the volumetric water flux through the fracture rather than a response to only the fluid velocity. The slope of the relationship between the degree of ALS cooling and flow depends on the characteristics of the matrix, borehole geometry and, critically, the position of the heater relative to flow and the measuring point. For any given set of geometric parameters, the log-linear relationship changes at critical flow rates which occur as increasing flow makes the heat transfer through portions of the borehole wall become uniform. Ultimately above a flow rate of approximately 10^{-4} m^2/s in the fracture, the amplitude of the thermal aberration becomes near constant and resolution of further increases in flow is poor to nonexistent. The results indicate that a consistent lower limit exists for the detection of flow ($5.6x10^{-7}$ m^2/sec per metre across the fracture). This lower limit is above what would be expected based on the large number of flow zones identified with the ALS technique and the flow rates indicated by other analyses. However within the individual analysis paths that has led to the inconsistency are several opportunities for improvement and there is considerable potential for reconciliation of the discrepancy.

The consistencies in observations from the Smoker model are not however conclusive proof that this is the root cause of the patterns observed and more analysis is required. As with other aspects of the ALS process, these observations create an internally consistent model of behavior but one against which methods of independent corroboration are unavailable.

In conclusion, the modelling indicates that there is considerable likelihood that the ALS techniques can be used to quantifiably predict ambient flow within a fracture. It appears likely that flow will need to be determined with the use of the TVP probe and a system of type curves based on thermal decay rates for a particular borehole condition (diameter, thermal conductivity of the rock ambient temperature etc.). The details of that relationship are beyond the scope of this work and some modification of the Smoker model to specifically address the ALS process and improved simulation of the borehole is advisable to increase confidence in the relationships.

5.3 Models: General Summary and Conclusions

Field data presented here, as well as in Chapters 3 and 4 show the ALS technique is a robust tool for the identification of many flow zones and provides a qualitative indication of water movement through the rock. However, the nuances of the thermal decay are still incompletely understood and the confidence limits are not yet fully established. Incremental steps in the process of refining the ALS technique from basic identification and qualitative comparison, to a quantitative estimate of the amount of water moving

through the fractures requires a better appreciation of the details of the heating process and subsequent thermal recovery as temperatures return to ambient levels. A critical issue is the lack of other techniques against which to compare results that can be applied at the level of detail that temperature logging provides and the scale at which fractures facilitate flow. Numerical modelling provides a method for simulating the processes at the level of detail required to improve understanding of the ALS and thermal processes.

Convection is ignored in many of the applications of temperature logging for identifying fractures presented in the previous chapters because although the investigations extend to below 100 m depth and well beyond the quasi steady state that defines the homothermic zone, the boreholes have not yet reached a point where the temperature consistently increases with depth. In instances where the temperature does increase with depth, the temperature logs tend to exhibit small scale irregularity and the possibility of convection exists. In addition, even in those boreholes where the overall thermal gradients are not conducive to convection, the underside of the negative aberration that forms at a fracture as a result of the ALS process has a gradient that could create thermal instability. Although the potential for convection in boreholes has been recognized for almost a century and its theoretical basis has been well developed (e.g. Raleigh number, Hale; 1937), the details of the phenomena remain the subject of ongoing research (e.g. Cermak et al., 2008; Berthold and Börner, 2008). These recent simulations still apply several simplifications to the process including representing the borehole as a two-dimensional plane, essentially convection within a thin plate rather than a cylinder. Since convection is controlled by the balance of forces created by buoyancy and friction against the borehole wall it follows that a two-dimensional simulation would underestimate the frictional forces present in a borehole and thereby over estimate the tendency for convection. These simulations (eg. Cermak et al, 2008) also often ignore heat transfer at the solid-water interface. Since the thermal conductivity of the rock would be 4-5 times that of water, energy transfer to the rock would dampen the thermal contrasts within the borehole and also reduce the tendency towards convection. In spite of long standing appreciation of the presence convection in a borehole, there is opportunity to improve understanding and simulation of the phenomena.

The TVP is shown to respond in a fashion that identifies the likely presence of convection, particularly in passive (background) logs. A prudent assumption is that some distortion of thermal/flow patterns will have occurred as a result of the movement of the protective cage through the water column but given the background variations observed (approximately 0.001 C˚) that is minimal. The field data indicate that convection is not as prevalent in the ALS technique cooling logs as it is in passive logging, likely because the horizontal thermal gradients are larger than the vertical gradients during much of the thermal recovery. The three-dimensional Smoker model, albeit adapted in a non-rigorous fashion to simulate the

ALS process in a lined borehole[15], has provided results that are consistent with observed field data. The field data and simulations demonstrate that convection is a three-dimensional phenomena and that for understanding the ALS process two-dimensional simplifications are inappropriate.

Flow in a fracture around a borehole which has been heated superficially appears to be a simple system, but these numerical investigations have shown it to be complex with multi parameter dependence. Subtle refinements of the model indicate strong promise for the quantification of flow from ALS data but also that several factors control the details of the log-linear relationship between the additional cooling that occurs at the fracture and the volumetric flow through the discontinuity. A potential scheme for quantifying the flow from ALS data will require knowledge of parameters such as the geometry and the thermal characteristics of the system. Many of these parameters are measurable or reasonably assumed. The ALS process can be used to estimate the thermal conductivity of the rock and the TVP used to determine the position of the heater in the borehole, but parameters such as flow direction will require additional work to resolve which is beyond the scope of this thesis and presents an opportunity for further investigation.

[15] The Smoker model as adapted accounts for heat transfer between the borehole and the rock, but density-dependent fluid flow within the open borehole is based simply on Darcy's Law, and there is no provision for friction at the borehole wall.

5.4 Tables

Table 5-2: Relative temperature drop during cooling as a function of flow rate

						Relative **temperature** drop (°C)					
H @ A,C	**v(m/sec)**	**∇h**	**2b**	**2bv**	**Log(2bv)**	**A4.5**	**A5**	**A5.25**	**C4.5**	**C5**	**C5.25**
D37,D54	0.00153	0.00750	0.00050	7.66E-07	-6.116	0.0051	0.0026	0.0022	0.0081	0.0034	0.0027
D22.D23	0.00306	0.00375	0.00100	3.06E-06	-5.514	0.0281	0.015	0.0122	0.0243	0.0118	0.0096
D14,D16	0.00613	0.00750	0.00100	6.13E-06	-5.213	0.049	0.0253	0.0205	0.0355	0.0175	0.0142
D18,D19	0.01225	0.01500	0.00100	1.23E-05	-4.912	0.0676	0.0343	0.0278	0.0453	0.0224	0.0182
D38	0.01225	0.00750	0.00141	1.73E-05	-4.762	0.0737	0.0376	0.0305			
D60	0.00501	0.00024	0.00502	2.52E-05	-4.599				0.0503	0.0255	0.0207
D53,D57	0.01010	0.00078	0.00398	4.02E-05	-4.396	0.0849	0.0433	0.035	0.0534	0.0269	0.0217
D39,D55	0.01531	0.00075	0.00500	7.66E-05	-4.116	0.0954	0.0482	0.0391	0.0562	0.0281	0.0226
D52,D58	0.06003	0.00265	0.00527	3.16E-04	-3.500	0.0968	0.0487	0.0392	0.0575	0.0279	0.0223
D50	0.31646	0.38750	0.00100	3.16E-04	-3.500	0.0939	0.0479	0.0389			
D51,D56	0.15366	0.00470	0.00632	9.72E-04	-3.012	0.0946	0.048	0.039	0.0613	0.0294	0.0234

Table 5-1: Summary of slopes and inflection points

		Heater Up-Gradient		**Heater Down-Gradient**	
Day	**Flow**	**Slope** $\Delta T/Lg(m^2,$	**Start** m^2/s	**Slope** $\Delta T/lg(m^2$	**Start** m^2/s
4.5	Low	0.0524	$10^{-6.15}$	0.0290	$10^{-6.40}$
	Intermediate	0.0335	$10^{-4.75}$		
	High	0.0002	$10^{-4.11}$	0.0040	$10^{-4.55}$
5.0	Low	0.0266	$10^{-6.16}$	0.0151	$10^{-6.32}$
	Intermediate	0.0164	$10^{-4.75}$		
	High	0.0000	$10^{-4.11}$	0.0012	$10^{-4.55}$
5.25	Low	0.0215	$10^{-6.16}$	0.0123	$10^{-6.32}$
	Intermediate	0.0133	$10^{-4.75}$		
	High	0.0002	$10^{-4.11}$	0.0009	$10^{-4.55}$

Table 5-3: Critical Flow

Aperture		Velocity			Flow
micron	metre	(m/sec)	(m/day)	(km/yr)	(m^2/s)
100	1.0 E-04	6.0 E-03	480.3	175.3	160.370
200	2.0 E-04	2.8 E-03	240.2	87.7	40.093
400	4.0 E-04	1.4 E-03	120.1	43.8	10.023
600	6.0 E-04	9.3 E-04	80.1	29.2	4.455
800	8.0 E-04	7.0 E-04	60.0	21.9	2.506
1000	1.0 E-03	5.6 E-04	48.0	17.5	1.604
2000	2.0 E-03	2.8 E-04	24.0	8.8	0.401
3000	3.0 E-03	1.9 E-04	16.0	5.8	0.178
4000	4.0 E-03	1.4 E-04	12.0	4.4	0.100
5000	5.0 E-03	1.1 E-04	9.6	3.5	0.064
10000	1.0 E-02	5.6 E-05	4.8	1.8	0.016
20000	2.0 E-02	2.8 E-05	2.4	0.9	0.004

5.5 Chapter 5 Figures

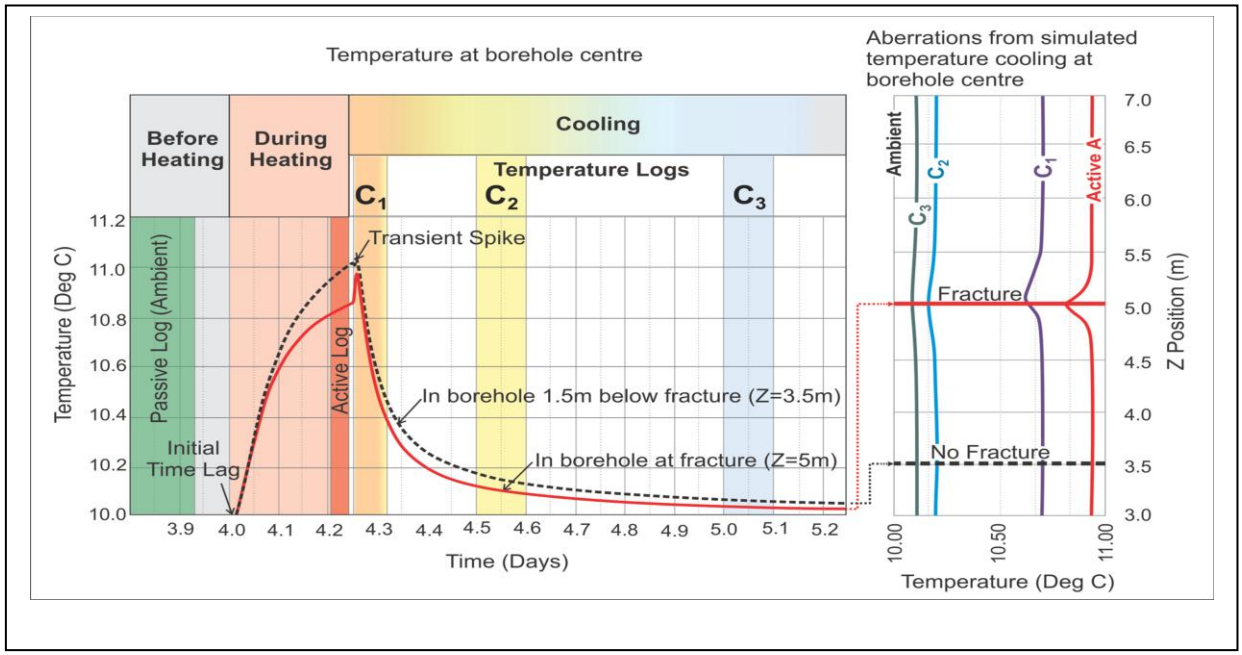

Figure 5-1 Predicted Response Base Case *(Figure 3-2: Chapter 3)*
Simulated temperature at the borehole centre during heating and cooling within a rock mass containing a single fracture. Following heating the hole, temperature profiling, is done on three occasions (1 hour intervals), referred to as cooling logs (C_1, C_2, C_3). Aberrations become less apparent as temperature decreases successively with each log as the water in the lined hole returns to the ambient (passive) condition. The active profile is obtained just before heating ceases

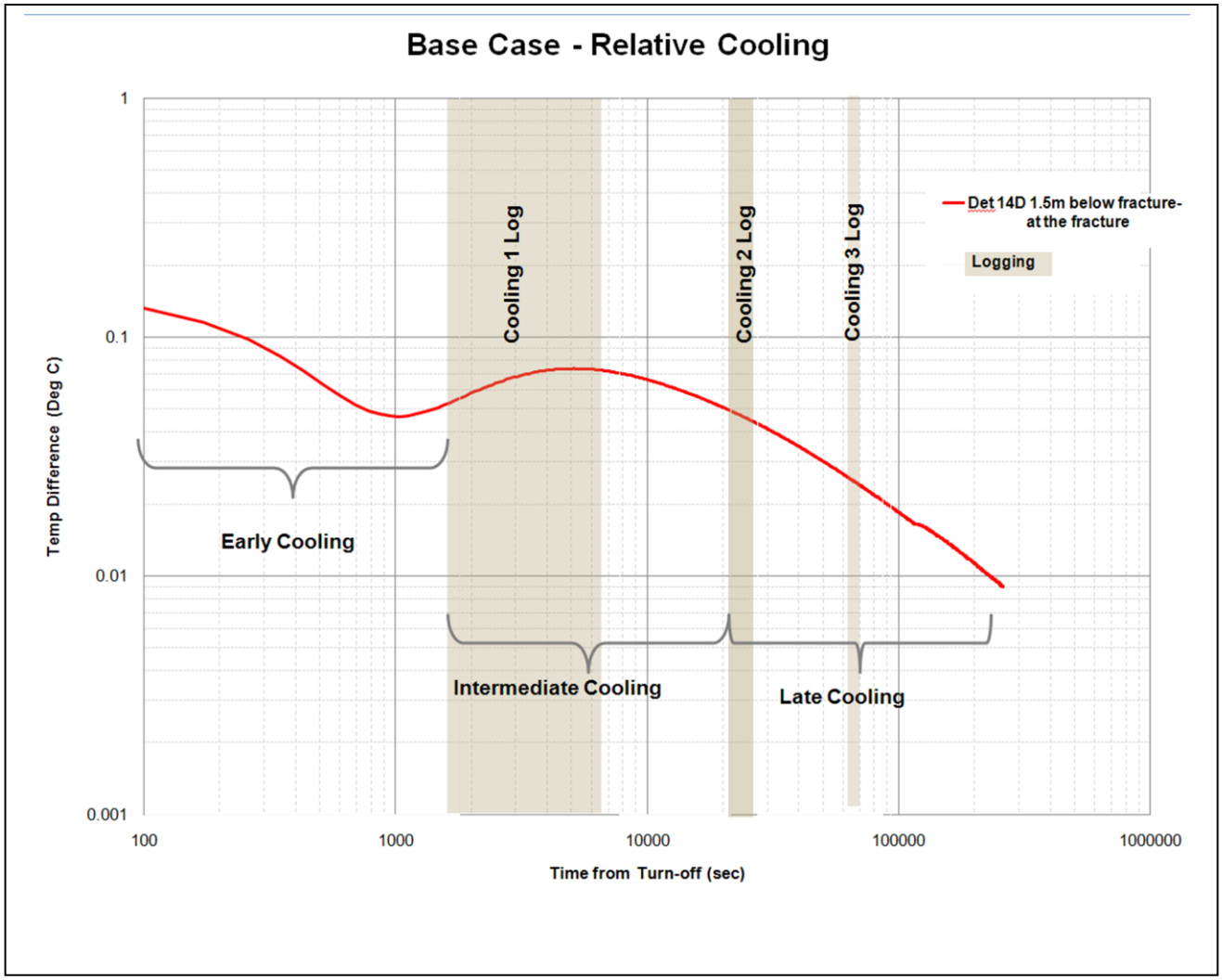

Figure 5-2: Log-Log plot of base case relative cooling with components of the ALS cooling cycle.
The relative cooling response (°C) center of the borehole (reference 1.5m below –at the fracture) plotted against time from turnoff, note early and intermediate response can be complex but linear decay in late time. Details discussed in main text

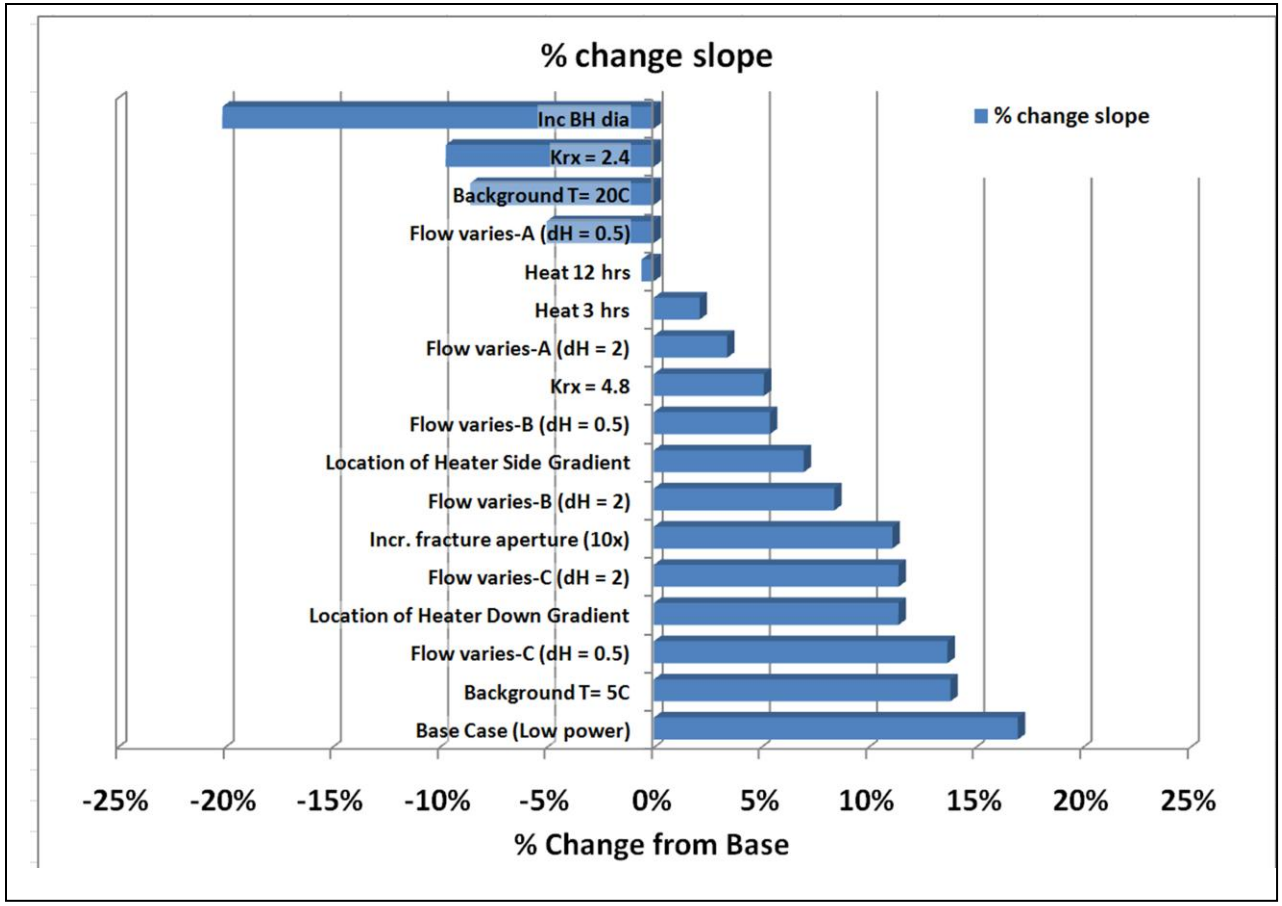

Figure 5-3: Summary of sensitivity analysis results;
percent effect on the slope of the relative cooling over late time as parameters of the model are varied relative to the base case.
Note although largest effects occur with parameters that can be measured or estimated (borehole diameter, background temperature and rock thermal conductivity), but location of heater are (A vs B or C) and velocity are also important controlling parameters. For details refer to appendix A.

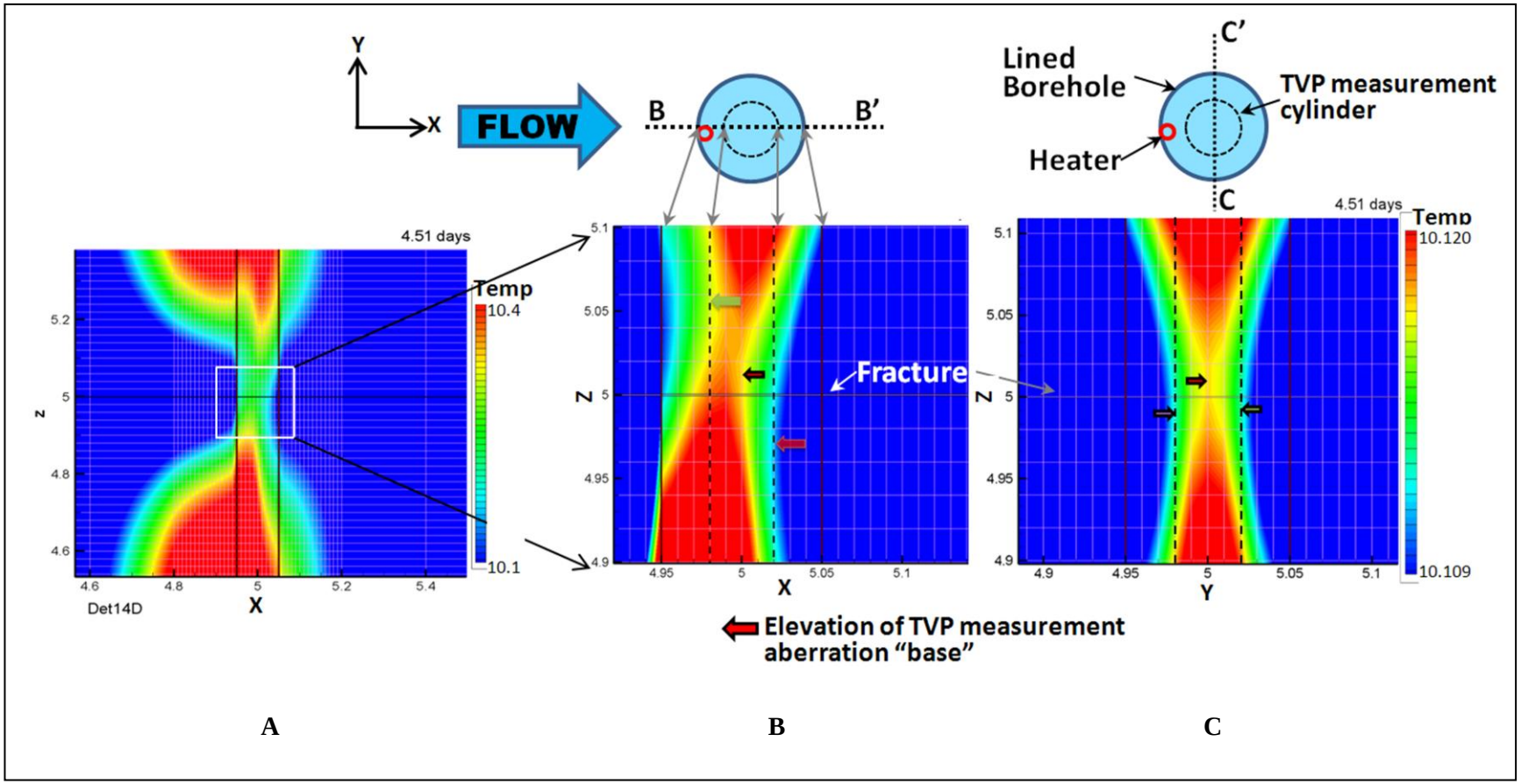

Figure 5-4: Detailed base case thermal pattern along (A, B) and across flow direction (C).
The of thermal patterns are distorted on the Y=5.00 plane (A&B) and although symmetric, variable on the X=5.00 plane (C). These patterns could not be duplicated with either 2 dimensional or rotational symmetry, detailed 3 dimensional models are required. Arrows indicate elevation of the lowest temperature (base) that would be measured by the sensor.

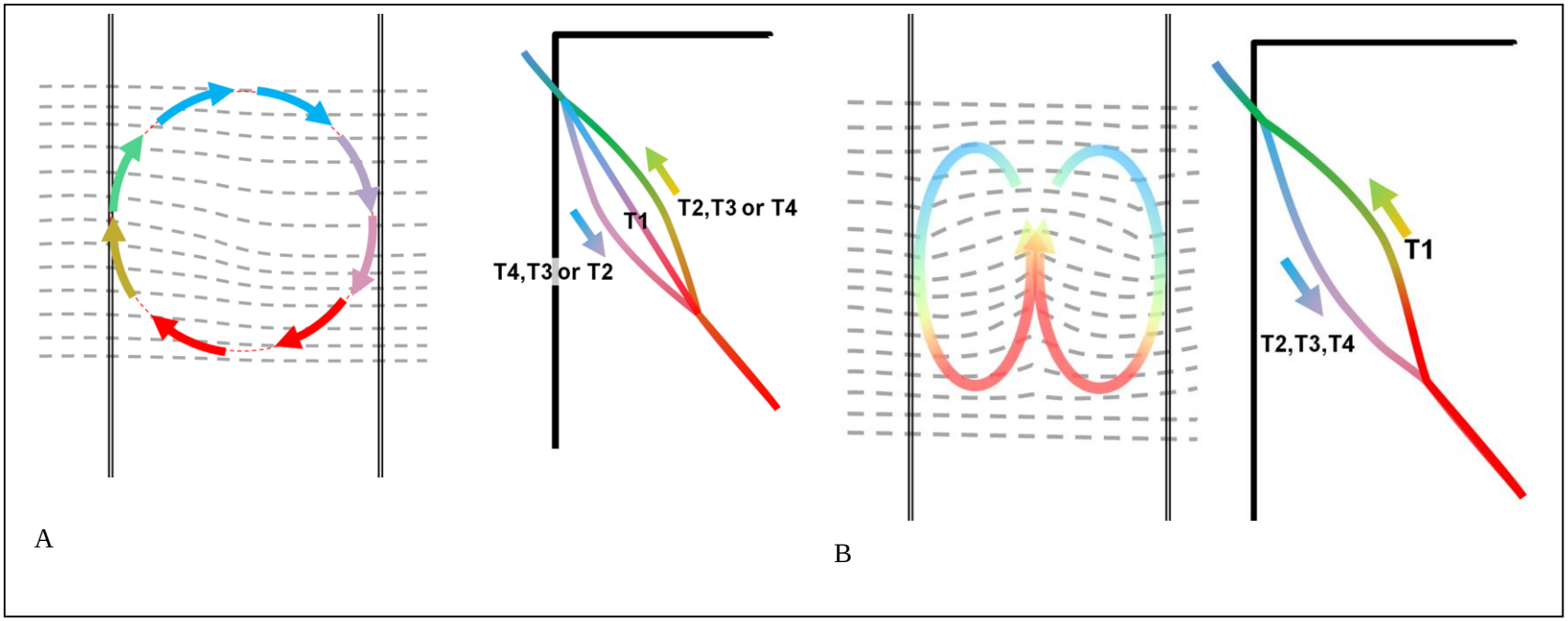

Figure 5-5 A- Circular convection cell model, B- Cylindrical "Donut" convection cell model
A- For a circular convection cell measured by the TVP, T1 would vary almost linearly with depth, the sensor on the upward flow side (T2, T3 or T4) would bow in a convex shape with depth and the other sensors towards the down flow side would be concave. B-For a cylindrical "donut" shaped convection cell, T1 would measure up flow, convex shape and T2, T3 and T4 would all measure downward flow and have a concave pattern. Note in either case, the measured temperature profiles would depend on the relative dimensions of the convection cell (controlled by borehole diameter) and the diameter of the probe. Dashed lines represent hydraulic gradients resulting from density variations controlling flow.

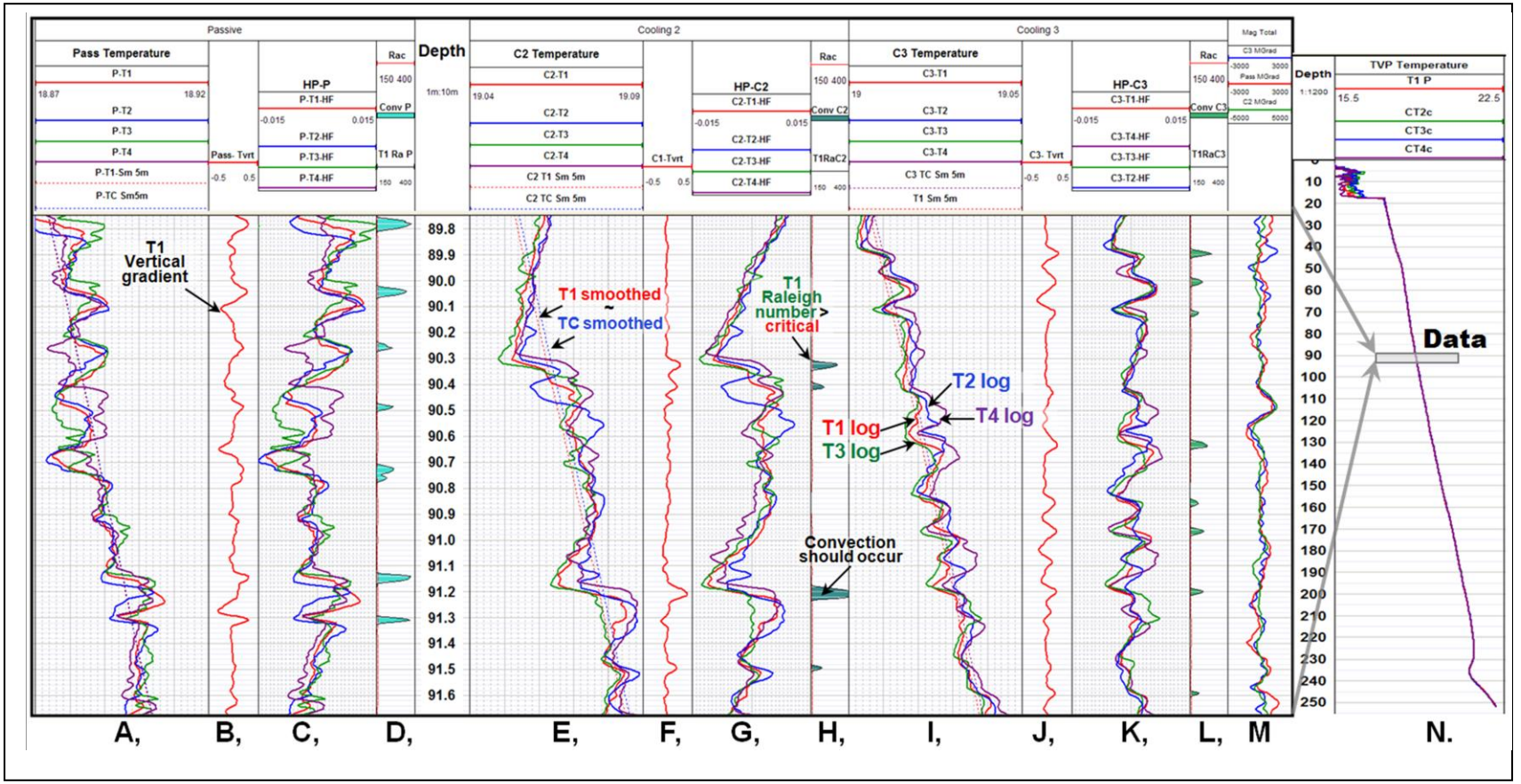

Figure 5-6A: Example ALS test results from C6, Santa Suzanne Field Laboratory, Simi Mtns, Ca.
In an overall regime of increasing temperature with depth conducive to convection detailed examination of temperature values in borehole indicate anti correlation indicative of convection under passive conditions and becomes orderly during thermal recovery from ALS heating. (Details in Figure 6B and 6C). A- TVP sensors T1,T2,T3 &T4 passive data set, smoothed T1 and TC (Temp. range: 18.87-18.92˚C) B-vertical thermal gradient T1(from A,-0.5 to 0.5˚C/m), C-Thermal Deviation (from A, -0.015 to 0.015˚C), D-Raleigh Number T1(A) and critical Raleigh Threshold, E-TVP sensors T1,T2,T3 &T4 Cooling 2 data set, smoothed T1 and TC (all 19.04-19.09˚C), F, G & H – same as B, C & D for Cooling 2 data set, I-TVP sensors T1,T2,T3 &T4 Cooling 3 data set, smoothed T1 and TC (all 19.00-19.05˚C), J,K&L – same as B, C & D for Cooling 3 data set, M-deviation TVP total magnetic field (passive, C2 and C3) -3000to 3000 nT used for detailed alignment of temperature data, N- Passive temperature data - complete borehole (all 15.5-22.5˚C)

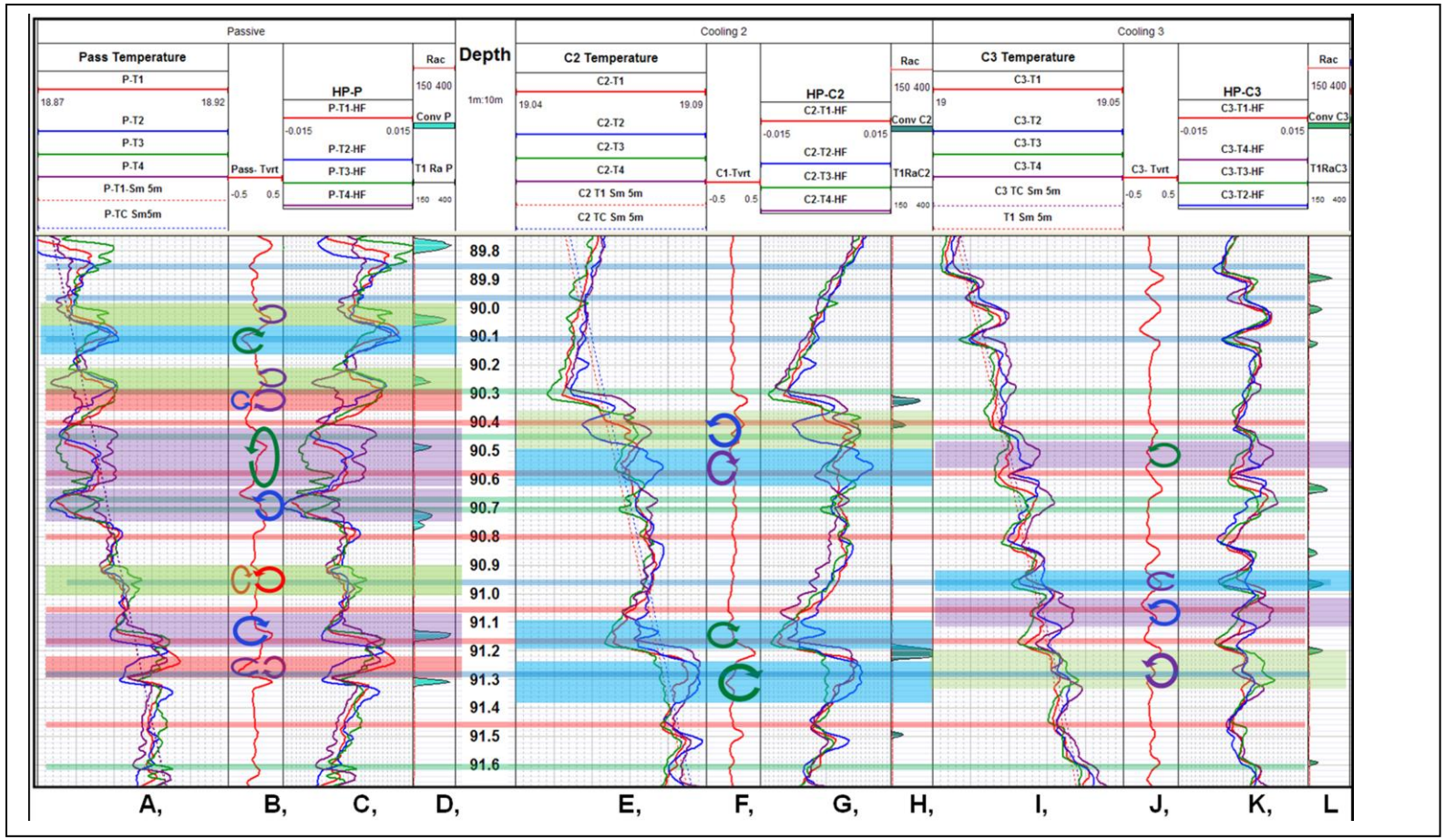

Figure 5-6B: Example ALS test results from C6 (Figure 6) with flow zones and possible convection cells highlighted.
Interpretation of convection (circular arrows) based on temperature distributions across borehole and flow zones. Note higher propensity for borehole fluid to convect under ambient conditions. (Further details in Figure 6C and text).
A-L Columns – as per Figure 6A, Green lines – interpreted flow zones (distinct in C2, weak in C3), Blue lines – interpreted flow zones (distinct in C3, weak in C2), Red lines – interpreted flow zones (distinct in both C2 &C3). Convection cells indicated by shading with upwards motion at T1(red), T2(blue), T3(green) and T4 (purple) and primary downwards indicators as arrows (same colour scheme), position relative to center of column indicates relative location of cell in borehole (assuming T2 on left side of column).

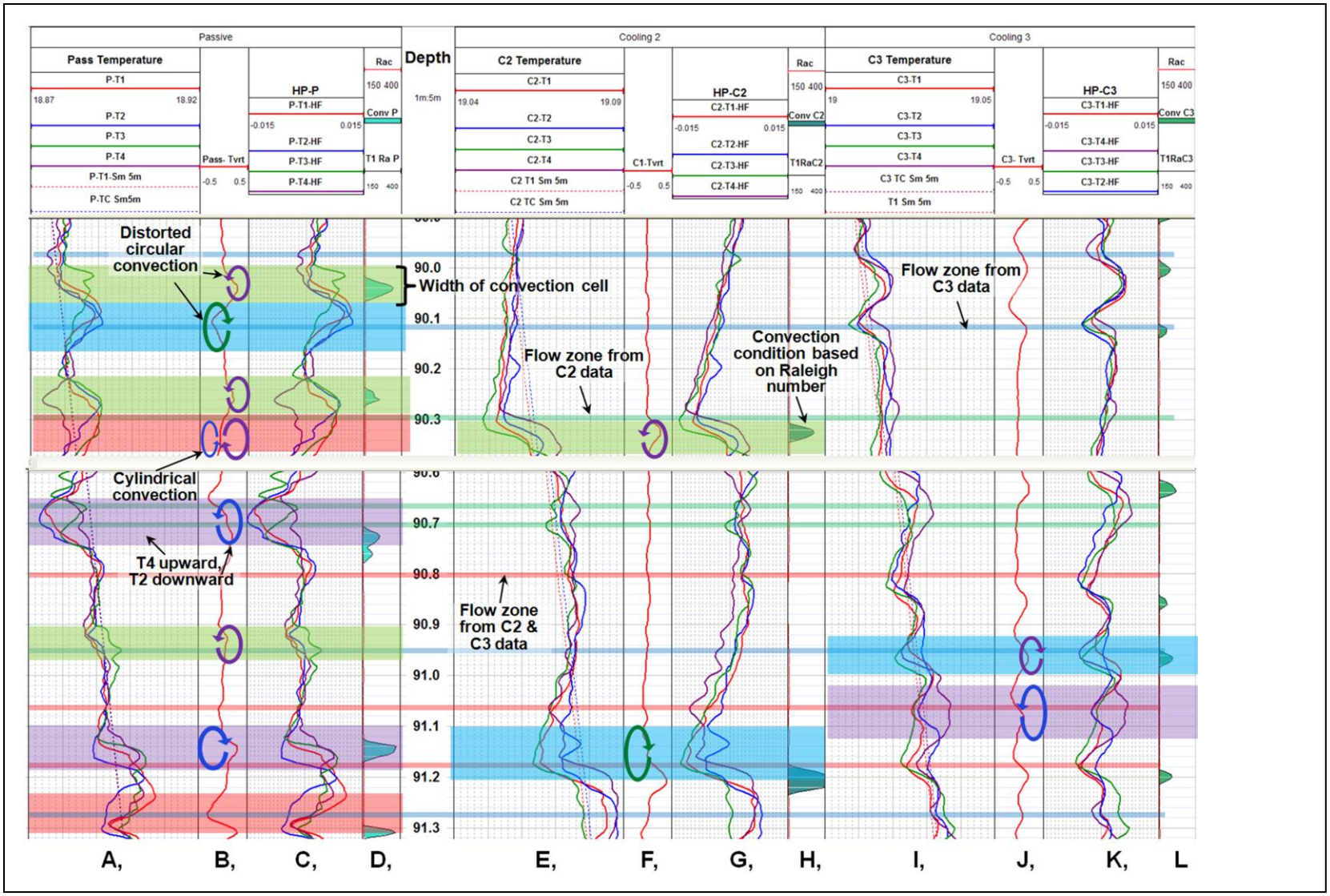

Figure 5-6C Expanded examples from Figure 5-6 of flow zones and possible convection cells based on temperature differences greater than 0.01C°.

A-L Columns – as per Figure 6A, Interpretation as per Figure 6B.

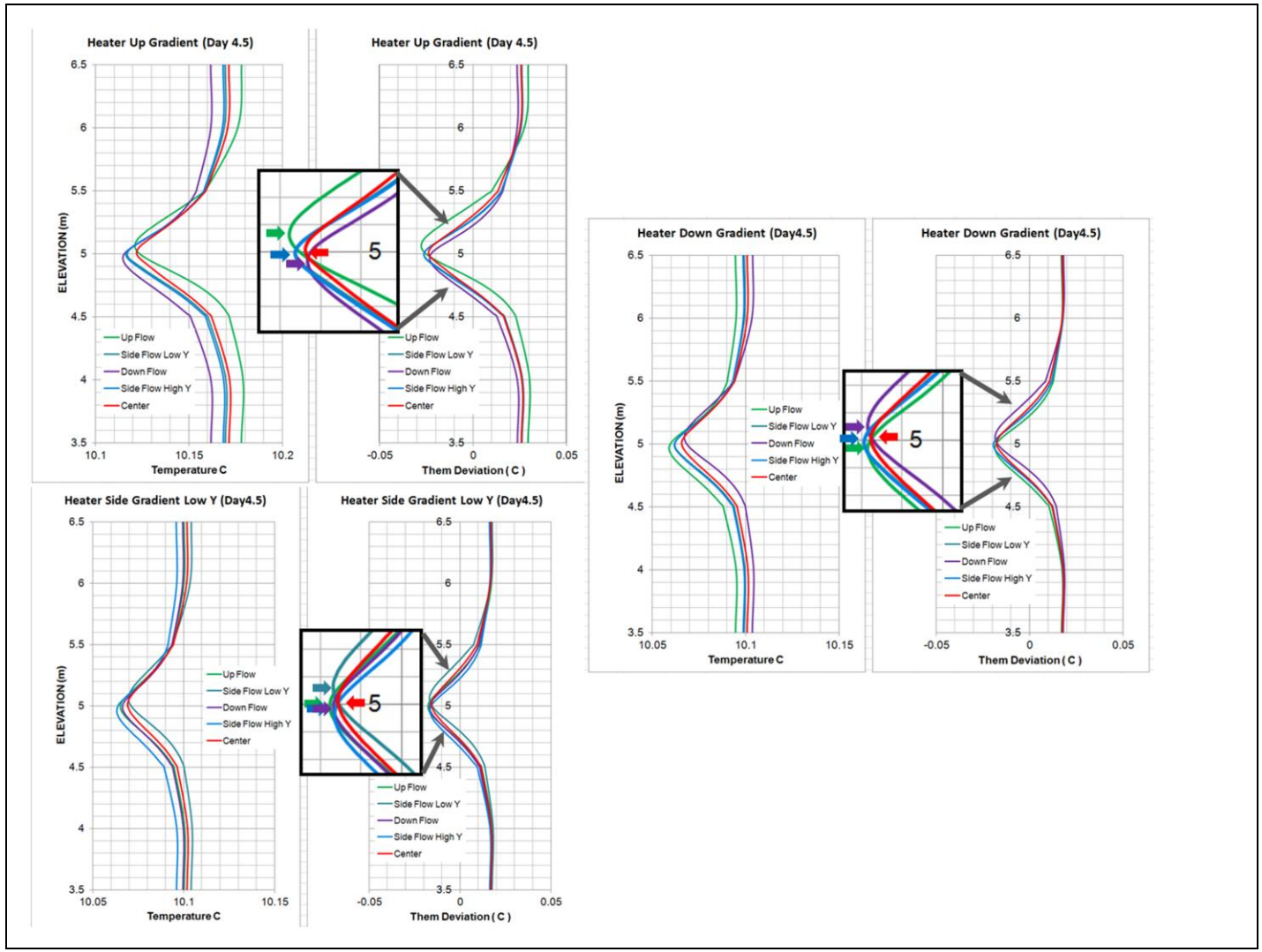

Figure 5-7: Details of simulated vertical C2 profiles (heater up, side and down-gradient)
Show vertical displacement of trough around TVP measurement cylinder and possible error in identifying elevation of fracture. Although the details of the Smoker simulation differ from the field example, the general characteristics are similar. Profiles along TVP measurement cylinder and center of borehole from Smoker models – base case, heater down gradient and heater side gradient. Arrows indicate elevation of the lowest temperature on profile, the "base" of the aberration.

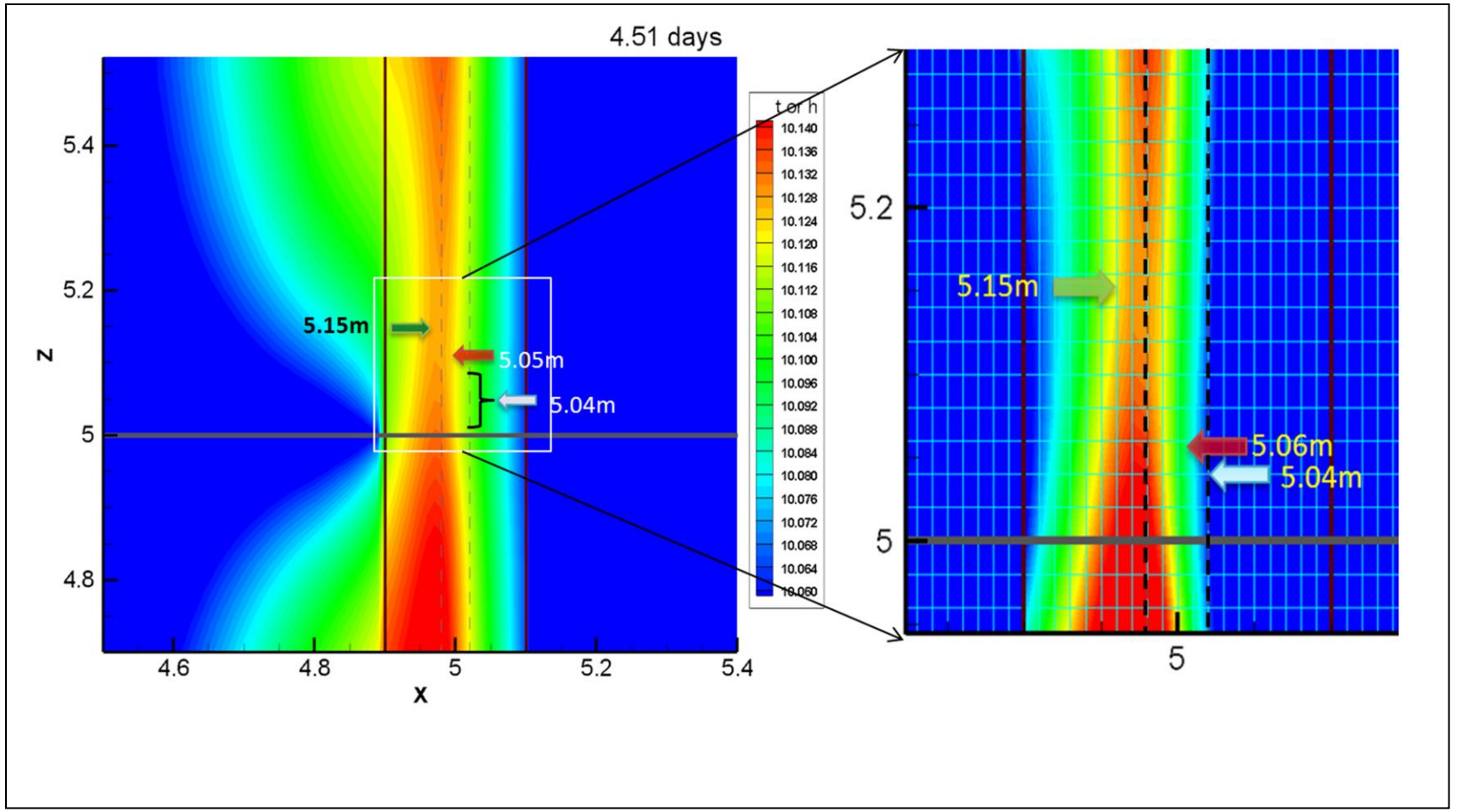

Figure 5-8: Details of simulated temperature distribution (20 cm hole) at 4.51 days (C2)
Show vertical and lateral variations in temperature. Note all troughs are centered above fracture, laterally offset and vertically stretched relative to base case (Figure 4) implying borehole diameter strongly influences the characteristics of convection.
Arrows indicate minimum values on TVP measurement cylinder (T2, T3 or T4) and at center of borehole (T1). Heater up-gradient, other parameters as in base case. Grid in expanded view shows location of model elements.

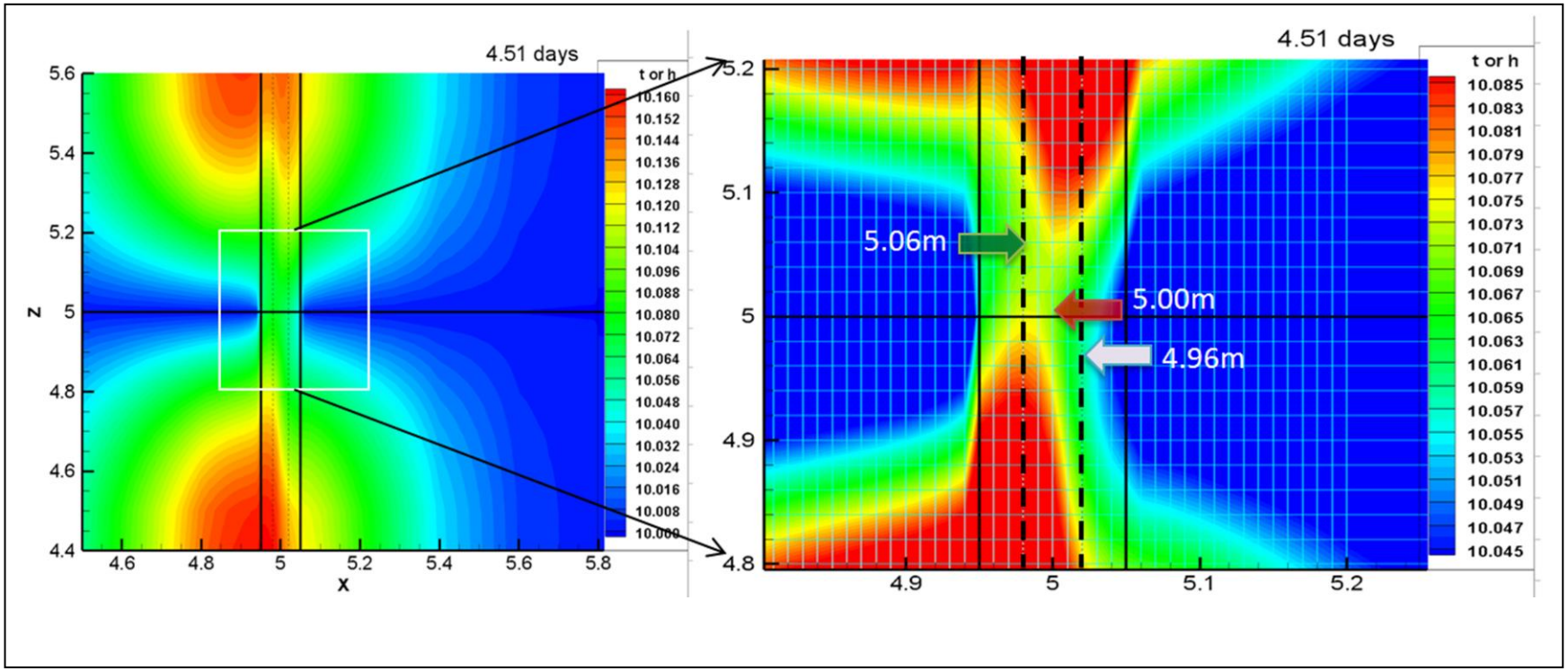

Figure 5-9 Details of Simulated Temperature Distribution (High Flow) 4.51 days (C2).
Note T1 is the best estimate of fracture elevation, the span of the aberration increases to approximately 1m, and is highly distortion laterally across the borehole with increased flow. Flow set at 4.5x10-3 m^2/s. Arrows indicate minimum values on TVP measurement cylinder (T2,T3 or T4) and at center of borehole (T1). Heater up-gradient, other parameters as in base case. Grid in expanded view shows location of model elements.

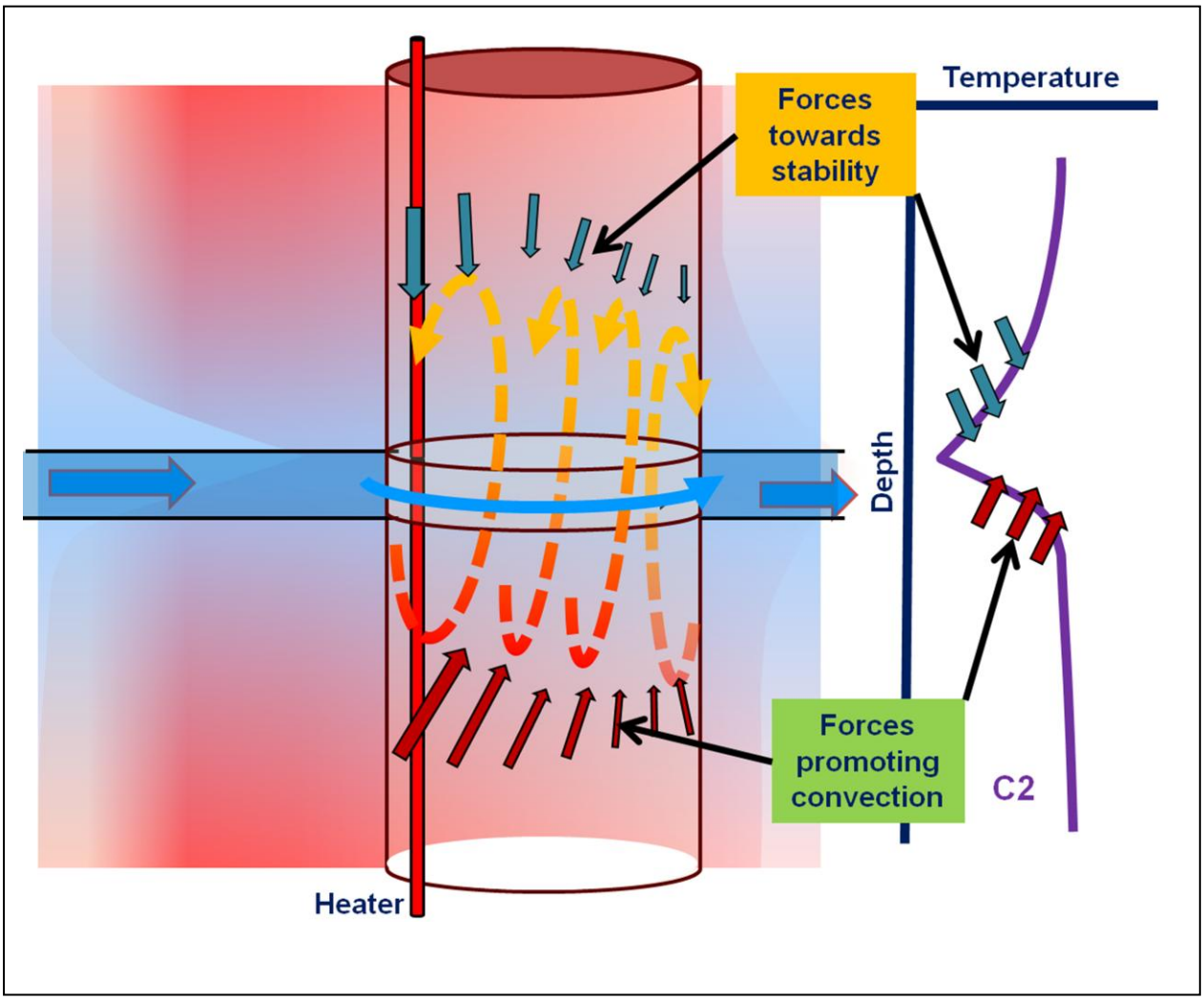

Figure 5-10: Schematic of a conceptual model for convection in the lined borehole at fracture during ALS thermal recovery.

The water in the borehole at the elevation of the fracture will be cooler than that above and below. Below the fracture, the condition of cool over warm water will promote convection and above the fracture warm over cooler water will tend to stabilize the environment. Friction (not considered by Smoker) would tend to impede flow along the borehole wall and therefore the convection cell should rise in the center of the hole and move downwards at the sides. However both the thermal gradients and consequently convection patterns will depend on the location of the heater relative to flow as well as the amount of flow and other characteristics of the system and therefore this conceptual model is an oversimplification of the situation Two dimensional simplification would be inappropriate..

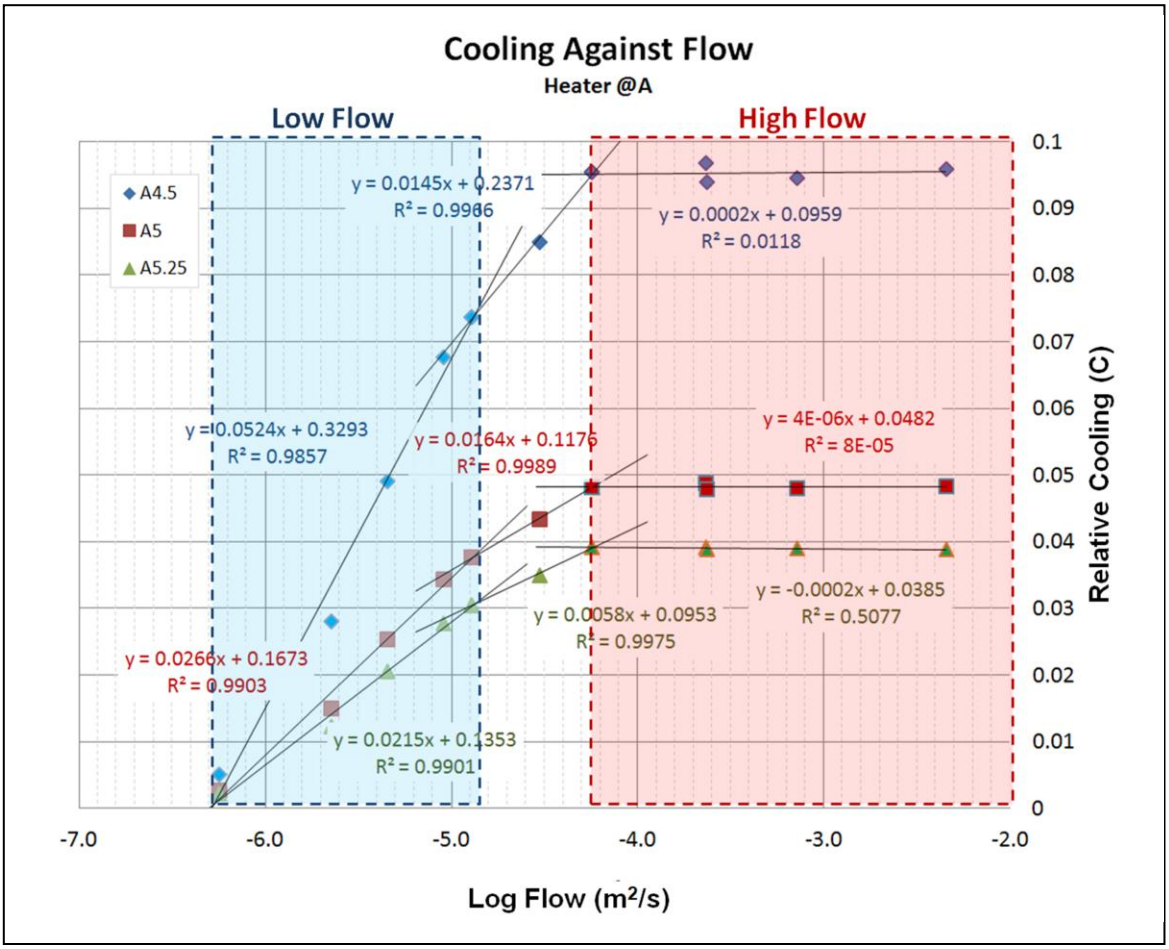

Figure 5-11: Relative Cooling against flow rate (Heater at A, up-gradient).
Cooling varies linearly with the log of the water flow rate through the fracture, in three distinct regimes designated as low, intermediate and high flow. The lower limit of detection is at ~10-6.2m^2/s and at flow rates above ~10-4.1m^2/s the relative cooling does not change with increased flow rates. A4.5= heater at A, 4.5 days into simulation (C2 condition). A5= heater at A, 5 d into simulation (C3 condition). A5.25= heater at A, 5.25 d into simulation (C4 condition).

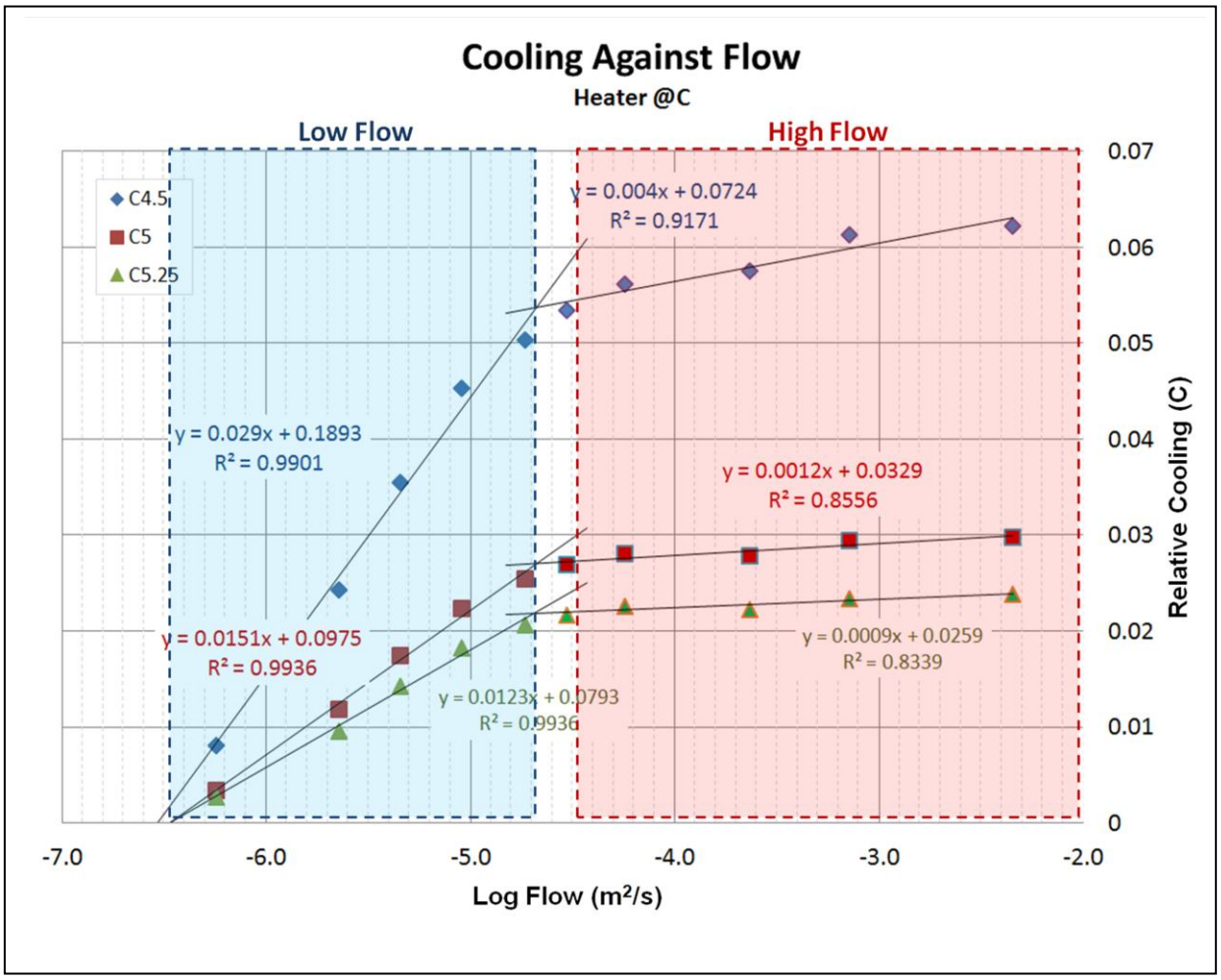

Figure 5-12: Temperature drop against flow rate (Heater at C, down-gradient).
Cooling varies linearly with the log of the water flow rate through the fracture, in two distinct regimes designated as low and, high flow. Intermediate flow may not exist or occurs under limited conditions. The lower limit of detection is at ~10-6.3m^2/s and at flow rates above ~10-4.6m^2/s the sensitivity of relative cooling to increased flow rates decreases dramatically. C4.5= heater at C, 4.5d into simulation (C2 condition). C5= heater at C, 5d into simulation (C3 condition). C5.25= heater at C, 5.25d into simulation (C4 condition).

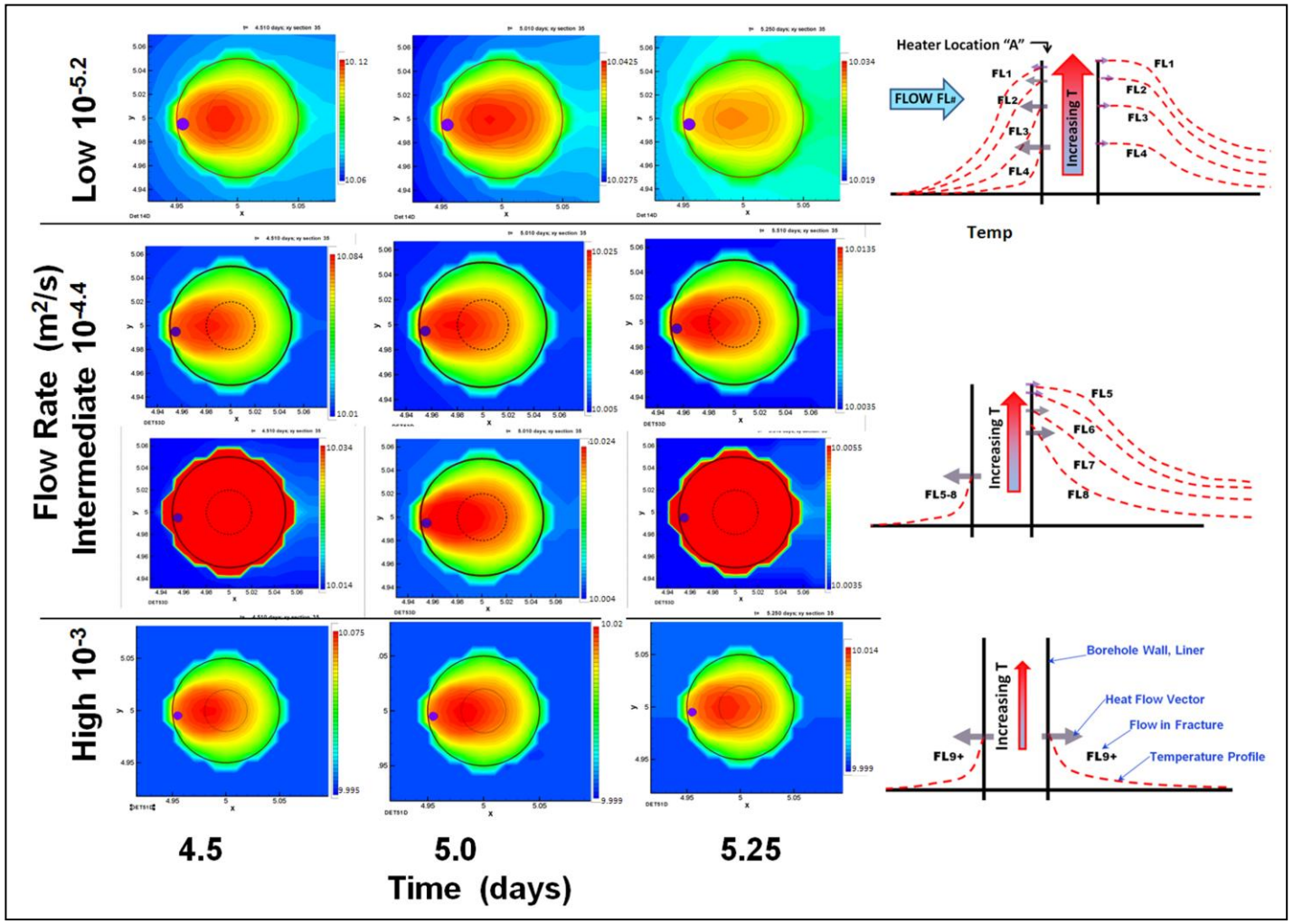

Figure 5-13: Enlarged view: Temperature distribution in borehole during late recovery with varying flow rates (heater at A). Schematics depict X-T temperature pattern through the center of borehole with progressively increasing flow FL1 to 9+. Heat transfer at the borehole wall is controlled by the temperature gradient across the liner. Within the low flow regime the thermal gradient varies around the circumference of the borehole as the flow rate increases. At ~10-6.3m2/s and above the thermal gradient on up-gradient side of the borehole is constant but the thermal gradient down gradient side continues to vary with flow rate until a rate of ~10-4.1m2/s. At high flow rates the gradient is constant on all sides and a maximum relative cooling is reached. Colour schemes vary to highlight temperature patterns around borehole. Intermediate time is presented at two colour schemes to show both temperature variations within the borehole and down gradient temperature patterns. Time 4.5d=C2 condition), 5d=C3 condition and 5.25d=C4 condition. Grey arrows represent relative heat flow, increasing with higher temperature gradient. See text for further discussion.

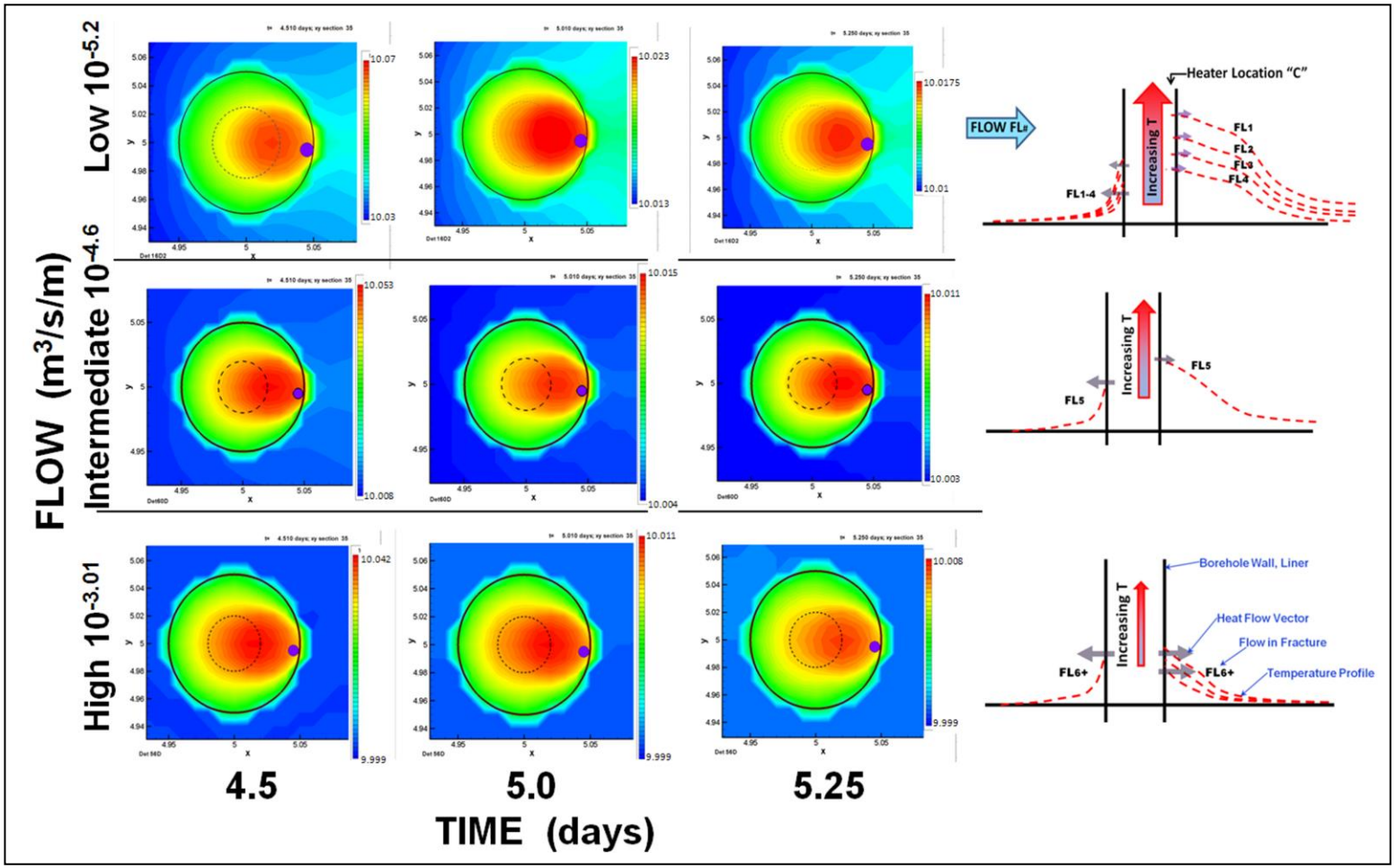

Figure 5-14: Enlarged view: Temperature distribution in borehole during late recovery with varying flow rates (Heater at C). Schematics depict X-T temperature pattern through center of borehole with progressively increasing flow FL1 to 6+. With the heater on the down-gradient side of the borehole much of the thermal decay occurs beyond the borehole and thermal gradients on around the borehole are relatively lower than in Figure 13. Within the low flow regime the thermal gradient varies around the circumference of the borehole as the flow rate increases. At a flow rate of ~10-4.6m2/s (intermediate) and above (high) the thermal gradient on up-gradient side of the borehole is constant but the thermal gradient on the down-gradient side continues to vary gradually with the flow rate as the store of heat dissipates down-gradient. Colour schemes vary to highlight temperature patterns around borehole. Time 4.5d=C2 condition), 5d=C3 condition and 5.25d=C4 condition. Grey arrows represent relative heat flow, increasing with higher temperature gradient. See text for further discussion.

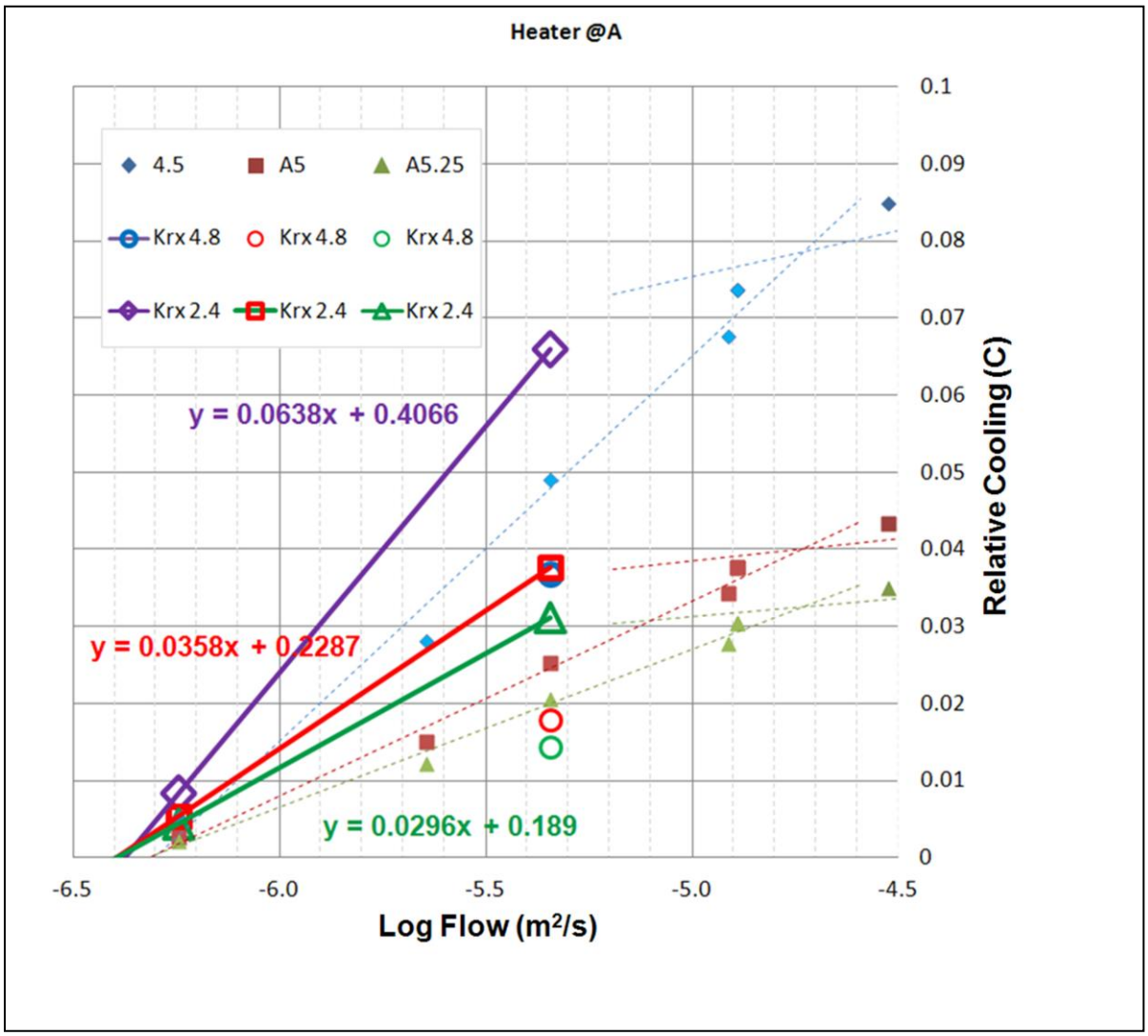

Figure 5-15: Change in Relative cooling vs. flow rate for different rock thermal conductivities; Heater at A. Although the slope of low flow relationship decreases with increasing rock thermal conductivity, the lower limit of detection is approximately that same. 2 additional points for rock thermal conductivity = 2.4W/m^2/C show approximate low flow trend. One additional point for rock thermal conductivity = 4.8W/m^2/C show comparison against base conditions (3.6 W/m^2/C). Time 4.5d=C2 condition), 5d=C3 condition and 5.25d=C4 condition. See text for further discussion.

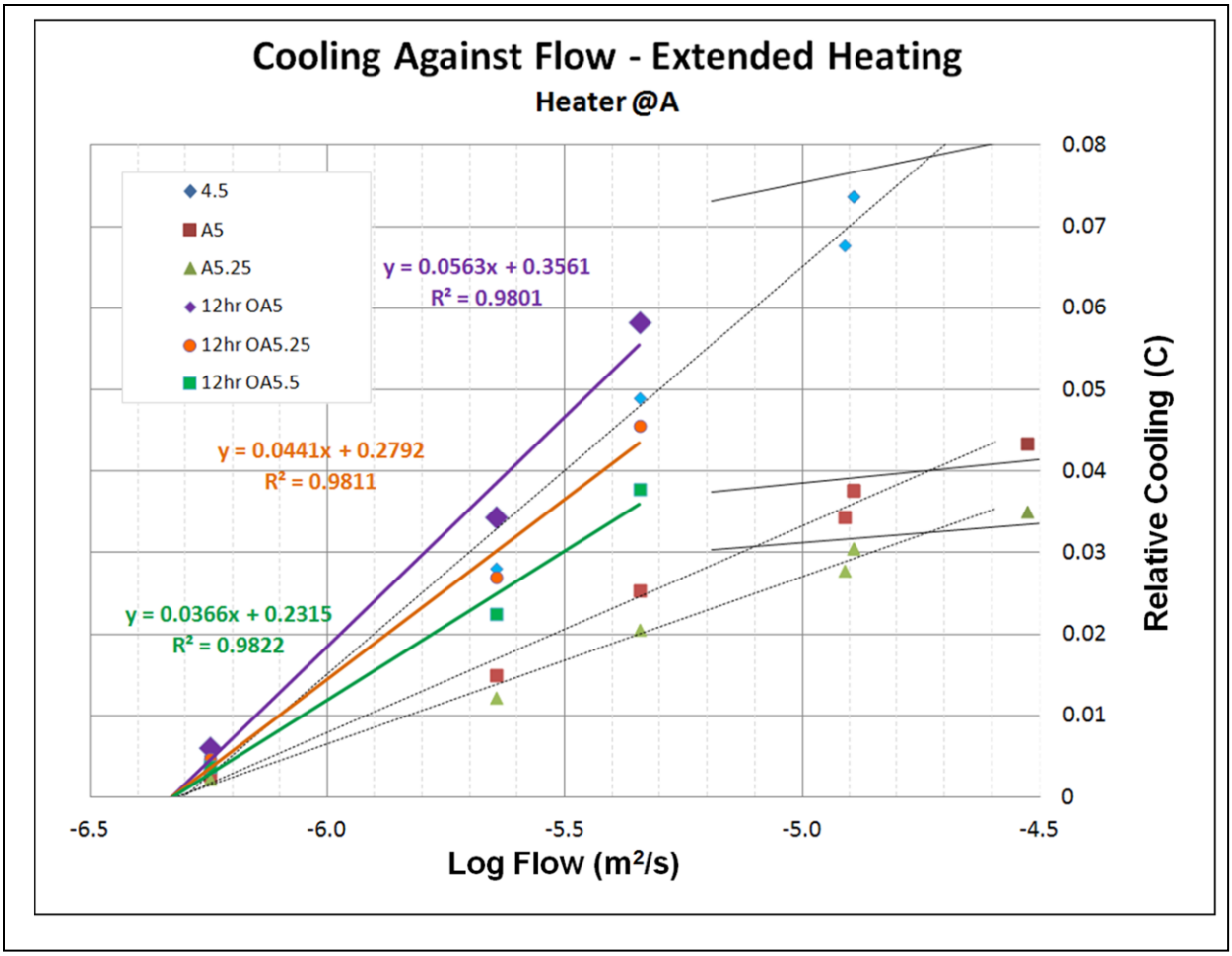

Figure 5-16: Relative cooling vs. flow rate for different heating times; Heater at A.
Increasing the amount of heat energy stored in the rock increases the slope of the low flow relationship implying that quantification of flow will require normalization to length of heating. Note the lower limit of detection remains the same in all examples presented suggesting that is a fundamental characteristic of the ALS process. 3 additional points for heating time increased to 12hrs. Show comparison against base conditions (6hrs). Increased duration of heating alters designation of cooling logs, Time 5d=C2 condition, 5.25d=C2.5 condition and 5.5d=C3 condition. See text for further discussion.

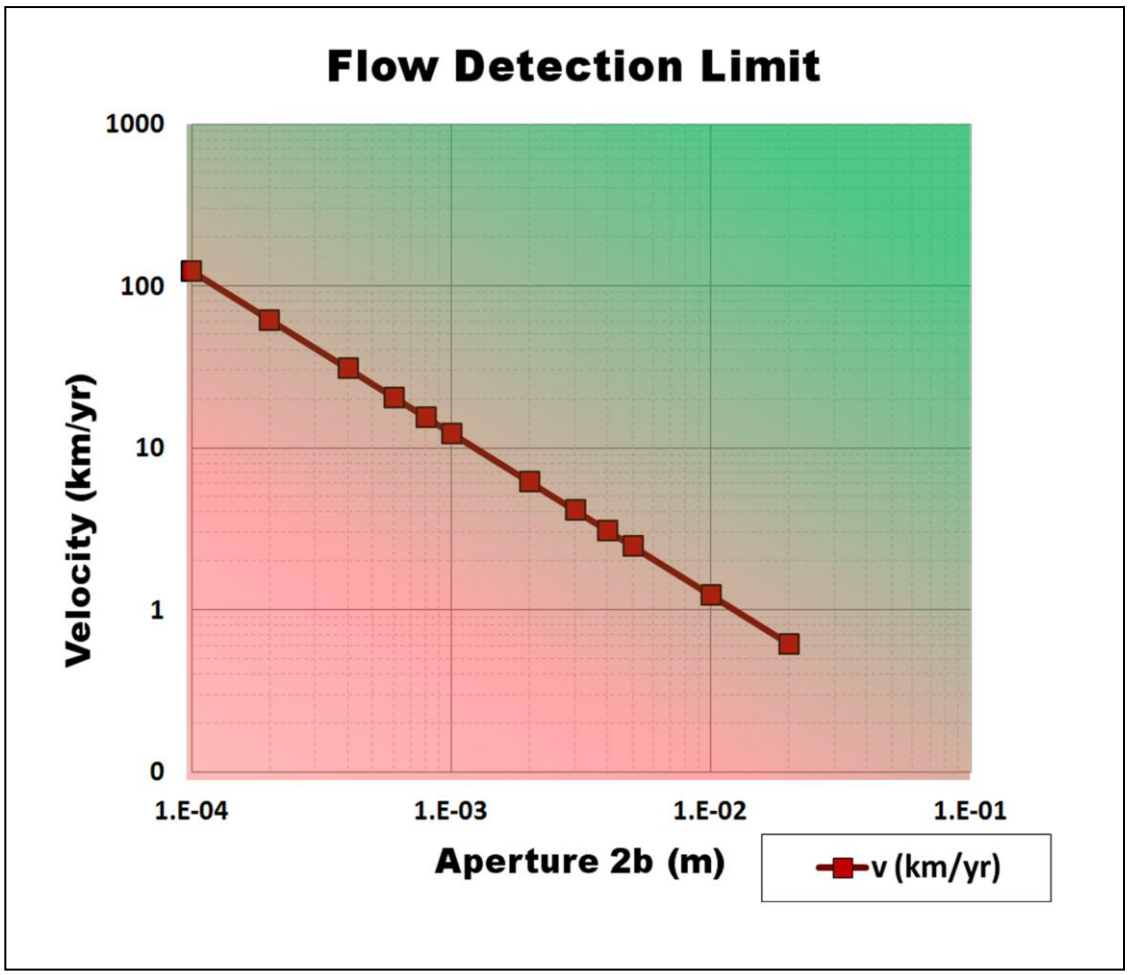

Figure 5-17: Theoretical Applicability of ALS Technique
Based on threshold and velocity- fracture aperture relationship (Eq3), when velocity and fracture aperture lie in green zone, flow is detectable with the ALS technique; flow is not detectable in pink zone. Detection limit is inconsistent with number of flow zones identified in field data implying figure may be overly conservative. See text for further discussion.

Chapter 6
Summary and Conclusions

The fundamental limitations to the use of temperature logging as a method for identifying groundwater flow through fractured rock have been identified, better understood and overcome. Both the increased resolution achieved by temperature sensor manufacturers and the advent of borehole liners designed to avoid chemical cross contamination have been effectively utilized in new techniques to identify many more flow zones than previously interpreted from temperature logs. The historic reliance on natural thermal disequilibrium has been documented and eliminated with the ALS technique. The complexity of the thermal response of the system is better appreciated; the thermal vector probe (TVP) has been developed and implemented to characterize the thermal field in high detail, thereby improving our understanding of ambient groundwater flow in fractured rock.

Key observations and insights achieved in this work include:

1. Although it has been long recognized that cross-connection compromises resolution of flow zones with temperature logs, the price of the compromise is herein documented. In example presented some of the missed zones are shown to facilitate high amounts of flow and based on rock core data are critical conduits contaminant transport.
2. Cross-connected flow is shown to have similarly negative implications for other techniques such as flow meters wherein important flow zones are not identified.
3. The results of open-hole temperature and flow meter logging therefore depend on the depth of drilling and which flow zones are deemed as most important can vary with the transmissivity of the deepest fractures intersected.
4. Interpretations made in the presence of cross-connected flow in the examples presented misplace emphasis on the shallowest and deepest hydraulically transmissive fractures leading to erroneous conclusions with regards to which flow zones control contaminant distribution. This realization has critical implications on other aspects of hydrogeologic investigations such as the design of multilevel installations.
5. Temperature logging in a lined borehole avoids the distortion of the data typically caused by hydraulic cross connection and provides an ambient (natural) thermal profile with improved resolution of flow zones.

6. The thermal deviation log is introduced and shown to be an improved representation of lined-hole temperature data, better emphasizing and representing the influence of individual flow zones.
7. The "change log" is developed to highlight the temporal variations in flow and, together with the thermal deviation log from temperature profiles collected in lined boreholes, provide a better qualitative ranking of flow zones and potential importance to contaminant distribution.
8. Although an improvement on previous interpretations of flow, passive temperature logging within a lined hole is shown to miss some deep flow zones because the process relies on thermal disequilibrium driven from surface to create temperature aberrations.
9. The concept of the heterothermic-homothermic boundary as the limit of shallow thermal dis-equibrium (Drogue, 1985) is given passing reference in the literature. A conceptual model for the importance of the boundary on the applicability of temperature logs is presented.
10. Historically the hetro-homothermic boundary in published accounts is relatively shallow (10-25m) although sometimes it is obscured by cross-connected flow. The identification of the boundary is shown to depend on the resolution of the sensor, sensor calibration and the time scale chosen. The data herein shows the hetro-homothermic boundary to be at 35-100mbgs at the Southern Ontario test sites, varying in depth considerably between locations. Some thin, deep zones of variable temperature persist below the boundary (presumably because of lateral flow), and therefore what is considered "invariant" is a qualitative assessment provided by the interpreter. Any discussion of the hetro-homothermic boundary should be accompanied by a description of the criteria used for its definition.
11. It is the contrast between the temperature of the water flowing in a fracture and the rock matrix that creates a variation on a temperature profile and consequently the size of the aberrations in passive logs will vary with the degree of thermal disequilibrium, decreasing in amplitude deeper in a borehole. Standard temperature logs are therefore an inconsistent indicator of flow with sensitivity decreasing with depth and a finite limit of applicability.
12. The active line source (ALS) technique is shown to overcome both the depth limitation imposed by the reliance on natural thermal disequilibrium as well as normalizing the cause-effect relationship making temperature aberrations a more consistent indicator flow throughout the borehole. The ALS technique extends the applicability of temperature logs such that heater design is the only depth limitation to applicability (450m is the deepest deployment to date) and the results provide a relatively uniform basis of comparison throughout the interval tested.
13. Fundamental to successful application of the ALS technique is a low data collection speed to minimize disturbance of the water column and high data density to adequately characterize the details of the temperature aberrations observed. It is the data density combined with the high

sensor resolution that allow individual thermal aberrations of much less than 0.01 C° to be resolved with 15 to 20 readings in a consistent and reproducible manner in this study.

14. The size of the temperature aberrations during thermal recovery after ALS heating, the accelerated cooling at a flowing fracture relative to background is defined as "relative cooling". Relative cooling decreases systematically with time, but it is also dependent on the position of the heater relative to the flow direction, as well as site conditions (e.g. background temperature, thermal conductivity of the rock and borehole diameter). The effect of these other factors is particularly strong immediately after the heater is turned off, in what is designated as the "early" and "intermediate" cooling portions of the thermal recovery process.
15. The thermal recovery stabilizes and relative cooling decreases linearly against log(time) in the portion of thermal recovery designate as "late time", after recovery has gone on for the same length of time as the borehole was originally heated. Logs collected at the beginning of late time provide the best compromise of sampling the largest aberration within a stable thermal decay.
16. The practical implications of understanding the thermal recovery process has led to a standardization of the ALS technique to a process that includes a background (passive log), heating for 5-6 hrs (near the end of which an "active" log is collected), and three data sets (cooling logs, C1-C3) during thermal recovery. The first (C1) cooling log is collected shortly after the heater is turned off, the second (C2) at the start of late time and C3 approximately a day after the initiation of heating. C2 and C3 are the primary data sets used for identification and comparison of flow zones.
17. The temperature vector probe (TVP) has been designed to continuously measure the vector components (as a gradient) and direction of the thermal field (as a densely spaced series of vectors along the length of the borehole). Four thermistors distributed in a tetrahedral pattern as well as three orthogonal components of the earth's magnetic field with directional magnetometers are simultaneously measured. Calibration procedures have been refined for the thermistors and matrix based rotational algorithms developed so that: the horizontal and vertical components of the total temperature gradient (vector), the direction of the horizontal component of the temperature field relative to magnetic north and the inclination of the total temperature vector from the horizontal are determined.
18. The TVP responds to the ALS process in an expected and consistent manner, facilitating a highly detailed analysis of thermal disequilibrium as well as the gradual return towards the original passive state. Most importantly the data provide a reproducible assessment of the cooling aberrations that result from groundwater flow through fractures.

19. Time-Elevation-Head (TEH) sections, a new method for presenting hydraulic head data from multilevel installations was developed and used for a detailed comparison of the broad characteristics of hydro-stratigraphy and the temperature field over the length of a borehole.
20. The TVP data along the length of a borehole can be divided into thermal subunits based on systematic variations in the magnitude and orientation of the components of the thermal field. In the example shown the thermal subunits coincide with changes in hydro-stratigraphy as defined by variations in hydraulic pressure on a TEH section.
21. Based on the magnetometer response of the TVP, temperature data sets (passive and three cooling) are aligned to an estimated 0.02m, a level of accuracy previously unattainable. Confidence in alignment allows for detailed comparison of the response of individual thermistors as well as the temperature field characteristics through the thermal recovery process. The level of detail achieved by the probe and superior alignment of separate data sets improves analysis of the effects of flow through the fracture as well as an assessment of thermal convection as a potential complicating factor in the interpretation.
22. In the boreholes studied where temperature increased with depth, variability in response consistent with convection occurs in portions of the passive data (either from single or multi-sensor probes). Interpretation of the TVP probe data under background conditions suggests that convection occurs as complex patterns of circular and cylindrical water movement. Typically the cells extend over distances of 0.1 to 0.2m, can occupy all or part of the borehole annulus, and have no readily apparent systematic pattern to the circulation direction.
23. The number of convection cells decreases during ALS thermal recovery, presumably as a result of the dominance of the horizontal gradient demonstrating another advantage of employing the technique.
24. The TVP data shows the thermal patterns within the borehole can be complex. Consequently, even though the ALS techniques simplifies the patterns and increases resolution, identification of flow is improved by the ability to examine thermal patterns concurrently with four thermistors rather than data from a single sensor probe.
25. Although the Smoker model used to analyze TVP and ALS response is a guide rather than a rigorous numerical simulation of the processes, the results of modeling a simple single fracture system confirm the complexity of the thermal field in and around a borehole through the process of thermal recovery. This is a conservative assessment as a more complete numerical simulation would be expected to provide a more complex result.
26. The numerical simulations show that the temperature field in the borehole is variable in four dimensions (three spatial and temporal) and thermal patterns consistent with convection are

predicted to occur during ALS cooling. The multidimensional variations imply that assumptions commonly used in the literature (eg. Berthold, S and F. Börner, 2008; Cermak et al., 2008) to simplify the analysis of convection in a borehole as a two dimension model are likely inappropriate.

27. Numerical modeling indicates that groundwater flux rather than velocity is the controlling factor in creating a temperature aberration in response to the ALS technique.
28. The simulations indicate the lower limit of flow detectable by the ALS technique is approximately $5.6x10^{-7}$ m^3/sec per m across the fracture (m^2/s). The limit is consistent regardless of varying some of the system parameters; however more testing is required to confirm the lower limit is constant in all circumstances. The simulations predict that above a rate of approximately 10^{-4} m^2/s the water movement creates a strong thermal aberration but differences in the flow rate cannot be resolved. Based on the predicted lower limit of detectable flow, an inconsistency exists between the large numbers of flow zones identified with the ALS technique at some locations and site conceptual models that have small aperture fractures with limited flow. Although the inconsistency is likely rooted in assumptions used to establish either or both the model of the ALS process or the simulations of site conditions, resolution of the issue is an opportunity for future research.
29. The ALS process is controlled by geometric factors (e.g. heater location relative to flow direction and borehole diameter), physical properties (e.g. thermal conductivity of the rock and background temperature) and the movement of water through the fracture. Many of the other factors are known, can be measured, or reasonably estimated with the TVP probe and therefore there is strong potential for quantifying flow. Additional work is required to move beyond the qualitative identification and comparison of flow zones to quantitative estimates of flow and direction.

The interpretations of flow in the bedrock drawn from these temperature data are generally consistent with other techniques that measure critical aspects of the system (fracture location, transmissivity etc.). However, there is currently no comparable method for directly measuring ambient flow in fractured rock to confirm the accuracy of the interpretations presented herein. Some discrepancies remain between the number and characterization of flow zones with the results of core logging, hydraulic testing as well as other geophysical and hydro-physical techniques. Some differences are reasonably expected because data are rarely collected concurrently, both borehole and hydrogeologic conditions vary over time. None of the techniques employed in a borehole measure exactly the same parameter and therefore commonality of conclusions is by inference, not observation. Additionally the study of flow through fractured rock is a complex emerging field, almost all of the techniques and

the fundamental assumptions upon which these are interpreted are the subject of ongoing research and will each continue to evolve for some time.

Through this study understanding of the processes as well as identification and the qualitative comparison of flow zones has improved. This increased understanding has also heightened appreciation for the complexities of the thermal and hydrogeologic processes and presented new opportunities for advancing research. Specifically:

1. Since there are no current techniques against which to assess the ALS interpretation, advancement of the process will rely heavily on the use of numerical models such as Smoker. Although the current results of numerical simulations appear reasonable and are consistent with field data, the model should be adapted to more rigorously simulate water movement in a borehole. This would facilitate additional modeling with multiple fractures and varying more parameters with added confidence. Ultimately the goal is to research the quantification of flow based on a "type curve" system.
2. There is a need to critically assess the implications of the results on understanding of flow through fractured rock. The ALS technique indicates many more flow zones exist than other techniques employed to date. The number of flow zones identified by the ALS is similar to the combined number of discrete fractures and "vuggy" layers identified in the dolomitic rocks inferring the importance of the latter. There may be a continuum of transmissivity in "flow zones" some that will be obvious in core and others that are more subtle. Recognizing these additional conduits and numerical simulation of such flow may be difficult, but provides another opportunity for advancement of understanding.
3. As the science of investigation of flow through fractured rock matures, new characterization techniques are being continuously developed and the broader understanding of hydrogeologic systems evolves (eg. hydrostratigraphic units, Meyer et al 2008). It is important to continuously review, re-assess and refine temperature techniques to compliment these.
4. The advancements in temperature logging presented herein are largely focused on technique development and better understanding of the hydraulic conditions within individual boreholes. Many opportunities exist for improved understanding of broader site wide hydrogeologic conditions by examination of the temperature data from a multi-hole basis and site wide implications of the results.

Temperature logging has become an underutilized tool for several reasons including sensor resolution, cross-connected flow and dependence on thermal disequilibrium. These limitations have

all now been overcome at a high level of detail. Although the detection and characterization of ambient flow is of critical importance in the investigation and numerical simulation of contaminated fractured rock sites, the measurement of this flow is extremely difficult. This work confirms that temperature logging procedures and interpretation can be refined and combined with other technologies to improve detection and characterization of flow in fractured rock and has made advances in that process. With improved understanding and the high resolution the temperature data presented comes both a heightened appreciation of the complexity of the interrelationship between thermal patterns and groundwater flow through fractured rock as well as the tools for even further insights. A technique that alters a parameter cannot be used to measure it, and therefore direct measurement of low levels of ambient groundwater flow in boreholes through fractured rock is unlikely. Consequently other physical properties of the system must be used to infer the water movement. Temperature is such a property, with strong potential to achieve a quantifiable measurement well beyond the qualitative improvements in characterization of groundwater flow in fractured rock achieved herein.

Appendix A

Identifying and Assessing Ambient Groundwater Flow Through Fractured Rock: Revitalizing the Role of Temperature Logging with New Approaches and Technologies

Peeter Pehme, Beth Parker, and John A. Cherry

A1. Overview

The popularity of temperature logging for identifying groundwater flow in fractured rock has waned relative to newer and more sophisticated geophysical and hydrophysical technologies. The declining interest can largely be attributed to a lack of precision, over simplification by cross-connected flow in the borehole, and depth limitations imposed dependence on heterothermic conditions to create aberrations on thermal profiles. Yet for their advances, straddle packer testing, borehole dilution, and flow meters are applied with portions of the borehole open to cross connection and often under hydraulic stresses that that does not reflect ambient flow in the formation. There is no accepted technique for identification or assessing the amount of ambient horizontal flow in fractured rock.

The utility of temperature profiles in rock boreholes for identifying hydraulically active fractures has recently advanced by the use of (i) improved sensors with resolution approaching 0.001 C°, (ii) flexible impermeable liners and iii) the active line source (ALS) method to overcome the depth limitations while standardizing the basis for comparison of flow zones. The borehole liner prevents vertical cross-connected water flow between fractures and hydrologic units thereby restoring the ambient groundwater flow condition that would have existed without the hole present. The ALS process, wherein the entire length of the static water column in the lined-hole is heated and high resolution temperature profiles are repeatedly measured to observe the dissipation of thermal energy, was applied in sandstone and dolostone to depths of up to 400m for comparison to results using the same procedures without heating. The interpretation identifies many hydraulically active fractures under ambient flow conditions without the depth related bias, beyond the limits of conventional temperature profiles and provides an improved basis for assessing the relative magnitude of ambient flow based on the comparison of the size of the temperature variations.

A2.**Background:**

Although temperature profiles are reported to have been collected in water wells by James D. Forbes and William Thompson (aka Lord Kelvin) as early as the mid 1800's (Burchfield, 1975), the application of the technique for identifying flow in fractures is sparsely discussed in the literature until the late 1960s. Trainer (1968) recognized that flow zones in dolomitic rocks of the Lockport formation (Niagara County N.Y.) created abrupt offsets in temperature profiles of boreholes. Seasonal variations in surface temperatures propagating downward with cross-connected flow within boreholes provided the thermal disequilibrium that allowed flow zones to be interpreted and Trainer was able to laterally correlate these features over the span of a kilometer. Conway (1977) improved the identification of flow features by calculating the thermal gradient over a few metres which enhanced correlation between boreholes. Drogue (1985) superimposed seasonally varying thermal profiles from the same borehole to depict a cone of time-dependant variability the width of which decreases from surface and identified a characteristic boundary beyond which the temperature is stable and gradually increasing with depth. Drogue designated the shallow thermally variable portion of the profiles as "heterothermic", the deeper portions "homothermic", and identified the boundary between the two at approximately 25m in an example from Southern France.

Keys and Brown (1977) noted that lateral flow through fractures moving from an injection well creates discrete aberrations (peaks or troughs) in temperature profiles. The identification of fractures based on discrete aberrations was subsequently used by many (e.g. Sillman & Robinson, 1989; Malard & Chapuis,1995; Bideau & Drogue,1993; Robinson et al,1993 and Ge,1998) but commonly the identification of flow zones suffered in the presence of cross-connected flow. Although fluid temperature logs are regularly collected in a typical geophysical logging suite through fractured rock, but (based on the number of citations) interest in the technique has waned; the data has become of secondary value and is rarely relied upon in deference to several other techniques such as flow meters, FEC logging, and a variety of transmissivity measuring methods. In a review of the use of heat for groundwater insights Anderson (2005) cited over 200 references of which only seven focused on identification of flow in boreholes through fractured rock.

We attribute the declining reliance on temperature logging for providing identification of flow through fractures to two primary factors; historically poor resolution of temperature probes (until recently sensors could not resolve variations of less than 0.1C°), and the negative effects of borehole hydraulic cross-connection (e.g. Bidaux and Drogue, 1993; Robinson et al.,1993; and Genthon et al., 2005). The effects of borehole hydraulic cross connection are a ubiquitous problem influencing all

forms of testing in open boreholes through fractured rock. For example, Price et al (1993) and Sterling et al (2005) demonstrated the impacts of hydraulic cross connection by showing substantial differences between ambient and cross connected hydrochemistry.

These fundamental limitations to the application of temperature profiles in fractured rock have now been overcome. The resolution of temperature probes used in borehole logging has improved to the order of 0.001 C° (e.g. Pehme et al, 2007a; Berthold and Börner, 2008), which greatly enhances the detection limits of flow from temperature logs. A recent advance in borehole technologies, the installation of flexible fabric impermeable liners to restrict hydraulic cross connection in bedrock boreholes is an increasingly common practice (Keller, 2007). A cylindrical liner that has a diameter slightly greater than the borehole is everted down the entire length of the hole by adding water to the inside and once in place, the water level is maintained above the highest formation head so that the liner is inflated tightly against the borehole wall. Pehme et al (2010) show by means of high resolution temperature profiling that the water column inside the inflated liner is essentially motionless, and that after a period allowing thermal equilibration, the water column takes on the temperature distribution of the rock mass surrounding the borehole. They present high resolution temperature profiling in four holes in fractured dolostone and sandstone to show that many more hydraulically active fractures are identified by profiling inside lined holes relative to the identification in the same holes without the liners (Figure A1, columns B and C). However in the process of overcoming these limitations to the application of temperature logs, two additional requirements influencing the resolution of flow from temperature logs have been highlighted, specifically data density and depth constraints imposed by the need for thermal disequilibrium. This manuscript discusses the additional limitations and approaches to eliminating these as part of the revitalization of temperature profiling for identification of flow through fractured rock.

A3. **Data Resolution:**

The advent of a gradient log over short distances (Conway, 1977) was well suited to improving resolution of discrete flow zones in temperature data in a cross-connected open hole because both flow in and out of the borehole manifest as either a step or inflection in the temperature profile. However, in the case of a lined borehole, where flow in a fracture results in a narrow spike or trough in the temperature profile, a gradient log calculated in this manner distorts the original pattern of the aberration in the profile and creates a bimodal anomaly. Pehme et al (2010) describe an alternative

approach, the "variability log", but which we prefer to refer to as a "thermal deviation log"[16], which is calculated by first smoothing the temperature profile over a broad interval (5 metres is suggested), and then subtracting the result from the original data. The thermal deviation log suppresses the broad temperature changes created in the near surface heterothermic zone and deeper geothermal gradients while better honoring the original shape of the narrow temperature changes that occur due to water movement.

A critical aspect of the analysis of aberrations on a temperature profile that is sometimes overlooked, but which becomes particularly evident as the resolution of the probe improves and greater detail is demanded from the interpretation, is that the data density must be increased to adequately resolve the subtle aberrations and logging speed commensurately decreased to match the sampling time constant of the sensor. The IFG probe has a time constant of 0.5s, can be sampled at 2Hz, and when data is collected at a nearly constant speed between 0.5 and 0.7 m/min, can be processed to a constant depth interval consistent with the nominal sampling distance of 0.005 m. In our experience typical contractor SOPs specify logging rates for temperature of 2-3 m/min or more and sampling intervals that are at 0.1 m to 0.3m and greater.

To examine the ramifications of broader sampling the open and lined-hole temperature logs presented by Pehme et al (2010) that were originally collected at a 0.005m data density were re-sampled by extracting the closest data point to a 0.1m and 0.3m data interval. The corresponding gradient and thermal deviation logs (columns $H_{10,30}$, $J_{10,30}$ and $K_{10,30}$) are shown in Figure A1 for the open-hole data as well as the first ((16/02/04) and last (12/04/04) lined-hole data sets. At the scale of the entire borehole there is only a slight smoothing of the result, with a minor deterioration in resolution with the coarser sampling intervals. All of the major irregularities are represented in all three data densities and identification of those does not noticeably deteriorate. Note that re-sampling does not include the additional smoothing that would result from an increase in logging speed.

However the compromise associated with under-sampling becomes more apparent at a higher level of detail. Figure A2 shows a window of selected data from UW1 (Figure A1) between the depths of

[16] In statistical parlance the difference between an individual data point and the mean value of the complete data set is termed "the deviation" (refer to a standard statistical text, e.g. Sokal and Rohlf, 1981) while the variance is the mean square of the deviations. Although individual deviations of the members of a data set would be calculated based on the mean of the entire data set and not a sliding mean, we suggest that the "variability log" described by Pehme et al (2010) would be more correctly termed a "thermal deviation log", using the qualifier to differentiate it from a "borehole deviation log" used to depict the systematic changes in the angle of a borehole from the vertical, and subsequently adopt the term.

47.5-52.0mbgs with the 0.10m and 0.30m sampling points superimposed on the original logs. The distinct aberration in the open and 12/04/04 lined-hole temperature logs 51.30 mbgs is drastically dampened in at a 0.10m sampling interval and essentially un-resolvable at a 0.30m data spacing. Several subtle irregularities exist between 48 and 49mbgs which are of larger amplitude than the sensor sensitivity, are represented by many readings in each of the original logs and can be identified in multiple data sets, but cannot be inferred at either of the coarser sampling intervals. It is important to note that although the similarities in the patterns (peaks and troughs) coincide between the three lined-hole temperature logs (even though these are collected at approximately one month intervals over a thermal recovery from an open-hole to an ambient temperature condition), there is yet no independent means to corroborate that these irregularities result from water flow within the rock. However no further analysis could be undertaken to resolve this issue on the coarser data sets as the patterns either do not appear in the data or are inadequately resolved.

A4.**Reliance on Thermal Disequilibrium**

Although implied by many, and seemingly intuitive, the requirement for disequilibrium as an additional fundamental limitation to application of temperature logs for identifying flow through fractures is emphasized by the data collected in the lining of the borehole. In a lined hole, without environmentally driven thermal disequilibrium below the limit of the heterothermic zone, the temperature of the rock and any water moving through fractures will be the same and flow would not be detectable by way of a temperature log as shown schematically in Figure A3. Between the shallow subsurface where the thermal disequilibrium tends to be large and the upper limit of homothermic zone where thermal uniformity makes flow undetectable, intermediate degrees of temperature contrast must exist between the water flowing through the fractures and the surrounding rock. It follows that for two fractures with the same rate of groundwater flow, but each with a different temperature contrast between the water and the matrix, the size of the aberration on a temperature profile will be different. The practical implication of this premise is that a comparison of the magnitude of aberrations on a temperature profile is not always a reliable basis for inferring of the amount of water moving in the fractures throughout the borehole and sensitivity will depend on the degree of disequilibrium, in most cases decreasing with depth.

Figure A4 shows an expanded portion of the data in UW1 deeper, over the lower limit of the heterothermic zone. These data highlight the fact that the depth of the heterothermic-homothermic boundary will depend in part on the resolution of the probe used. At a 0.1 C° sensor resolution the boundary would be set at approximately 80 mbgs whereas with the higher sensitivity sensor there is

clear separation between the profiles to 85 mbgs and a subtle offset to 112 mbgs. The irregularity of the thermal deviation representations of the lined-hole temperature profiles decrease distinctly at 80, 85 and 112mbgs as well. However the packer testing results show available transmissivity and rock core contamination implies flow has occurred throughout the depth interval and although neither confirm flow was occurring when the temperature data were collected, these results are consistent with the temperature logs having declining resolution of flow immediately above the hetero-homothermic boundary.

A comparison of the open-hole temperature profile represented as a gradient log with the thermal deviation version emphasizes the advantages of the latter when interpreting discrete aberrations rather than steps or inflections. The gradient log is un-interpretable from the perspective of individual flow zones whereas the thermal deviation representation of the open-hole data maintains the character of the individual aberrations. A complication that remains is that in many cases when a pattern of thermal deviations is identified the interpreter does not have apriori knowledge of whether the water in the fracture is warmer or cooler than the surrounding rock. Molson et al (2007) showed that the polarity of a temperature anomaly can vary over short distances, likely due to small localized changes in the flow pattern as the water winds through a fracture network. Consequently in a thermal profile with closely spaced temperature variations and a poorly defined base level such as in UW1 it can be unclear whether peaks or troughs represent the flow in fractures. With the advantage of several temperature logs over time exhibiting a systematic tendency of cooling it is reasonable to interpret that the resulting negative deflections are potential flow zones, but that could not be concluded with only one data set.

Several investigators (e.g., Beck et. al. 1971; Shen and Beck, 1986 and Lee et. al., 2003) have formulated the relationship between the effects of heating and cooling of a borehole and the thermal distributions within rock in order to estimate ambient formation temperatures after drilling and mud circulation or to estimate the thermal properties of the matrix at discrete depths within a borehole. These works led to the concept of intentionally creating thermal disequilibrium using the active line source (ALS) technique described by Greenhouse and Pehme (2002) and Pehme et al (2007a&b) to gather the same information along the entire length of the hole. In the ALS process, temperature logs are collected both while a borehole is warmed with a line heater and during the subsequent thermal recovery to ambient conditions after the heater is turned off to estimate the variations in the relative apparent thermal conductivity of the rock mass from plots of either or both the ln-linear steady state temperature increase during heating, or decline during thermal recovery. As a limitation to the process Greenhouse and Pehme (2002) note that the borehole fluid is difficult to heat and that it cools

more rapidly where hydraulically active fractures are interpreted to exist based on other data. Pehme et al (2007a&b) suggest that the ALS technique has potential to be used to enhance thermal anomalies due to flow.

Since its introduction the ALS process has evolved and been refined for the purposes of identifying flow in fractures to optimize results and fit within an efficient work flow. The concept is shown schematically in Figure A5, the borehole is heated for 4-6 hours with a line heater that provides approximately 20W/m uniformly along its length to create a cylinder of excess heat around the borehole. Water flowing through fractures under ambient pressure conditions is in thermal disequilibrium near the borehole and manifests as negative aberrations on temperature logs. The typical data collection sequence has three stages consisting of a background (passive) log, an ”active” log during heating, and three “cooling” logs collected through the period of thermal recovery.

Figure A6 shows an example of the results of an ALS test in borehole MW7679 in Guelph Ontario. The borehole is also drilled through the Lockport dolomite, approximately 15 kilometers northeast of UW1. Above 43mbgs the borehole diameter is nominally 15.2 cm diameter and below that it is a 10 cm hole. The passive (background) thermal deviation log has numerous irregularities indicating flow zones above 60mbgs but is relatively uniform below. The borehole was heated for 5 hrs at 22.7 W/m and an active log was initiated an hour before the heater was turned off. Cooling logs were initiated 0.5 hrs (C1), 5 hrs (C2) and 20 hrs (C3) after the heating ceased. The temperature of the larger diameter (upper) portion of the borehole was increased by approximately 1C° and the lower, smaller diameter portion by approximately 2 C°. There is a gradual change in the character of the cooling logs from large amplitude, very narrow negative inflections in C1 to fewer, broader, more uniform zones of cooling as time progresses through C2 and C3. There is a consistent repeatability of the shape and relative size of the broader (approximately 1 m wide) negative inflections throughout the borehole. The expanded view of the portion of the borehole from 70-80mbgs shows repeatability of many of the narrow inflections in the C1 overprinted on the broader lows of the C2 thermal deviation log. However, by the time the C3 data are collected generally the thin inflections can no longer be resolved. The nominal width of the narrow aberrations is between 0.1 and 0.2m and the detailed shape of these would not be adequately resolved at similar data spacing supporting the need for very high data density. The original passive thermal deviation log through this section of the borehole displays none of these aberrations in the temperature profile and these potential flow zones could only be identified by way of the ALS technique.

Timing of ALS tests within the overall workflow in a borehole is important because the interpretation of the results is based on the premise that the initial passive log represents the ambient background temperature distribution in a borehole. The thermal regime should be allowed to stabilize after installation of the liner, however the time required for that to occur depends on the activities undertaken before lining, as well as the degree and duration of the thermal instability introduced. The drilling procedures, the temperature contrast between the air or drill water and the rock mass, the degree of cross-connected flow and the duration that each occurred influence the time required for thermal stabilization. The lack of a systematic progression of temperature from the second (C2) cooling log to the third (C3) and towards the temperatures of the original passive (P) log is an indicator that the environment was unstable during testing.

A5. Summary and Conclusions

The application of temperature logging to the detection of flow through fractures has evolved from originally using the thermal disequilibrium created by cross-connected flow through a borehole to detect some of the primary flow zones in a rock mass - to the recognition that other more subtle flow features exist but are masked by the borehole water movement, - to the current appreciation that not only are minor flow zones being masked by cross-connected flow but critically important ones can be as well. However, removable liners are now available to eliminate the cross-connected flow and place the borehole into an ambient thermal stratification. Sensor sensitivity has increased dramatically and the detection of many more flow zones that represent a broad range of flow conditions has improved. As the potential importance of resolving these subtle variations in response is realized, it becomes critical that data density is also increased and that data presentation be revised from the basic gradient to approaches such as the “thermal deviation” to honour the detail of the temperature aberrations.

The elimination of cross-connected flow removes one of the contributors to thermal dis-equilibrium deeper in the borehole (below the hetero-homothermic boundary). Once eliminated, the absence highlights the degree to which temperature logs depend on thermal dis-equilibrium to detect flow through fractured rock. The ALS technique holds promise for creating required temperature contrasts in a controlled fashion and improving the detection of flow zones, but requires further development to fully understand the process and the mechanisms that control it.

A6. Appendix A - Figures

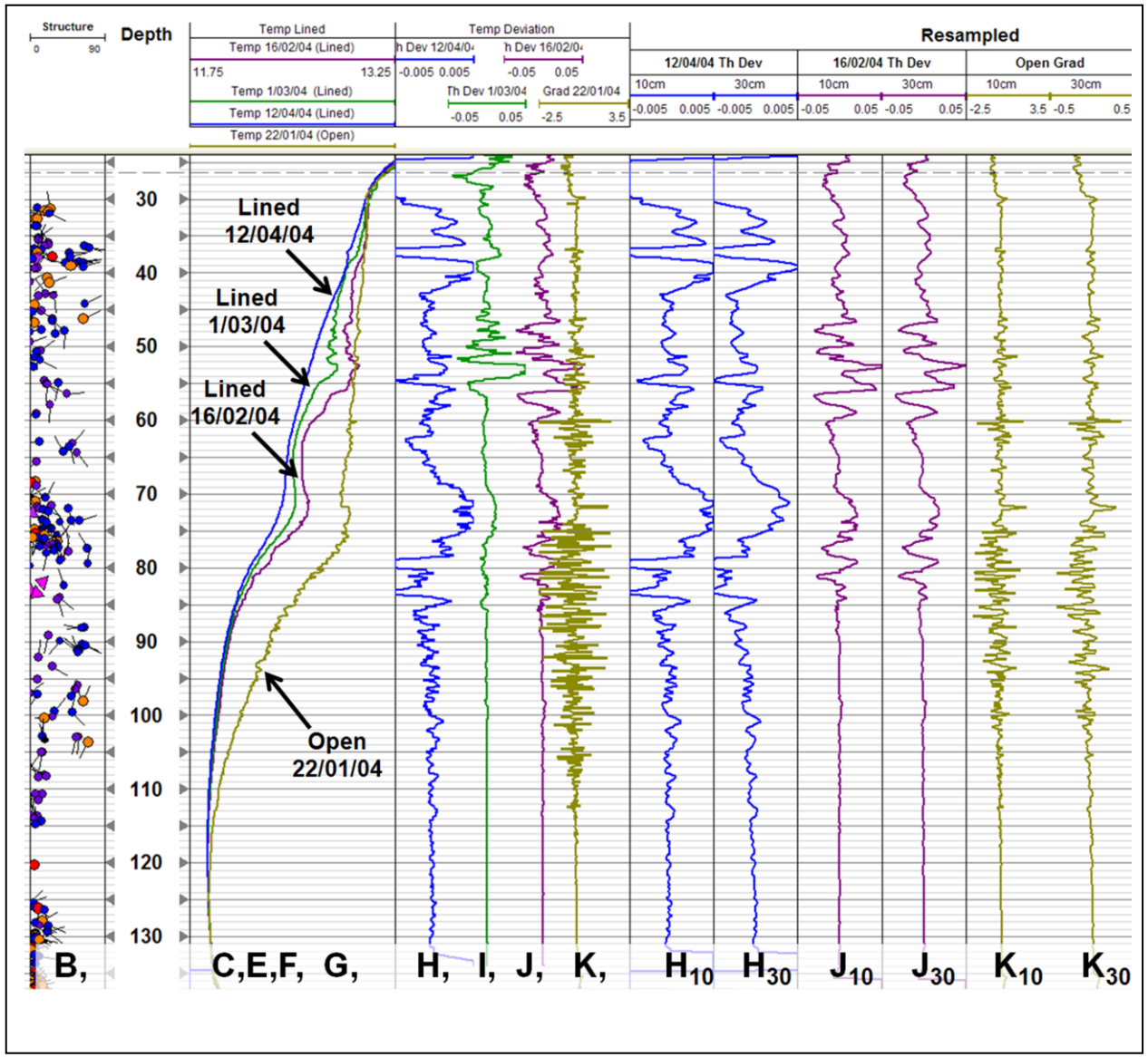

Figure A1: Open and Lined-hole temperature logs from UW1 (Lockport formation), Cambridge Ontario.

Column labelling is consistent with subsequent figures: B), interpretation of discontinuities from acoustic televiewer amplitude image , passive temperature logs collected in the lined boreholes 12/04/2004 (C-blue), 1/03/2004 (E-green), and 16/02/2004 (F-purple), and open borehole 22/01/2004 (G-gold); lined-hole thermal deviation logs 12/04/2004 (H), 1/03/2004 (I) and 16/02/2004 (J); open-hole 22/01/2004 gradient log (K); H_{10}& H_{30} thermal deviation log based on re-sampling 12/04/2004 (C) at 10cm and 30cm intervals respectively; J_{10} & J_{30} thermal deviation log based on re-sampling 16/02/2004 (J) at 10cm and 30cm intervals respectively; K_{10} & K_{30} gradient log based on re-sampling Open-hole 22/01/2004 (K) at 10cm and 30cm intervals respectively; (columns C-K from Pehme et al (2010).

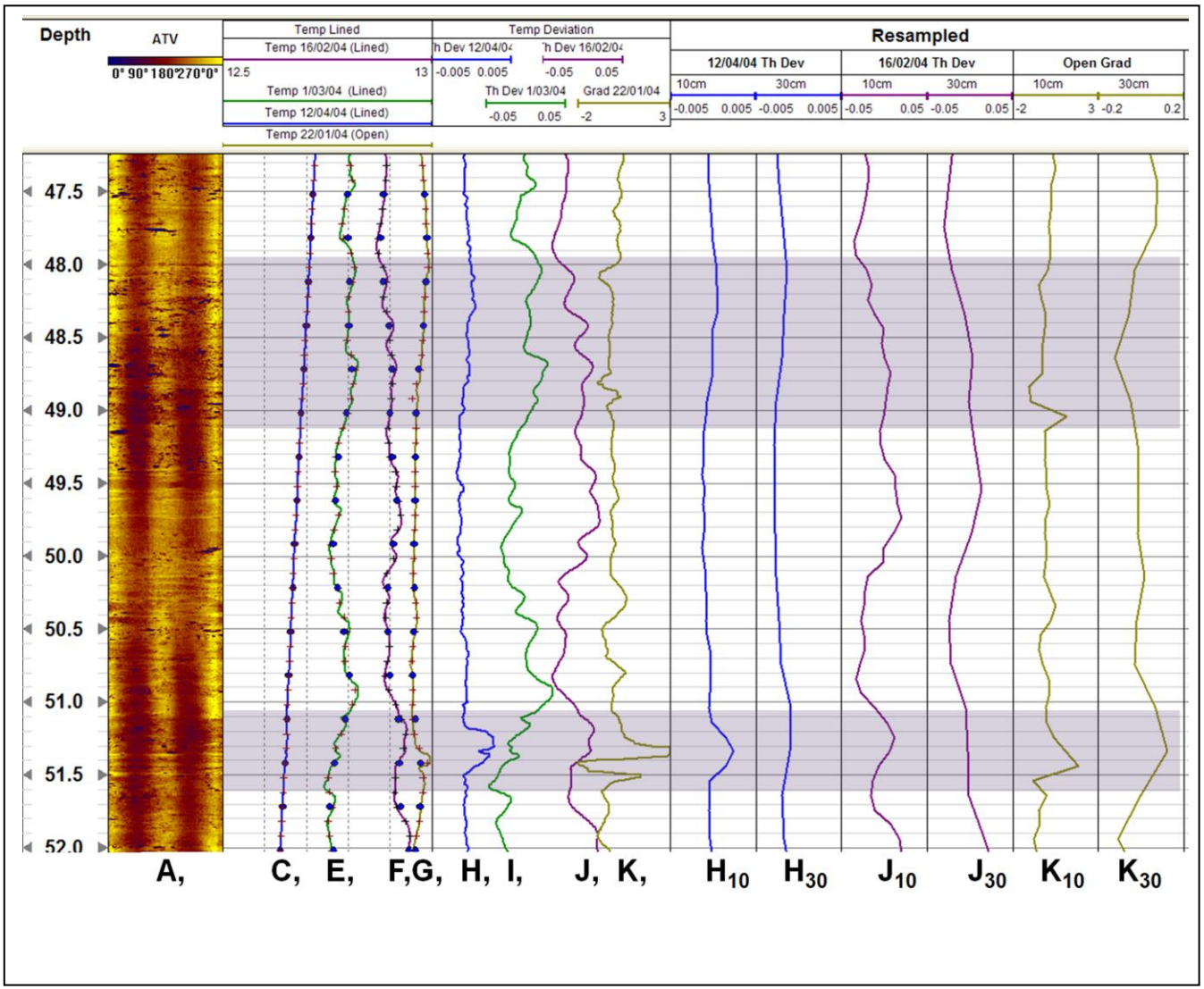

Figure A2: Expanded portion of open and lined-hole temperature logs from UW1 (Lockport formation), Cambridge Ontario. Column labeling is consistent with other figures: A) acoustic televiewer amplitude image, passive temperature logs collected in the lined boreholes 12/04/2004 (C-blue), 1/03/2004 (E-green), and 16/02/2004 (F-purple), and open borehole 22/01/2004 (G-gold); lined-hole thermal deviation logs 12/04/2004 (H), 1/03/2004 (I) and 16/02/2004 (J); open-hole 22/01/2004 gradient log (K); H_{10}& H_{30} thermal deviation log based on re-sampling 12/04/2004 (C) at 10cm(+) and 30cm (•) intervals respectively; J_{10} & J_{30} thermal deviation log based on re-sampling 16/02/2004 (J) at 10cm(+) and 30cm (•) intervals respectively; K_{10} & K_{30} gradient log based on re-sampling Open-hole 22/01/2004 (K) at 10cm(+) and 30cm (•) intervals respectively; columns C-K from Pehme et al (2010).

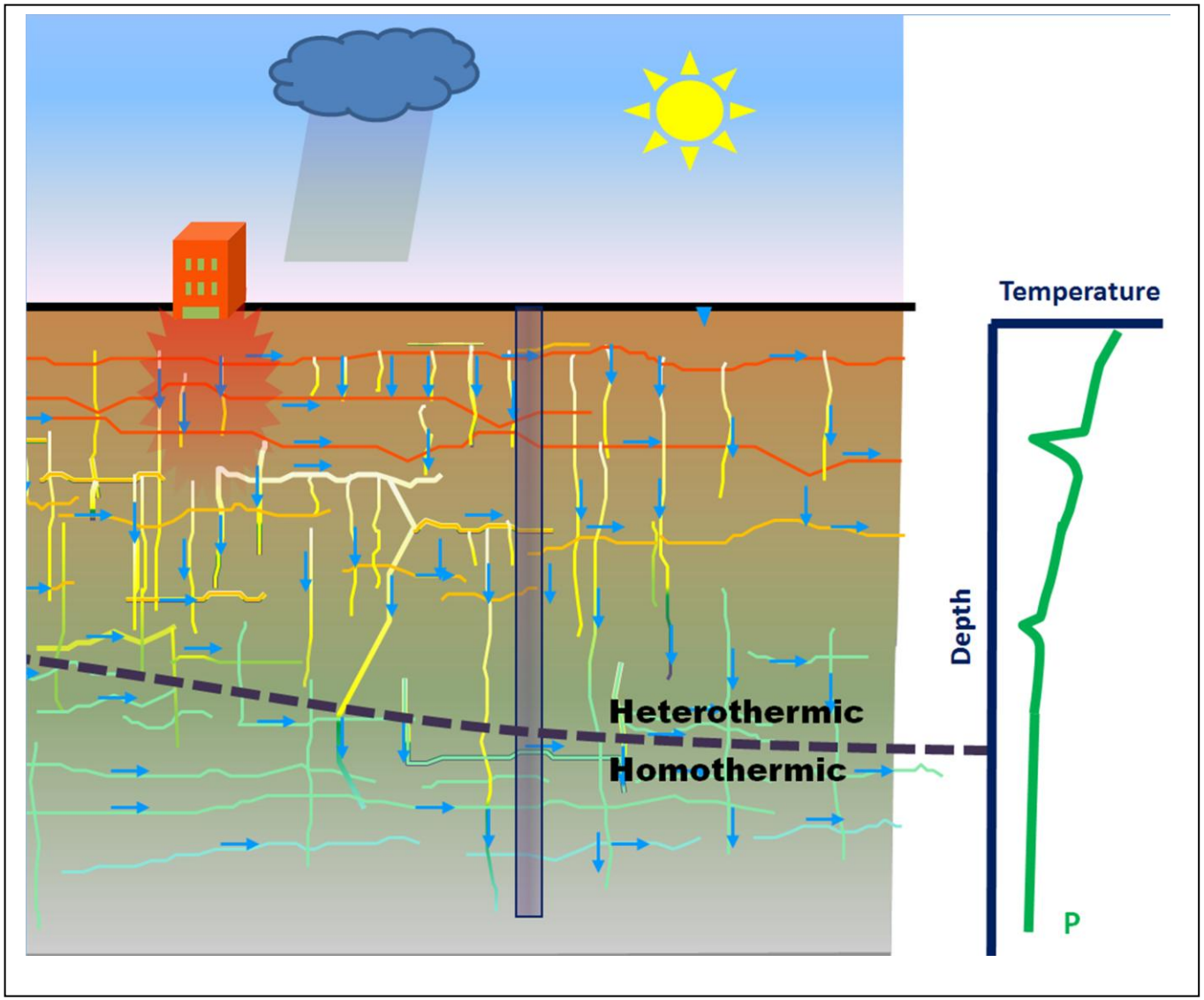

Figure A3: Schematic representation of the heterothermic-homothermic boundary. The propagation environmentally thermal disequilibrium is controlled by groundwater flow in the rock. The temperature profile shows the implications on resolving equivalent flow zones with a temperature log at a high (large aberration), moderate (small aberration), and no thermal dis-equilibrium (no response).

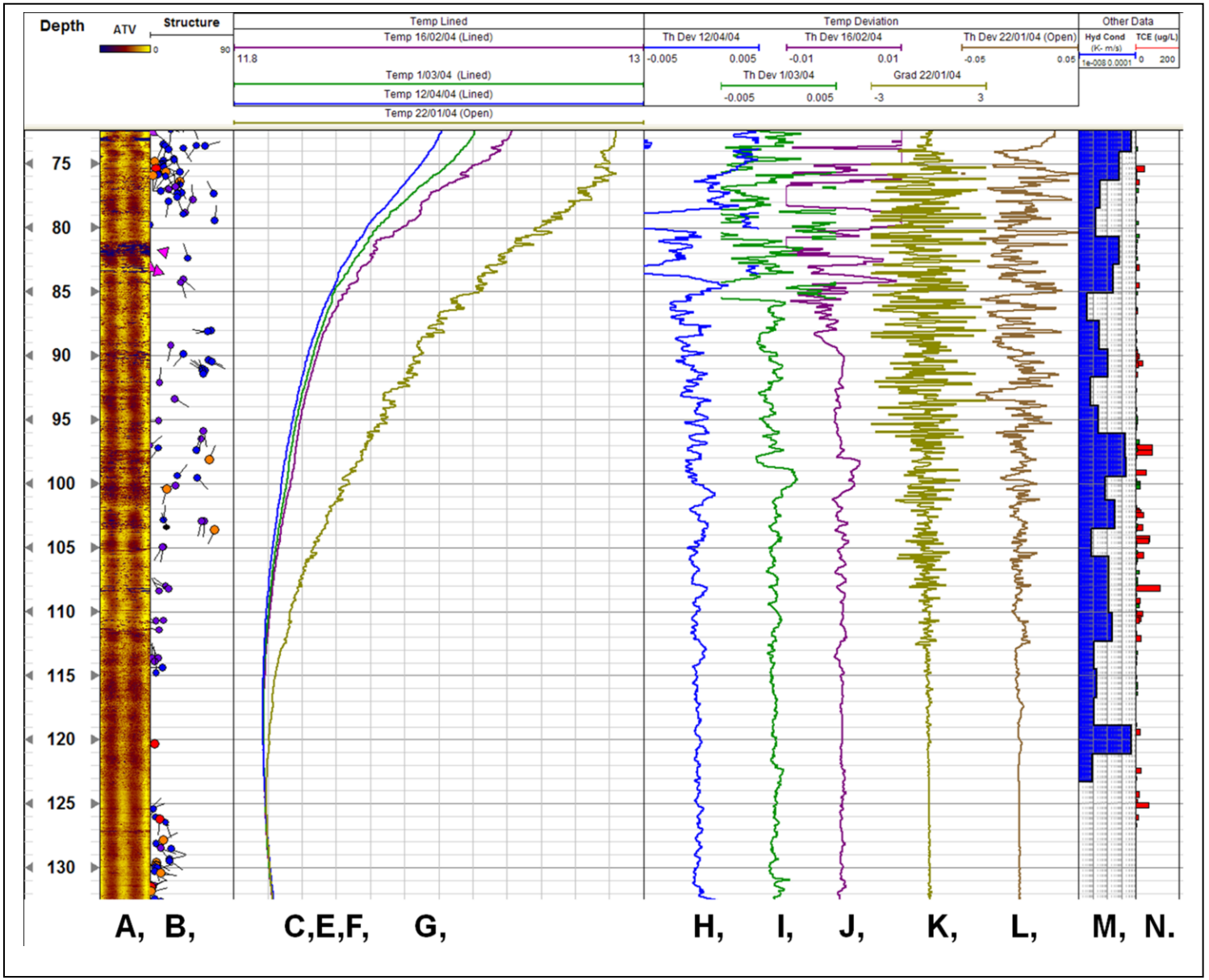

Figure A4: Expanded view of UW1 data. (A) acoustic televiewer amplitude image, (B) interpretation of discontinuities from A, passive temperature logs collected in the lined boreholes 12/04/2004 (C-blue), 1/03/2004 (E-green), and 16/02/2004 (F-purple), and open borehole on 22/01/2004 (G-gold); lined-hole thermal deviation logs 12/04/2004 (H), 1/03/2004 (I) and 16/02/2004 (J); open-hole 22/01/2004 gradient log (K) and thermal deviation log (L); (M) hydraulic conductivity from packer testing (at a log scale), (N) TCE rock core analysis ug/L (red, quantifiable; blue and green, below detection limit). (columns C-K from Pehme et al (2010).

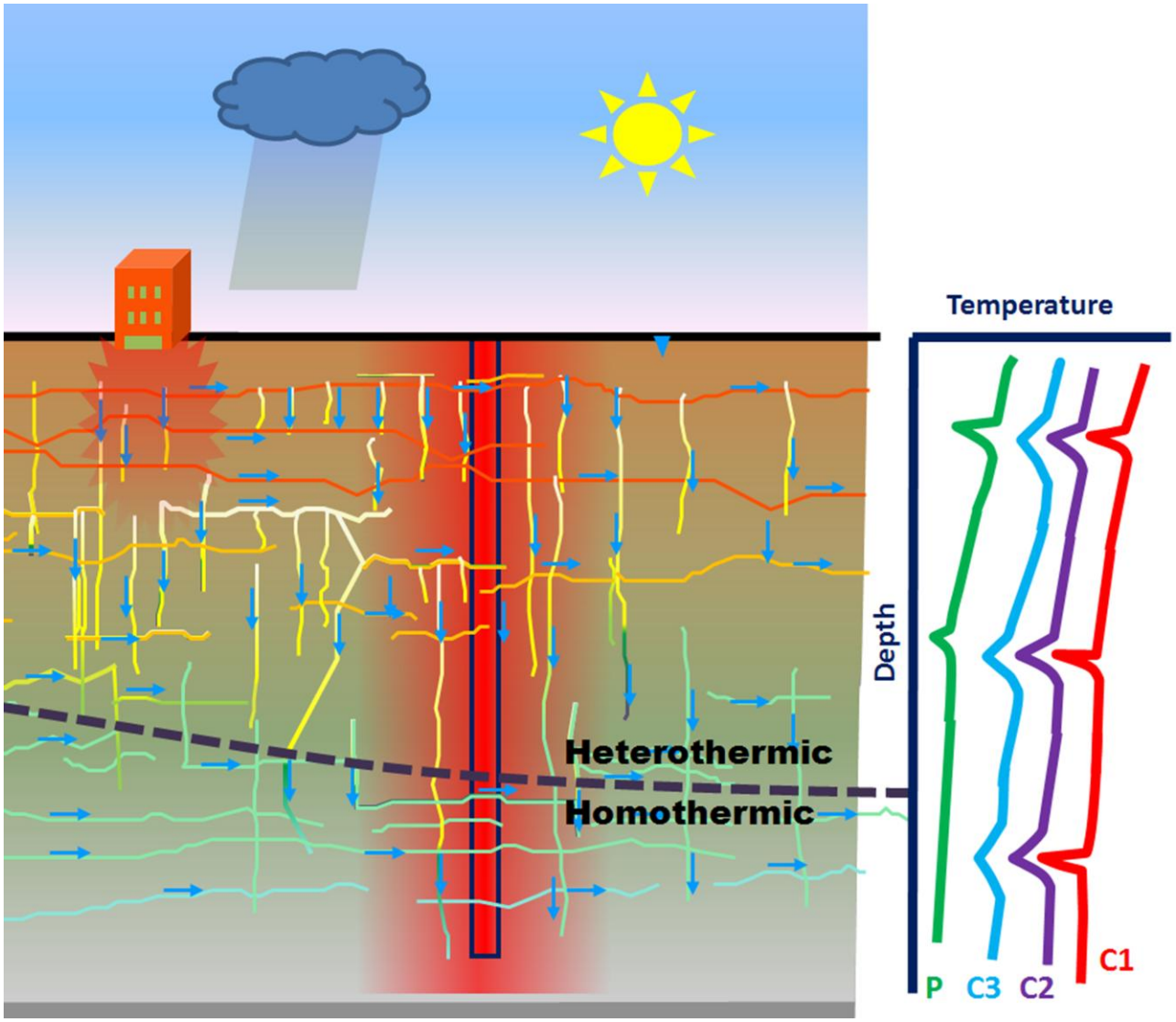

Figure A5: Schematic representation of the ALS technique.
The aberrations on cooling logs are all negative and independent of hetero-homothermic boundary.

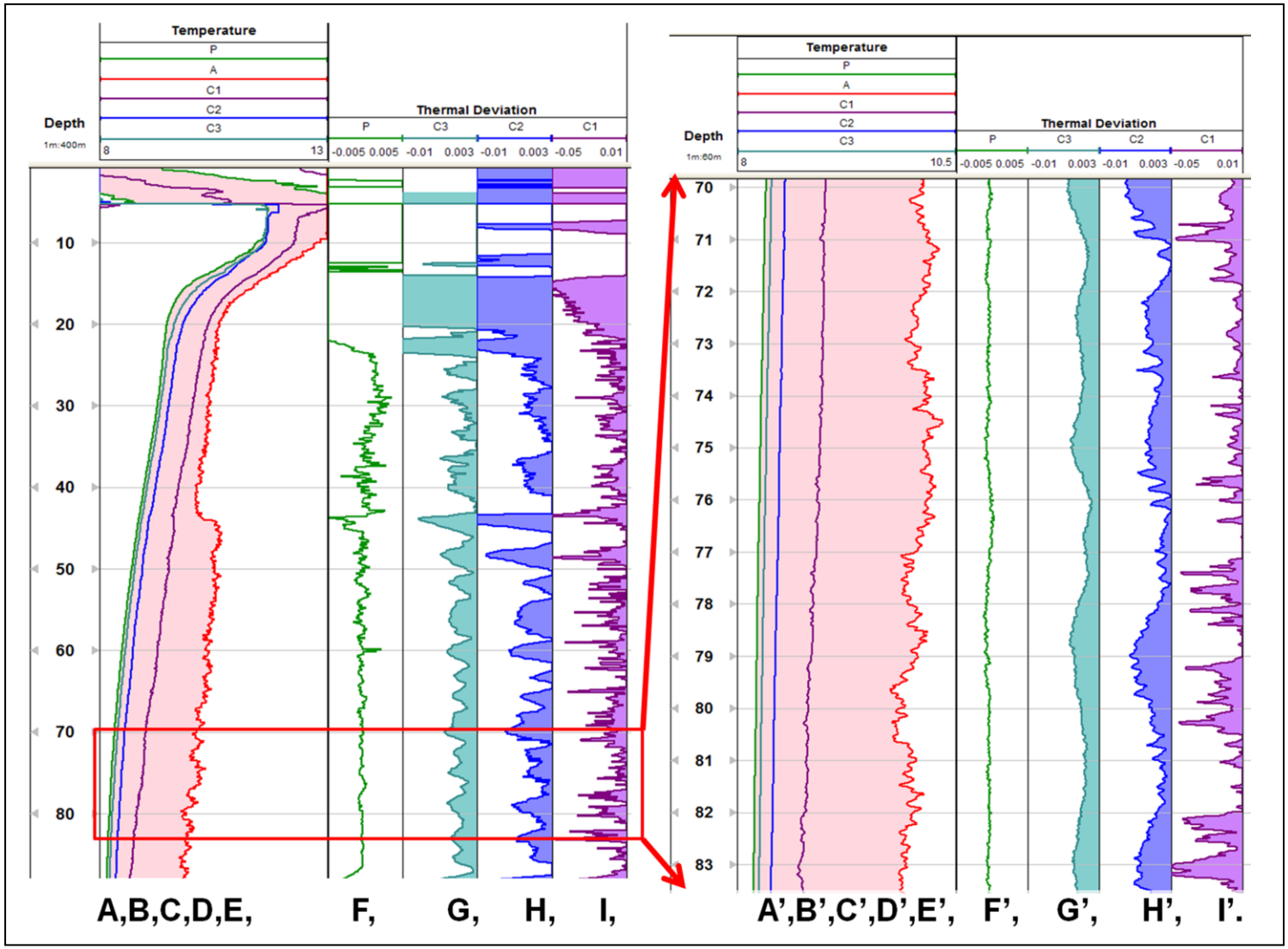

Figure A6: Example of an ALS Test MW7679 Guelph, Ontario.
A Passive Temperature, B,C,D- Cooling Logs C3,C2,C1, E-Active Temperature during heating (all Temperature logs 8.0-13.0), D- Thermal Deviation (Passive (A),-0.005 to 0.005), G- Thermal Deviation (C3(B),-0.01 to 0.003), H- Thermal Deviation (C2(C),-0.01 to 0.003), I-Thermal Deviation (C1(D),-0.05 to 0.01). A' through I' as per A through I with expanded vertical scale.
** All data in C° **

A7. **Appendix A - References:**

Anderson, M.P. 2005. Heat as a ground water tracer. Ground Water 43, no. 6: 951-968

Berthold, S and F. Börner, 2008, Detection of free vertical convection and double-diffusion in groundwater monitoring wells with geophysical borehole measurements. Environmental Geology 54, 1547-1566.

Beck A.E., F.M. Anglin and J.H. Sass 1971. Analysis of Heat Flow-in situ Thermal Conductivity Measurements. Canadian Journal of Earth Sciences, Vol 8, No 1 pp 1-19.

Bidaux, P., and C. Drogue. 1993. Calculation of low-range flow velocities in fractured carbonate media from borehole hydrochemical logging data comparison with thermometric results. Ground Water 31, no.1: 19-26.

Burchfield, J.D. Lord Kelvin and the Age of the Earth, 1975, Sci. Hist. Pub., New York. 260pp.

Conway, J.G. 1977. Deconvolution of Temperature Gradient Logs, Geophysics, Vol 42, no. 4 pp.823-837

Drogue, C. 1885. Geothermal gradients and groundwater circulations in fissured and karstic rocks: The role played by the structure of the permeable network. J. Geodynamics,no.4, pp.219-231.

Ge, S. 1998, Estimation of groundwater velocity in localized fracture zones from well temperature profiles, Journal of Volocanology and Geothermal Research 84, pg93-101.

Genthon, P., A. Bataille, A. Fromant, D. D'Hulst, and F. Bourges. 2005. Temperature as a marker for karstic waters hydrodynamics. Inferences from 1 year recording at La Peyrére cave (Ariège, France). Journal of Hydrology 311, no. 1-4: 157-171

Greenhouse, John P. and P.E. Pehme, 2002, Monitoring the Temperature in a Sleeved Borehole: Implications for Fracture Detection, Proceedings of the 55th Canadian Geotechnical and 3rd Joint IAH-CNC and CGS Groundwater Specialty

Keller, C., 2007, Liners and Packers: Similarities and Differences. 2007 NGWA/U.S. EPA Fractured Rock Conference: State of the Science and Measuring Success in Remediation, Portland, Maine. September 24-26, 2007

Keys, W.S., and R.F. Brown. 1978. The use of temperature logs to trace the movement of injected water. Ground Water 16, no. 1: 32-48.

Malard F., and R. Chapuis. 1995. Temperature logging to describe the movement of sewage-polluted surface water infiltrating into a fractured rock aquifer. Journal of Hydrology 173, no. 1-4: 191-217.

Lee Tien-Chang, A.D. Duchkov and S.G. Morozov, 2003, Determination of thermal properties and formation temperature from borehole thermal recovery data, Geophysics Vol 68, No8, pp.1835-1846

Molson J., P. Pehme, J. Cherry, and B. Parker. 2007. Numerical analysis of HEAT transport within fractured sedimentary rock: Implications for temperature probes. In 2007 NGWA/U.S. EPA Fractured Rock Conference: State of the Science and Measuring Success in Remediation, Portland, Maine, 24-26 September 2007.

Pehme, P., J.P. Greenhouse and B.L. Parker, 2007a, The Active Line Source Temperature Logging Technique and its application in fractured rock hydrogeology, Journal of Environmental and Engineering Geophysics, V 12 No 4 pp. 307-322.

Pehme, P.E., B.L Parker, J.A. Cherry and J.P. Greenhouse, 2007c, The Potential for Compromised Interpretations When Based on Open Borehole Geophysical Data in Fractured Rock. 2007 NGWA/U.S. EPA Fractured Rock Conference: State of the Science and Measuring Success in Remediation, Portland, Maine. September 24-26, 2007

Pehme, P.E., Parker B.L, Cherry J.A. and Greenhouse J. P., 2010, Improved Resolution of Ambient Flow through Fractured Rock with Temperature Logs, Ground Water, Vol 28, No 2 pp.191-211.

Price, M. and A. Williams, 1993. The Influence of Unlined Borehole on Groundwater Chemistry: A Comparative Study Using Pore-Water Extraction and Packer Sampling, J.IWEM Water and Environment Journal 7 651-659

Robinson R., S. Stilliman, and C. Cady. 1993. Identifying fracture interconnections between boreholes using natural temperature profiling: II. Application to fractured dolomite. Log Analyst 34, no. 1: 69-77.

Shen, P.Y. and A.E. Beck, 1986. Stabilization of bottom hole temperature with finite circulation time and fluid flow. Geophysical Journal of the Royal Astronomical Society, 86, 63-90

Silliman, S., and R. Robinson. 1989. Identifying fracture interconnections between boreholes using natural temperature profiling: I. Conceptual basis. Ground Water 27, no. 3: 393-402.

Sokal R.R. and F.J. Rohlf. 1981. Biometry: The principles and practice of statistics in biological research. W.H. Freeman and Company, San Francisco, 859 pp.

Sterling, S.N., B.L. Parker, J.A. Cherry, J.H. Williams, J.W. Lane Jr., and F.P. Haeni. 2005. Vertical cross contamination of trichloroethylene in a borehole in fractured sandstone. Ground Water 43, no. 4: 557-573.

Trainer, F.W. 1968. Temperature profiles in water wells as indicators of bedrock fractures. Professional Paper 600-B, Washington DC: USGS.

Appendix B

Numerical Investigations Of Groundwater Flow And Thermal Patterns With Implications For Interpreting High Resolution Temperature Logging Data.

Final Version November, 2011.

Peeter Pehme,

Edited by Dr. John Molson & Dr. Emil Frind.

B1. Overview

As hydrogeologic investigators increasingly focus on issues within fractured rock, the need for tools to characterize flow within the fractures is growing. Temperature logging was the original borehole geophysical tool applied to the problem, but has decreased in importance relative to more sophisticated technologies. However, with improvements in electronics allowing temperature differences of a few thousandths of a degree to be resolved, new field techniques such as using the FLUTe liner to restrict borehole cross-connected flow, and the active line source (ALS) approach controlling disequilibrium, thermal logging applications are in a revival. High resolution temperature logging is one of few viable techniques for characterizing ambient flow within fractures although currently only at a "qualitative interpretation" level, allowing relative comparisons of flow but it cannot yet be used as a quantifiable measurement tool.

This report numerically explores the interaction of heat, supplied by the ALS process, and water moving through a fracture, to assess the controlling and limiting factors of the potential for a quantitative analysis of fracture flow. A finely discretized model of the intersection of a lined borehole and a single horizontal fracture is developed and the code "Smoker" (Molson and Frind 2005), which numerically simulates the flow of water and heat transport through a fractured rock system, is used to imitate the ALS process. The influence on the temperature patterns of system parameters that are controllable (i.e. amount / length of heating, borehole diameter), uncontrolled factors of the process (heater location) and natural system characteristics (i.e. background temperature, rock thermal conductivity, fracture aperture and hydraulic gradient) are systematically varied individually and in pairs. The results are analyzed both in terms of absolute temperature and

based on relative cooling which emphasizes the effect of the water movement in the fracture. The ALS process is divided into stages and the influence of the changing parameters on each of the stages is documented and compared.

The results show the importance of the location of the heater relative to the flow direction and help explain previously unresolved observations in field data e.g. temperature measurements occasionally increase after the heater is turned off. The parameters which influence the logarithmic rate of cooling are ranked in terms of relative influence and collectively indicate that the temperature response cannot simply be related to flow alone. However, most of the other critical factors such as borehole diameter and rock thermal conductivity can be measured and their influence accounted for. Resolution of the position of the heater relative to flow will require measurements with multiple temperature sensors. The results indicate that the excess cooling at the fracture relates to volumetric flow (flux) rather than velocity. Flux cannot be quantified with a single simple equation based on the thermal response but will likely require a series of "type curves" which account for the important but measurable parameters.

B2. Acknowledgments

The author would like to acknowledge Dr. John Molson for numerous hours invested in providing guidance, discussion and constructive review of this work. Dr. Emil Frind also graciously contributed valuable insights and edits that improved this manuscript.

P. Pehme.

B3. Introduction

This manuscript is the culminating summary of an independent study course (Earth 692) which focused on the influence of the physical characteristics of a fractured rock system on the temperature distribution around a fracture-borehole intersection. In addition to exploring the thermal process of an active line source (ALS) test, the objective is also to develop an appreciation for the broader influence of physical and geometric parameters on the distribution of heat as well as refine the process of temperature logging as part of a study of groundwater flow in fractured rock. The final goal is to assess the potential for determining fracture flow rates based on measured temperature profiles and specifically address the potential for application of the newly-developed temperature vector probe (TVP) as a geophysical characterization tool.

The study is undertaken by creating a numerical model that simulates a field situation typical of southern Ontario which includes a borehole drilled through dolomite that has been sealed with a liner. To simplify the analysis, the borehole is assumed to intersect a single horizontal fracture in the model. The process of temperature logging of the borehole with the ALS technique (Pehme et al., 2007a) is simulated. After establishing that the model is a reasonable representation of field conditions, a sensitivity analysis is completed by systematically varying (increasing and decreasing) various parameters of the model. The parameters tested are generally divided between those that can be controlled (e.g. borehole diameter, timing etc) and others that cannot (e.g. the thermal conductivity of the rock, fracture aperture, etc). Insights into the factors controlling thermal patterns in the borehole are developed by comparing the predicted temperature variations in the borehole as individual parameters are varied in a systematic fashion. Those results are then compared to the simulated effects of varying flow rates through the fracture to develop a strategy for quantifying flow rates from the temperature data.

B2.1. Conceptual Models in Fractured Rock Investigations

Fractured rock sites are broadly conceptualized as either an equivalent porous medium or are described based on the nature of the flow through the fracture system. The models that form the framework for describing the nature of the fracturing are further subdivided into two groups Parker (2007), referred to as the "super highway" in which groundwater flow is controlled by a limited number of major fractures and the newer, "discrete fracture network" (DFN) model, in which some larger fractures exist but flow is predominantly controlled by many inter-connected small fractures. There is an increasing body of evidence (Sterling et. al., 2003, Parker 2007, Meyer et. al., 2007) that the DFN model has broad application, particularly in sedimentary rock. The primary support for the DFN model comes from the general observation that many contaminant plumes are often not as extensive as expected from the measurement of hydraulic gradients and subsequent groundwater velocity estimates. Parker et. al. (1994) used detailed chemical analyses of rock matrix samples to develop and confirm the applicability of a model wherein retardation results from the spreading of the plume through numerous small fractures and subsequent diffusion of contaminant into the matrix. Other forms of data (core logging, video logs and geophysical logs (acoustic televiewer and caliper)) support the premise that numerous fractures exist, but do not confirm groundwater movement. Likewise straddle packer testing (Novakowski et al., 2005) and FLUTe liner profiling (Keller et al., 2008) identify hydraulically conductive zones (fractures), but only under artificially applied pressure and do not provide insight into fracture flow under ambient conditions. Several techniques exist for detecting flow in an open borehole of which heat-pulse and impeller flow meters are most commonly

employed (Paillet, 1999). Electromagnetic flow detection (Moltz et al. 1994) and fluid conductivity logging (Tsang et al., 1990) have seen limited use. All of these techniques suffer in the presence of cross-connected flow in the open borehole annulus which commonly occurs. Pehme et al. (2010) demonstrate that open hole geophysical and hydrophysical measurements can be misleading and that temperature profiles in lined boreholes provide a superior method for identifying the presence of water moving through fractures. Other techniques, including KVA (Kerrfoot 1992), Posiva (Kukkonen et al. 2005), Colloidal Boreholescope (Kearl 1997) and Borehole Doppler (SonTek, 1996) use a variety of approaches to restrict annular flow while measuring flow but see very limited use based on their representation in the literature. Wilson et. al. (2001) tested these alternative technologies (with the exception of Posiva) and found the repeatability of results poor.

B3.1. Temperature logging

B3.1.1. Historical Perspective

It has long been recognized that subsurface temperature can provide insights into groundwater movement. The distortion of the patterns in heat energy transfer by groundwater can be used to identify surface water infiltration, broad patterns of groundwater movement as well as flow through fractures (Anderson 2005). Drogue (1985) superimposed seasonally varying thermal profiles from the same borehole to depict a cone of time-dependant variability decreasing from surface below which the temperature is stable and gradually increasing with depth. Drogue designated the shallow thermally variable portion of the profiles as “heterothermic”, the deeper portions “homothermic” and identified the boundary between the two at approximately 25m (measurements ± 0.02C°) in an example from Southern France.

The general premise for the use of temperature profiles to identify hydraulically active fractures is that changes in groundwater temperature at shallow depths (e.g. due to seasonal variations in the temperature of recharge water) are propagated by groundwater transport to substantial depth in the rock. Temperature profiles measured in open rock boreholes intercepting fractures may exhibit small-scale aberrations (anomalies) caused by the flow of relatively warm or cool water in and out of those fractures. Trainer (1968) traced laterally continuous bedding plane fractures in a carbonate rock aquifer for several hundred metres by correlating inflections in temperature profiles. Drury (1984), Droque (1985), Sillman and Robertson (1989) and Malard and Chauis (1995) provide other field examples where borehole temperature measurements were used to identify fracture locations.

Bidaux et al (1993) compared hydrochemical logging with temperature profiles for identifying flow velocities in fractured carbonate media at a site in southern France. They concluded that, although temperature data worked well in high flow conditions, the technique was poor at identifying low-flow zones. Bidaux's data suffered from both the low resolution of their temperature probe and vertical flow in the open borehole, as did Drogue's (1985) temperature profiles measured at the same site. Robinson et al (1993) identify vertical flow in open boreholes as well as the lack of sensitivity of the technology used as the major limitations of temperature measurements for identifying hydraulically active fractures.

B3.1.2. Current State-of-the-Art

Temperature logging is generally not considered a high priority amongst the suite of possible borehole geophysical tools. Although many probes measure internal instrument temperature, the fluid temperature is usually only measured along with the fluid electrical resistivity in specifically designed probes. The data are collected as the probe moves downward through the water column with a temperature sensor set at the bottom of the probe to minimize disturbance of the water column. Most probes (e.g. Mount Sopris, Century, Robertson, Oyo etc) measure to an accuracy of ±0.1-1°C and a resolution of 0.01 to 0.1C°. Manufacturer-recommended logging speeds are 3-5m/min, and typical data density is often at approximately 0.1-0.3m (1 ft) resulting in poor resolution temperature profiles. In addition these results are often masked by cross-connected flow in an open borehole or the interpretation is complicated in some circumstances by convection within the borehole (discussed further below), all factors leading to temperature data rarely being given much consideration. This conclusion is supported by the fact that in a recent review of temperature literature (Anderson, 2005) which included over 200 references, only seven papers were cited on fracture detection with temperature logs.

Hardware improvements have yielded probes that now measure borehole fluid temperature variations to a few thousandths of a Celsius degree (Greenhouse and Pehme 2002; Berthold and Börner 2008). Recent advances in field techniques, particularly when conducted in a borehole with cross-connected flow restricted by the use of a FLUTe liner, show promise for detecting ambient flow in fractures (Greenhouse and Pehme 2002; Pehme et al. 2007a,b & c). These techniques are being continuously refined to improve resolution and progress from a qualitative to quantitative analysis.

The Parker-Cherry group uses a probe manufactured by Instruments for Geophysics (IFG) in Brampton, Ontario. The single parameter device measures fluid temperature with an accuracy of 0.1°C yet can resolve changes in temperature of approximately 0.001C° (IFG 1993)[17]. The sequence of depth-temperature data are collected at a rate of twice a second. By lowering the probe at a near constant rate between 0.5 and 1.5 m/min (depending on the circumstances), data are collected at a nominal interval density of approximately 0.004 to 0.013 m. The data are subsequently splined and re-sampled to a consistent depth increment that is commensurate to the original data density (i.e. 0.005 to 0.015m for the extremes of the range) for additional processing.

In any approach relying on temperature changes as a diagnostic tool, thermal convection in the borehole can be an important consideration (Sammel, 1968). The issue of water movement as a result of either thermal or chemically driven density variations was most recently dealt with by Berthold and Börner (2008) who investigated the issue of thermal profiles and convection within a borehole. Thermally driven water movement, convection[18], occurs when a temperature increase with depth creates an unstable condition such that the resulting density variations cause buoyancy forces to overcome the frictional forces tending towards stability. Berthold and Börner (2008) provide a review of background equations including the rationale and development of the critical Raleigh Number. Whereas heat conduction is controlled by Equation B 9, convective flow in a borehole is described by the Navier-Stokes equations (Equation B-5 and Equation B 7) and which relate flow to the balance between forces driving and limiting water movement:

Equation B-5 $$\frac{\partial \rho}{\partial t} + \rho \cdot div\vec{v} = 0$$

[17] The sensor (thermistor) measures the varying resistivity of a small wire with changing fluid temperature. The device is calibrated in a bath over a range of approximately 50C° and although changes are resolved in detail, the actual temperature measured is subject to the resolution of the calibration system.

[18] The use of the term "convection" varies between disciplines. The engineering community tends to use "forced convection" when the water movement is a function of hydraulic pressures where hydrogeologists would use "advection". Throughout this text "convection" will be used to describe flow resulting from density contrasts caused by temperature changes and "advection" to refer to the movement of water driven by head contrasts.

However, convective flow only occurs when the Raleigh number, Ra_t (Equation B- 8), is above a critical threshold, approximated for a column by Gershuni and Zhukhovitskii (1976) as Ra_c (Equation B-5).

Equation B 7

$$\frac{\partial \vec{v}}{\partial t} + \vec{v}(grad\,\vec{v}) = \vec{f'} - \frac{1}{\rho} grad\,p + \frac{\eta}{\rho} div(grad\vec{v}) + \frac{\eta + \eta'}{\rho} grad\,div\vec{v}$$

with velocity $\vec{v}$, time t, force density $\vec{f}'$(gravity per mass), density ρ, pressure p, viscosity η, a second temperature dependant friction coefficient η'

Equation B 9 $\overrightarrow{J_T} = \lambda \cdot grad\,T$

with the temperature T, thermal flux $\vec{J}_T$ and heat conductivity λ.

Equation B- 8 $Ra_t = \frac{\beta g \nabla T}{D_t \eta} r^4$

where β is the thermal expansion coefficient, ∇T the temperature gradient, D_t the thermal diffusivity and r the characteristic length (the radius in the case of a vertical channel (Gershuni and Zhukhovitskii,1976)).

Equation B 6

$$Ra_c = \frac{96}{5(1 + 103\tilde{\lambda})}\left[3(33 + 103\tilde{\lambda}) - \sqrt{3(2567 + 14794\tilde{\lambda} + 26927\tilde{\lambda}^2)}\right]$$

where $\tilde{\lambda} = {}^{\lambda_{fluid}}\!/_{\lambda_{surrounding\ material}}$ (Gershuni and Zhukhovitskii 1976)

Berhold and Börner (2008) provide two approaches to recognizing convection; a cause-based approach wherein Ra_t is compared to the critical number Ra_c; and an effect-orientated approach where the linear representation of the gradient is removed from the data and all the resulting variations are attributed to convection. Interestingly Berhold and Börner allocate all temperature variations to convection cells and do not attribute any of the variation in the temperature profile to result from flow in the fractures, the focus of the G360 group's work.

B.3.1.2.1. The Active Line Source (ALS) Process

Various approaches to the mathematical analysis of heating and cooling about a borehole are summarized by Lee et. al. (2003). These works primarily focus on predicting the true formation temperatures after the borehole is cooled during drilling in petroleum and deep geothermal applications. The earliest approach to estimating formation temperature was graphical, using "Horner plots" (Horner, 1951) and subsequently empirically relations were developed that applied to specific geographic areas in the southern US. Analytical solutions to the problem of radial heat flow from a cylindrical source form much of the classic reference Carslaw and Jaeger (1959) and their solutions have been used extensively for analogous hydrogeologic models. The theoretical model for the temperature rise about a cylinder producing heat at a constant rate (Equation B-10) was developed by Jaeger (1956). Subsequent investigators have developed various approaches to solving this equation set under different boundary conditions and simplifying assumptions.

Equation B-10: *from Jeager (1956)*

$\Delta T = \left(\frac{Q}{\lambda}\right) G(h, \alpha, \tau)$ where:

$h = {}^{\lambda}/_{aH}$,

$\alpha = {}^{2\pi a^2 \rho c}/_{S}$,

$\tau = {}^{\kappa t}/_{a^2}$ where,

$G(h, \alpha, \tau) = \frac{2\alpha^2}{\pi^3} \int_0^\infty \left[\frac{1-e^{(-ru^2)}}{u^3 \Delta(u)}\right] \partial u$ and,

$\Delta(u) = [uJ_0(u) - (\alpha - hu^2)J_1(u)]^2 + [uY_0(u) - (\alpha - hu^2)Y_1(u)]^2$

where $J_n(u)$ and $Y_n(u)$ are Bessel functions of the first and second kinds and order n.

λ= thermal conductivity (mcal/cm s °C)
κ= thermal diffusivity (x10^{-3} cm^2/s)
c= specific heat (cal/g°C) of rock
ρ= density (g/cm^3)
t= time (sec)
T= temperature (°C)
a= effective borehole radius (cm)
Q= power input of heater/unit length (mcal/cm s)
H= thermal conductance (mcal/cm^2 s °C) of contact layer between probe and rock
S= effective heat capacity/unit length (cal/cm s °C)

In their summaries Luheshi (1983); Shen and Beck (1986); and Lee et. al., (2003) divide the analytical solutions to the problem of heat flow from a borehole into three basic groups: i) the line

source approach which assumes constant heat transfer from the drilling fluid (mud), ii) the zero circulation model which assumes the rock adjacent to the borehole instantaneously becomes the temperature of the mud and, iii) the instant heating model in which there is a very short duration injection of heat rather than cooling. The analytic solutions have evolved with each generation adding additional variables to the equations such as varying mud properties (Lee 1983), followed by Shen and Beck's (1986) adaption of the line source model to include borehole radius as well as both radial and unidirectional fluid flow. These approaches are all limited by the simplifying assumptions used to reduce the number of variable parameters and have generally poor field data comparisons because of inadequate data quality and limited recovery times. Shen and Beck (1986) concede: "*Because of the stringent requirement of analytic solutions, the method presented in this work is, by necessity, limited to those models which possess a high degree of symmetry and simplicity. When a more accurate simulation of field condition is desired, computer modeling must be used.*") Lee et. al. (2003) adopted an iterative generational convergence using elaborate statistical focusing of forward and reverse models to improve parameter estimates but again poor data quality led to an uncertain result.

Although most of these approaches are designed to determine true formation temperature, adaption of these equations led to devices that attempted to estimate formation thermal conductivity at point locations along the borehole such as those proposed by Beck (1957) and later by others (e.g. Hyndman et. al 1979; Lister 1979; Jemsek and VonHerzen 1989). Beck et al's (1971) derivation led to the concept of using the active line source (ALS) technique described by Greenhouse and Pehme (2002) and Pehme et al (2007a&b) to determine the thermal conductivity of rock along the entire hole by collecting temperature logs while a borehole is warmed with a line heater and during subsequent thermal recovery to ambient conditions after the heater is turned off. They adopted Shen and Beck's (1986) approach that the thermal conductivity of the rock (λ_{rx}) can be estimated from the slope the temperature vs ln(t) function when time is adequately long (Equation B-11). The corresponding relationship during thermal recovery is Equation B-12. Greenhouse and Pehme's (2002) work showed that the heating process tended to be irregular (noisy), while the cooling is more uniform and is therefore more commonly applied in practise. They note that the borehole tends to be more difficult to heat and that it cools more rapidly where hydraulically active fractures are interpreted to exist based on other data.

Equation B-11

$$\frac{\Delta T}{\Delta \ln t} \rightarrow \frac{Q}{4\pi\lambda_{rx}} \quad (\boldsymbol{Heating})$$

Equation B-12 $\frac{\Delta T}{\Delta \ln(\frac{t}{t_c})} \rightarrow \frac{Q}{4\pi\lambda_{rx}}$ ***(Cooling)***

t_c= time from end of heating (sec)

A fundamental limitation to the application of temperature logging for identification of flow through fractures is that the water must be in thermal disequilibrium with the surrounding rock to create an anomaly. Without thermal transience and transport of warmer or cooler water through the fracture network, temperature profiles in boreholes would show only the near surface variations caused by environmental changes and the geothermal gradient. This transition is essentially a hetero-homothermic boundary presented by Drouge (1985) although when originally defined, cross-connected flow complicated the interpretation. Molson et al (2007) use the numerical model Smoker (Molson and Frind, 2005, see details in Section B4.2) to demonstrate that typical annual temperature variations experienced in Southern Ontario could drive thermal disequilibrium at scales detectable with modern temperature probes to depths of 50 metres and more. Pehme et al (2007a) demonstrate that anomalies can exist beyond 100 metres. However, generally the deeper a fracture is within the stratigraphic sequence (excluding deep geothermal sources), the further it would be from heat sources and sinks, and the greater the likelihood that the water and the rock are at the same temperature, a situation which would render the water moving through the fracture undetectable with a simple (passive) temperature profile.

Pehme et. al. (in prep-a) show that improvements in temperature logging realized by improved sensors and elimination of cross-connected flow with the FLUTe liner has highlighted a third limitation, a depth related constraint presented schematically in Figure B1A. Below the limit of the heterothermic zone, without environmentally driven thermal disequilibrium, the temperature of the rock and any water moving through fractures will be the same and not be detectable by way of a temperature log. Between the shallow subsurface where the thermal disequilibrium tends to be large and the upper limit of heterothermic zone where thermal uniformity makes flow undetectable, intermediate degrees of temperature contrast must exist between the water flowing through the fractures and the surrounding rock. It follows that for two fractures with the same rate of groundwater flow, but each with a different temperature contrast between the water and the matrix, the size of the aberration on a temperature profile will be different. Pehme et al (in prep-a) show that the ALS technique can be used to induce an artificial disequilibrium and create thermal anomalies where none are detected under ambient thermal conditions (Figure B1B-heating and Figure B1C-thermal recovery). In addition a complication in the identification of fracture flow in passive logs is that the interpreter does not have apriori knowledge of whether the water in the fracture is warmer or cooler than the surrounding rock. Molson (in prep) has shown that the polarity of a temperature anomaly (i.e. the fluid temperature relative to the surrounding rock) can vary likely due to small localized changes in the flow pattern as the water winds through a fracture network. The ALS process simplifies

temperature patterns because the water in the borehole is initially heated and then allowed to recover towards ambient temperatures, allowing the interpreter to reasonably assume that the water flowing through the fractures is cooler than the matrix which will cause negative inflections in the temperature profile. Based on publications, the Parker-Cherry group are currently the sole practitioners of the ALS process. The process as it is currently applied is summarized in Table B1.

Table B1: Details of data collection steps in the ALS process (Pehme et al., *In prep-a*)

Stage- Figure B1		Details	Purpose/Comments
1	Background	The ambient temperature of the fluid column in the borehole is recorded prior to the addition of heat. **P-** A "passive" log is collected at a slow rate of descent (0.5-0.7 m/min),	Provides base against which to access: amount of heat added values towards which recovery progresses basis for assessment of overall borehole thermal stability (see C3) optimally completed the afternoon prior to heating
2	Heating	Energy is added with a line heater (typically at 15-20 W/m for 5-6 hrs) uniformly down borehole **A** – Active log collected (1.5-2m/min),	estimate amount of heat added data tends to be noisy (irregular) which is presumed to be primarily caused by small changes in the distance between the heat source and sensor(s) power depends on heater(s) used and voltage applied timed to end near end of heating cycle
3	Recovery	**C1** – Log collected during cooling, starting approx. ½ hour after heater turned off (1-1.5 m/min)	heater may be removed depending on logistical considerations provides indication of the early stages of cooling most variable of the recovery logs
		C2 – Cooling log started at approximately the same length of time after the heater is turned off as total heating (i.e. usually ~5½-6½ hrs after end of heating), logging rate approx. 0.8-1m/min	designated as start of "late" time theoretical start of linear decay (Shen and Beck 1986, Pehme et al 2007a), used to estimate thermal conductivity
		C3 – logged the next day (approx. 24hrs after the start of heating) at 0.5-0.7 m/min	well into late stage recovery used in estimation of thermal conductivity compared against P log to access recovery process and overall thermal stability

The industry standard method for accentuating small variations in a temperature profile (both in vertical extent and temperature difference) is a gradient log. Gradient logs are calculated from the original data by dividing the difference in temperature over a short distance (often successive readings) by that distance. This approach tends to work well in an open hole with cross-connected flow because flow in fractures is often identifiable based on steps in a temperature profile. However, in the case of a lined borehole where flow in a fracture results in a narrow spike or trough in the temperature profile, a gradient log calculated in this manner distorts the original pattern of the aberration in the profile and creates a bimodal anomaly. Pehme et al (*2010*) describe an alternative approach, a "variability log", which is calculated by first smoothing the temperature profile over a broad interval (5 metres is suggested), and then subtracting the result from the original data. The variability log suppresses the broad temperature changes created in the near-surface heterothermic zone and deeper geothermal gradients while better honouring the original shape of the narrow temperature changes that occur due to water movement.

Another approach to processing recovery data in the ALS process is the "cooling log" which was developed to isolate and improve representation of the cooling process at each fracture (Pehme et. al *in prep-a and described in detail on page 213*). The goal of the cooling log is to isolate and depict the cooling at each fracture caused by the flow of water. As is the case with the variability log, shallow heterothermic and deep geothermal changes are removed, as are broad temperature variations resulting from changing geologic properties, creating a better qualitative comparison of the degree of cooling at each fracture. However, as in the case with the variability log, offsets in the background temperature in the form of step patterns (e.g. at the water table) are distorted and lengthened, appearing in the cooling log as a broad saw-toothed pattern.

B3.1.3. Future

The focus of the Parker-Cherry group's research in applying temperature techniques in fractured rock is to progress from a qualitative identification of aberrations in a temperature profile to quantitative analysis of flow within individual fractures. A better understanding of the interaction and processes of heating and measuring the temperature in a borehole through fractured rock is required to move this research forward. As is demonstrated here, even in a simple system with a borehole intersecting a single fracture in a uniform medium, a highly detailed 3D analysis of heat transfer of a non-symmetrical system over short time periods is beyond analytical solutions. Because of the very small temperature variations created and measured, numerical modelling is required to resolve the dynamic conditions and subtle variations in the temperature patterns resulting from the ALS process.

Pehme et al *(in prep-b)* describe a new probe, the Thermal Vector Probe (TVP), which was built to measure direction and magnitude of the temperature vector on a continuous basis along the length of the lined borehole. The probe utilizes four temperature sensors spaced a few centimetres apart in a 3 dimensional array to calculate the magnitude of the horizontal and vertical components of the temperature vector and is combined with either an optical gyro or orthogonal magnetometers to determine the probe rotation and thereby the vector direction. Pehme et al *(in prep-a)* demonstrate that the thermal vector can be consistently disturbed and recovered through the ALS process confirming validity of the measurement. Combined with the ALS technique to create disequilibrium, this approach has potential for estimating both quantity and direction of ambient groundwater flow.

B4. Numerical Modelling of Heat Transport

Several pioneers of hydrogeology adapted the equations governing heat transport such as summarized by Carslaw and Jaeger (1959) for their analysis of flow problems and pumping tests (eg. Theis). Although thermal processes are generally well documented and have been extensively modelled, an initial literature search (see below) has indicated that research that addresses fractured rock is sparse and even less deals with the level of detail required in this case. Beyond the hydrogeologic community, heat flow through rock (fractured or otherwise) has been extensively investigated within many diverse disciplines and for a broad variety of purposes by those involved in: construction, geothermal energy, energy storage, nuclear waste disposal, industrial minerals, mining and the oil industry, to name but a few. A complete review of these fields is beyond the scope of this exercise and we concentrate here on a sampling of the hydrogeologically orientated work available.

B4.1. Modelling Heat

Numerous authors have incorporated thermal affects into groundwater models. The vast majority of these deal with density and convection issues with respect to large scale transport in porous (unfractured) media (e.g. Molson et. al. 1992). Su et al. (2006) successfully simulated the response of a multi sensor temperature installation above a sand-clay interface using the code TOUGH2 (Pruess et al 1999), and small elements to conduct a sensitivity analysis. Some (e.g. Brookfield et. al. 2009) have adapted existing hydrogeologic models such as “Hydrogeosphere” to consider temperature and deal with broader ecosystem (surface and groundwater) interactions and issues of global warming. Of the few that have worked within rock environments, fewer still have dealt with individual fractures and at the scale attempted here. For example Bataillé et. al (2006) represented a group of fissures as an individual vertical fracture in simulating geothermal convection, but their scale spans several kilometres and the fracture zone is 35m thick. Anderson et al (2005) provide an extensive review of

the use of temperature techniques in hydrogeologic applications. Of the more than 200 references, only 7 deal with flow through fractured rock, none of which emphasise modelling of the response. Existing modelling work focuses instead on the use of temperature as a tracer for recharge and discharge in a much broader perspective than a single fracture (e.g. Bredehoeft and Papadopulos, 1965; Bundschuh, 1993; and Ferguson et. al 2003). Although Ge (1998) provided an analytical solution comparing the thermal anomaly from a "single" fracture to the broader thermal gradient to estimate flow velocity, their data reflected an anomaly that spanned several hundred metres and flow through a zone estimated to be over 20m thick.

As part of their investigation of convection in a borehole, Berthold and Börner (2008) used a finite element code (COMSOL Multiphysics v3.3) to simulate detailed water movement and thermal variations, comparing their results to laboratory and field data. The authors chose to deal with the simulations in a 2D space; citing "computing time reasons" as the justification for avoiding a 3D simulation. However their treatment of the problem is fundamentally flawed in that by assuming a 2D representation, the borehole becomes a vertical plate of water thus reducing both the friction and the heat transfer to the rock and consequently increasing the tendency for convection. In the absence of flow, the situation would have symmetry in radial coordinates, but not in a cartesian representation, thus their 2D representation was inappropriate. Intuitively one would then expect convection to appear as a vertically extended doughnut shape rather than the sphere Berthold and Börner show. In spite of these simplifications they predict convection cells to be of approximately the same vertical dimensions as the variations herein observed and noted in our field data. With the exception of Su et al. (2006, discussed above) who worked in an unconsolidated aquifer, a reference was not identified that deals with the level of detail to be undertaken here.

B4.2. The "Smoker" Model

To explore the theoretical basis for stabilization of a lined borehole, we turn to the "Smoker" model (Molson 2006), a refined version of Heatflow (Molson and Frind 2006), for modeling three-dimensional groundwater flow and heat transport within a fractured porous medium. These finite element models have been tested and applied over the last decade by Yang et al (1996a,b;1995), Molson et al. (1992), Molson and Frind (1994), Markel et. al (2006) and Molson et. al. (in prep). Smoker was designed to simulate water movement through discrete fractures and in the surrounding matrix while accounting for density variations as a result of temperature changes. The rock mass (and overlying overburden) is represented using 3D deformable elements and fractures are treated as 2D

planar surfaces imbedded onto the element surfaces. The code derives a solution for the nonlinear transient coupled system defined by a set of flow and heat transport equations.

Matrix flow is defined by Equation B-13:

Equation B-13 $$\frac{\partial}{\partial x_i}\left[K_{i,j}(T)\left(\frac{\Psi}{\partial x_j}+\rho_r(T)\right)\right]-\sum_{k=1}^{N} Q_k(t)\cdot\delta(x_k,y_k,z_k)=S_s\frac{\partial\Psi}{\partial t}$$

where $K_{i,j}(T)$ is the temperature dependent hydraulic conductivity tensor, Ψ is the equivalent freshwater head, $\rho_t(T)$ is the temperature dependent relative density of water, Q_k is the fluid volume flux from a source or sink located at (x_k,y_k,z_k), S_s is the specific storage and t is time. Smoker applies Equation B-14 to describe the change in temperature through the matrix elements (Molson, *In Prep*)

Equation B-14 $$\frac{\partial T}{\partial t}=\frac{\partial}{\partial x_i}\left[\left(\kappa+\frac{D_{i,j}}{R}\right)\frac{dT}{dx_j}\right]-\frac{\partial}{\partial x_i}\left(\frac{v_i}{R}T\right)+\sum_{k=1}^{N}\frac{Q_k(t)T_k(t)}{R\theta}\delta(x_{k'},y_{k'},z_{k'},)$$

where R is the thermal retardation, given by

Equation B-15 $$R=\frac{C_o}{S\theta c_w\rho_w}$$

and κ the equivalent rock thermal diffusivity,

Equation B-16 $$\kappa=\lambda/C_o \qquad \textbf{and where}$$

Equation B-17 $$C_o=S\theta c_w\rho_w+(1-\theta)c_s\rho_s$$

with c_w, c_s the specific heat and ρ_w, ρ_s the density of the water and solids respectively

Other constants and values used in the base case are provided in Table B2.

Fractures:

Fractures are treated as a 2 dimensional surface on the face of an element. Temperature (T') in a fracture (horizontal xy, for example) is given by Equation B-18:

Equation B-18 $$\frac{\partial T'}{\partial t}=\frac{\partial}{\partial x}\left(\frac{\lambda_w}{c_w\rho_w}\frac{dT'}{dx}\right)+\frac{\partial}{\partial y}\left(\frac{\lambda_w}{c_w\rho_w}\frac{dT'}{dy}\right)+\frac{\lambda_m}{c_w\rho_w b}\left[\frac{dT'}{dz}\right]_{z=\pm b}-\frac{\partial(\overline{v}_x T')}{\partial x}-\frac{\partial(\overline{v}_y T')}{\partial y}$$

Molson and Frind (2006) relate velocity (v,ms^{-1}) to the hydraulic gradient (∇h) with the relationship

Equation B-19 $$v=\frac{-(2b)^2}{12\mu}\rho g\nabla h$$

wherein 2b is the full fracture aperture (m), ρ is the water density (1000 kgm^{-3}) and g the gravitational acceleration (9.8 ms^{-2}). The viscosity of water, μ varies with temperature according to Equation 5-4 (Molson and Frind, 2006).[19]

Equation B-20 $$\mu(T) = 0.001787 * e^{(3.073\times10^{-2}T+1.303\times10^{-4}T^2)}$$

The main routine organizes the input file and parameters that define the matrix grid, fractures and boundary conditions. The main program then iterates within each time step using a flow loop embedded within a broader heat transport loop to solve the governing equations. Each of the loops employ subroutines to determine variable parameters, solve the matrix equations, and then checks for convergence, first in flow and then for transport. Molson (2010) provides further details.

Table B2: Additional parameters and default value

T'	°C	10	Fracture (water) Temp
T	°C	10	Initial matrix (solids & water) Temperature
$\overline{v_{x,y}}$	m/s	$\frac{-(2b)^2}{12u}\rho_w g\nabla h_{x,y}$	Velocity of water in fracture *(x or y direction)*
$\lambda_{w,m}$	$\frac{J}{ms°C}$	0.57 , 3.65	thermal conductivity (water and "aquifer" (porous matrix))
$c_{w,s}$	$\frac{J}{kg°C}$	4174.0	Specific heat of water or solid *(Molson et. al in prep)*
$\rho_w(T)$	kg/m^3	$\rho_o\{1+[-6.562\times10^6+2.166\times10^{-8}(T-4)](T-4)^2\}$	Density of water
Θ	m^3/m^3	0.05	Porosity
K	m/s	9.8x10^{-10}, 1	Hydraulic Conductivity-rock, borehole
S_s	m^{-1}	0	Specific storage
Q_k	m^3/s	0	Fluid volume influx (internal)
2b	m	.001	Fracture aperture *(base case)*
$\mu(T)$	$\frac{kg}{ms}$	$0.001787 * e^{(3.073\times10^{-2}T+1.303\times10^{-4}T^2)}$	Viscosity of water
g	$\frac{m}{s^2}$	9.8	Gravitational acceleration
∇h	m/m	Varies (nominally 0.15)	Hydraulic head gradient (-)

[19] Equation 5-3 shows that the velocity estimate is sensitive to the viscosity. Other researchers (e.g. Berthold and Börner (2008)) use other equations to estimate μ which can lead to a 35% difference in velocity values. See B7.2.7 for addition discussion.

It is important to note that Smoker **does not** however, provide a rigorous representation of flow within a pipe, or in our case a lined borehole, as these features are represented using 1D line elements (Molson pers. 2006). From this perspective we must weigh the results of the modeling as a guide to understanding temperature distributions within a borehole and compare those results to field data to confirm relevance. Key traits of the model and the particular implications on these simulations and analysis described here are summarized in Table B 3:

Table B 3: Key characteristics of the Smoker model and implications with respect to this work

Saturated flow	No implication
The model allows for thermal (buoyancy) convection within a fractured porous medium	Although convection is viable within the 3D elements representing the matrix, the code is not intended to have elements that are only water. If the thermal gradients are adequate convection should occur in the modeled borehole, but the details of the convection will not be entirely accurate because subtle influences (3) are unaccounted for.
Flow through a pipe or conduit is assumed one-dimensional and based on Darcy's Law and the cubic law.	Accurate representation of fluid flow in a borehole would incorporate characteristics such as friction, rugosity etc which are not considered.
The elements are rectilinear	The shape of the simulated borehole is approximate and has sharp corners, increasing the flow distance (see below)
Angled fractures cannot be represented	The system represented is simple and horizontal; this has no implications on this work.
Fluids and solids are in local thermal equilibrium at the grain scale	The treatment of individual elements in the borehole as water or in the rock as matrix material should make the subdivision within the elements inconsequential.
Temperatures >0, <100	No implication
No phase changes or chemical reactions	No implication
Well bore storage and well losses are neglected	The well is lined and therefore no implication

B5. Methodology

B5.1. Approach

The modelling exercises that are herein described are designed to simulate the field procedures and the measurements made through the ALS process. Although a typically a borehole tested is 100-150m deep with potentially a hundred to two hundred fractures (flow zones) or more to develop an understanding of influence of the various parameters the system is drastically simplified. Water migration in a fractured rock and its subsequent influence on the heat distribution about a borehole are studied by designing a model with a single, planer horizontal fracture and a single, lined borehole.

Flow across the system is induced with a constant gradient between fixed hydraulic heads at the up-gradient and down-gradient boundaries. An initial uniform background temperature of 10°C is established with a fixed up-gradient boundary temperature. The borehole is then heated with a "line heater" and the system is allowed to return to thermal equilibrium. The simulated cycle is repeated using various physical and geometric parameters and the effects on the transient temperature distribution are analyzed by interpreting the model data sets.

The results are compared using data processing methods analogous to those routinely employed during field work to both explore the system dynamics and parameter sensitivity as well as to gain insight into how these variations would appear in field results. By systematically varying (increasing and decreasing) individual parameters, the sensitivity of the system and the ALS technique to each parameter can be ranked.

B5.2. Base Model

The base model consists of a single horizontal fracture embedded in a low permeability, porous matrix. A critical aspect of the model is that the heated well and vicinity is adequately discretized to accurately represent the detailed flow and temperature variations that might occur in and around the borehole.

The three-dimensional (3D) model is shown schematically in Figure B2, with X (left to right), Y (front to back) and Z (bottom to top) dimensions of 20, 10 and 10 metres respectively. A single horizontal fracture with an aperture of 1 mm is placed at Z=5 metres, within a matrix having characteristics similar to those of dolomite (porosity of 0.05, hydraulic and thermal conductivities of 9.8E-10 m/sec (Burns, 2005) and 3.6 J/m/s/ºC (Appendix B - Table 6, from Molson, 2006) respectively. Detail within the model is provided by discretizing a square column (0.4 m per side) around the "borehole" into 1 cm elements (Figure B3**Error! Reference source not ound.**). The 0.5 m thick horizontal slabs above and below the fracture are refined with 2 cm elements in the z direction. The complete details of dimensions and

Table B4: Model Geometry

Direction	Extent (m)	# of Elements	Size (m)
X	**0.0 - 4.8**	**24**	**0.20**
	4.8 - 5.2	**40**	**0.01**
	5.2 - 10.0	**24**	**0.20**
	10.0 - 20.0	**10**	**1.00**
Y	**0.0 - 4.8**	**24**	**0.20**
	4.8 - 5.2	**40**	**0.01**
	5.2 - 10.0	**24**	**0.20**
Z	**0.0 - 4.5**	**9**	**0.50**
	4.5 - 5.5	**50**	**0.02**
	5.5 - 10.0	**9**	**0.50**

discretization of the model are provided in Table 4 and all physical parameters used in the model are provided in Table 2 and Appendix A.

A 10 cm diameter vertical borehole is simulated at X=5, Y=5 by creating a "cylinder" of elements (Figure B3b) with a porosity of 1, hydraulic conductivity 1 m/s and the thermal conductivity of water (0.57 J/m/s/ºC). The FLUTe liner is 3 mm thick, most of which is weaved nylon material which would be saturated under normal operation (C. Keller pers. comm.) and its thermal conductivity is therefore assumed to be that of water, ignoring the thin coating of urethane that makes the liner impermeable. The hydraulic conductivity of the outer elements of the borehole are decreased to $1x10^{-55}$ m/s to restrict movement of water into the borehole as would a liner. A plug, 1 element thick, of low permeability was added in the upper and lower ends of the borehole to restrict the development of a "head" gradient within the borehole annulus. All the elements are set to the initial conditions of a head of 0 metres and temperature of 10 °C. The upper, lower, front and back sides are designated to be "no flow" boundaries with zero temperature gradient. The vertical up and down gradient boundaries (X=0, 20m) were both designated as constant head with the up gradient end (X=0) a fixed temperature (10°C for base case) and the down gradient end (X=20m) a zero gradient boundary. The input file (Smoker.data) used for the base case is provided in Appendix A.

At the beginning of the simulation the head at the X=0 end is changed and maintained at a constant 0.15 metres creating horizontal flow in the positive X direction. The model is time-stepped through 4 days to attain steady state conditions prior to turning on the heater. A time increment of 0.001days (1.44 min) was used throughout each simulation. To simulate a typical ALS field test, at the start of day 4, the heater is turned on for a period of 6 hours and then turned off. The model was initially allowed to continue through to 12 days, well beyond the time required for the system to return to initial conditions, which was later shortened to 8 days to shorten run times. At the beginning of the process the standard field procedure was to use a heater with an output of 5 W/m, but part way through the exercise the standard field technique was modified to increase the heater output. All models were rerun with the heat source providing 20 W/m[20], a typical heater being 150m long with a 240 Volt power supply.

[20] Outside surface area of each element is $0.0008m^2$ (4 x 0.01m x 0.02m), heater output is 20 W/m, with 50 elements/m vertically 0.4 W/ element (20/50) is required, which converts to $500W/m^2$ (0.4/0.0008).

B5.3. Model Testing and Calibration

Prior to beginning the sensitivity analysis to rank the influence of system parameters, it is important to test that the numerical model accurately represents the conditions and processes being considered. Although the Smoker code has been validated in the literature for flow and heat transport on the scale of tens and hundreds of metres (Molson et al. 1992, Palmer et al. 1992 and Yang et al. 1996a,b), the code has not been tested when dealing with variations in temperature of a few thousandths of a degree at the centimetre scale. Since it is impractical to test these conditions in the lab, conceptual testing as well as calibration against field data are used to establish confidence in the model results.

"Conceptual testing" in this context (Section 3.3.1 – 3.3.3) refers to judging the quality of the base model response on the criteria of meeting the anticipated physical characteristics of the system. In this case the key comparison factors are:

- symmetric flow conditions within the fracture around the borehole,
- no (or very low) flow within the borehole, and
- the ability to meet theoretical thermal decay rates.

The first two criteria are assessed based on head distributions and are a robust, controlled basis for comparison that are predictable throughout the model. The third test is based on whether the thermal recovery in the model behaves in the manner anticipated by an analytical model which is itself the subject of ongoing research. To this end the thermal conductivity of the rock predicted from the recovery and the analytic solution in Equation B-12 is compared to the values originally introduced into the model, although recognizing the analytic solution is subject to a number of assumptions.

The calibration of the model (Section 3.3.4-3.3.5) is based on comparing the predicted thermal patterns against temperature logs collected in the field, specifically:

- Similarity to field data in magnitude, symmetry and extent of the temperature variation anomalies in the vertical dimension,
- Similarity to field data in the temporal patterns of heating and recovery during an ALS test.

Because the details of the temperature variations through the ALS process observed in the field are expected to vary based on both geometry and the physical characteristics of the rock and the fractures, as well as the flow field, an exact comparison to the model results is unattainable and a reasonable similarity is deemed as adequate. The base model underwent 14 refinements (parameter adjustments) to achieve an adequate representation of field conditions (Section 3.4).

B5.3.1. Flow symmetry

Figure B4 represents the steady-state head distribution within the fracture. As expected with constant head boundaries at either end of the model, the pattern shows a uniform gradient ($7.5x10^{-3}$) across the fracture plane. shows the water flow in the fracture around the borehole as velocity vectors. The vectors beyond the area shown are uniform and parallel to the right. Based on these results we anticipate the flow velocity in the fracture to be a minimum along the central Y=5 plane as the water diverges around the liner at X=4.95 and as it re-converges down gradient of the liner at X=5.05. Maximum velocities are anticipated along the lateral sides of the liner as the water increases speed to circumvent the borehole and return to a uniform flow field down gradient. A full appreciation of this pattern is important to understand the temperature distributions described below.

Figure B6 displays the head distribution in the vertical plane at Y=5m in the vicinity of the borehole-fracture intersection immediately prior to heating. With the exception of the borehole which is set at a higher pressure than the surrounding rock, the head gradient is linear as anticipated from the boundary conditions. Apparent from a detailed comparison against the model grid, the head contours are very slightly skewed, implying that a minor vertical gradient (approximately $2x10^{-4}$) exists throughout the model domain independent of the fracture and the borehole. The pattern is likely an artefact of iteration of the model and although it could create a minor downward component to the flow, the effect is assumed insignificant.

B5.3.2. No flow condition (in borehole)

A basic assumption of the ALS process and temperature logging within a lined borehole in general is that the water is stagnant, the liner having sealed all vertical or cross-hole flow. The appropriate time at which to examine this premise is just before heating is initiated, as once energy is introduced into the system, convection could occur and drive water movement. The detailed head distribution within the borehole adjacent to the fracture is shown in Figure B7 (colour zones are altered to highlight local variability). The simulated hydraulic head within the liner varies by less than 10^{-7} m at 3.98 days (immediately before heating), confirming the hydraulic integrity of the simulated liner and that no appreciable horizontal flow exists prior to heating.

Details of the vertical head distribution within the liner in the vicinity of the fracture immediately prior to the beginning of heating are shown in

Figure B8. A uniform downward gradient of approximately $2x10^{-4}$ is evident which is consistent with that observed throughout the model domain.

Various attempts at changing the model parameters did not eliminate this small downward gradient from either the liner or the matrix. The cause remains uncertain but is likely related to numerical error. Through most of the model domain the horizontal gradient is two orders of magnitude larger and given the low permeability of the matrix and liner relative to the fracture, the existence of the vertical gradient should not appreciably alter the desired flow patterns. However, since the portion of the model of primary interest is the borehole which has no appreciable horizontal head gradient, the effects of vertical advective flow could influence the thermal patterns; this issue is considered in the subsequent analysis and discussed further below.

B5.3.3. Internal Consistency and the ALS approach

The third approach adopted to assessing the internal consistency of the results was to compare the simulated estimate of thermal conductivity (based on the thermal decay) with the input value parameters. The ALS technique as presented by Pehme et al. (2007a) is intended to estimate the thermal conductivity of the matrix as described above (Section 1.2.2.1). shows the temperature plotted against $Ln(t/t_c)$ for the low and high power base case, 1½ metres from the fracture. The ratio of the slope of the high power output model over that of the low power is 3.9 which closely approximates that of the ratio of the power outputs (4.0). However the estimate of the rock thermal conductivity for the low and high power cases[21] using Equation B-12 are 6.1 and 6.5 $J/(ms°C)$ respectively, almost twice the 3.6 $J/(ms°C)$ used in the model. Given the limited range of values documented in earth materials, this discrepancy is large.

Among the many basic assumptions of the analytical derivation provided by Shen and Beck (1986) are that adequate time exists for both heating and cooling to become steady state, radial symmetry, as well as that the temperature is measured at the heater, all of which are violated in both the field application and this modelling process. However, additional model runs indicated that the rate of background decay varied a minimal amount (to 6.3 $J/(ms°C)$) when the temperature is measured at the heater. When thermal recovery data produced when the heater is down-gradient of the borehole (see Section 4.2.3) is used, the estimate of the thermal conductivity based on the model almost doubles (to 11.5 $J/(ms°C)$). However when the flow is removed (heater up-gradient) the thermal

[21] The base model was run with both low 5W/m and high 20W/m heater outputs, see Section 3.4 for details.

conductivity is essentially the same ($6.7\,J/(ms°C)$). Estimates of thermal conductivity using recovery data after varying the duration of heating (see section 4.2.2 for simulation details) varied from $14.7\,J/(ms°C)$ to $2.49\,J/(ms°C)$ for 3 and 12 hours of heating respectively. Lee et al (2003) establish a strict specification for the time required to estimate thermal conductivity: "*The asymptotic approximation is good to 1% from the exact line source solution if* $r^2/4\kappa(t-t_D)\leq 0.01$ *…*" (where $(t-t_D)$ is equivalent to the cooling time t_c, r the borehole radius (0.05m) and κ the thermal diffusivity $1.47\text{x}10^{-6}$ m^2/s in our case). Based on this specification, the model would require 236 hr to reach an appropriate asymptotic estimate; a time that is well beyond the practical implementation of the line source technique given the limits on the introduction of energy and the current resolution of temperature probes.

The inconsistency between the analytical solution, the field measurement of rock thermal conductivity, and the results on the Smoker model requires further investigation, but the implication is that the discrepancy results because the complexity of the practical details of heating a borehole and measuring the thermal recovery with a temperature probe violates the simplifying assumptions used to develop the analytic equations. Given the number of subtle variations to the analytical approach developed by various authors and the duration (from the early 1950's to present) of the effort to refine these without in most cases achieving good correlation with field data, it is likely that the fundamental assumptions rarely apply. Shen and Beck (1986) emphasize the limitations of idealizing the process to arrive at an analytical solution and although they anticipate a radius dependent deviation for the ln-linear time based estimate of thermal conductivity if adequate time is not allowed, based on these results their estimate that t_c should be at least the same as t_h appears to be inadequate. Pehme et at (2007) use the qualifying term "apparent" to describe their thermal conductivity estimate in recognition of the potential geometric and time dependant errors. It seems that the additional qualifier of "relative" is appropriate as the estimate is condition specific and a better used to comparison of conditions along the length of a specific borehole rather than an absolute estimate thermal conductivity. The specific issue of rock thermal conductivity and how it influences the detection of flow in fractures with the ALS is specifically dealt with later in this text.

B5.3.4. Comparison with field data

shows a comparison of the vertical distribution of temperature (as predicted from the base case model immediately after heating) with data collected during a typical ALS test conducted in dolomitic rock (in this case MW25 at the Guelph Site). The field temperature logs are also presented as cooling logs used to highlight negative inflections (see details in B7.1.2). In both the model and the

field data the width of the thermal aberration spans approximately 20cm in depth. The model results can be used to capture a moment in time accurately, however in the field logging process it is difficult to acquire an exact moment in the overall process at a specific depth and therefore the times displayed in the field data will not exactly compare with those portrayed in the model. Although the model is not an exact duplication of the field results because the timing, geometry and the flow details in the field example are unknown, it is clear that the pattern (the approximate breadth and shape) of the cooling curve is reasonably approximated by the model. Within the model limitations and assumptions, the simulation reasonably represents the characteristics of an anomaly observed in the field.

B5.3.5. Comparison with temporal variations in field data

To examine whether the model reasonably predicts variations in temperature in the rock mass over time,Figure B11 compares the observed temperatures in portions of the data with few variations in MW79 (i.e. few fractures) from the Guelph site (when hole is 5 inch (red) and 10 inch (blue) diameters) and UW7 (a 5 inch borehole from the Cambridge site) (orange)[22]. In both field cases heating occurred for 5 hrs and special runs of the base case model (designated as "E") were conducted to reflect those situations. For the model "base case", data from both the fracture depth and 1.5m below (the un-fractured "reference" response) are provided. Whereas offsets in the timing of the field data, the degree of fracturing (which creates some ambiguity in the identification of a "reference" portion within the field log) and uncertainty about geometry (the relative location of the heater and the sensor) in the field data will somewhat distort the results, Figure B11shows that the temperatures during heating and cooling are reasonably similar in both boreholes and are well approximated by the model. In both cases the field data demonstrate slightly higher temperatures than the model, particularly during heating. This would be anticipated if the field probe and the heater were slightly closer than simulated. Neither the geometric nor temporal variations of the model match the field data exactly. However, the uncertainties in the time and geometry in the field results are such that, based on these calibration examples, we can conclude that the model as designed provides a reasonable base which can be used to examine the sensitivity of the ALS heating process to the variations in design parameters and physical properties.

[22] This section compares the field data and the base model results, the nuances of the time dependent variation in predicted temperature are discussed in detail in Section B7.1.3.

B6. Parameter Matrix

Having tested the model, various parameters were systematically adjusted to examine the impact on the temperature distribution predicted during the ALS process. The parameters considered are geometry (i.e. the location of the heater relative to flow and borehole diameter), physical characteristics of the rock (thermal conductivity, background temperature), technical design options to the testing process (duration of heating, amount of energy used) and factors related to water movement in the fracture (velocity, fracture aperture). The parameter adjustments associated with the various model runs are shown schematically in Figure B12and summarized in Table B5Table B1.

Table B5: Model Parameter Summary and Adjustment Matrix

	Test Sequence (Det ##)				Trend being Tested	Heater Location
Low Power	14	15	16	31	Location of heater (*up-, transverse- & down- gradient; center)*	varies
	22	14	18		Flow varies ∇H = (*0.5, 1, 2*) x base	A
	21	15	20		Flow varies ∇H = (*0.5, 1, 2*) x base	B
	23	16	19		Flow varies ∇H = (*0.5, 1, 2*) x base	C
	14	24	25		Varying thermal cond. (λrx=3.6,4.8 & 2.4 $^{W}/_{mC^\circ}$)	A
	16	26			Varying thermal cond. (λrx=3.6 & 2.4 $^{W}/_{mC^\circ}$)	C
	27	14	28		Varying background temp of Rx *(5 ℃, 10 ℃ & 20 ℃)*	A
	14	35			Inc Frac aperture (*10X to 1cm)*	A
	14	17			Heat time (*inc to 24 hrs)*	
	14E	14D			Inc Power (from 5.8 to 20.0 W/m)	
High Power (D)	14	15	16		Location of heater (up, side & down gradient)	varies
	22	14	18		Velocity varies ∇H = (0.5, 1, 2) x base	A
	21	15	20		Velocity varies ∇H = (0.5, 1, 2) x base	B
	23	16	19		Velocity varies ∇H = (0.5, 1, 2) x base	C
	14	24	25		Varying thermal cond. (λrx =3.6,4.8 & 2.4 W/mC°)	A
	16	26			Varying thermal cond. (λrx =3.6 & 2.4 W/mC°)	C
	27	14	28		Varying background temp of Rx (5°C, 10°C & 20°C)	A
	14	35			Inc Frac aperture (10X to 1 cm)	A
	16	36			Inc Frac aperture (/10 to 100μm)	A
	14	40			Inc BH dia (to 20 cm)	A
	14	41			Inc BH dia (to 20 cm)	A-
	40	41			Inc BH dia (to 20 cm)	A-
	16	42			Inc BH dia (to 20 cm)	C

Note: Numbering is not sequential to allow for future work and cataloguing of tests

In most cases the parameters are varied about the central value used in the base case DET14D (i.e. the critical parameter is first increased above the base case value and then decreased). Early in the process it became apparent that the location of the heater relative to flow has a significant impact on the results (discussed in detail below) and therefore in some cases a similar set of parameter variations was repeated with the heater at a different location.

Over the duration of the modelling exercise, field procedures were altered such that the energy output by the heater was increased from 4.8 W/m to almost 20.0 W/m and many models were consequently re-run with the increased power to be more representative of current field conditions. The increase in power simply accentuates the observed effects making presentation of both versions redundant and since the high powered version is most representative of current field practices, the examples provided herein use only the high power versions of the model.

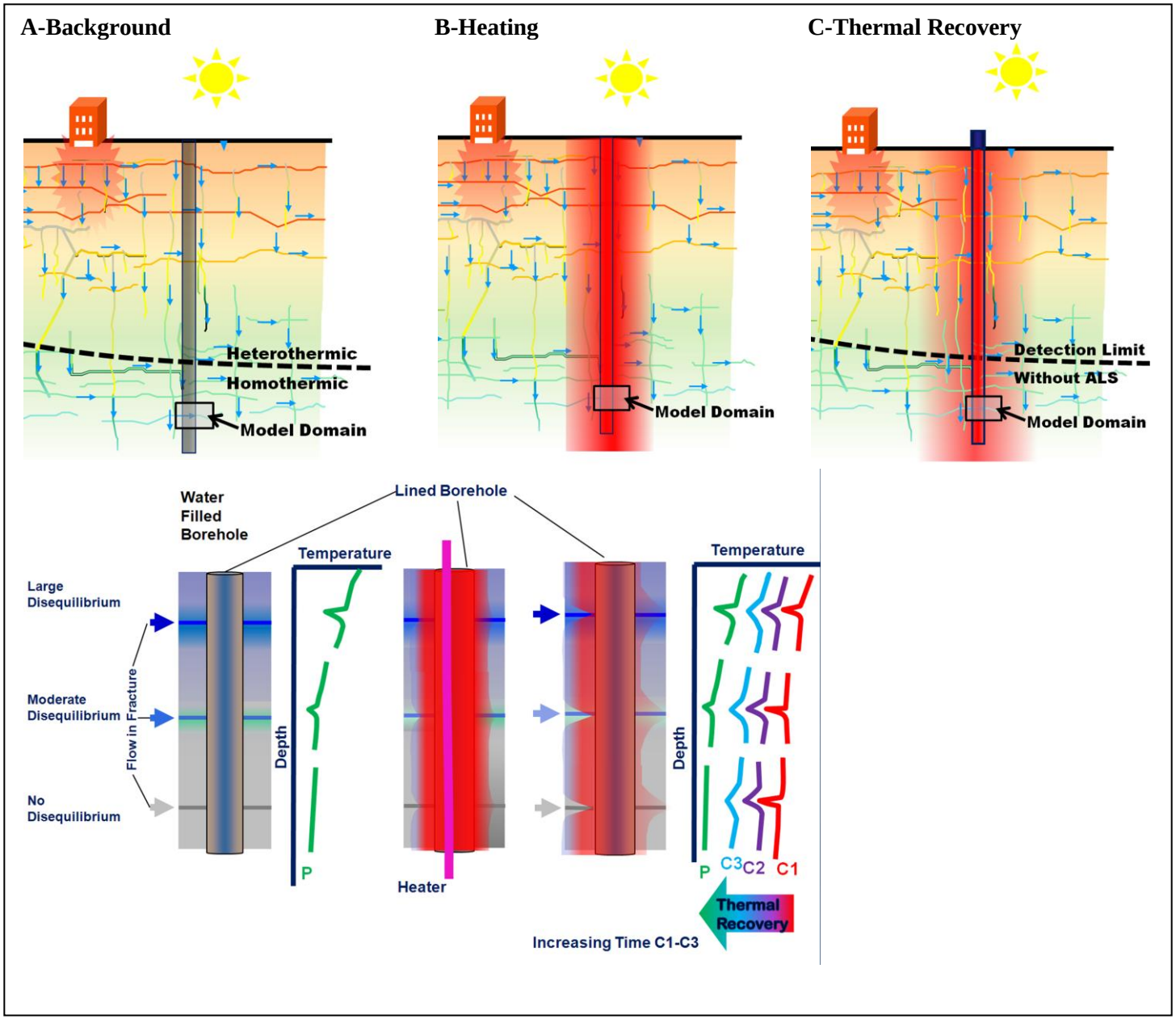

Figure B1: Schematic Hetero-Homothermic Boundary and the ALS Process. *Thermal disequilibrium exists in heterothermic layer but not deeper in homothermic zone. Consequently for the same amount of flow the aberration on Passive (background) temperature profile (P) varies in size above hetero-homothermic boundary and does not exist below. Heating during ALS process creates artificial dis-equilibrium making flow detectable in C1, C2 and C3 temperature logs collected during thermal recovery. Conceptual model domain is shown.*

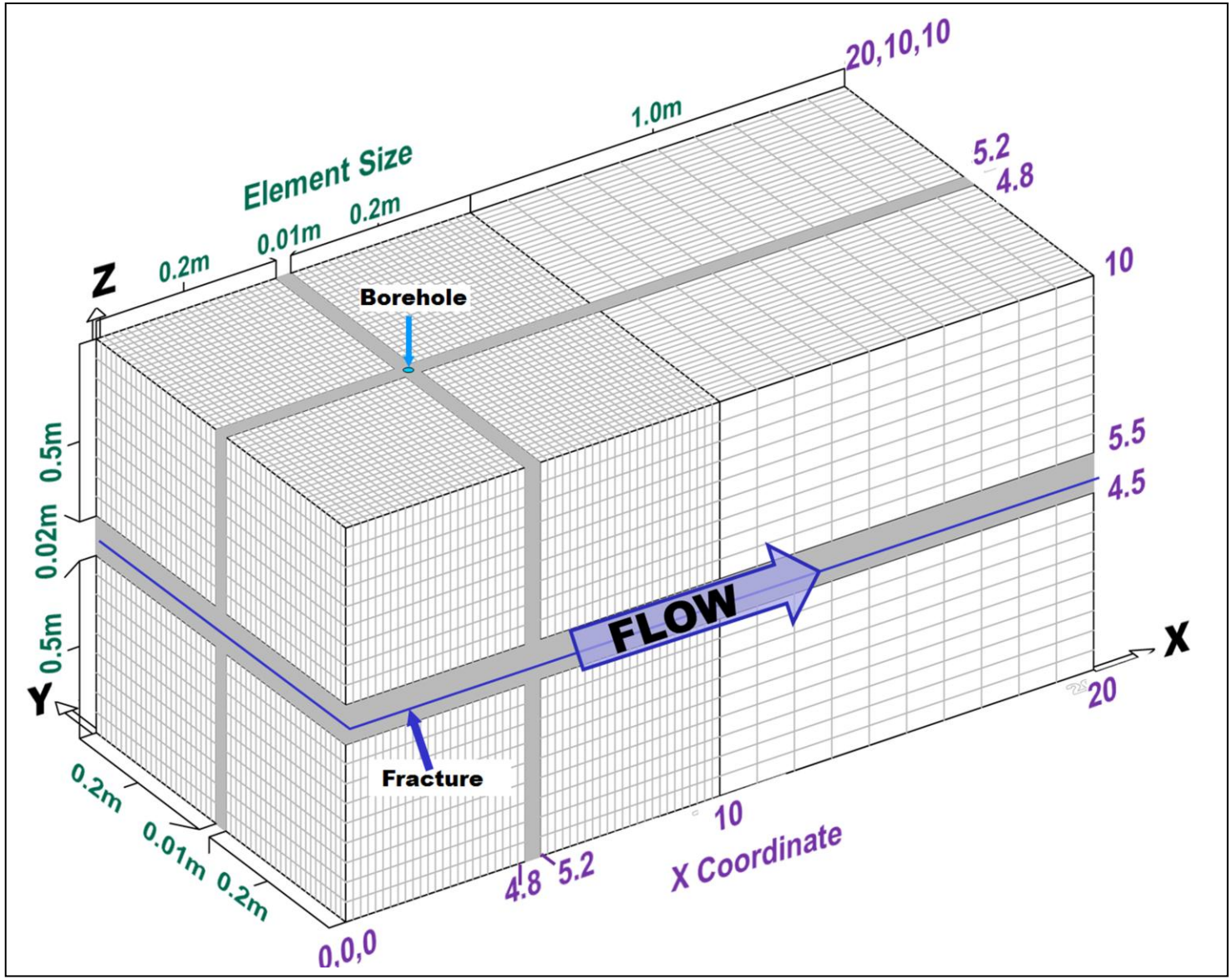

Figure B2: Schematic representation of the model.
The element dimensions are shown in green for each grid section. The coordinates of each section boundary (in metres) are shown in purple.

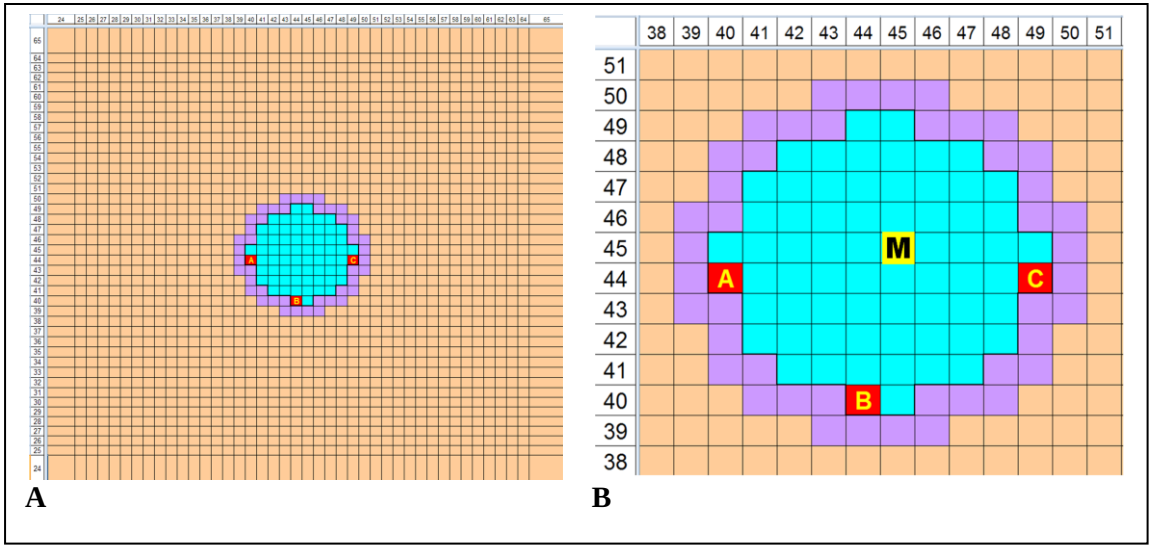

Figure B3: Schematic plan views of the liner surrounding the borehole within model, flow in fracture is from left to right. *(Tan-fracture surface, cyan-water in borehole, purple-liner, red-heater locations)* ***A-*** *Broad view showing 1cm x 1cm x 2cm elements,* ***B-*** *Expanded view detailing borehole elements heated in various model scenarios, Heater positions at A,B and C, M=measuring point.*

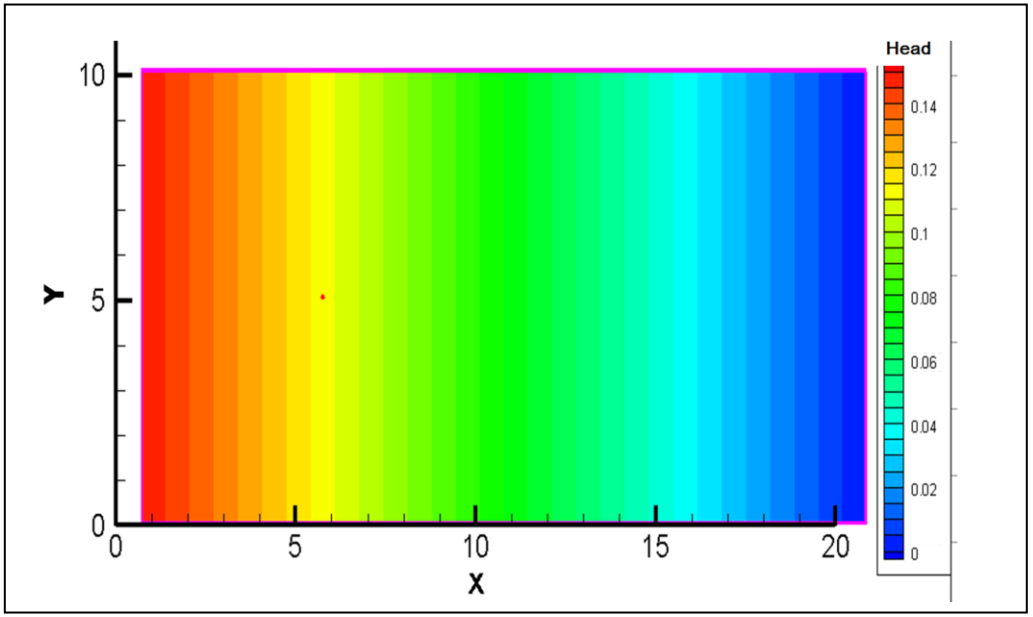

Figure B4: Steady state hydraulic head distribution pattern in the fracture – horizontal plane.
Values presented in colour scale are in metres.

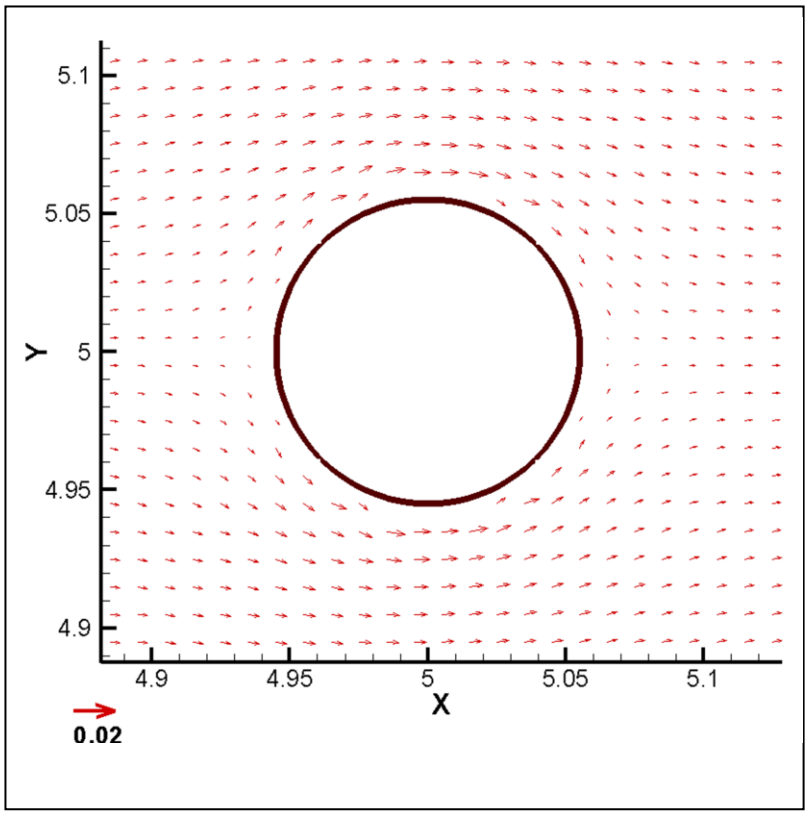

Figure B5: The velocity distribution for flow in the fracture.
∇h=0.0075, velocity in m/s, circle represents borehole liner

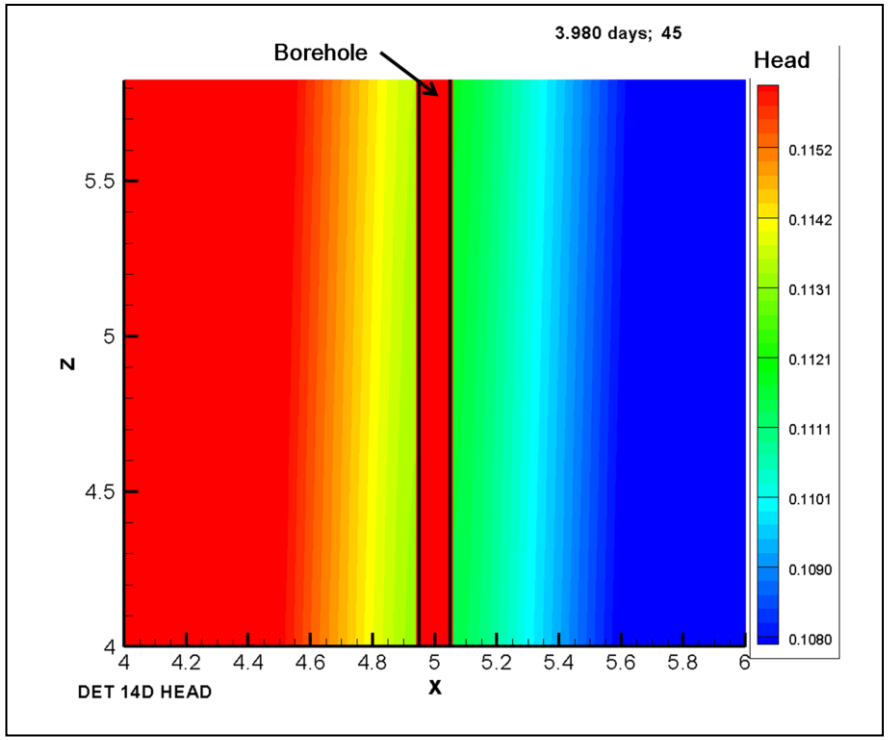

Figure B6: Steady state head distribution around borehole – vertical plane Y=5m. *Values presented in colour scale are in metres.*

.

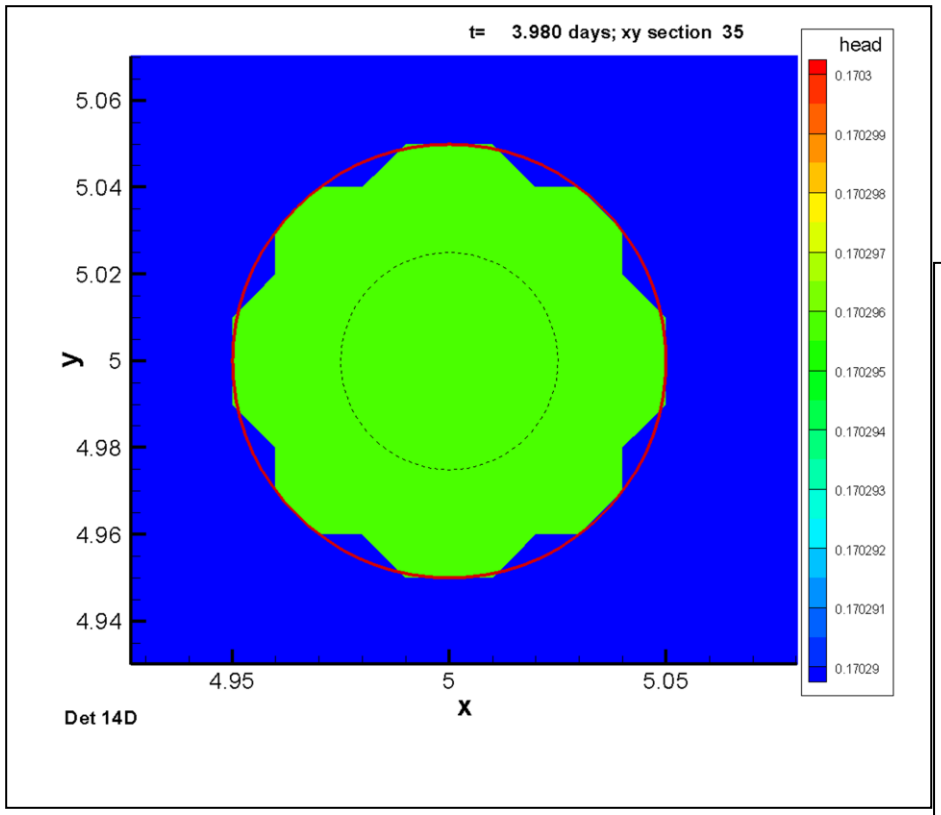

Figure B7: Head distribution around borehole – horizontal plane immediately before heating

Values presented in colour scale are in metres. Light green nodes are borehole and liner.

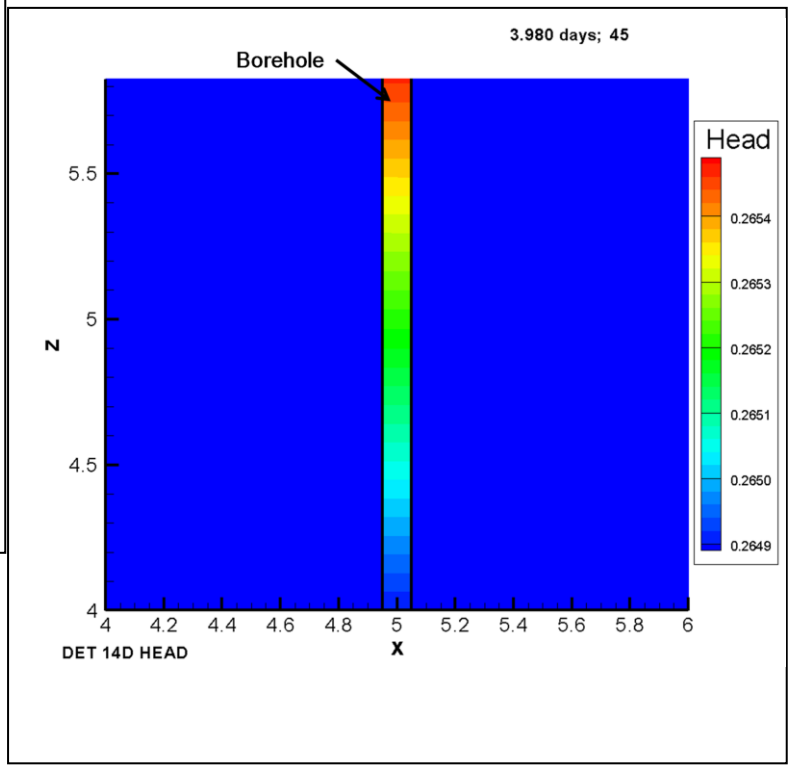

Figure B8: Head distribution pattern in borehole before heating– vertical plane

Values presented in colour scale are in metres. Coloured band represents borehole.

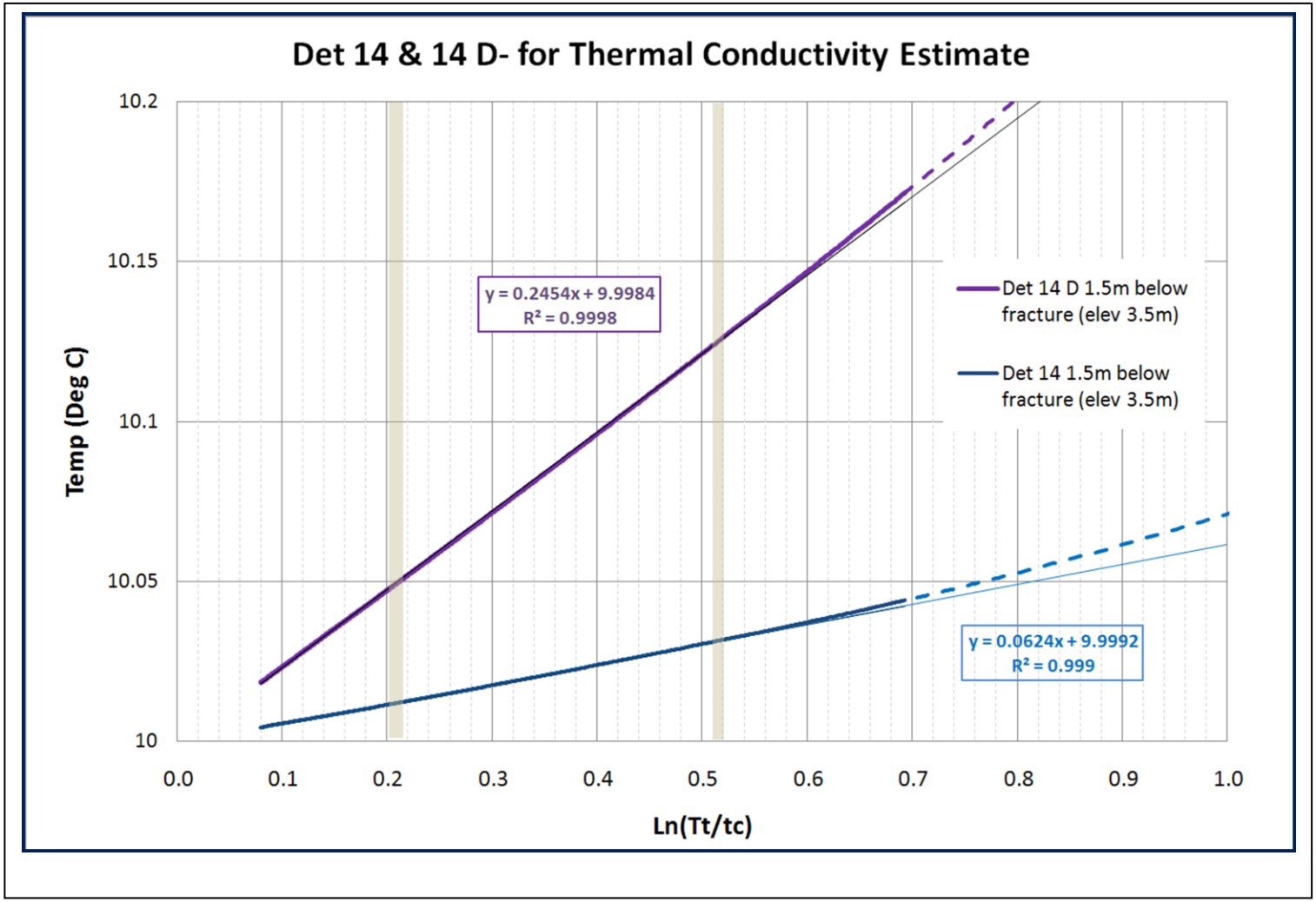

Figure B9: Inverse estimate of K_{rx} using base model.

t=time, t_c=time from turnoff of heater. Solid portion of lines used for linear regression.

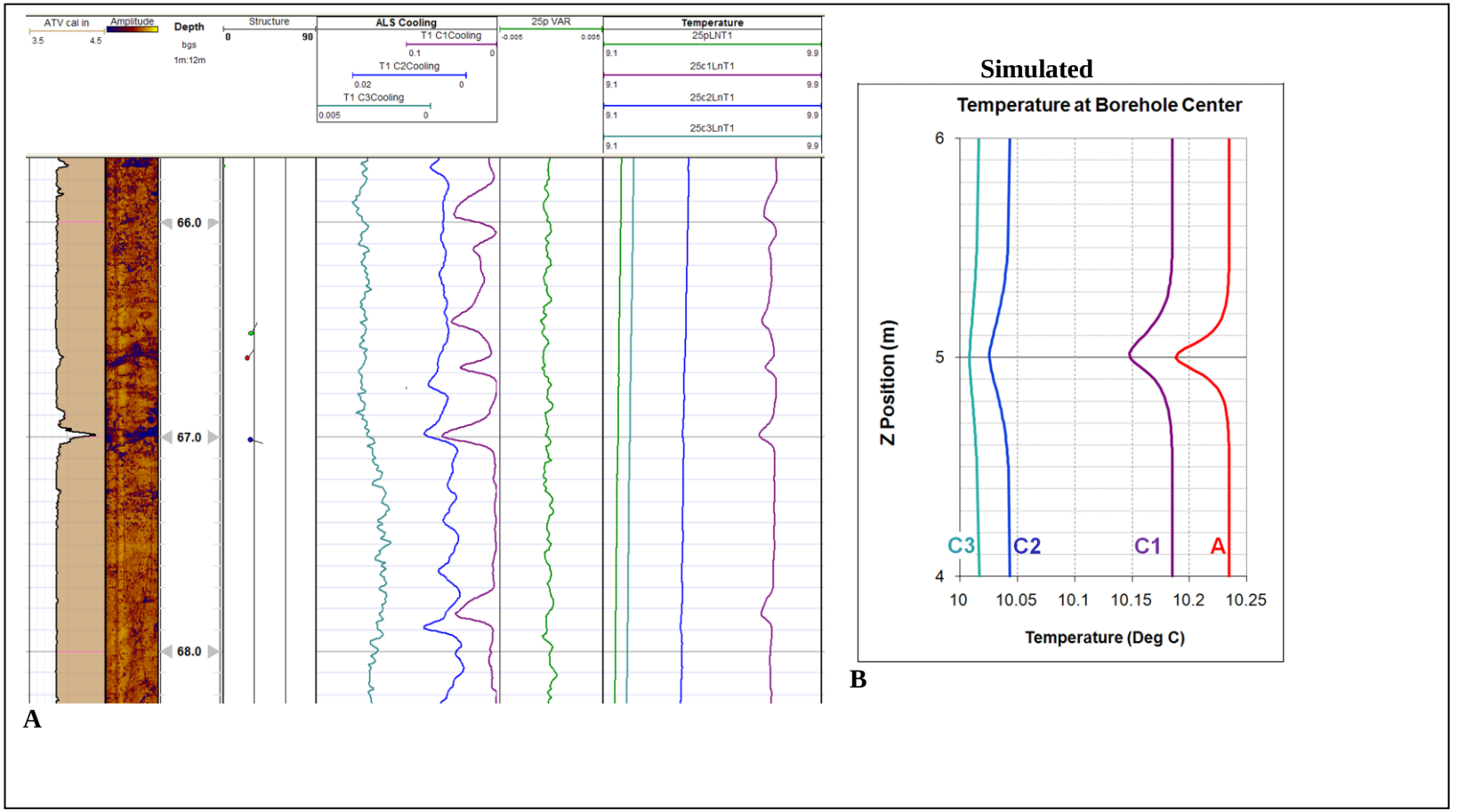

Figure B 10: Detailed comparison of vertical temperature variation.
A-field data MW25 Guelph, Ontario, from the left logs: virtual caliper, acoustic televiewer (ATV), structural interpretation of ATV, cooling (span) of C1(0.1C°),C2 (0.02C°) &C3 (0.005C°), passive variability (±0.0005°C), passive, C1,C2 & C3 temperature (note scales vary) B-Det 14 (base model) response to flow though fracture at A=4.249, C1=4.26, C2=4.5 & C3=5 days (turnoff at 4.25 days). Note similarity of scales between anomalies in field data and model.

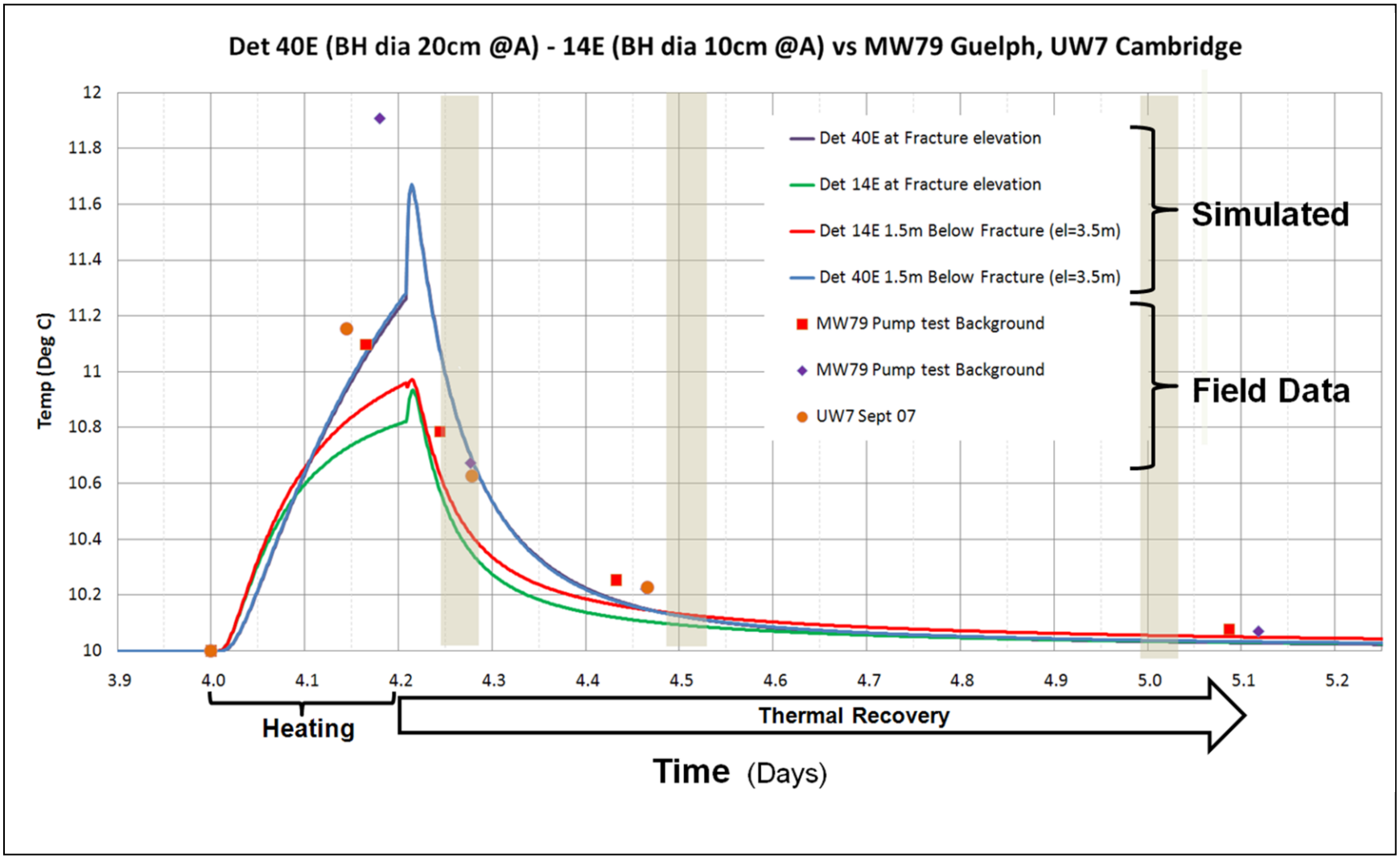

Figure B11: Detailed comparison of temporal temperature variation during ALS testing.
Field data UW7 Cambridge, MW79 Guelph Ontario,

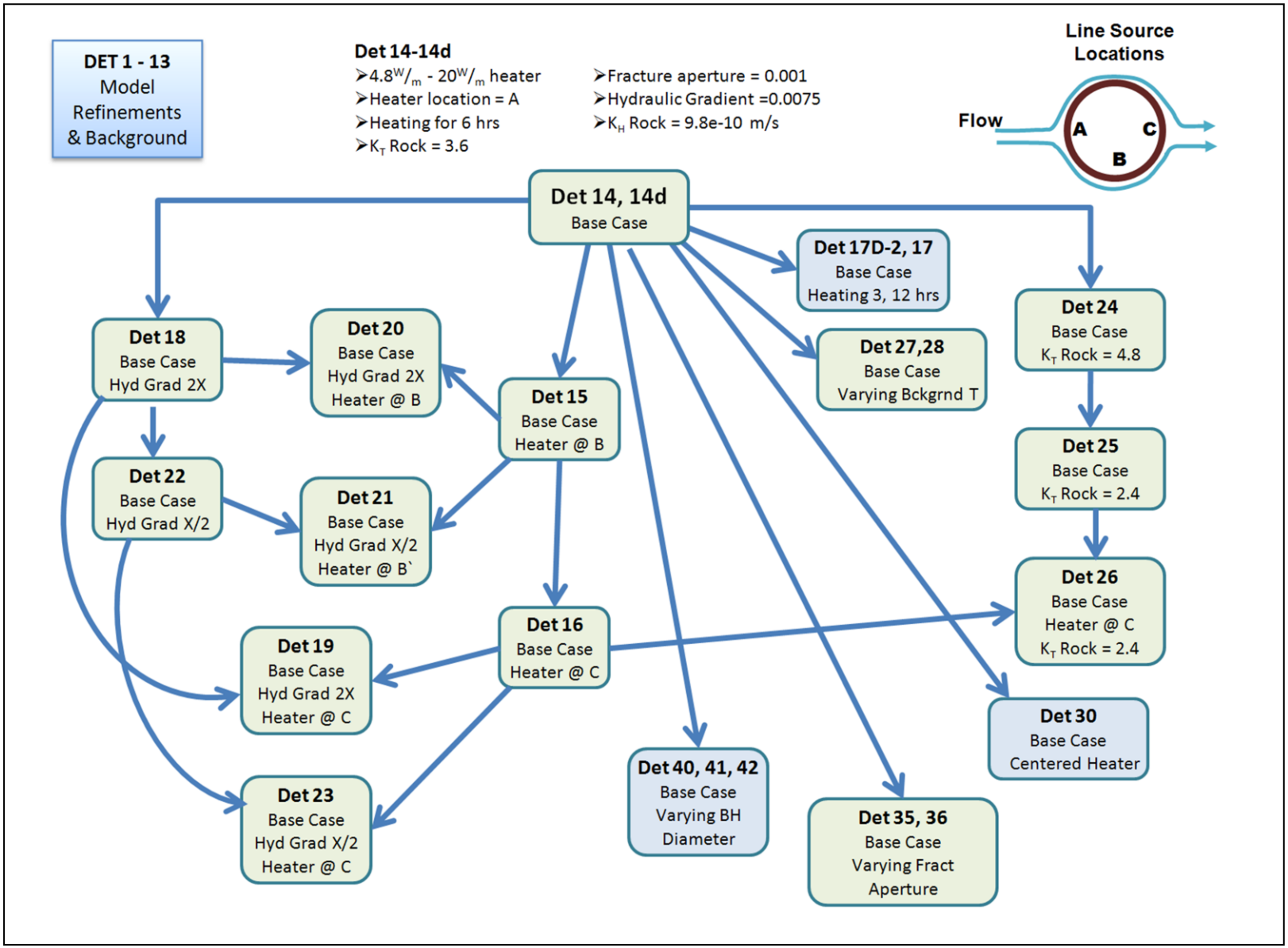

Figure B12: Schematic representation of model parameter variations.
Note: Numbering is not sequential to allow for future work and cataloguing of tests.

B7. Results & Discussion

The results of the modelling exercise and sensitivity analysis follow. As each parameter is varied, the temperature at the center of the borehole at the fracture intersection, at 1.5 m below the fracture (the "no flow" reference), and the effective cooling (details below) are compared with the appropriate base case. The effects of the changing parameters on the thermal recovery process are ranked and compared based on their influence on the rate of effective cooling. The implications of this comparison on the interpretation field results and quantifying flow are discussed.

B7.1. Data Presentation

The Parker-Cherry research group is continuously refining and improving data processing and presentation methods. For field data these processes are generally intended to isolate the temperature variations occurring at a single fracture from the broader changes that occur over the length of the borehole as a result of either deep geothermal or shallow environmental influences. Having isolated small scale variations, the emphasis has turned to insuring that variations at specific depths are accurately characterized. Modelling is used to understand which variations are representative of water movement versus instrument or process variability (noise). Some of the approaches isolating individual variations, such as the "variability log", have been previously published (Pehme et al. 2010) while others, for example the "cooling log" are yet unpublished. The results of the modelling are presented using these techniques as a basis for comparison.

B7.1.1. The Variability Log

The variability log is essentially a high-pass filter wherein a temperature profile is smoothed using a moving average that typically spans 5 metres to create a base that represents the broad temperature variations over the borehole. That base is then subtracted from the original data to emphasise the small scale variability. This process is similar to Berthold and Börner's (2008) subtraction of a linear trend (the geothermal gradient) to highlight variations which they attribute to convection only. The P-C research group has adopted the variability log approach because it not only eliminates the overall geothermal gradient but the procedure also minimizes the broader changes caused by varying lithologies and near-surface environmentally driven heterothermic affects. Although the variability log improves the representation of temperature aberrations associated with a fracture in a lined hole, it does not work as well in a cross-connected borehole where the temperature variations tend to be "steps" which are broadened by the filtering procedure.

B7.1.2. The Cooling Log

The "cooling log" has evolved from the variability log and is specifically intended to highlight the effects of the ALS technique. In a typical background (passive) temperature log, the interpreter cannot be certain whether the water moving through a fracture is warmer or cooler than the surrounding rock and therefore could create either a positive or negative deflection from the general trend. However in the ALS technique, the disequilibrium is controlled by the heating process, and it is reasonable to assume that water moving through the fractures will be preferentially cooling the local environment around a fracture and therefore will create negative variations from the broader trend. A "cooling log" is based on the assumption that over a given span (2-4 metres is typically used) the warmest readings represent that portion of the formation least influenced by the cooling effects of flow in fractures and provides a "best estimate" of the temperature of the rock mass. It follows that the negative deviations from that value result from any water movement.

The process of isolating the cooling effect from the trend is shown in Figure B13. A base log is created by assigning the maximum temperature within a window (±1 m) at each depth along a temperature profile. The resulting stepwise log is smoothed using a 1 metre wide boxcar filter to create a base (i.e. the presumed representation of the temperature of the rock). The original data is subtracted from that base to create a series of spikes that represent the cooling occurring at intervals down the borehole. The modelling simulates a comparatively simple geometry and the effect of the cooling log is achieved by the computationally more efficient process of subtracting the temperature predicted in the center of the borehole at the depth of the fracture from a reference temperature (the center value 1.5 metres below the fracture[23]).

B7.1.3. Components of a Heating Cycle

The ALS process involves a cycle of heating and cooling. To facilitate discussion, the response is subdivided into components as shown in Figure B14 which is shaded to highlight the time periods when data would be typically collected in a field implementation of the ALS technique: the passive, active and cooling logs (1, 2 and 3). In this case the shading represents the duration of logging for a 100m deep borehole at 0.7m/min, the actual time spent collecting each of the logs would vary with the depth of the hole and the logging speed. The cycle is subdivided into stages as follows:

[23] The reference value at 1.5m is chosen because the distance = ½ x (2m max temp window + 1m smoothing filter).

Background – Is the ambient temperature prior to the initiation of heating. In field data this would be any time after the thermal variability caused by previous work in the borehole has dissipated. Natural variability due to weather/seasons and human influences such as local pumping wells can cause changes in the background temperature. Background is therefore collected as close to the beginning of heating as is practical (usually the day before). For the purposes herein, model stabilization was deemed to have occurred after 4 days based on uniform temperature and hydraulic gradients;

Heating – The heating stage is the entire time that the heater is on. The simulated temperature shows an initial time lag that is required for energy to move from the heater located along the up-gradient side of the borehole to the center of the hole. Following the lag the temperature rapidly increases as a response to heating. The rate of temperature increase steadily declines with time. This is consistent with field observations (Pehme et al 2007a) and the theoretical analysis of Beck et. al (1971) which predicts a ln-normal temperature increase with a slope proportional to the thermal conductivity of the rock (Equation B-12). In practical applications however, these data are often highly variable, the likely reasons for which are discussed later in this text.

Early Cooling – The early cooling period is the portion of the ALS cycle immediately after the heater is turned off in which in some cases the temperature at the center of the borehole continues to increase because of the heater-measurement point offset distance and the energy stored in the rock. The increase in temperature is due to heat transport into the borehole from up-gradient because of water flow in the fracture (see section 4.2.3 Heater Position for detailed discussion of influences and figures). Early cooling continues until the temperature returns to the maximum achieved during heating. The duration and size of the heat pulse varies with several parameters including those that are being analysed here which are discussed in detail throughout this text. Depending on early cooling behaviour, some or all of C1 may be collected within this stage of the cycle.

Intermediate Cooling – The intermediate cooling stage is defined as the period between early and late cooling. During this period the rate of declining borehole temperature is initially very rapid, but the rate of decline decreases towards steady state as the borehole approaches late cooling. Although the end of intermediate cooling is clearly established by the start of late cooling (see below), the beginning of intermediate cooling and its duration can vary.

Late Cooling – Late cooling begins when the heater has been turned off as long as the original heating occurred. For example, in most of the models, heating occurred from 4 to 4.25 days (a duration of 0.25 days) and therefore late cooling begins 0.25 days after the heater is turned off (at 4.5 days). For practical

reasons the late cooling ends when the effects of the ALS process are no longer measurable (i.e. 0.001 C° above background). The late cooling stage of the ALS cycle corresponds to the portion of the thermal recovery after heating that Shen and Beck (1986) showed to be the initiation of linear proportionality when plotting temperature against time from the end of heating on a ln-linear scale. Subsequently Greenhouse and Pehme (2002) have used data from this period to estimate the thermal conductivity of the rock mass.

When comparing the field data collected using the ALS process (see Table B1 for details of geophysical logs) to these modelling results it is important to note that for some temperature logs (e.g. the active (A) and first cooling (C1) logs in particular) the upper and lower parts of the hole may be at different stages of the heating cycle when the data are collected for a particular profile. When analysing the thermal behaviour at a given depth based on a combination of logs (C1, C2 and C3) the interpreter must consider that data collected deeper in the hole are further along the cooling cycle than data collected at a shallower depth because of the time required to log the borehole.

Because of the ln-linear relationship and the need to expand early time scales when changes occur rapidly and compress later changes which are gradual, we also adopt a standard of plotting temperature against the log of time from the end of heating such as in Figure B15and Figure B16. Figure B15shows the results of the base case at the fracture and 1.5m below against the log of time from turn-off relative to the stages described above and the typical field data collected (C1, C2 and C3). Note that the model does not predict a true straight line decline in temperature, which was also the case observed in the field data presented by Pehme et al (2007a). Note also that the early cooling variations are greater in the data at the fracture (red) than at the "reference" point 1.5 metres below (purple). The causes for this nonlinearity will be discussed later in the text.

Figure B16 shows the relative cooling for the base case, i.e. the reference temperature (from 1.5 metres below the fracture) minus the temperature at the fracture, isolating the influence of the water moving through the fracture on the thermal patterns, a plot of values equivalent to the "cooling log" against time on a log-log scale. As above, Figure B16 includes the three stages of cooling and the approximate time spans of field data collection in a typical implementation of the ALS technique in a 100m deep borehole. Although in the base case the effect of the fracture initially decreases towards the end of early cooling and into the beginning of the intermediate stage of cooling, the contrast in temperature increases again before the difference begins a linear decline (at a log-log scale) throughout late cooling. These patterns and comparisons against them will be the basis of our assessment of the effects of varying parameters and their influence on the temperature response.

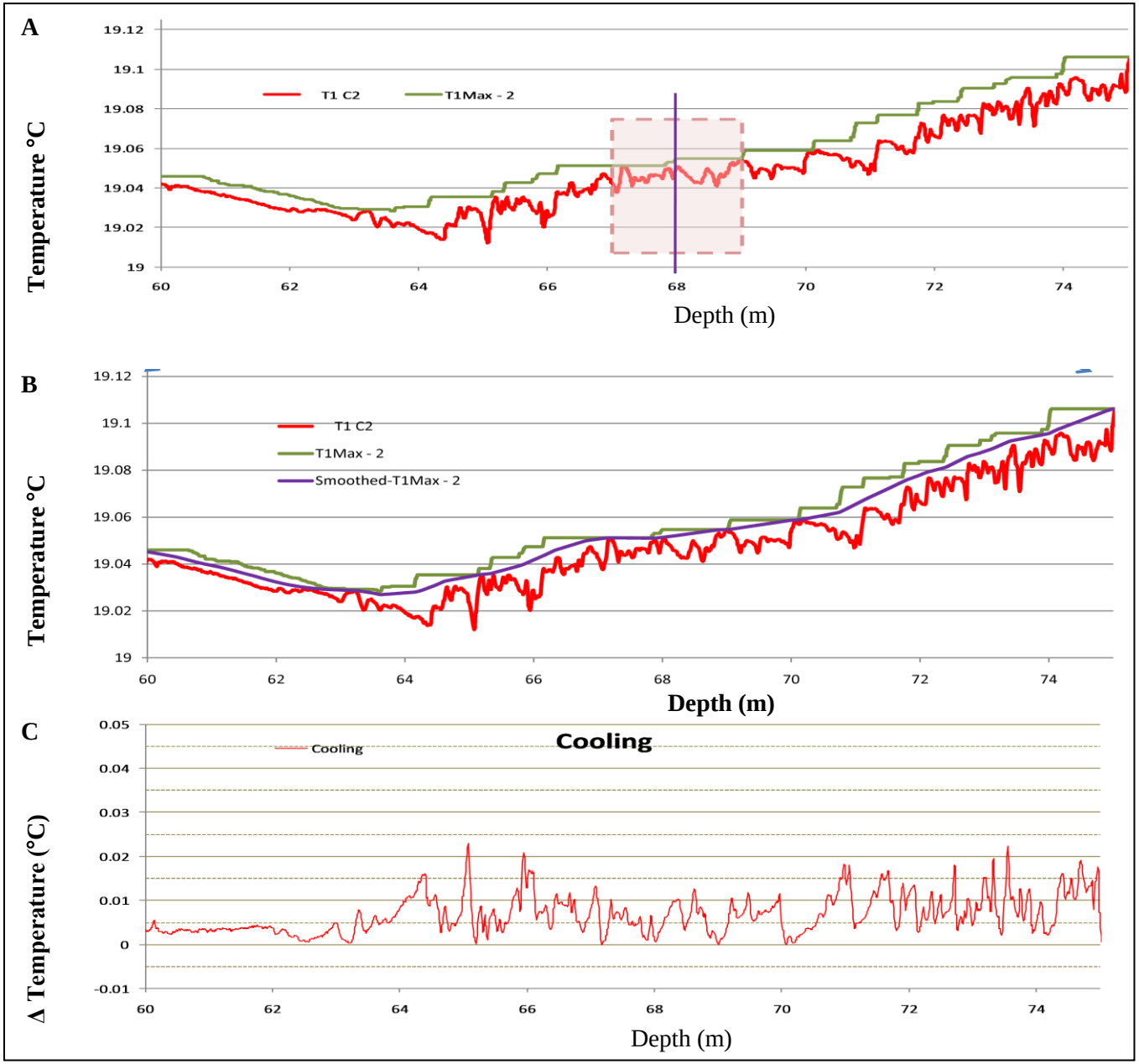

Figure B13: Cooling Log Calculation Procedure. **A**-*Maximum temperature within a 2m window assigned to each point creates stepwise plot,* **B**-*stepwise maximum temp plot smoothed over 2m moving average window,* **C**-*Original temperature log subtracted from smoothed maximum temperature log to create "cooling log"*

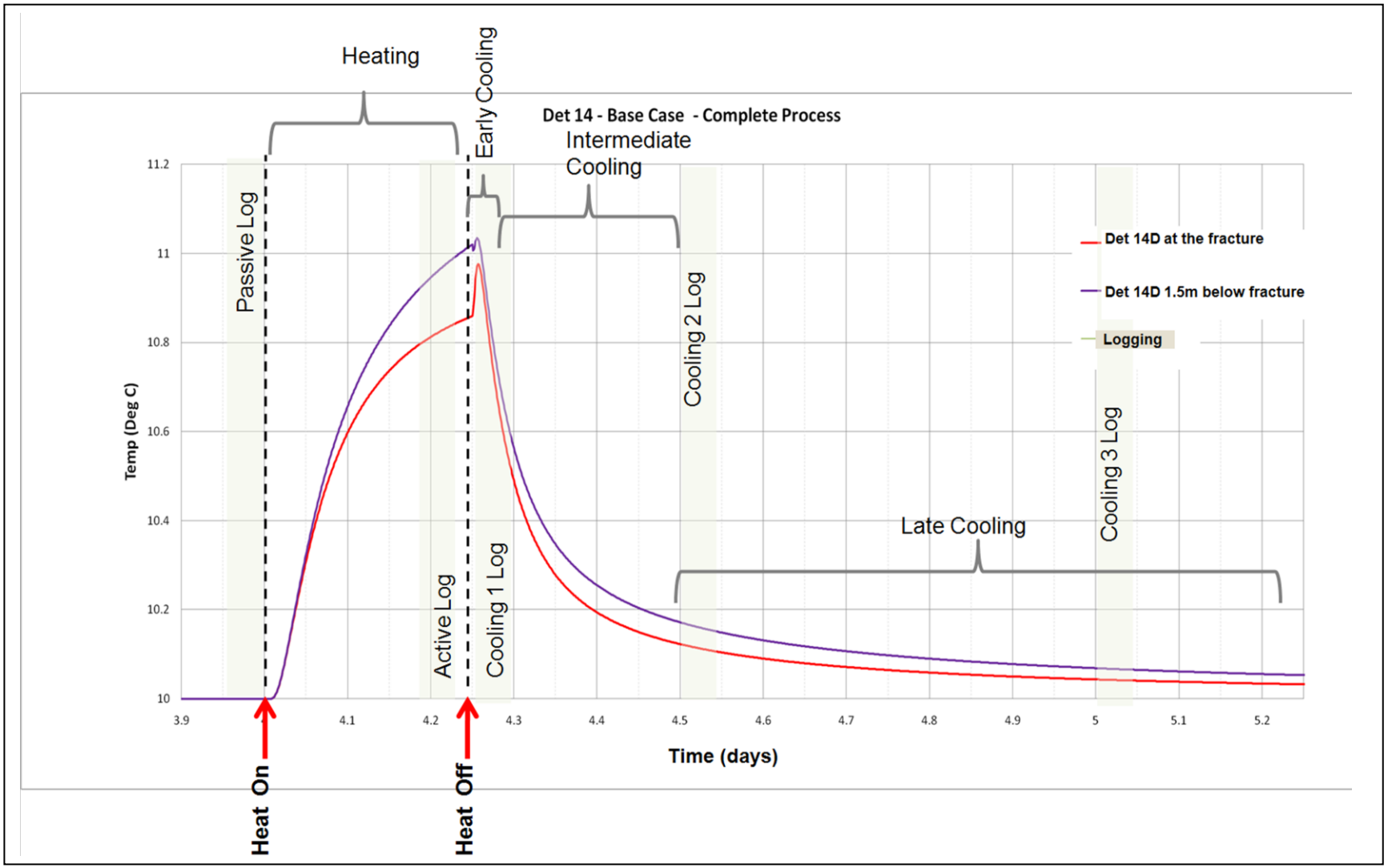

Figure B14: Components of the ALS heating – cooling cycle.

The temperature response (℃) at the center of the borehole at the fracture (red) and 1.5m below the fracture (purple) plotted against time. Details discussed in main text.

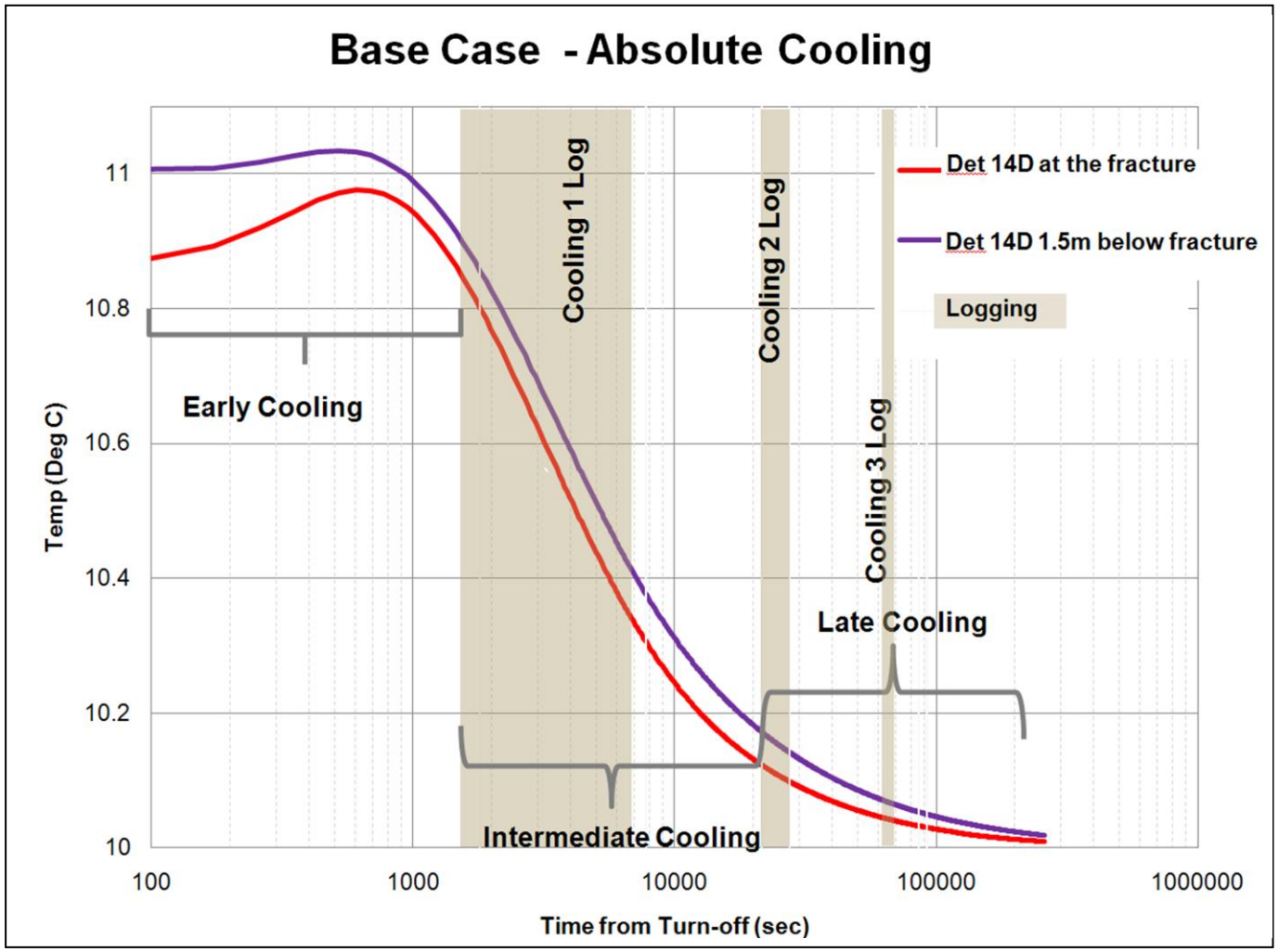

Figure B15: Log ALS heating – cooling cycle. The temperature response (°C) at the center of the borehole (red) and 1.5m below the fracture (purple) plotted against time from heater turn off. Details discussed in main text.

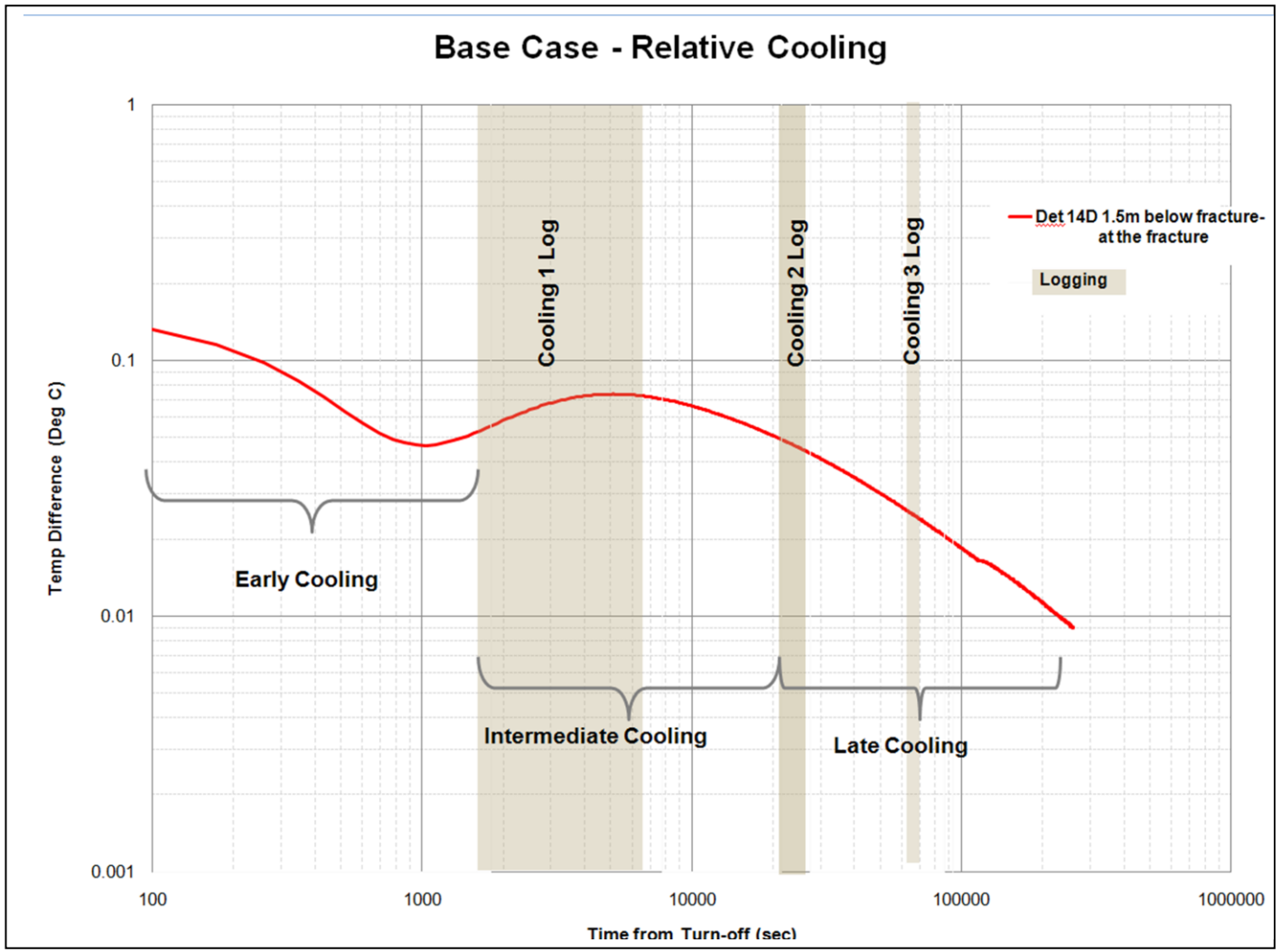

Figure B16: Cooling components of the ALS heating – cooling cycle.
The relative temperature response (°C) center of the borehole (reference 1.5m below –at the fracture) plotted against time from turnoff. Details discussed in main text.

B7.2. Response at Borehole Center

The following section focuses on predictions of the borehole temperature along the center of the borehole, analogous to the results of a centralized single sensor temperature probe. The sequence of parameter variation is:

1. heater output,
2. duration of heating,
3. heater position,
4. borehole diameter,
5. rock thermal conductivity,
6. background temperature,
7. hydraulic gradient (with varying heater locations), and
8. fracture aperture.

Those aspects of the process that are under the investigators' control (power output, duration of heating) are addressed first. Then other aspects of the approach that are not well controlled, e.g. the location of the heater around the circumference of the borehole as well as the borehole diameter are examined. Finally the influence of parameters beyond investigator control such as the matrix thermal conductivity and background temperatures are tested, ending with system characteristics that dictate water movement in the fracture (i.e. hydraulic gradient and fracture aperture).

B7.2.1. Heat Source – power output (W/m)

Figure B17 compares the model results of the ALS process where the power output of the heater was increased from 5.8 W/m to 20 W/m. Additional power accentuates the magnitude of the characteristics of the heating-recovery curve. The change in power does not, however, influence the timing of the features of the growth-decay curve. Consequently the temperature decay varies considerably more through the early cooling as the heat is increased, particularly in the vicinity of the fracture and consequently the relative cooling is more variable as well. An important factor is that unlike above where the slope of the line changes with the power introduced, the slope of the log-log plot of relative recovery is relatively independent of the power input (1.844 for Det14 and 1.769 for Det14D). The converse also applies; any reduction in power will dampen the response and reduce the effects of the water moving through the fracture.

B7.2.2. Heat Source – duration

Figure B18 shows the effect of varying the duration of heating from 3 to 6 (base case) and to 12 hrs. Since the definition of early, intermediate and late stages of the process are based on the duration of heating, the timing of these stages are different for each case as would be when logging is undertaken. The logging times for the base case are shaded, while the initiation of logging is represented as coloured circles for the shorter and longer heating times. The logging events when the borehole is heating 12 hr (Det17) have been proportionally spaced to capture the cooling process.

During heating the curves are similar in all three cases, with the water flow increasing the separation between the temperature at the fracture and that at the reference point (1.5 m below) with time. During early cooling the flow of water in the fracture causes a similar sized peak to occur in all three cases. In the case of the 3hr heating, the water flow in the fracture has not yet induced an adequately large difference in temperature from the reference and consequently for a short period during early cooling the peak temperature adjacent to the fracture is higher than at the reference depth creating negative relative cooling values which cannot be represented on a log-log scale. The slope of the relative cooling is similar in all three cases (-0.717, -0.701, -0.697) through the respective (short to long) late times. Although the implication is that the cooling process could be adequately sampled with a shorter heating period, the working window (the time between the end of early time transient variations and when adequate signal exists for measurement) becomes shorter with less heat. The available time for logging relative to the length of the borehole places practical constraints on the implementation of the process (an issue addressed further in the conclusions).

B7.2.3. Heater Position

An aspect of the ALS process beyond the control of the investigator is the position of the heater in the borehole. Based on the author's experience with hundreds of boreholes logged using acoustic televiewer probes[24], it is very unlikely that any borehole is perfectly vertical, but almost all will either gradually deviate or in the case of longer holes occasionally corkscrew with depth. The bottom end of the heater has a load attached which, along with the weight of the cable itself, places the cable under tension. During the insertion, the heater is lowered to the bottom and then placed under tension, lifting the weight approximately a metre off the deepest portion of the liner to avoid added stresses on the material.

[24] a sonde which is primarily intended to measure borehole diameter and surface reflectivity with a sonic pulse but also assesses borehole deviation.

Although there may be some frictional cohesion between the liner and the heater, it is reasonable to assume that:

1) the heater is along the side of the borehole rather than the middle,

2) the gravitational and tensional forces on the heater are greater than any frictional forces and

3) the heater will follow the shortest path from the bottom to the surface.

Given the opposing forces of tension and gravity, the heater will likely follow the shortest route to the bottom of a near vertical borehole, tending to the high side of the hole near the surface and the low side towards the bottom, but that cannot be certain in all cases. Since everything about the system except flow is radially symmetric about the center of the borehole, the heater position is examined relative to the flow direction and an XZ plane through the center of the borehole. For convenience, three positions for the heater are simulated (refer to Figure B3b) which are designated relative to flow as:

- on the up-gradient side of the borehole (along elements centered at X=4.955m, Y=4.995m, Z=0.25-9.75m),
- side gradient, half way around the borehole (elements X=4.995m,Y=4.955m, Z=0.25-9.75m),

and

- down gradient (elements X=5.045,Y=4.995m, Z=0.25-9.75m).

Figure B19 shows the simulated response at the fracture and 1.5 metres below when the heater is at A (Det14D), B (Det15D) and C (Det16D) (Figure B3) with all other parameters as in the base case. With the exception of the first half of the heating stage, the temperature with the heater up-gradient at A is consistently higher than when the heater is either side- or down-gradient. As is the case in other tests, the response is predicted to be more variable at the fracture than at 1.5m away for all heater positions. The maximum temperature is expected to be over 11^{o}C with the heater up-gradient in comparison to 10.7^{o}C with the heater down-gradient, approximately a 30% larger increase relative to the 10^{o}C initial temperature. The temperatures during early thermal recovery (Figure B19b) increase by approximately 0.1 C^{o} at the fracture before starting to cool when the heater is up-gradient, much more than in any of the other conditions plotted. The peak temperature occurs the earliest when the heater is side-gradient (B), followed by down-gradient (C) and the longest delay is when the heater is up-gradient (A), approximately 300 s (50min) after the side-gradient case. This result would have particular significance when characterizing flow by comparing early and intermediate temperature recovery logs and will be discussed

further in the conclusions. The plots of relative cooling (Figure B19c) highlight the degree of variation in the early and intermediate cooling time windows when the heater is at A. Although the direct plots of temperature (Figure B19 a&b) show differences when the heater is side or down- gradient (at B and C) the relative cooling is essentially the same. Although the relative temperature in the up-gradient case is warmer than the other two conditions, the log-rates of cooling (slope on the log-log plot) are similar ($-.701_A$ vs $-.750_B$ and -7.81_C) and are relatively independent of the heater location in the borehole.

A comparison of the changes in the temperature around the borehole helps identify the cause of the predicted temperature patterns. Figure B20 shows plan view representations of the temperature patterns in the fracture plane at approximately 5,500, 22,000 and 65,000 seconds (1.5, 6.1 and 18.1hrs) after the heater is turned off. The temperature patterns result from a combination of the affects of geometry, water movement and the comparatively higher thermal conductivity of the rock on the outside of the liner relative to that of the water in the borehole. When the heater is up gradient (A), much of the thermal energy remains in the rock after heating stops and slowly moves towards the temperature sensor. When the line source is side (B) or down (C) gradient, most of the energy that has been stored in the rock is transported away from the thermistor after the heater is turned off. Note that in cases B and C, the thermal gradient in the hole increases towards the heater location at all times, while in the case of an up-gradient heater (A) the reservoir of heat energy in the rock and the symmetry of the heat transport by flow essentially eliminate the horizontal thermal gradient in the borehole soon after the heater is turned off.

To put the temperature comparison between the fracture and the reference into context, it is useful to compare other, broader perspectives of the process. Plots of the vertical temperature distributions in various configurations are shown inFigure B21. Although the range of the temperatures being considered in any particular case is small, compared to the overall differences in temperature under conditions A, B and C it is large, and therefore two different colour scales are presented. In addition when the heater is side gradient (B), the variations are no longer symmetric about the XZ plane (Y=5). The YZ slice (X=5) is provided as well.

As anticipated from discussions above, Figure B21 shows that the fracture is in all cases cooler than the rock with the exception being down-gradient of the borehole in the local zone of the heater influence. The zone initially (4.35 days) impacted by the addition of heat extends approximately one metre down-gradient at the fracture. However as the water moving through the fracture dissipates the excess energy quicker than does the rock, the temperature approaches ambient levels much earlier at the fracture. Consequently, a distinct horizontal thermal gradient towards the location of the heater is predicted above and below, but not at the fracture. The vertical thermal gradient is largest in magnitude slightly above and

below the fracture (~0.1m), although in opposite directions. These observations apply in a broad sense; however the temperature pattern within the borehole is not symmetric about the fracture. There are subtle patterns in addition to the trends described, with the side below the fracture warmer than the upper implying that the warm water is rising, i.e. the model predicts convection to be occurring (shown schematically in Figure B22). The disruption extends approximately 0.8m below and 0.6m above the fracture with the water rising on the side of the borehole near the heater. The scale of these convection cells is slightly smaller than those predicted by Berthold and Börner (2008) under ambient thermal gradients. The asymmetry is consistent with the thermal gradient below the fracture promoting convection while the condition of warm water above cooler water would be conducive to thermal stability. Further study of these patterns including thresholds for occurrence, comparison with head profiles and field data are warranted but beyond the scope of this effort.

B7.2.4. Borehole Diameter

The base case has a 10 cm (3.93") borehole which is a commonly used borehole size when core samples are retrieved for testing rock chemistry or geotechnical properties. Although it is relatively rare for smaller boreholes to be drilled when multilevel installations are planned, larger 5, 6, 8 and even 10 inch holes may be used in some cases to provide either larger core samples or to allow more sampling ports[25]. In addition, portions of boreholes are often enlarged beyond the intended diameter due to either poor drilling technique or a weakly consolidated matrix. Given that the base case is close to the smallest size a borehole is likely to be, only the possibility of the borehole being larger is examined.

Figure B23 shows the effect of increasing the borehole diameter to 20cm (~8in). Note that the heater has been moved to remain against the up-gradient borehole wall. Overall the response is dampened by the increase in the amount of water between the probe and the heat source. The early time rise is more gradual than in the base case. The latent peak in the 8 inch borehole has a similar, dampened shape at both the fracture and 1.5m below. At the fracture the late time response is similar to the base case but is only slightly cooler than temperatures 1.5 m below.

[25] The number of ports in a FLUTe multilevel installation depends on the diameter of the borehole, while a Westbay system is controlled by the vertical spacing of seals and ports while the Waterloo system multilevel system is fixed at maximum of 7 ports.

The relative cooling is consistently at a lower temperature than that of the base case. The relative cooling is highly variable and unstable (negative) at early time as the temperature in the fracture is temporarily warmer than at 1.5m below and consequently cannot be presented at a log scale. Through late time the slope of the cooling is -0.561, 20% less than the base case and the intercept-slope ratio is 54% less. The implication is that borehole diameter is an important consideration in the interpretation and quantification of the response.

Table B6: Typical* range of thermal conductivity of various rock types

Type	k_{rx} (W/m·K)
Limestone	2.0 - 3.3
Sandstone	1.6 - 2.1
Granite	1.7 - 4
Shale	1.3 - 3.0
Slate	1.8 - 2.9
Schist	1.7 - 3.8
Calcite	3.5 - 3.9
Quartz	3.0

Values compiled by Molson and Frind (2006)
* a range of values exist for each rock type, other authors provide slightly different values, see Appendix C

B7.2.5. Thermal Conductivity Contrast

The version of Smoker used herein requires a bulk rock thermal conductivity value including both matrix and water. The thermal conductivity of water is essentially constant over the range of temperatures dealt with in this exercise (Bejean 1993), as it would be in most field applications. However, the thermal conductivity of the host rock could vary considerably. Table B6 provides a subset of a summary of bulk thermal conductivity values provided by various sources as compiled by Molson and Frind (2006) which is included as Appendix B. Within each rock type there is a range of thermal possible conductivity values depending on mineralogy, porosity or the nature of how the minerals are bound to each other (their genesis). Beck (1976) among others has provided formulas for determining effective thermal conductivity values along and across bedding. An analysis of the nuances of the various possible permutations of thermal conductivity is beyond the scope of this effort, but a simplified scenario of 3 possibilities is examined.

Figure B24 compares the base case (k_{rx}=3.6 W/Km, based on Appendix BB: Table 6) with scenarios where the rock thermal conductivity is either 33% lower (k_{rx}=2.4 W/K m, Det25) or comparably higher (k_{rx}=4.8 W/K m, Det24). Since the rate of temperature change can be used to estimate the thermal conductivity of the rock (Pehme et al. 2007a) the raw curves are expected to vary considerably as is the case. The rate of temperature increase during heating is inversely related to the thermal conductivity of the rock because the heat energy dissipation from the vicinity of the borehole depends on k_{rx}. The effectiveness of the fracture water flow in suppressing the rate of temperature increase relative to background decreases with a larger k_{rx}, i.e. the difference between the temperatures at the fracture versus that 1.5m below as the heater is turned off is smaller when k_{rx} is higher.

The pattern of early time decay varies only slightly with k_{rx} at 1.5 m below the fracture. However, the delayed temperature increase at the fracture becomes much larger and lasts longer with a smaller k_{rx} than

with a larger value. The influence of the thermal conductivity of the rock on the early time peak is related to the storage of heat in the rock and subsequent release. The rate at which the temperature decays through intermediate time also increases when k_{rx} is low as compared to when k_{rx} is high. It follows that k_{rx} also has implications on the heater up vs down gradient as discussed above (4.2.3).

Figure B24c shows that the relative cooling increases in variability at early and intermediate time with decreasing k_{rx}. The log-log rate of decline of relative cooling over late time is 5% larger when k_{rx} is increased by 33% over the background case and 10% smaller when k_{rx} is 33% smaller indicating that the effect of varying k_{rx} is not linearly related to log time, The effect decreases when the thermal conductivity of the rock is high and it is an increasingly important factor as k_{rx} approaches the range most commonly expected at sedimentary rock sites.

B7.2.6. Background Temperature

Another factor beyond the investigator's control is the background temperature. Background temperature can vary both geographically according to where the work is being conducted, but also because of other factors such as elevation, local topography, vegetation and proximity to heat sources such as buildings etc. To examine the effects of broadly varying rock temperature on the ALS process the background temperature of the base case 10°C (values typical of southern Ontario) is halved to 5°C (Det 27, representing northern regions) and doubled to 20°C (Det 28, typical of Southern California). The results of these simulations are shown in Figure B25.

The thermal response to the heating portion of the ALS process varies considerably with background temperature. The maximum temperature increase within the borehole is approximately 0.2 C° higher (above ambient) in a 20°C environment than when background is 5°C. During cooling, the characteristic early time peak at both the fracture and 1.5m below both increases in amplitude and exists for a shorter time (narrows) as the background temperature increases. These patterns are consistent with a higher rate of lateral heat dissipation in a cooler environment than in a warm one. Referring to Figure B26 which displays the pattern of the energy increase (at 4.27 and 4.45 days) in both plan and section, the colour scheme of each case is consistent relative to the respective background. A single yellow contour is added to each image to show the extent of above the respective background (i.e. at 5.002, 10.002 and 20.002 °C) to indicate the limit of the measurable impact of heating. In all cases the detection limit becomes broader with background temperature. A higher, narrower relative peak is maintained when the background is 20°C than when background is at 5°C. In a colder environment the energy is drawn out into the rock and away from the borehole resulting in lower temperature increases in the borehole above ambient levels as shown schematically in Figure B26d. Note that this phenomenon only occurs at the fracture, the overall

width of the zone of influence away from the fracture is the same in both Det27 and Det28. Since the duration of "early time" depends on the pattern, that stage in the decay process is shorter when the background temperature is higher. As a consequence of the overall increase in temperature being larger at higher background temperatures, the rate of temperature decline through the intermediate stage is also higher.

The plot of relative cooling Figure B25c provides a different perspective on the patterns. The first cooling log (C1) would be started within early time in all three cases, albeit the characteristic dip in values is muted when the background temperature is cooler. Most importantly the decline of the relative temperature is greater in the 5°C case than in the 20°C scenario. This situation continues through late time with the slope at 5°C being -0.798 LT/Lt (13.9% above the base case) and -0.633 LT/Lt (8.6% less than the base case) at 20°C. However, the intercept-slope ratios are similar (Table B7) to most of the other cases tested.

The model predicts that the background temperature is an important consideration, especially when interpreting the raw data. Pre-normalization, the variability and the rate at which the temperature changes occur are greater in a warm environment than when the background is cool. Although the model predicts eventual similarity in thermal recovery, this does not occur within the maximum time intervals currently used for data collection.

B7.2.7. Hydraulic Gradient

The ultimate goal of the ALS process is the characterization of water flow in fractures, and therefore a key parameter is the effect of varying water velocity within the fracture. In this case the velocity is varied by halving and doubling the hydraulic gradient across the model from 3.75×10^{-3} in Det 22 through 7.50×10^{-3} in the base case to 1.5×10^{-2} in Det18. The velocity of the water for the three cases is 2.27×10^{-3}, 4.53×10^{-3} and 9.06×10^{-3} m/s, respectively, based on Equation 5-3. Because of the strong influence of the location of the heater on the predicted temperature, the effect of varying water velocity is examined with the heater at the three positions A, B and C.

Figure B27 plots the modeled response for the three flow velocities with the heater up-gradient at A. The simulated temperature at 1.5 m below the fracture for Det18 ($\nabla h = 1.5 \times 10^{-2}$) is within a few thousandths C° of the base case ($\nabla h = 7.5 \times 10^{-3}$) throughout the entire heating-cooling cycle (i.e. overlap) and both are distinctly warmer than the temperature at the reference depth in Det22 ($\nabla h = 3.75 \times 10^{-3}$) during heating. The implication of the reference varying is that an offset of 1.5 metres is not sufficient to be entirely independent of the fracture and that the vertical influence of the water in the fracture is a function of the

velocity (or flow). However once some level of influence is achieved, the reference temperature becomes independent of increasing velocity. It is also important to note that as the heater is turned off the temperature at the fracture for the base case is greater (by approximately 0.06 C°) than when the water velocity is either higher or lower, implying that the temperature at the borehole is partially a function of the transport of heat energy back towards the borehole. The implication is that an optimum water velocity exists that maximizes the temperature for the energy input than if the water velocity is higher or lower and a simple assumption that "the coolest zones at maximum heating represent the most flow" is inappropriate. Figure B28 shows vertical profiles through the borehole for each test at 4.24 days, immediately before the heater is turned off. A detailed representation of the temperature distribution at the fracture and 1.5 m below is shown as well as a plot of the difference in temperature at 0.5 and 1.5 m below the fracture for both the centerline and at the heater. Although, a vertical gradient is not apparent in the at 1.5m below the fracture cross-sections a calculation of the gradient between 4 and 3.5m across the borehole (Figure B28D) shows a gradient does exist and it reverses at the liner-heater boundary (X=4.95). These results also highlight the issue of what is the appropriate distance along the borehole at which to determine a "reference" temperature? In this single fracture model the choice is simply a compromise between the effects of the fracture and model boundaries. But in the field, the practical choice of background is largely limited by fracture frequency. Given the generally high frequency of fractures typically estimated from other techniques (rock core, ATV etc.), the 0.33 $^{frac}/_{m}$ is optimistically assuming a low fracture frequency and it would be unrealistic to chose a temperature further from the fracture as background. Through intermediate and late recovery, all three curves measured from 1.5m away overlie each other and therefore relative cooling remains a viable base for characterization at these later stages.

Referring to the relative temperatures in Figure B27, the low-velocity case is particularly variable as the temperature at the fracture is higher than that at background during early cooling, presumably because the water brings additional heat energy towards the borehole which does not occur away from the fracture. Although the raw temperature data exhibit a complex relationship with water velocity, the relative cooling is systematic, varying in a consistent manner, showing greater and more uniform cooling throughout recovery, with increased water velocity. There is a slight but systematic increase in slope at a log scale through late recovery time from -0.666 (Det 22) to -0.725 (Det 18), a range that spans 8.4% relative to the slope of the background case (Table B7).

Figure B29 shows the thermal response as the head gradient is increased and the heater is at the side of the borehole off-center of the flow (at B) where Det21 is the lowest velocity and Det20 the highest. Again the background temperatures for the intermediate and high velocity cases are essentially the same, but the response for the low velocity situation is at a higher background temperature (a reverse of the situation

above). With the heater at A and B, the recovery during the intermediate and late cooling at 1.5m below the fracture is the same in all three cases. The response is less complex than when the heater is at A with the background curves always warmer than the corresponding values at the fracture and the higher velocity response always cooler than the lower velocity cases. Again the relative cooling is greater and more uniform with increasing water velocity. The log slope in late time increases by 2.8% of the base case (from -0.739 to -0.760) through the range of velocities used.

When the heat source is moved down-gradient (to C) (Figure B30), again the background response of the high (Det19) and the intermediate (Det16) hydraulic gradients are the same, both being greater than the low velocity case (Det23) as occurred when the heater was at A. As predicted with the other heater locations, the background values are similar through intermediate and late decay regardless of the water velocity. With the heater down gradient, both the high and low velocity curves grow in a similar fashion at the fracture and neither is as warm as the mid-velocity simulation although the span of temperature (lowest to highest) is much lower than with the heater up-gradient. These complex trends are resolved through intermediate and late decay again with the temperatures becoming consistently lower with increasing water velocity through the fracture. The relative cooling curves are similar to those described earlier in this section in that the curves are all stable and more uniform with increasing water velocity. At the lowest velocity the transient peak extends later in time than the other two cases. The log slopes of the late time decays are all similar ranging in value from -0.781 (both Det 16 and Det 19) to -0.797 (Det 23) a range of 2% of the base case.

These simulations indicate that although the character of the thermal response is complex and varies considerably with the hydraulic gradient (water velocity) the representation of the response in terms of cooling varies in a comparatively consistent manner. The log rate of cooling in late time decay is similar (varying by less than 3%) regardless of velocity or whether the heater is side or down gradient. The log slope varies slightly more (by approximately 9%) when the heater is up gradient (at A), however the decay curves maintain a consistent increase in cooling and distinct separation as the velocity increases.

B7.2.8. Fracture Aperture

The remaining factor controlling the flow of water flow in Equation 5-3 is the fracture aperture (2b). Since the term is squared, variations in aperture should have considerable effect. In addition, although the hydraulic head in field situations will tend to change gradually over broad areas, the aperture could vary considerably over short distances. Since portions of the fracture are closed to support the overlying rock mass, while other parts of the fracture disproportionally facilitate flow, a situation which in some cases is accentuated by variable long term chemical dissolution or precipitation, fractures are generally described

as having an "effective" fracture aperture. The aperture observed at the borehole wall will depend on where chance has directed the drill to intersect a particular fracture and although the hydraulic gradient varies gradually the fracture aperture is a local condition.

To investigate this effect, the aperture in the base case with the heater up gradient (Det14D) of 2b=0.001m is increased 10 fold to 0.01m (Det35) and decreased by a factor of 10 to 0.0001m (Det36), (Figure B31). In the case of Det36 the temperature at background and at the fracture are the same. The water moving at a velocity $6.1x10^{-5}$ m/sec (5.29 m/day) based on Equation 5-3 is too low to create a measureable anomaly with the ALS technique. In the case of Det35 the resulting velocity is very high (0.6125 m/sec) and the effect is distinct. The general trend of greater cooling with increased velocity is consistent with section B7.2.7 and the log slope value is -0.779. As occurred in previous simulations, the water moving through the fracture has influenced temperatures 1.5m below during early recovery, but that effect does not extend into the periods of intermediate and late cooling. Of note is that the character of the early recovery, the size and duration of the transient peak, are very similar in both Det14D and Det35 with only a minor offset even though the water velocity in the later case is one hundred times higher implying relatively little change in character at high groundwater velocities.

B7.3. Summary

As temperature profiles are collected in the field, the thermal decay continuously progresses and consequently the times along the cooling curve at which measurements are taken change with depth. In many of the cases described, the temperatures observed at the fracture and 1.5m below were both sensitive to variation in a particular parameter during early and, in some cases intermediate, thermal decay resulting in complex patterns in the relative temperature. To simplify the comparison, the influence of the parameters is characterized based on the rate of recovery during late time thermal decay when all models predict consistent and simple changes in relative cooling. The effects of varying the different parameters on the log-log plot of relative cooling as a function of time from turnoff (t_c), are provided in Table B7as an assessment of relative impact on the results. The late-time decays are described in terms of the key parameters (slope, intercept, their ratio and R^2 fit) of the "best fit" line during late time recovery. In each case the parameter is compared against the appropriate base case (Det14d, unless otherwise noted) in terms of the percent change from the base. The R^2 fit values are all above 0.95 confirming that the late time decay data are well represented by straight lines in all cases. Figure B32compares the influence of the parameters on the late time relative decay as a histogram, sorted according to percent change in slope (blue), with the variation in intercept (red) alongside.

Although it is important to appreciate which parameters have the largest influence on the log rate of recovery, it is also critical to differentiate between parameters that are relatively uniform within a single borehole (e.g. background temperature) or those that tend to vary over a much broader scale such as geologic control (i.e. Krx) from those that are potentially variable at the scale of a fracture such as aperture. The largest change relative to background results from an increase in the borehole diameter. However diameter is generally a fairly constant parameter for a given borehole although washouts and large voids can occur. A suite of geophysical logging usually includes ATV data and/or a caliper log, both of which would detect a change in borehole diameter.

The amount of heat added will strongly influence the slope of the decay (not the intercept), but it is a controlled (or least readily measured) parameter. The third largest effect on the rate of log decay is the background temperature. Again, this parameter is also relatively constant at a particular location and is measured as part of the ALS process. If the heater is located at the side of the borehole or if the thermal conductivity of the rock decreases, the effect on the slope is within 5 to 10 percent of the base value. It is clear from Figure B32 that velocity, which is the critical system parameter controlled by hydraulic gradient and fracture aperture cannot be systematically characterized by either the rate or log rate of thermal recovery.

Table B7: Model Results Summary

	Parameters							Trend being Tested	Source @
	Slope	-% of Base	Inter	-% of Base	Int/Slp	% of Base	R2		
14	-0.820	17.0%	1.844	4.2%	-2.249	10.9%	0.959	Base Case (Low power)	A
14D	-0.701		1.769		-2.524		0.992	BASE CASE	A
17.2	-0.716	2.1%	1.572	-11.1%	-2.194	13.1%	0.992	Heat 3 hrs	A
17	-0.697	-0.6%	2.011	13.7%	-2.886	-14.3%	0.999	Heat 12 hrs	A
15	-0.750	7.0%	1.816	2.7%	-2.421	4.1%	0.996	Location of Heater Side Gradient	B
16	-0.781	11.4%	1.989	12.4%	-2.549	1.0%	0.996	Location of Heater Down Gradient	C
41	-0.56	-20.1%	0.651	-63.2%	-1.162	-54.0%	0.988	Inc BH dia	A-
22	-0.666	-5.0%	1.372	-22.4%	-2.062	-18.3%	0.997	Flow varies (dH = 0.5·b)	A
18	-0.725	3.4%	1.770	0.1%	-2.573	1.9%	0.997	Flow varies (dH = 2·b)	A
21	-0.739	1.5%*	1.558	-14.2%*	-2.108	12.9%*	0.996	Flow varies (dH = 0.5·b)	B
20	-0.760	1.3%*	1.980	9.0%*	-2.605	7.6%*	0.996	Flow varies (dH = 2·b)	B
23	-0.797	2.0%**	1.899	4.5%**	-2.381	6.6%**	0.996	Flow varies (dH = 0.5·b)	C
19	-0.781	0.0%**	2.097	5.4%**	-2.686	5.4%**	0.996	Flow varies (dH = 2·b)	C
24	-0.737	5.1%	1.791	1.2%	-2.430	3.7%	0.998	K_{rx} = 4.8	A
25	-0.633	-9.7%	1.611	-8.9%	-2.547	-0.9%	0.994	K_{rx} = 2.4	A
27	-0.798	13.8%	2.289	29.4%	-2.867	13.6%	0.999	Background T= 5C	A
28	-0.641	-8.6%	1.448	-18.1%	-2.261	-10.4%	0.983	Background T= 20C	A
35	-0.779	11.1%	2.422	36.9%	-3.108	23.1%	0.995	Incr. fracture aperture (10x)	A
36	Nil		Nil		Nil			Decr. fracture aperture (/10)	A

Det14D used as base except for: *Det15 used as base, ** Det16 used as base

Note: Since the slope represents a decay, the negative of the % change as plotted, i.e. an increase in the decay rate is a positive % change

Although other parameters influence the rate of cooling, the common characteristic amongst the simulations is that the late time temperature adjacent to the fracture is consistently less than that at the reference. We therefore look to the "relative cooling" and further explore its relationship to water velocity in the fracture. The relative cooling value and the accuracy of the analysis will depend on the ability to correctly characterize the other variables. Note, as observed when the head was varied (B7.2.5), the choice of the temperature at 1.5 m below the fracture as the "reference" raises several issues. Since the reference curves are shown to approach each other as recovery time increases, choosing an interpretive algorithm based later in time should improve the accuracy of the velocity estimate. This is unfortunately mitigated by decreasing temperature and consequently smaller relative cooling values with time.

Figure B33 shows a sub sampling of the relative cooling data from section B7.2.7 at three late recovery times 4.5, 5.0 and 5.25 days ($t_c = t_h$, $3t_h$ and $4t_h$ respectively) against the log of the water velocity with the heater at locations A, B and C. In all cases there is a linear relationship between Log(v_w) and the cooling. For all three heater locations the slopes of the lines steadily decline with time and the rate of cooling decreases considerably after the beginning of late recovery ($t_c = t_h$, 4.25d). The slope of cooling vs Log(v_w) is similar for all three heater locations for 5d and 5.25d with a shift in the lines depending on where the heater is located. The plots in Figure B33suggest a well predictable relationship can be established between the relative cooling and Log(v_w).

Two additional models were run: D37 to set a low velocity limit, and D38 which duplicated the previous high velocity with a different head-aperture combination (Figure B34). These additional points clearly do not fall on the linear relationships suggested by Figure B33. It is reasonable to speculate that the cooling is related to the amount of water (flow) moving past the borehole rather than simply the velocity. Further detailed analysis of the relationship between flow and the amount of cooling at late times is warranted but beyond the scope of this effort.

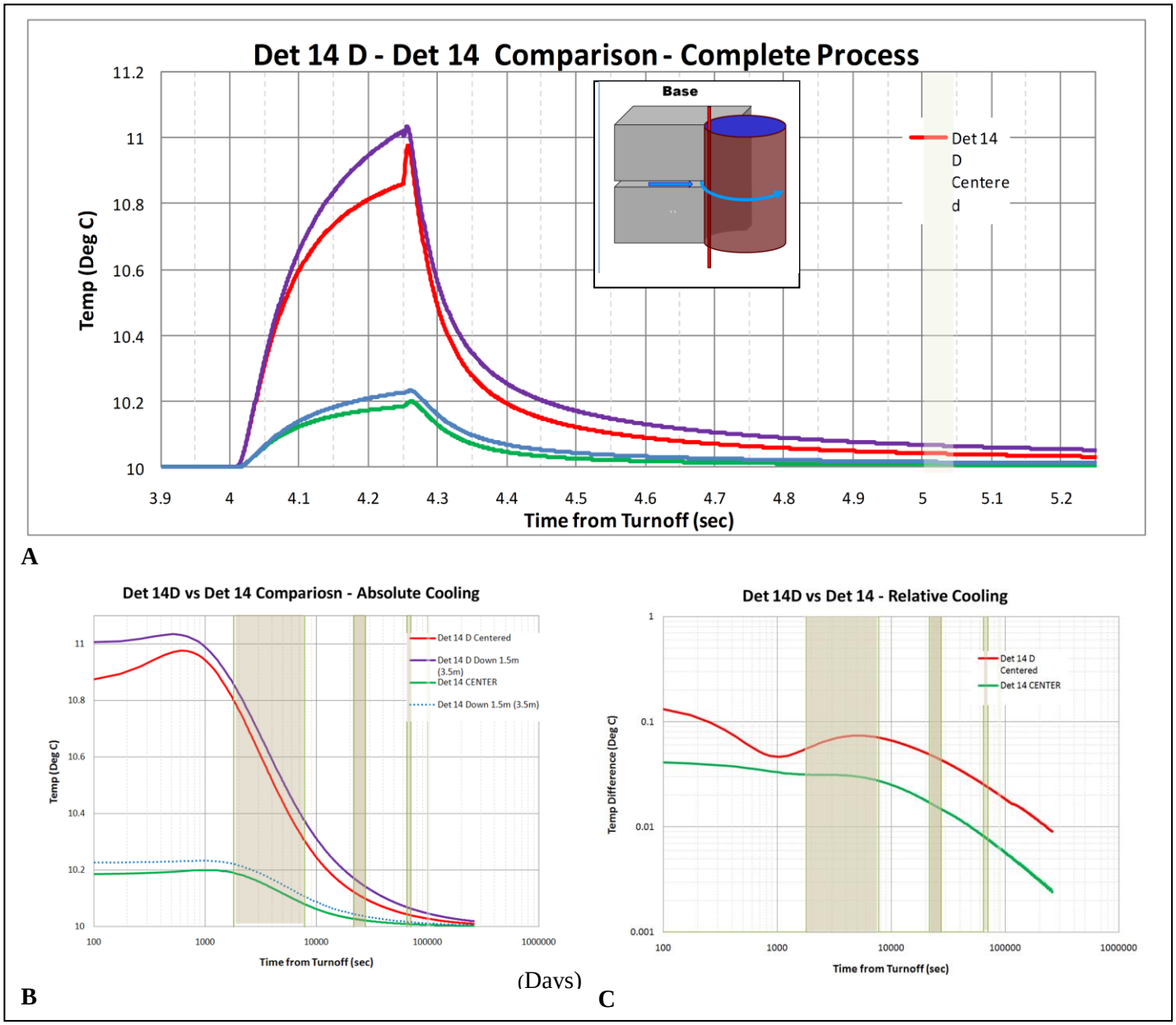

Figure B17: Effect of changing heat output, W/m.
A-The heating cycle (at fracture/background) for base case parameters 20W/m (red/purple) and 5.8 W/m (green/blue), **B-***Temperature in (A) plotted against log of time since turnoff* **C-***Relative cooling at fracture for high and low power outputs.*

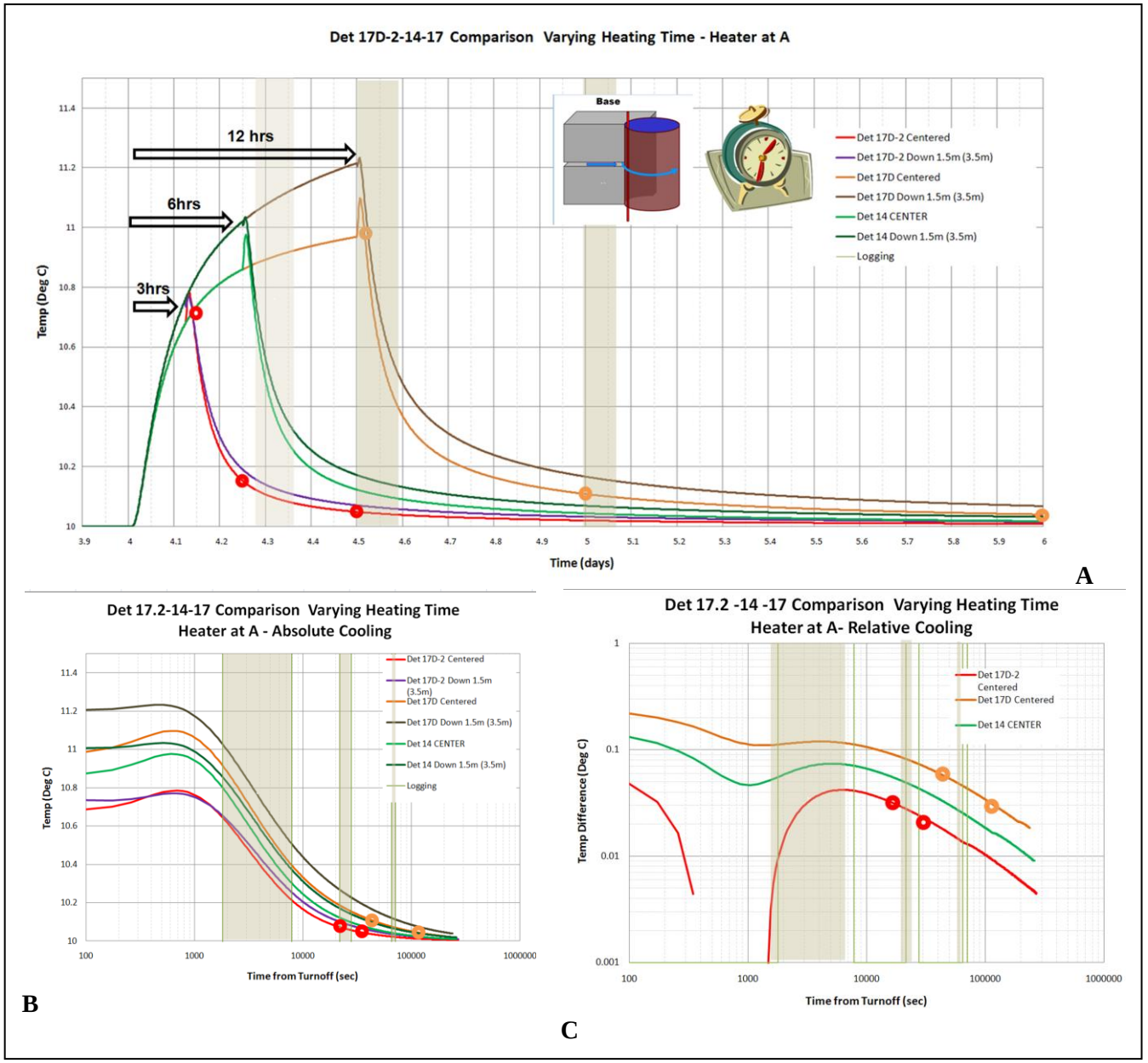

Figure B18: Effect of changing the duration of heating.
A-Complete heating cycle with heating for 0.125, 0.25(base) and 0.5 days, ***B-*** *Absolute Cooling* ***C-*** *Relative Cooling, Note: circles represent start of logging (heater at A, power output 20 W/m in all cases).*

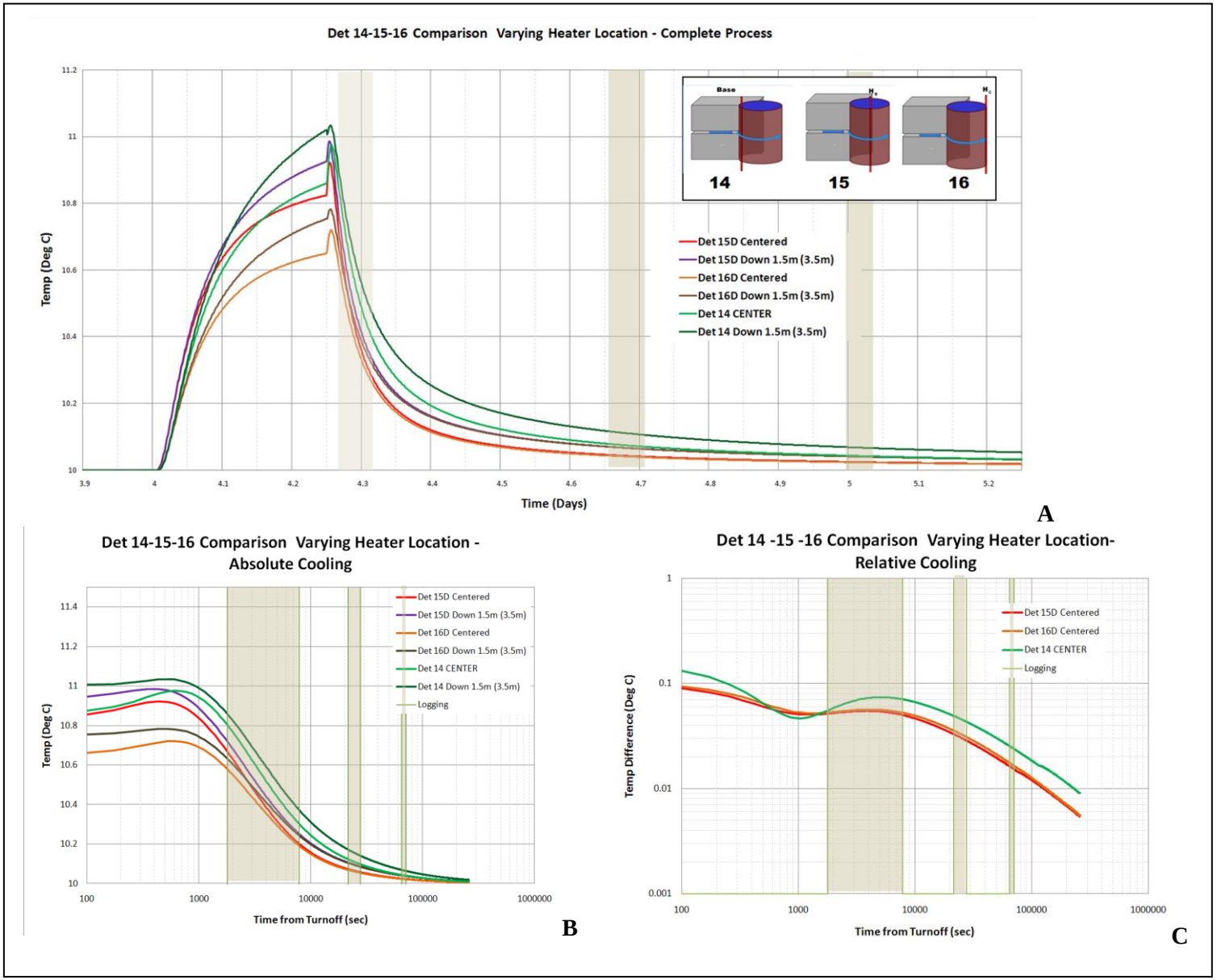

Figure B19: Effect of changing heater location. *A-Simulated temperature values at the center of the borehole, B- Temperature plotted as a function of log time since turn-off, C- Log relative temperature as function of log time since turn-off. Note plots are at fracture and 1.5m below for heater at A up-gradient (Det14-light and dark green), B side-gradient (Det15-red and purple) and C down-gradient (Det16-orange and brown).*

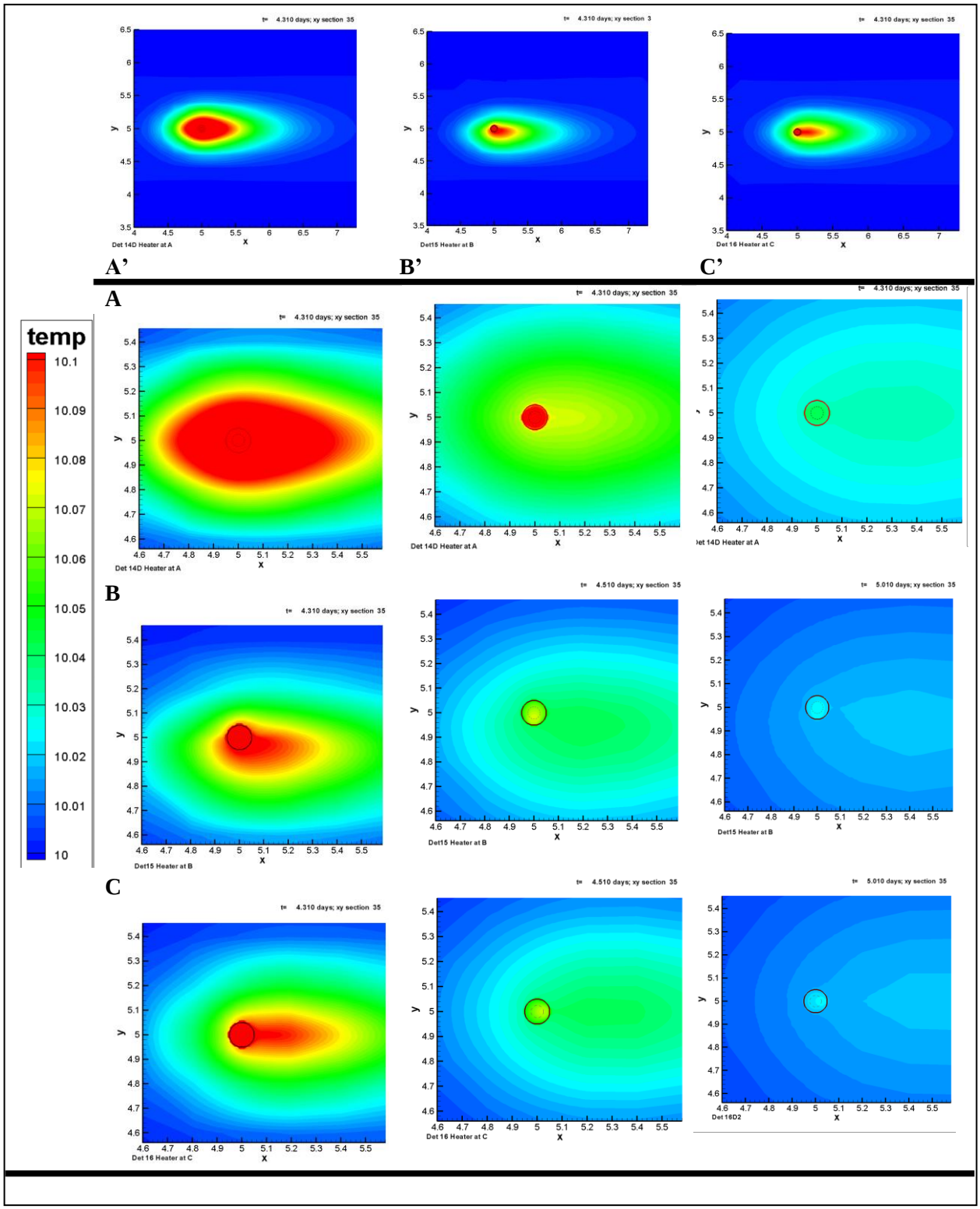

Figure B20: Plan view comparison (within fracture) with heater located A) up- gradient, B) side-gradient, and C) down-gradient within borehole.

The columns represent conditions at (from left – right) 5184 sec (day 4.31), 21600 sec (day 4.5) and 65664 sec (day 5.01), heating occurred from day 4-4.25. Day 4.31 with the heater at the 3 locations is also shown from a broader perspective in A',B' and C'.

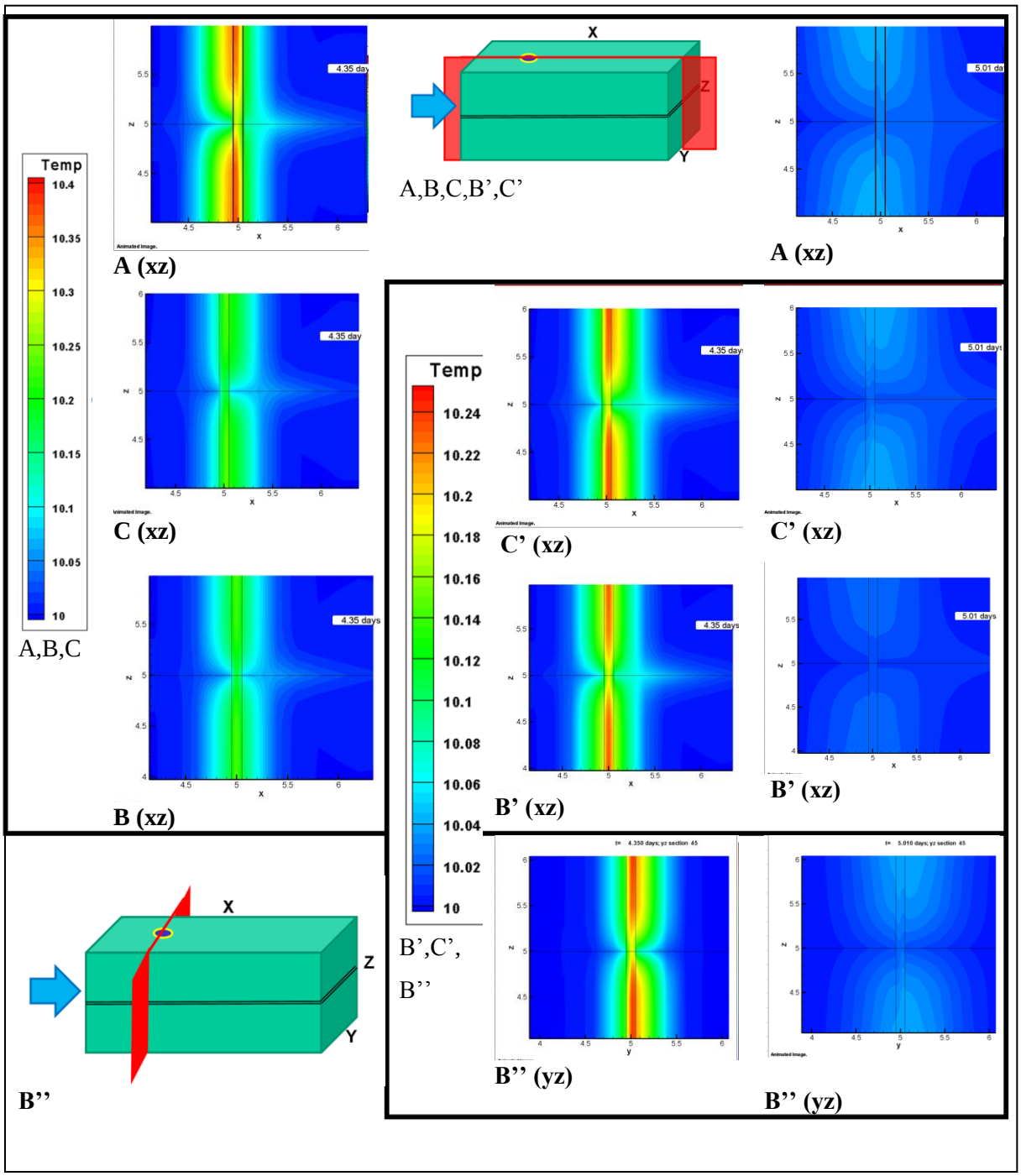

Figure B21: Vertical heat distribution view comparison with heater located A) up- gradient, B) side- gradient, and C) down-gradient within borehole.

The columns represent conditions at (from left – right) 5184 sec (day 4.31), and left most 65664 sec (day 5.01), heating extended from day 4-4.25. Two different colour scales are used, those marked prime are expanded to improve differentiation of temperature patterns, both xz and xy slices through the borehole are shown for the heater side flow (B).

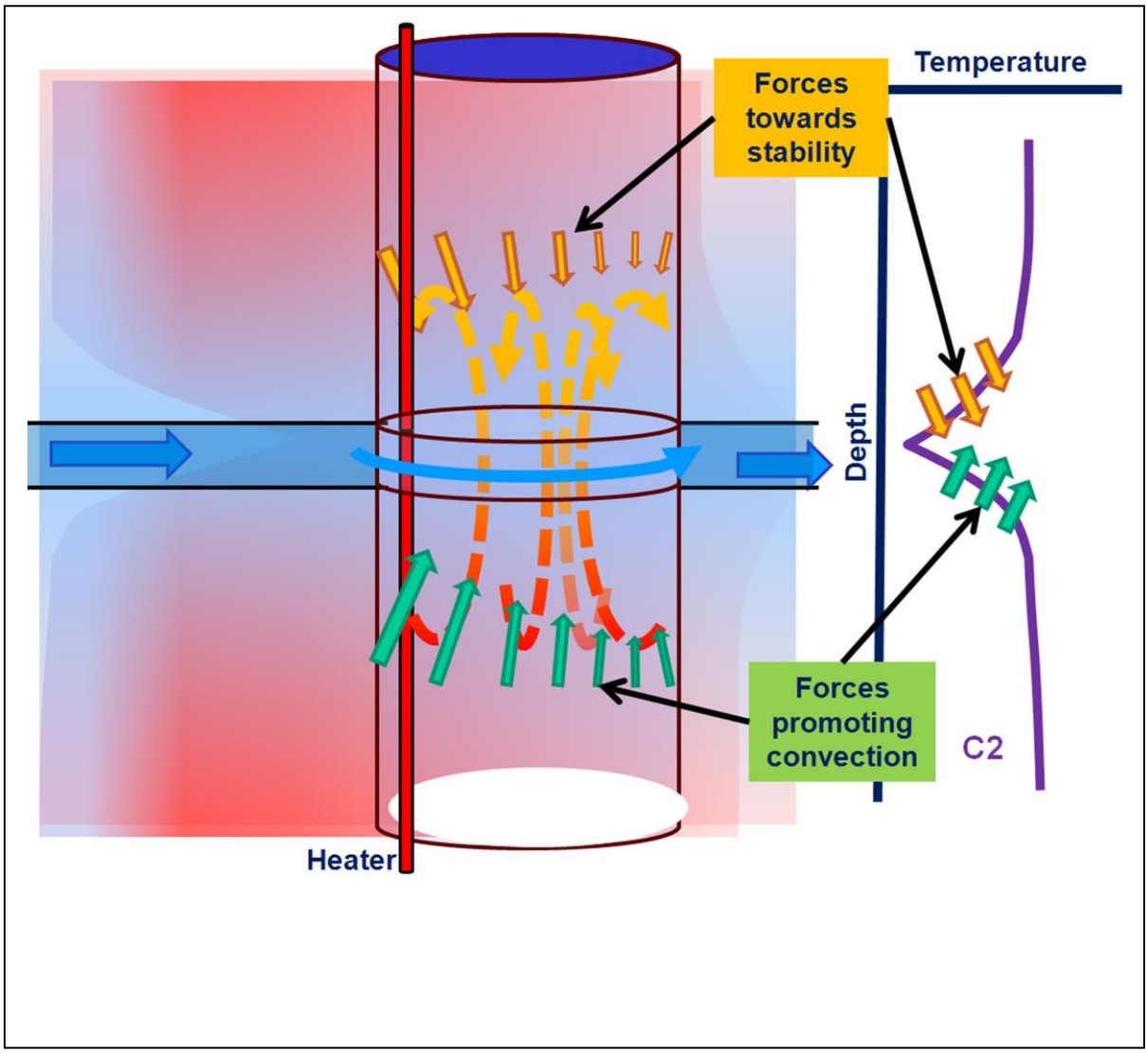

Figure B22: Schematic of a conceptual model for convection in the lined borehole at fracture during ALS thermal recovery.

The water in the borehole at the elevation to the fracture will be cooler than that above and below. Below the fracture, the condition of cool over warm water will promote convection and above the fracture warm over cooler water will tend to stabilize the environment. Friction (not considered by smoker) would tend to impede flow along the borehole wall and therefore the convection cell should rise in the center of the hole and move downwards at the sides. HOWEVER both the thermal gradients and consequently convection patterns will depend on the location of the heater relative to flow as well as the amount of flow and other characteristics of the system and therefore this conceptual model is an oversimplification of the situation.

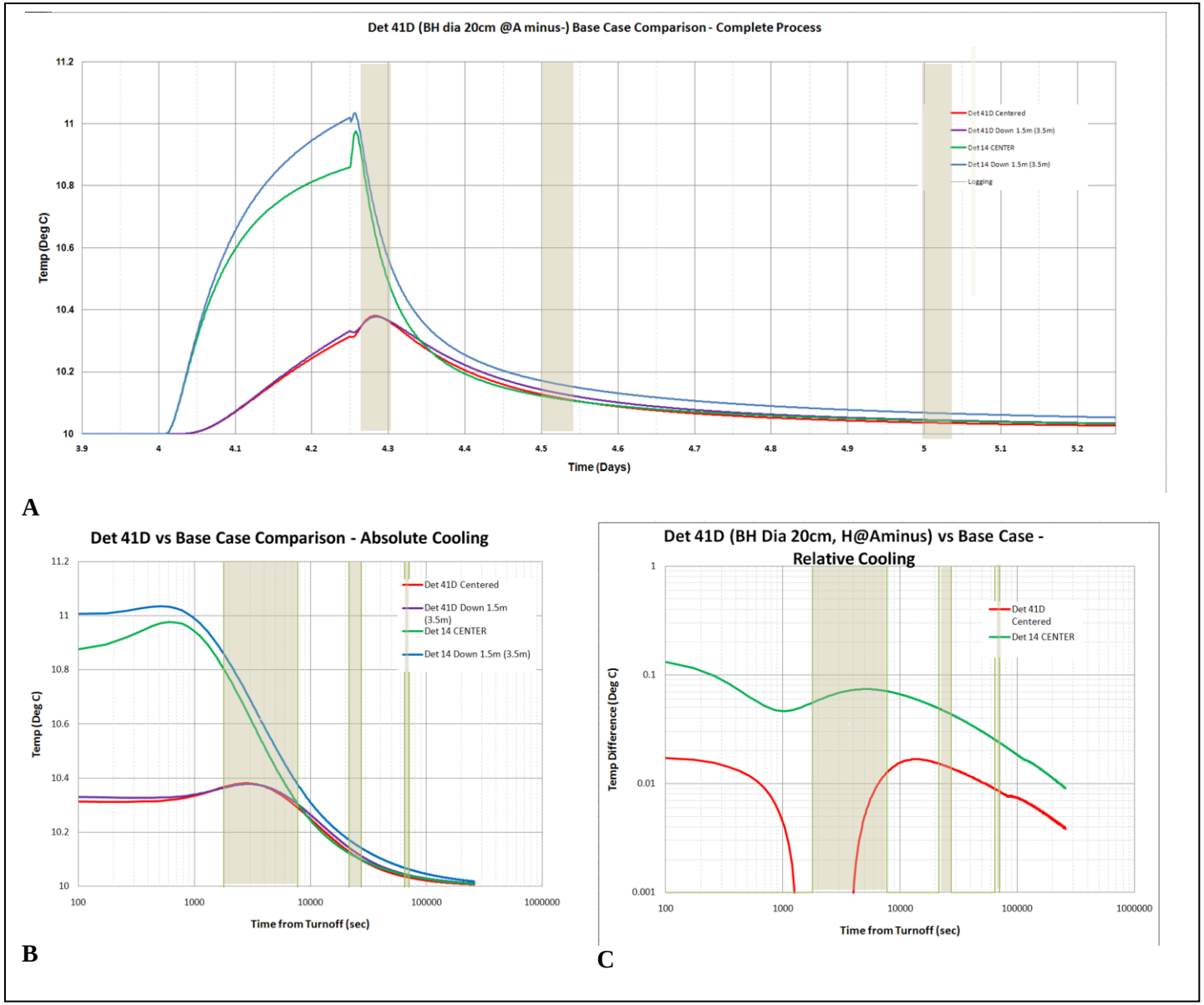

Figure B23: Effect of Borehole Diameter. ***A-****modeled temperature values at the center of the borehole,* ***B-****Temperature plotted as a function of the log of the time since turn-off,* ***C-****Log relative temperature as function of log time since turn-off. Note: Det41D borehole diameter 20cm.*

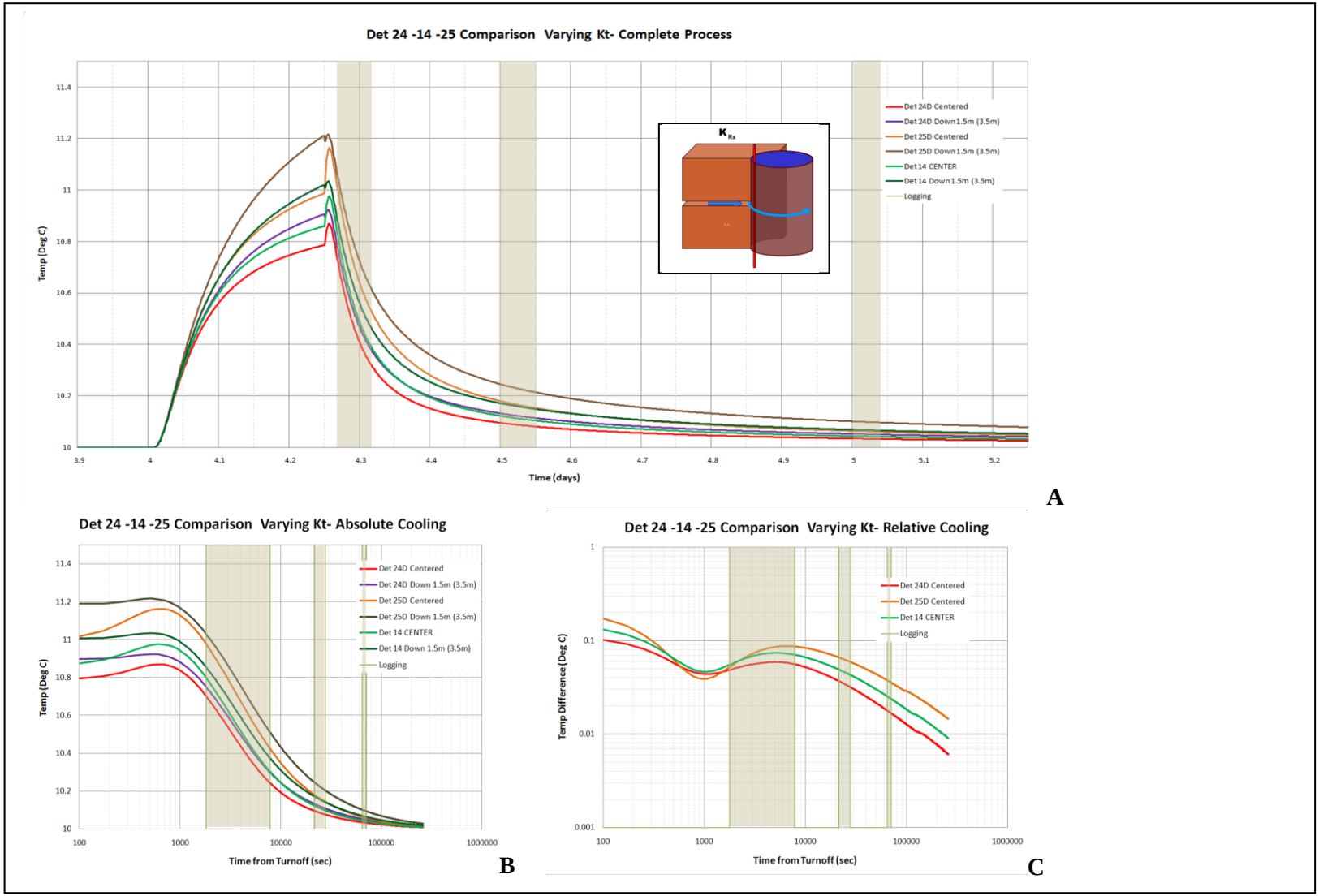

Figure B24: Effect of varying rock thermal conductivity.

A-modeled temperature values at the center of the borehole, B- Temperature plotted as a function of the log of the time since turn-off, C- Log relative temperature as function of log time since turn-off. Note: Det 24 - krx=4.8 W/K m, Det 14 - krx=3.6 W/K m and Det25 - krx=2.4 W/K m.

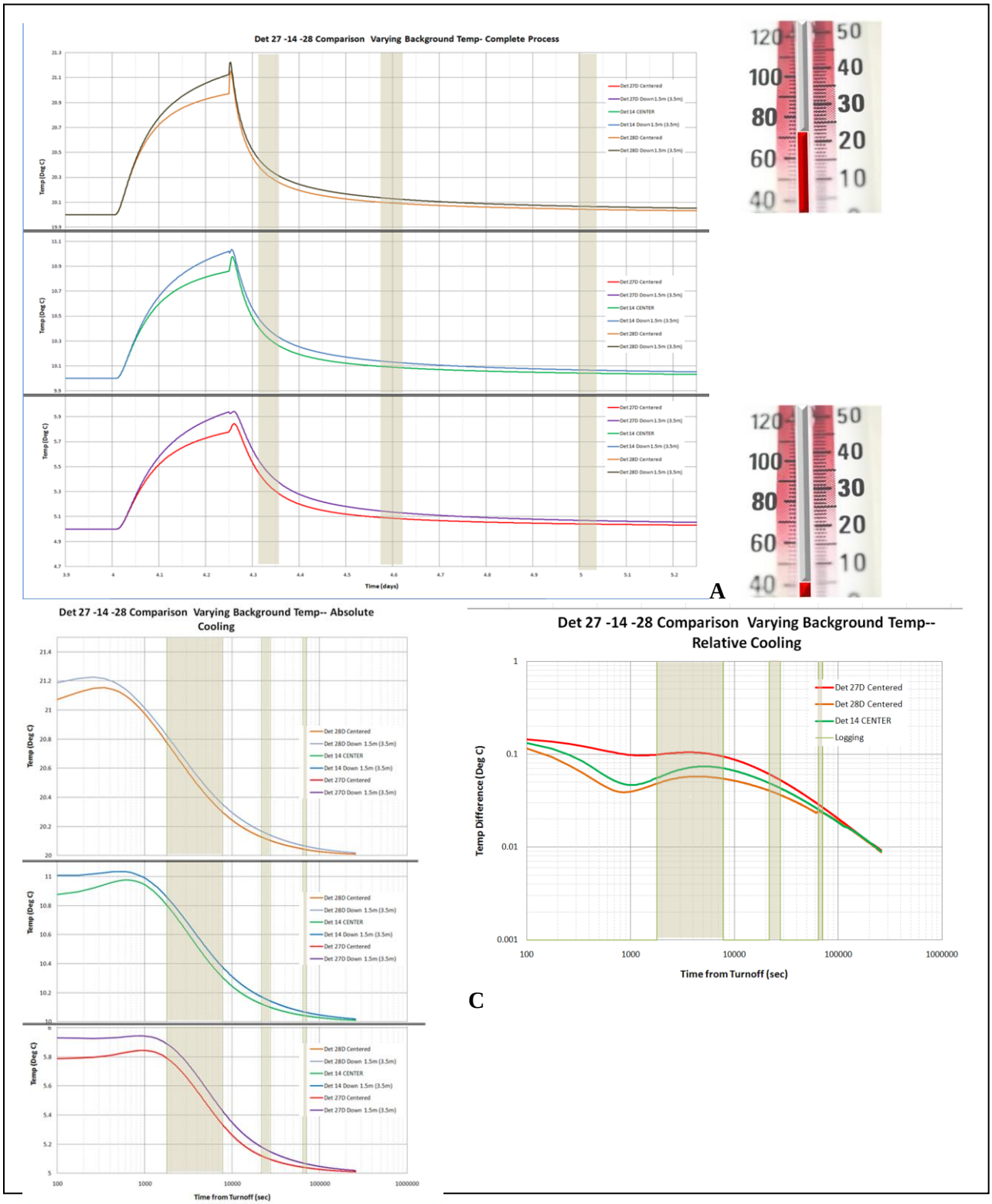

Figure B25: Effect of Changing Background Temperature.

A-modeled temperature values at the center of the borehole, B- Temperature plotted as a function of the log of the time since turn-off, C-Log relative temperature as function of log time since turn-off. Note: vertical scales in A and B include gaps, Background temperatures Det 27=5 ℃, Det 14=10 ℃ and Det 28=20 ℃.

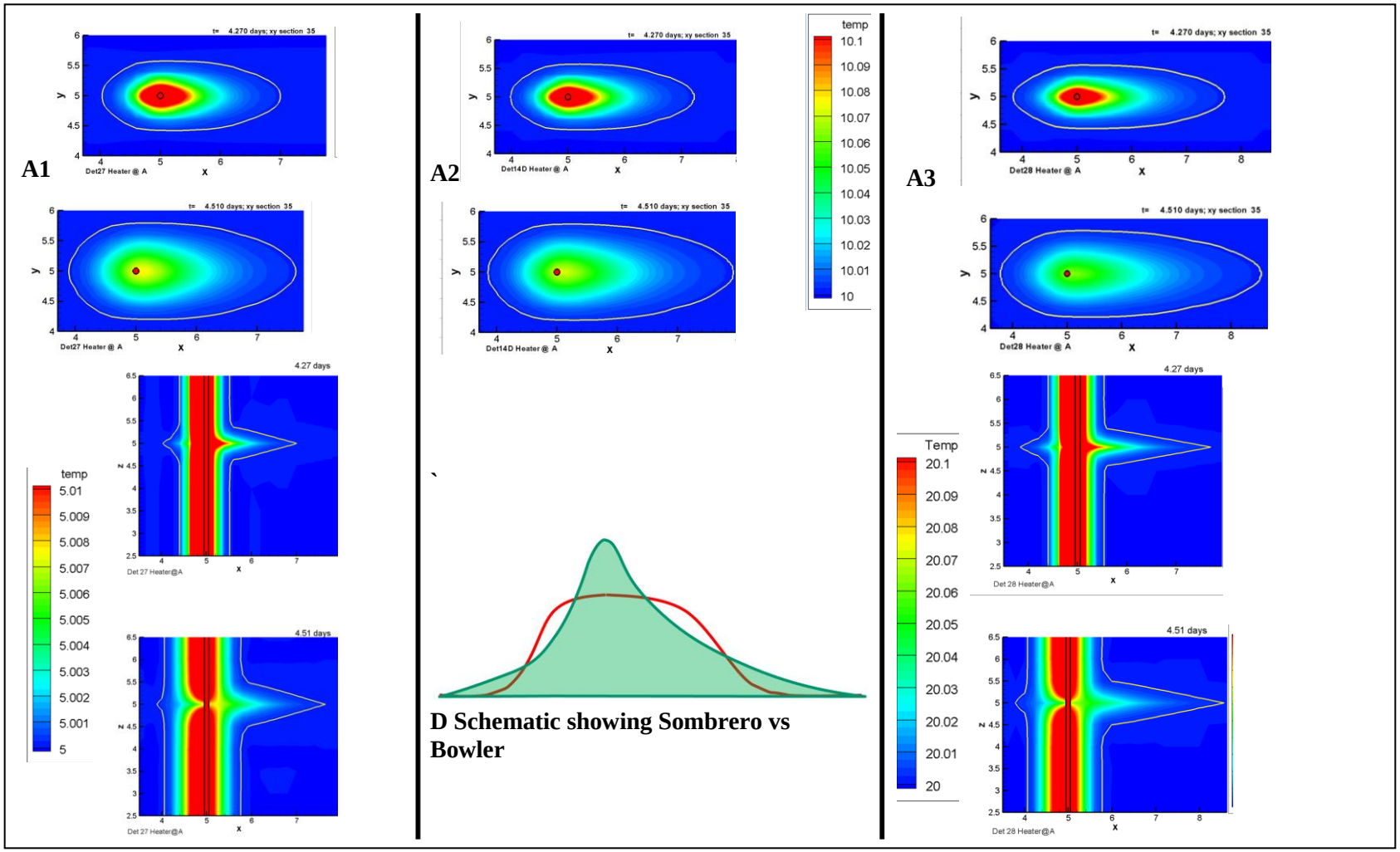

Figure B26: Breadth of the heat energy as background temperature increases.

At 4.27 and 4.51 days A1-Det27(5℃ base), A2-Det14(10℃ base) and A3-Det28(20℃ base). Note although the temperature scale of each group of images is different, the range is consistent. The yellow contour is 0.002C° above ambient temperature in each case (i.e. A-5.002℃, B-10.002℃ and C-20.002℃). These tend to be early time phenomena with minimal impact in late time. Conceptually A can be thought of as a "bowler" (red schematic) while C is a "sombrero", the green pattern.

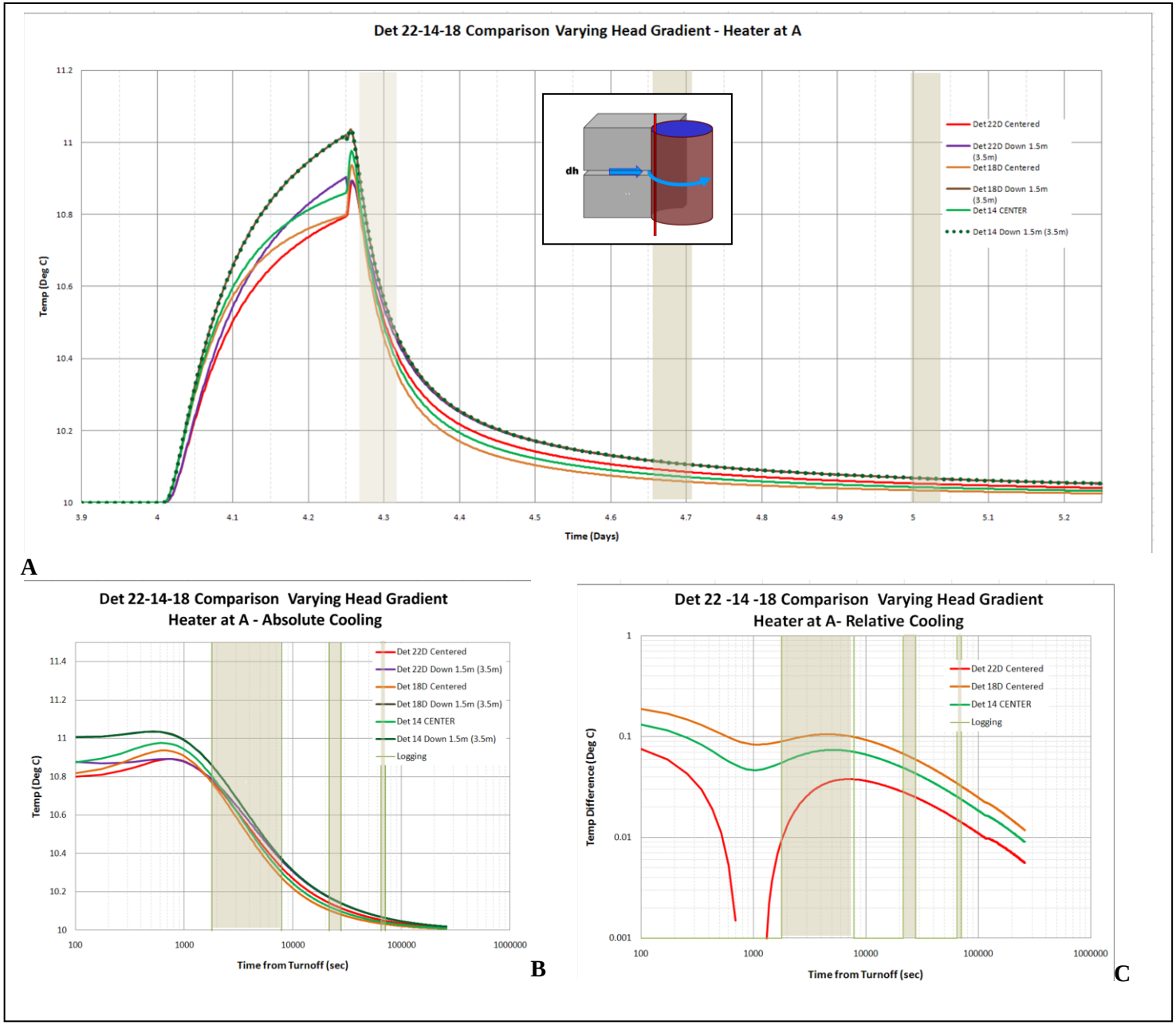

Figure B27: Effect of Changing Hydraulic Head Gradient (Water Velocity) with Heater at A. *Det22 dH = 0.075, Det14 dH=0.15 and Det18=0.30 Reference temperatures in Det18 and Det14 are overlie, Det 22 is lower. Representations A, B & C as previously.*

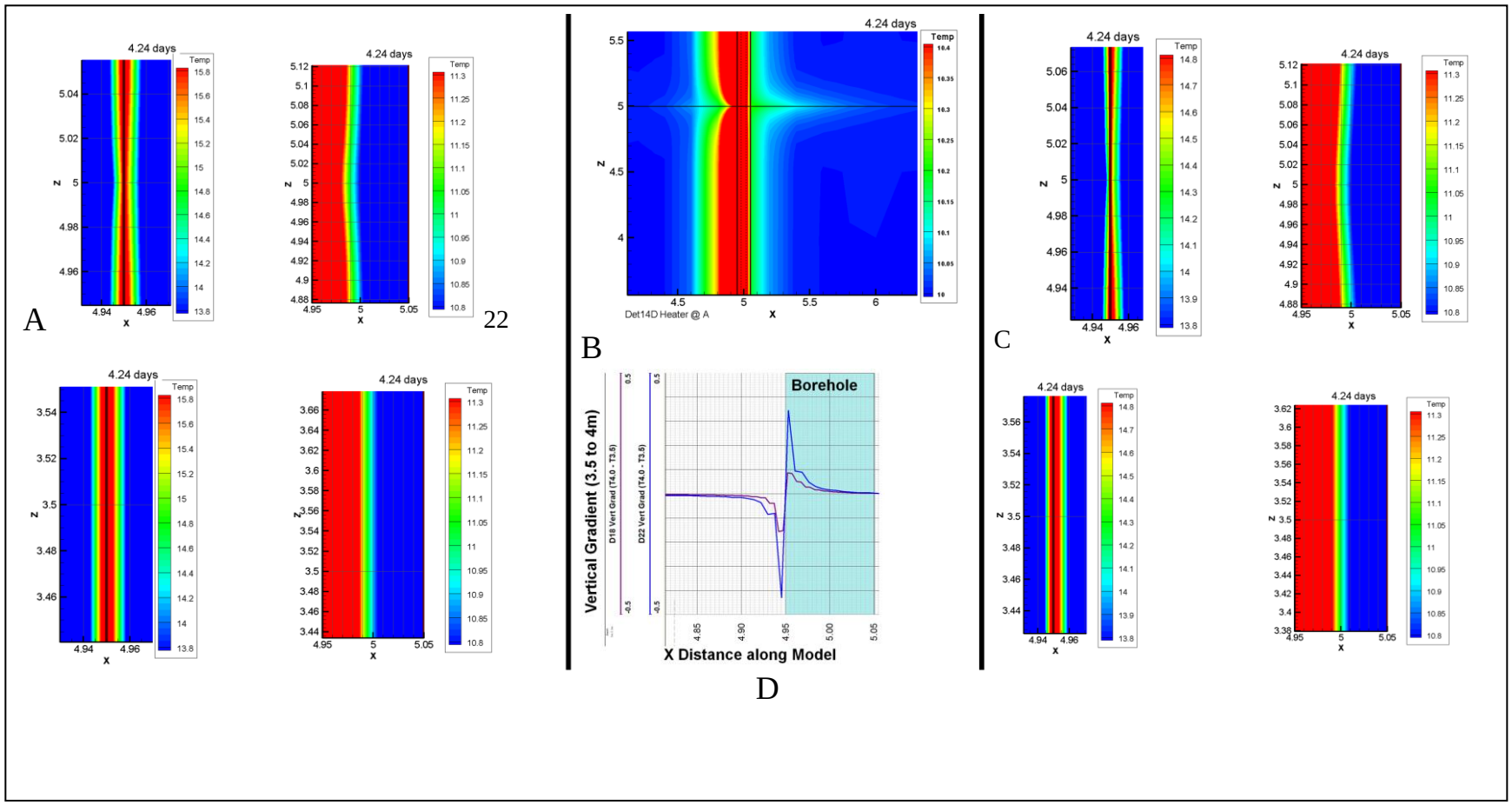

Figure B28: Influence of hydraulic gradient on temperature changes at reference.
At 4.24 days A-Det22, B-Det14 and C-Det18. Detailed temperature patterns are shown along the edge of the liner and across the borehole both at the fracture and the reference depth (3.5m). Although a vertical gradient is not apparent in the colour plot, the line plot (D) of the vertical gradient calculated between 3.5m and 4m elevations through the center of the borehole indicates a gradient does exist , reverses polarity at the line and decreases with increasing hydraulic gradient in the fracture.

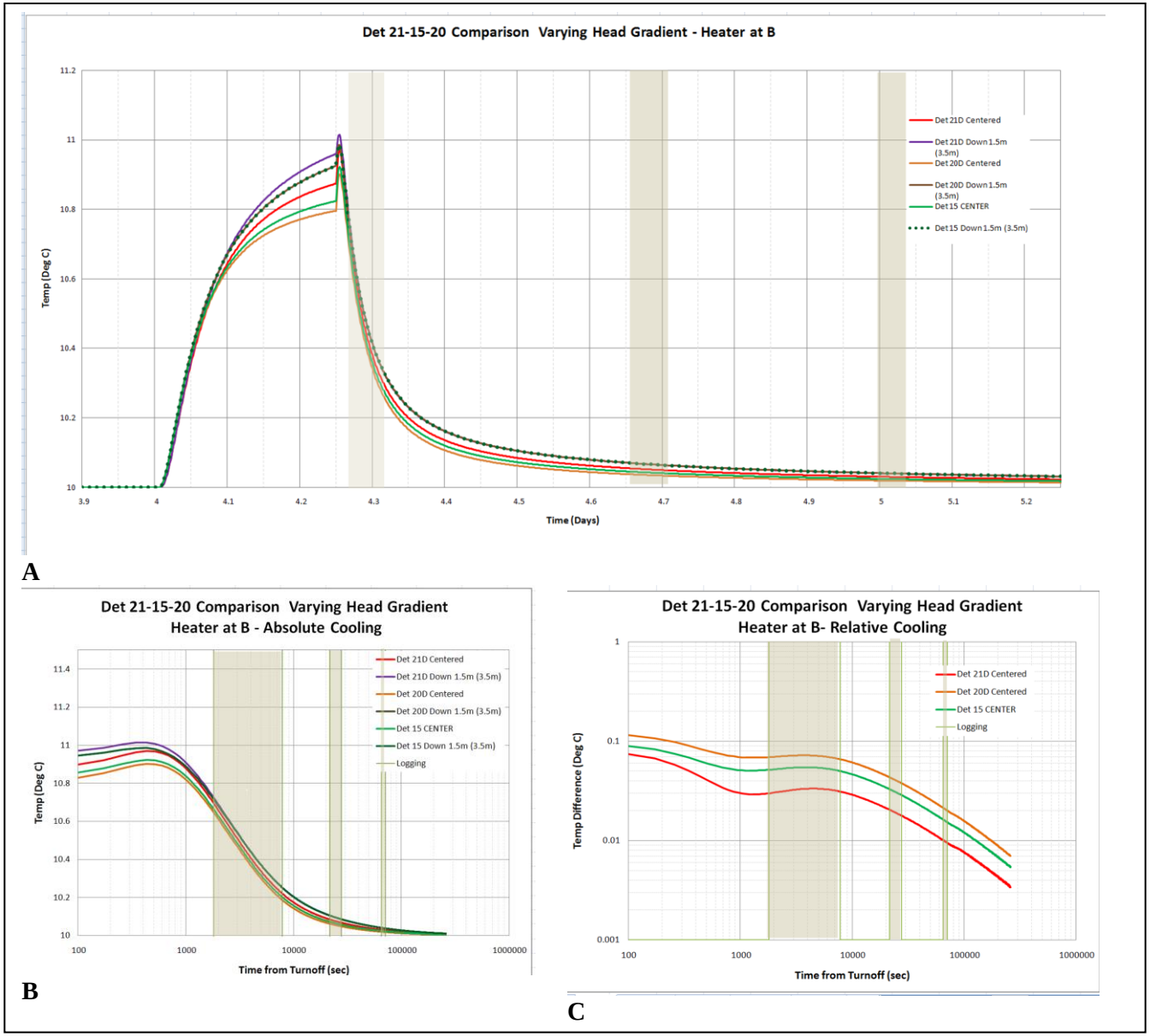

Figure B29: Effect of Changing Hydraulic Head Gradient (Water Velocity) Heater at B.

Representations A,B & C as previously. Det 21-dH = 0.075, Det 15 dH=0.15 and Det 20=0.30

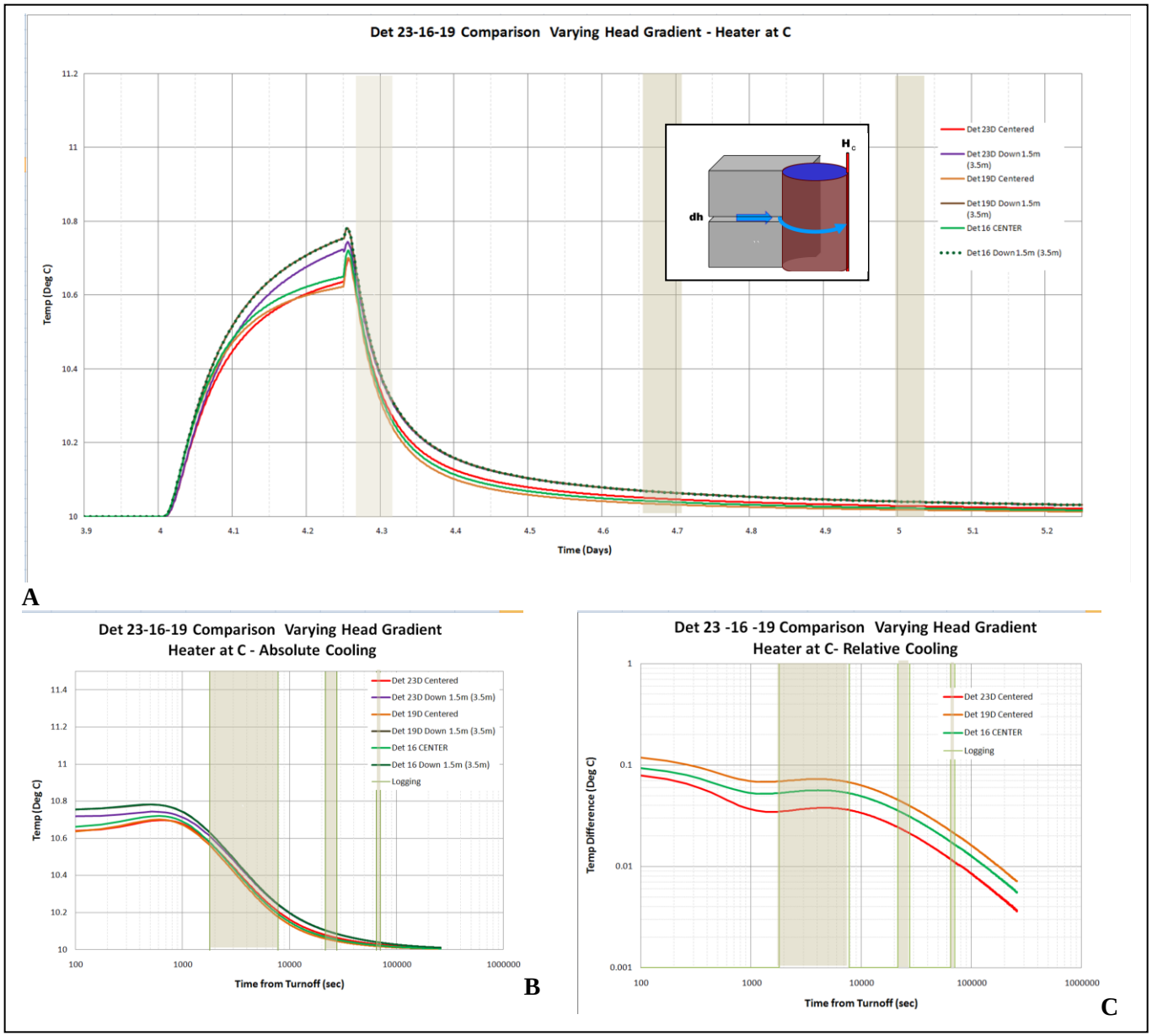

Figure B30: Effect of Changing Hydraulic Head Gradient (Water Velocity) Heater at C.
Representations A,B & C as previously. Det 23, dH = 0.075, Det16 dH=0.15 and Det19 DH=0.

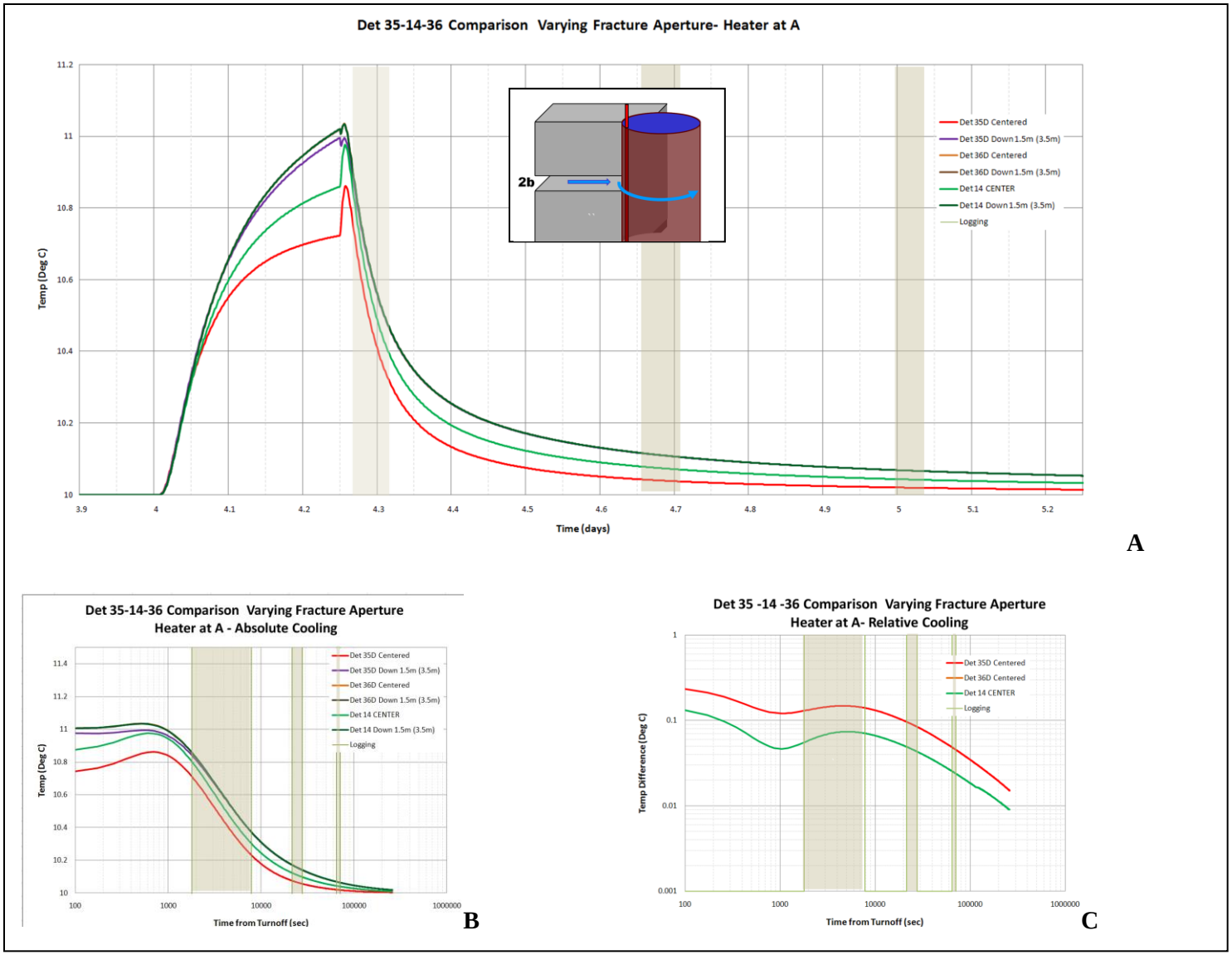

Figure B31: Effect of Changing Fracture Aperture Heater at A.

Representations A,B & C as previously. Note: 36 and 14 are almost the same. **9**

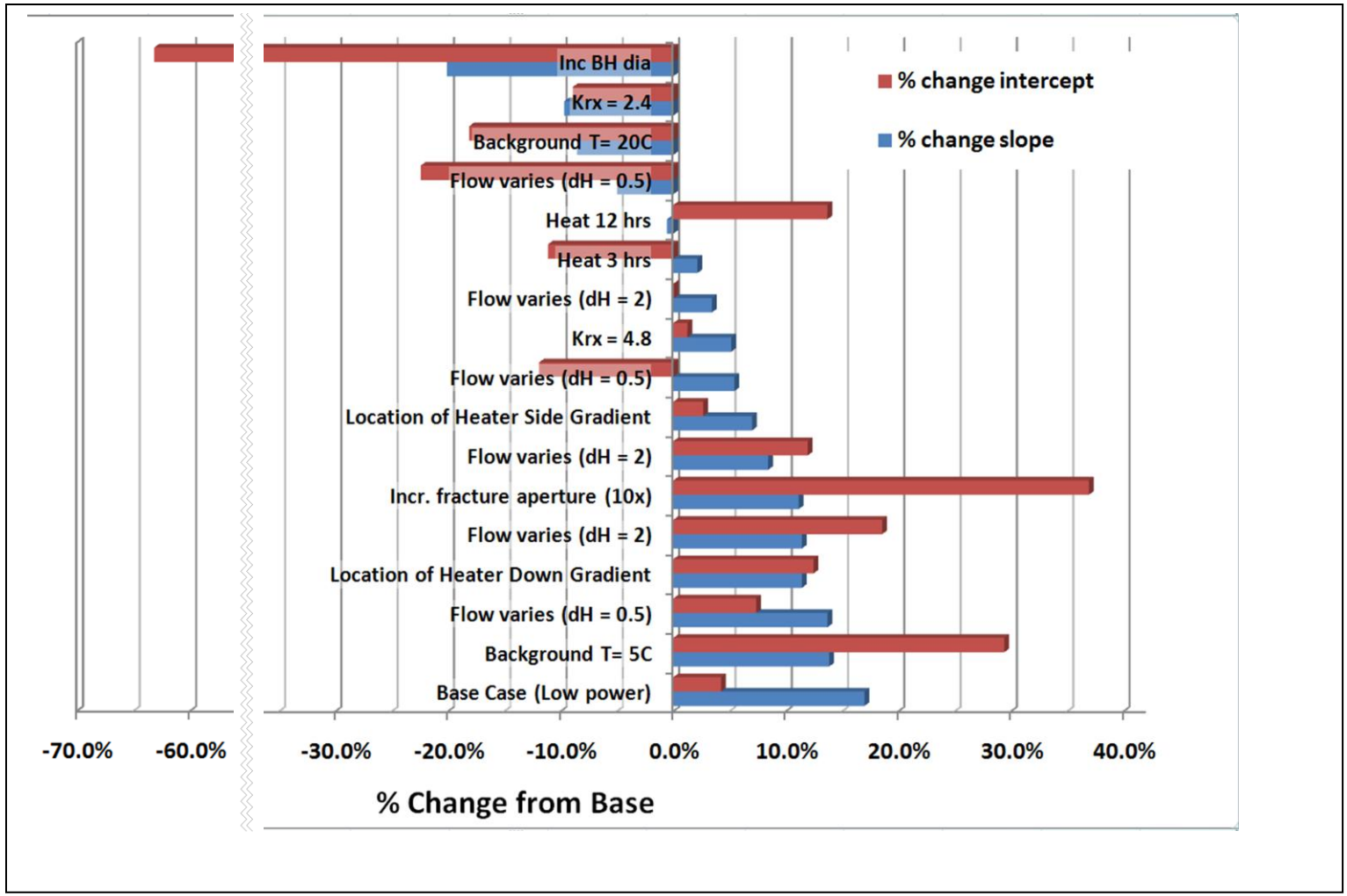

Figure B32: Influence of parameters on best fit line as a percent of base model.

Note: Since the slope represents thermal decay, the negative % change is plotted, ie an increase in the decay rate is a positive % change

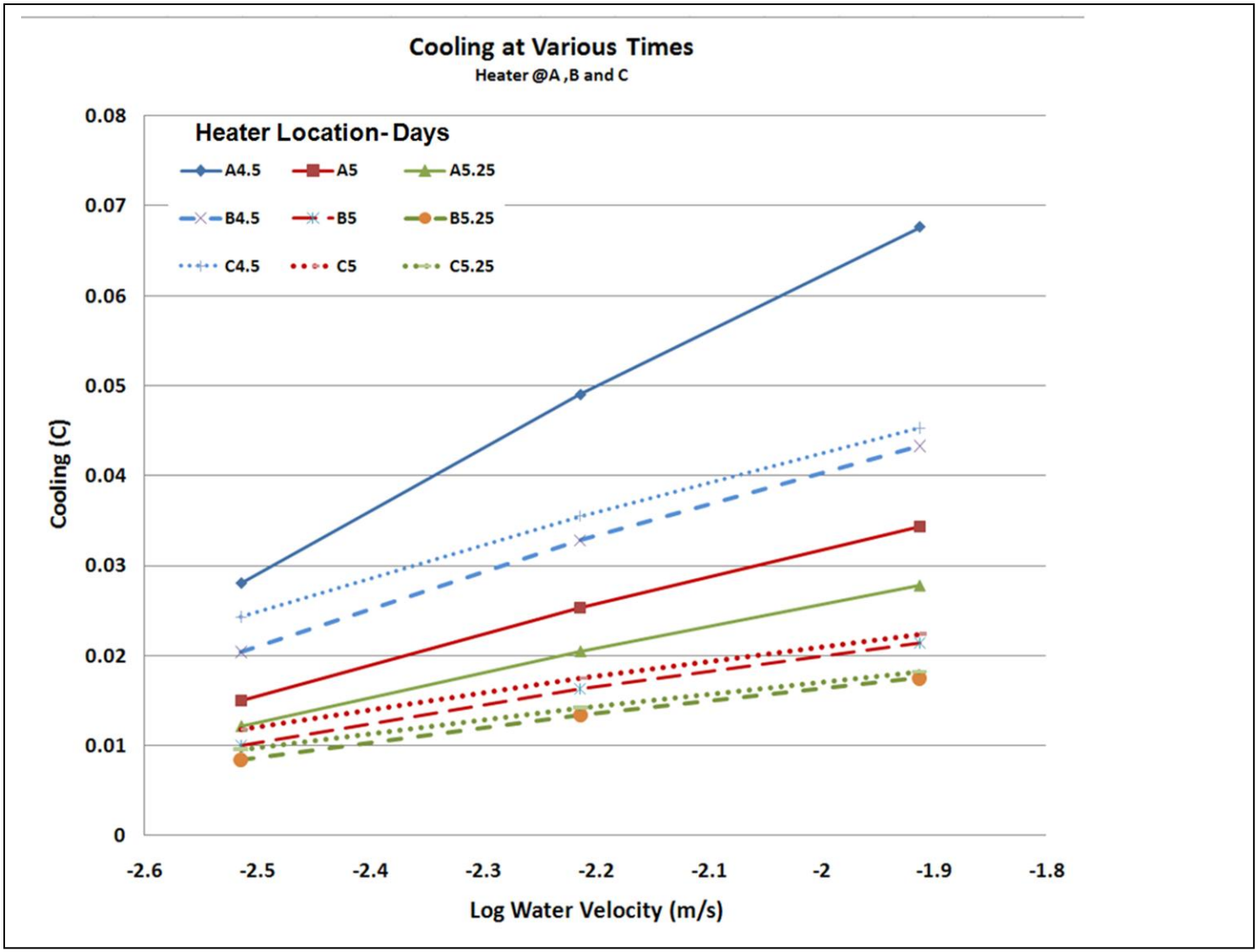

Figure B33: Superimposed Cooling at various times against velocity.

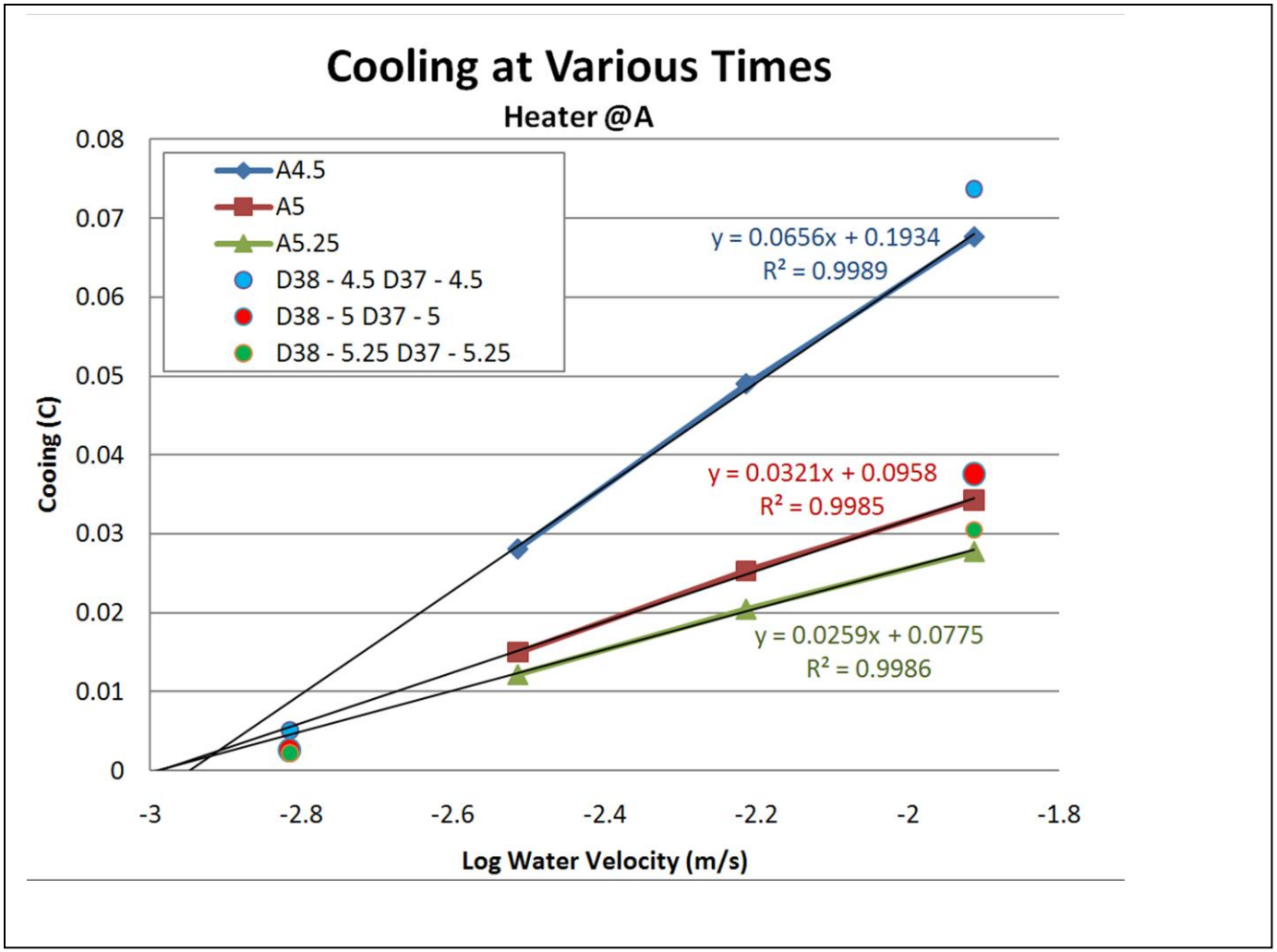

Figure B34: Cooling at various times against velocity with duplicate velocity points except with different aperture.

B8. Summary and Conclusions

The ALS technique, in various forms, has been used to identify flow through fractured sedimentary rock since the mid 1990s. Although a robust tool for the identification of many flow features, the nuances of the associated thermal decay are still poorly understood and the confidence limits are not yet established. A major step in the process of refining the ALS technique is to move beyond basic identification of the existence of flow to a qualitative comparison and ultimately to a quantitative estimate of the amount of water moving through the fractures. A precursor to that refinement is a better appreciation of the details of the heating process and subsequent thermal recovery as temperatures return to ambient levels; in particular understanding how the various parameters of the system impact the temperature logs and the subsequent interpretation of the results.

In this report, individual parameters of the simple single fracture model have been systematically varied; the results as described in Section 4 are summarized in Table B7 and inFigure B32. The predicted thermal variation is assessed both from the temperature in the center of the borehole at the fracture intersection and as an effective “relative cooling”, the difference between the measurement at the fracture and that at a reference point in the borehole adjacent to the unfractured matrix (1.5m below the fracture).

The conclusions derived from this sensitivity study are grouped according to the affect of the parameters on the thermal processes, and the implications for field applications. The key conclusions regarding the heating and thermal recovery process are:

1. Although basic plots of temperature against time are important from the perspective of understanding the data and providing appropriate quality control, the log-log plots of relative cooling provide the most insight into the process.
2. The ALS process can be effectively and consistently divided into four stages: heating, early, intermediate, and late cooling. Although all four provide insights into the processes, the thermal behaviour of the system is most consistent during late cooling.
3. Increasing the power output not only increases the energy introduced into the system (the temperature measured above background), but also accentuates the effect of the water moving through the fracture (relative cooling). However, the late time log-log rate of declining relative cooling is independent of power input.
4. Increasing the duration of heating reduces the variability in early cooling, improving the usefulness of that data.
5. The effect of the water moving through the fracture (relative cooling) increases with the duration of heating, but the log-log rate of decline is uninfluenced by the additional energy.

6. The time allocated to heating controls the maximum temperature and duration of the thermal decay. Inadequate separation (temperature change between logging runs) can become a problem for estimating thermal conductivity and other "thermal decay dependent" parameters if the duration of heating is too short.
7. Although different temperatures are measured when the heater is transverse or down-gradient, the relative cooling is essentially the same and both show a slightly lower response to water movement than when the heater is up-gradient. The log-log rate of decline in relative cooling is independent of the heater location.
8. The energy introduced during heating is stored in the rock adjacent to the borehole and is subsequently released, influencing the measured temperature as the water flow in the fracture transports the heat energy around the liner. Consequently the temperature at the center of the borehole can continue to temporarily increase after the heater is turned off. This effect is most pronounced when the heater is on the up-gradient side of the borehole, optimizing the geometry for the maximum flow of heat energy towards the temperature sensor.
9. When the heater is up-gradient, the relatively low thermal conductivity of the water compared to the rock, accentuated by the water movement, causes the energy to be conducted radially inward towards the center of the borehole from all sides, lowering the horizontal thermal gradient. In contrast when the heater is down or side gradient the energy in the rock moves away from the borehole and the horizontal gradient is higher and consistently towards the heater location.
10. The model indicates that convection may be occurring in the borehole in the vicinity of the fracture. However it also appears that the stratification of hot over cool water above the fracture is a stabilizing influence restricting the upward limit of the convection cell.
11. For a given amount of heating, increasing the borehole diameter decreases both the maximum temperature and the effect of the flow in the fracture (relative cooling). It is reasonable to hypothesise that the water between the temperature sensor and the borehole wall, fracture and heater has a dampening influence, muting the response and the resolution of flow. The muting effect delays responses and thereby extends the early time response later into the cooling cycle.
12. The ALS process is sensitive to the thermal conductivity of the rock. The early time response becomes more variable with decreasing rock thermal conductivity thereby complicating that portion of the curve, the relative cooling values increase and the log rate of decline decreases. Any quantitative analysis will require a reasonable estimate of the thermal conductivity of the rock mass. The value of 3.6 W/m·K used in the base case is towards the higher end of the range for sedimentary rock (Molson and Frind, 2006) and therefore the conclusions drawn from these analyses will tend to be conservative.

13. The model testing (section 3.3.3) suggests the application of the Shen and Beck (1986) analytic solution adopted by Pehme et al (2007a) is limited because the simplifying assumptions may not be met in practise and that the thermal conductivities derived are likely a better relative comparison than an absolute estimate.
14. The background temperature influences the temperature increase and relative cooling at early, intermediate and beginning of late times. However, as late time continues, the effect of the background temperature decreases and there is no appreciable difference in the relative cooling between background temperatures ranging from 5°C to 20°C. Whether background temperature is an important factor in an ultimate quantitative analysis will depend on the basis of the approach adopted, i.e. which portions of the thermal decay curve are used and how it is used. If the early portion of late time recovery is used, background temperature will be a factor, but can be accounted for as it is measured in the passive log of the ALS process.
15. In early time the observed "reference" temperature (1.5m below the fracture) is influenced by the presence of the flowing fracture as a result of secondary vertical migration of heat through the rock. There is no indication of a vertical thermal gradient in the borehole. Although the effect varies with flow, above a flow threshold the influence is constant. The amount of influence is larger when the heater is up-gradient, decreasing when the heater is transverse and down-gradient, reversing in the side flow case (i.e. background with a low velocity is warmer than medium and high velocity condition). In all cases this phenomenon disappears by the start of intermediate time and the background values are consistent (although at a different temperature depending on the heater location). The late time decay of reference temperatures is independent of flow.
16. When the borehole, flow and heater are symmetrically aligned relative to the X-Z plane, the temperature during heating and in early recovery time does not consistently vary with the water velocity (flow). The highest temperatures are observed at an intermediate water velocity when the balance the water flow moving energy towards the borehole from the up-gradient side and the heat transport by down-gradient advection is maximized. However, through intermediate and late time relative cooling, the decay consistently decreases with increasing water velocity in the fracture, independent of the geometry of the components, implying that the characteristics of the late decay are the most useful for estimating flow.
17. The observed temperature is directly related to the energy introduced and inversely a function of the dissipation of that energy, primarily depending on the thermal conductivity of the rock and the amount of water moving through the fracture. Within the range of parameters modelled herein, the relative cooling provides a simplified presentation of the complex relationship such that the amount of cooling is in some manner a function of the flow.

18. Based on the tabulated and graphical comparison of the influence of the various model parameters on the characteristics of the log-log decline of relative cooling, it is apparent that background temperature, borehole diameter, rock thermal conductivity and location of the heater can all have as much or more influence on the log-log *rate of decline* in relative cooling than does the velocity of water moving in the fracture. Quantitative analysis of water movement will not be resolved as a simple function of the rate of decay on either a log-linear or log-log scale because too many variables exist that could influence the response.
19. The fracture is always cooler than the matrix after heating and exploring the amount of relative cooling as a function of flow is the most promising method for the quantifying the amount of water movement. However, relative cooling is complicated by the location of the heater relative to flow, a situation that must be resolved by determining which side of the borehole the heater is on and the flow direction.
20. Although there appears to be a linear relationship between the relative cooling and the log of the water velocity, when the velocity is changed by varying the fracture aperture, the data no longer fits that relationship indicating that *total flux (m^3/s) rather velocity is likely the quantifiable parameter*.
21. All of the variables with the exception of the relative location of the heater and the amount of flow, can be determined with other technologies or estimated from the ALS process directly, suggesting that if the location of the heater can be determined, flux would remain the only variable.

These conclusions have practical impacts on field work and interpretation, specifically:

1. Every practical effort should be made to increase the amount of energy transferred to the formation. This can be achieved by either maximizing power output per metre or by increasing the time spent heating. If the duration of heating is increased, the logging intervals must be appropriately adjusted and in some cases the possible cost implications associated with that choice must be considered.
2. The early-time response can be highly variable depending on geometry etc. Although these data are useful and should be collected if possible, interpretation should consider potential variability. The stability (and usefulness) of the early time data increases with longer heating but is negatively impacted by increased power.
3. The current methodology of 5-6 hrs of heating is adequate in the situations considered but shortening the heating time would negatively impact resolution.
4. Early-time anomalies will appear much larger when the heater is up-gradient accentuating the negative implications on using early time data for comparative interpretations.

5. The borehole diameter should be as small as possible. However there are practical limitations to the minimum size possible both for temperature logging and other types of testing.
6. Borehole diameter is an important consideration and should be measured. Expect a dampened response as the diameter increases. Any quantitative analysis will require consideration of the diameter.
7. There is potential for resolving the flow direction if the location of the heater in the borehole can be determined. Resolution of thermal gradients holds promise for that purpose.
8. Use of multiple data runs for determining flow requires highly accurate vertical alignment of the profiles. An approach based on a single run would therefore be preferable or improvements to standard practices of depth alignment will be required.

B8.1. Potential Future Work

This modelling exercise has provided many insights into the heating and subsequent recovery associated with the ALS technique. It also suggests specific efforts required to continue the analysis and the progression towards estimating flow from temperature decay, specifically:

1. A relationship appears to exist between fluid flux and the relative cooling. That relationship requires further investigation and development.
2. Additional work is needed to resolve the thermal vector and its potential for resolving heater-flow geometry.
3. If the basis for quantifying flow does become relative cooling in some form of type curve comparison, separate type curves will be required for different borehole diameters, rock thermal conductivities and background temperatures.
4. This work should be expanded into a multi-fracture system. Careful consideration of the implementation of the model will be needed to minimize run times.
5. Additional work on the use the ALS results to estimate the thermal conductivity of the rock is needed.
6. To date the issue of convection has largely been ignored because natural thermal gradients are often too low to make it a concern. However the modelling has indicated that the lower side of a fracture is likely to have gradients conducive to convection, although the corresponding upper side would be a stabilizing influence. The issue of convection requires further investigation.
7. If multiple data sets are to be used together to determine flow or alternatively as a form of corroboration, strategies to improve and insure depth alignment will be required.

The ALS technique is a proven advancement in the detection of water flow through fractures, particularly in the deep homothermic portions of aquifers where the system is in thermal equilibrium. These results can be directly used to improve the qualitative interpretation of that data, has indicated promise for further advancement of the technique to a quantification of ambient flow around a lined borehole, and narrowed the approach to that end.

B9. Appendix B - References

Anderson, M.P. 2005, Heat as a Groundwater Tracer, Ground Water 43 (6), 951-968

Bataillé A., Geebthon P., Rabinowicz M. and Fritz B., 2006. Modeling the coupling between free and forced convection in a vertical permeable slot:Implications for the heat production of an Enhanced Geothermal System. Geothermics 35 p654-682.

Beck A.E. 1957, A steady state method for the rapid measurement of the thermal conductivity of rocks, Journal of Scientific Instruments V34, No 5 p186-189.

Beck A.E. 1976, An improved method of computing the thermal conductivity of fluid-filled sedimentary rocks, Geophysics V41, No 1 p133-144.

Beck, A.E, F.M. Anglin and J.H. Shaw, 1971. Analysis of heatflow data – *in situ* thermal conductivity measurements. Canadian Journal of Earth Sciences, **8**, 1-19.

Beck, A., J.C. Jaeger, and G. Newstead, 1956. The measurement of the thermal conductivities of rocks by observations in boreholes, Australian Journal of Physics, vol.9, no.2, pp.286-296,

Bejan, A, 1993. Heat Transfer, John Wiley & Sons, Inc. New York pp 675.

Berthold, S and F. Börner, 2008, Detection of free vertical convection and double-diffusion in groundwater monitoring wells with geophysical borehole measurements. Environmental Geology 54, 1547-1566.

Bidaux, Pascal and Claude Drogue, 1993. Calculation of Low-Range Flow Velocities in Fractured Carbonate Media from Borehole Hydrochemical Logging Data Comparison with Thermometric Results, Groundwater, 31, no.1, 19-26.

Blohm D, 2007. President, IFG Corporation Inc. Phone interview, September 12, Brampton, Ontario.

Bredehoeft J.D. and I.S. Papadopulos, 1965, Rates of Vertical Groundwater Movement Estimated from the Earth's Thermal Profile, Water Resources Research Vol1, No2 p325-328.

Brookfield A.E., E.A. Sudicky, Y.-J. Park and B. Conant Jr. 2009. Thermal transpprt modelling in a fully integrated surface/subsurface framework. Hydrol. Process. 23, p2150-2164.

Bundschuh, J. 1993. Modeling annual variations of spring and groundwater temperatures associated with shallow aquifer systems. Journal of Hydrogeology 142, no 4: 427-444.

Burns, L. 2005. Fracture network characteristics and velocities of groundwater, heat and contaminants in a dolostone aquifer in Cambridge, Ontario. Master's thesis, Department of Earth Sciences, University of Waterloo.

Carslaw, H.S. and J.C. Jaeger 1959. Conduction of Heat in Solids. 2nd ed. Oxford, UK: Clarendon Press.

Drogue, C. 1885. Geothermal gradients and groundwater circulations in fissured and karstic rocks: The role played by the structure of the permeable network. J. Geodynamics,no.4, pp.219-231.

Drury, M.J., 1984. Borehole temperature logging for the detection of water flow. Geoexploration, no. 22, pp.231-243.

Ferguson G., A.D. Woodbury, and G.L.D. Matile. 2003. Estimating deep recharge rates beneath an interlobate moraine using temperature logs. Ground Water 41, no. 5: 640-661.

Frind, E.O. 1982, Simulation of long-term transient density–dependent transport in groundwater, Adv. Water Resour., 5(2) 73-88.

Ge Shemin 1998, Estimation of groundwater velocity in localized fracture zones from well temperature profiles. Journal of Volcanology and Geothermal Research 84 p.93-101.

Gershuni G.Z.,and E.M. Zhukhovitskii, 1976, Convective stability of incompressible fluids. Keter Publishing House Jerusalum Ltd. ISBN:0706515625 9780706515626

Greenhouse, John P. and P.E. Pehme, 2002, Monitoring the Temperature in a Sleeved Borehole: Implications for Fracture Detection, Proceedings of the 55th Canadian Geotechnical and 3rd Joint IAH-CNC and CGS Groundwater Specialty Conferences, Niagara Falls, Ontario, October 20-23, 2002, Published by the Southern Ontario Section of the Canadian Geotechnical Society pp.

Horner, D.R. 1951 Pressure build up in wells. Proc. Third World Petroleum Congress, The Hague. p. 503

Hyndman, R.D., E.E. Davis and J.A. Wright, 1979. The measurement of marine geothermal heatflow by multi-penetration probe with digital acoustic telemetry and in situ thermal conductivity, Mar. Geolphys.Res., 4, 181-205.

IFG, 1993. Temperature Logging, Tech Note Ref: 9303-01-01, IFG Corporation, Brampton, Ontario, Canada. 4p

Jaeger, J.C., 1956. Conduction of heat in an infinite region bounded internally by a circular cylinder of a perfect conductor. Australian Journal of Physics, 9, pp. 316-321

Jemsek, J. and R.P. Herzen 1989. Measurement of insitu sediment thermal conductivity: continuous heating method with outrigged probe, in Hanbook of Seafloor Heat Flow, pp.91-120 eds Wright, J.A. & Luoden, K.E., CRC Press, Boca Raton, FL.

Kearl, P.M., 1997. Observations of particle movement in a monitoring well using the colloidal borescope: Journal of Hydrogeology, **200**, 323-344.

Keller, C.E., pers communication re liner design implications on thermal cond.

Keller, C.E., J.A. Cherry and B.L. Parker. 2008 for submission A new method for fracture identification and continuous hydraulic conductivity profiling in fractured rock boreholes. Ground Water.

Kerfoot, W.B. 1992, The use of flowmeters and slow release dyes to determine bedrock flow for wellhead protection, *in* Proceedings, The Sixth National Outdoor Action Conference on Aquifer Restoration, Ground Water Monitoring and Geophysical Methods, National Groundwater Association, May 11-13, 1992, Las Vegas, Nev., 755-763.

Kukkonen I., I. Suppala, A. Korpisalo and T Koskinen, 2005 TERO Borehole Logging Device and Test Measurements of Rock Thermal Properties in Olkiuoto, Posiva OY, Olkiluoto, Finland, 98p.

Lee Tien-Chang, 9182, Estimation of formation temperature and thermal property from dissipation of heat generated by drilling, Geophysics Vol 47, No11, pp.1577-1584.

Lee Tien-Chang, A.D. Duchkov and S.G. Morozov, 2003, Determination of thermal properties and formation temperature from borehole thermal recovery data, Geophysics Vol 68, No8, pp.1835-1846

Lister, C.R.B, 1979. The pulse probe method of conductivity measurement, Geophys. J. R. atsr. Soc. 57, pp. 451-461.

Lusheshi M.N., 1983, Estimation of formation temperature from borehole measurements, Geophys. J. R. atsr. Soc. 74, pp. 747-776.

Malard F. and R. Chapuis, 1995, Temperature logging to describe the movement of sewage-polluted surface water infiltrating into a fractured rock aquifer. J. of Hydrology no.173 pp. 191-217.

Markle J.M., R.A. Schincariol, J.H. Sass and J.W. Molson 2006, Characterizing the Two-Dimensional Thermal Conductivity Distribution in a Sand and Gravel Aquifer, Soil Science of America Journal 70, p1281-1294.

Meyer, J.R., B.L. Parker, and J.A. Cherry. 2007. Detailed hydraulic head profiles as essential data for defining hydrogeologic units in layered fractured sedimentary rock. Environmental Geology. DOI10.1007/s00254-007-1137-

Molson, J.W., 2006. Laval University, pers. discussion, November, Waterloo, Ontario.

Molson J.W., E.O. Frind and C.D. Palmer 1992, Thermal Energy Storage in an Unconfined Aquifer 2. Model Development, Validation and Application. Water Resources Research, Vol28, No10, p2857-2867.

Molson J.W. and E.O. Frind, 1994. Predicting the behavior of thermal energy in porous and discretely fractured media, Proceedings: *Eighth International Conference of the Association for Computer Methods and Advances in Geomechanics*, West Virginia University, May 1994.

Molson, J.W. and Frind, E.O., 2005 HEATFLOW/SMOKER, A 3D groundwater flow and thermal energy transport model, version 3.0, University of Wateroo.

Molson J.W. and E.O. Frind 2006, Heatflow, Ver 4.0, Density-Dependent Flow and Thermal Energy Transport Model in Three Dimensions, User Guide. Dept. Earth Sciences University of Waterloo.

Molson J.W., J. Cherry, B. Parker and L. Burns, In prep, Numerical Simulation of Thermal Transport In Fractured Dolostone at the Cambridge Research Site.

Molson J., P. Pehme, J. Cherry, and B. Parker, 2007, Numerical analysis of heat transport within fractured sedimentary rock: Implications for temperature probes. 2007 NGWA/U.S. EPA Fractured Rock Conference: State of the Science and Measuring Success in Remediation, Portland, Maine • September 24-26, 2007

Moltz F.J., G.K. Boman, S.C. Young and W.R. Waldrop, 1994, Borehole flowmeters: field application and data analysis. Journal of Hydrology, V163, pp. 347-371.

Novakowski K.S., Bickerton G., Lapcevic P., Voralek J., Ross N., 2005. Measurements of groundwater velocity in discrete rock fractures. Journal of Contaminant Hydrology 82: 44-60.

Oldenburgh and Pruess 1995. Dispersive transport dynamics in a strongly coupled groundwater-brine flow system. Water Resources Research 31:289-302.

Paillet F.L. 1999, Geophysical Reconnaissance in Bedrock Boreholes – Finding and Characterizing the Hydraulically Active Fractures, USGS Water-Resources Investigations Report 99-4018C, Toxic Substances Hydrogeology Program – Proceedings of the Technical Meeting, Charleston, South Carolina, March 8-12, 1999. D.W. Morganwalp and H.T. Buxton editors p 725-733

Palmer C.D., D.W. Blowes, E.O. Frind and J.W. Molson, 1992, Thermal Energy Storage in an Unconfined Aquifer 1. Field Injection Experiment. Water Resources Research, Vol28, No10, p2845-2856.

Parker, B.L., 2007, Investigating Contaminated Sites on Fractured Rock Using the DFN Approach, NGWA/U.S. EPA Fractured Rock Conference: State of the Science and Measuring Success in Remediation, Portland, Maine • September 150-168, 2007

Parker, B.L., R.W. Gillham and J.A. Cherry, 1994. Diffusive disappearance of immiscible phase organic solvents in fractured rock geologic. Ground Water, 32(5):805-820.

Pehme, P.E., Parker B.L, Cherry J.A. and Greenhouse J. P., 2010, Improved Resolution of Ambient Flow through Fractured Rock with Temperature Logs, Ground Water, Vol 28, No 2 pp.191-211.

Pehme, P.E., J.P. Greenhouse and B.L. Parker, 2007a, The Active Line Source temperature logging technique and its application in fractured rock hydrogeology, Journal of Environmental and Engineering Geophysics, Vol 12 No 4 pp. 307-322

Pehme, P.E., J. P. Greenhouse and B.L. Parker, 2007b,The Active Line Source (ALS) technique, a method to improve detection of hydraulically active fractures and estimate rock thermal conductivity, Proceedings of 60th Canadian Geotechnical Conference & 8th Joint IAH-CNC Groundwater Conference, Ottawa, Ontario.

Pehme, P.E., B.L. Parker, J.A. Cherry and J. P. Greenhouse, 2007c, The Potential for Compromised Interpretations When Based on Open Borehole Geophysical Data in Fractured Rock. 2007 NGWA/U.S.

EPA Fractured Rock Conference: State of the Science and Measuring Success in Remediation (#5017), Portland, Maine • September 24-26, 2007

Pehme, P.E., Cherry J.A. and Parker B.L, (In prep. –a) Induced thermal disequilibrium in boreholes to enhance detection of water flow in fractured rock, To be submitted to Journal of Hydrology.

Pehme P.E., B.L. Parker, J.A. Cherry and D. Blohm (in prep-b) A Temperature Probe for Fine Scale Resolution of Horizontal and Vertical Thermal Gradients in Fractured Rock To be submitted to Journal of Environmental and Engineering Geophysics,

Pruess, K., C. Oldenburg and G. Moridis, 1999. TOUGH2 user's guide, Version 2 Lawrence Berkley National Laboratory Report, LBNL-43134: Berkeley, California.

Robinson R., S. Stilliman and C. Cady, 1993, Identifying Fracture Interconnections between Boreholes Using Natural Temperature Profiling: II. Application to fractured Dolomite, Log Analyst 34, no. 1 pp. 69-77

Sammel, E.A. 1968. Convective flow and its effects on temperature logging in small diameter wells. Geophysics. V.33, no.6, pp.1004-1012.

Shen, P.Y. and A.E. Beck, 1986. Stabilization of bottom hole temperature with finite circulation time and fluid flow. Geophysical Journal of the Royal Astronomical Society, **86**, 63-90.

Silliman, S. and R. Robinson, 1989. Identifying fracture interconnections between boreholes using natural temperature profiling: I. Conceptual basis, Ground Water. V27, No.3. pp. 393-402.

SonTek Inc. 1996. Modified ADV for 3D velocity measurements in boreholes – Final project report. USGS Contract Number 1434-95-C-40232. SonTek: San Diego, California.

Sterling, S.N., B.L. Parker, J.A. Cherry, J.H. Williams, J.W. Lane Jr. and F.P. Haeni, 2003. Vertical Cross Contamination of Trichloroethylene in a Borehole in Fractured Sandstone. Ground Water, V43, No.4 pp. 557-573.

Su G.W., B.M. Friefield,C.M. Oldenburg, P.D. Jordan and P.F. Daley, 2006. Interpreting Velocities from Heat-Based Flow Sensors by Numerical Simulation, Ground Water. V44, No.3. pp 386-393.

Trainer, F.W. 1968. Temperature profiles in water wells as indicators of bedrock fractures. Professional Paper 600-B Washington DC: USGS.

Tsang, C.F., P. Hufschmied, and F.V. Hale 1990. Determination of fracture inflow parameters with a borehole fluid conductivity logging method: Water Resources Research, **26** no.4, 561-578.

Yang J., R.N. Edwards, J.W. Molson, E.A. Sudicky,1996a. Fracture-Induced Hydrothermal Convection in the Oceanic Crust and Interpretation of Heat-flow Data, Geophysical Research Letters Vol23 No9 p929-932.

Yang J., R.N. Edwards, J.W. Molson E.A. Sudicky,1996b. Three-dimensional numerical simulation of the hydrothermal system within the TAG-like sulfide mounds, Geophysical Research Letters Vol23 No23 p3475-3478.

Wilson J.T., W.A. Mandell, F.L. Paillet, E.R. Bayless, R.T. Hanson, P.M. Kearl, W.B. Kerfoot, M.W. Newhouse and W.H. Pedler, 2001. An Evaluation of Borehole Flowmeters used to Measure Horizontal Ground-Water Flow in Limestones of Indiana, Kentucky, and Tennessee, 1999. US Dept. of the Interior & USGS, Water-Resources Investigations Report 01-4139, pp 139.

B10. B- Appendix- A Base Case “Smoker.data” Input File

Base Case Smoker Input

```
THERMAL HEAT FLOW
Det 14
High detailed "round" liner
18/08/2010
0       0       0       0       0       0  1       0                    ; KPRT,KCN,KWT,KINT,KINTV,KGO,ksat,kmass
4       3       3                                                       ; ngx,ngy,ngz
4.80    5.20    10.0    20.0                                            ; xlim (m)-
4.80    5.20    10.0                                                    ; ylim -
4.5     5.5     10.0                                                    ; zlim -
24      40      24      10                                              ; nlx  -
24      40      24                                                      ; nly
9       50      9                                                       ; nlz
0       0.0                                                             ; nwtl, datum (flow)
40      45      34      34      1                                       ; breakthrough point
41      45      34      34      1                                       ; breakthrough point
42      45      34      34      1                                       ; breakthrough point
43      45      34      34      1                                       ; breakthrough point
44      45      34      34      1                                       ; breakthrough point
45      45      34      34      1                                       ; breakthrough point
46      45      34      34      1                                       ; breakthrough point
47      45      34      34      1                                       ; breakthrough point
48      45      34      34      1                                       ; breakthrough point
49      45      34      34      1                                       ; breakthrough point
41      41      34      34      1                                       ; breakthrough point
42      41      34      34      1                                       ; breakthrough point
43      41      34      34      1                                       ; breakthrough point
44      41      34      34      1                                       ; breakthrough point
45      41      34      34      1                                       ; breakthrough point
46      41      34      34      1                                       ; breakthrough point
47      41      34      34      1                                       ; breakthrough point
```

41	43	34	34	1						; breakthrough point
42	43	34	34	1						; breakthrough point
43	43	34	34	1						; breakthrough point
45	45	30	30	-1						; breakthrough point
1	38	1	88	34	34	2	6	0.001	1	;Low x All y single fract 2D fracture location, iloc,
38	51	1	38	34	34	2	6	0.001	1	;Mid x Low y single fract 2D fracture location, iloc,
38	51	51	88	34	34	2	6	0.001	1	;Mid x High y single fract 2D fracture location, iloc,
39	40	39	40	34	34	2	6	0.001	1	Lower left BH corner
39	39	41	42	34	34	2	6	0.001	1	Lower left BH corner
41	42	39	39	34	34	2	6	0.001	1	Lower left BH corner
39	40	49	50	34	34	2	6	0.001	1	Upper left BH corner
39	39	47	48	34	34	2	6	0.001	1	Upper left BH corner
41	42	50	50	34	34	2	6	0.001	1	Upper left BH corner
49	50	39	40	34	34	2	6	0.001	1	Lower right BH corner
47	48	39	39	34	34	2	6	0.001	1	Lower right BH corner
50	50	41	42	34	34	2	6	0.001	1	Lower right BH corner
49	50	49	50	34	34	2	6	0.001	1	Upper right BH corner
47	48	50	50	34	34	2	6	0.001	1	Upper right BH corner
50	50	47	48	34	34	2	6	0.001	1	Upper right BH corner
51	98	1	88	34	34	2	6	0.001	-1	;High x All y single fract 2D fracture location, iloc,
1	1	0	0	0	0					; B.C's flow SPECIFIED FOR **NODES** Imediately below
1	89	1	69	0.15	-1					; head at face 1 (left)
1	89	1	69	0.00	-1					; H2 at (m/s) adjusted up frm 59
1	586432	9.8E-	9.8E-10	9.8E-10	3.6	3.6	3.6	0.05	-1	; Use perm (1E-12 cm/sec>9.8E-10 m/sec and porosity
39	50	43	46	1	68	1.00E-	1.00E-	1.00E-	0.570.570.571.00E-1	; Liner Data Node Range X,Y,Z, HKx,HKy,HKz(m/s),
40	49	41	48	1	68	1.00E-	1.00E-	1.00E-	0.570.570.571.00E-1	; liner indexed K (m/s) Different way of entering same data
41	48	40	49	1	68	1.00E-	1.00E-	1.00E-	0.570.570.571.00E-1	; liner indexed K (m/s) Different way of entering same data
43	46	39	50	1	68	1.00E-	1.00E-	1.00E-	0.570.570.571.00E-1	; liner indexed K (m/s) Different way of entering same data
40	49	44	45	1	68	1.0E+00	1.0E+00	1.0E+00	0.570.570.571	1 ; Water in well indexed K (m/s) Different way of entering
41	48	42	47	1	68	1.0E+00	1.0E+00	1.0E+00	0.570.570.571	1
42	47	41	48	1	68	1.0E+00	1.0E+00	1.0E+00	0.570.570.571	1
44	45	40	49	1	68	1.0E+00	1.0E+00	1.0E+00	0.570.570.571	1
39	50	39	50	68	68	1.00E-	1.00E-	1.00E-	0.570.570.571.00E-1	; Plug in top of Liner Data Node Range X,Y,Z,
39	50	39	50	1	1	1.00E-	1.00E-	1.00E-	0.570.570.571.00E--1	; Plug in bottom of Liner Data Node Range X,Y,Z,
0.000										; specific storage SS
0	0.15									; init, h0 (flow initial condition)
1	0	0	0	0	0					; B.C.'s transport boundary types

1	89	1	69	10	-1				; Leftside boundary
1.2	1.2	0.3							; top: TCON, BZ SAT (m,s)
0.0	10.0	365	-45.0						; surfat min,amp,period,phase
0	0.0	0.0	0.0						; ivel,Vx,Vy,Vz (m/s) ivel=2 uniform fract v
0.100	0.010	0.005	0.0E+001						; AL, ATH, ATV, (m)DD(M^2/S), RETARD
4192	999.7	860.0	2850.0						; thermal properties (m,s) cw, rhow, cs, rhos
0.0E+000	.1	5.0							; latent heat, P,Q for Wu
1	99	1	89	1	69	10.0	10.0	-1	; temperature initial condition,
1.0E-03	0.01	0.0001	10	10					; ccp, cct, ccw, maxit1, maxit2
1.0	1.0	0.96							; over-relax factors for head, temp, tsa
45	0								; Y-Z Plane Section knox(1), knox(2), transverse print
45	0								; X-Z Plane Section knoy(1), knoy(2), longitudinal print
35	0								; X-Y Plane Section knoz(1), (2) for t1dx.plt
39	39	44	44	1	68	500.0	0.0	-1	; internal heat source fluxin W/m^2,decay
3.999	4.2510	4.2800	4.5	5.0					; five 3d print times (days)
0.0	4.0000	1.0E-0	20	1					;start t0 days,end t1,dt,kplot(days) time info +1 LOOKS
0.0	0.0	0							; hinc,rinc,iflux
0	0	0	0	0.0	-1				; surface temp patch
97	2	42	42	0.0E+001	0	-1			; **SOURCE** Node in X, Node in Y, From Z1 to z2, rate per
4.0	4.2500	1.0E-0	20	1					;start t0 days,end t1,dt,kplot(days) time info +1 LOOKS
0.0	0.0	1							; hinc,rinc,iflux
0	0	0	0	0.0	-1				; surface temp patch
45	45	66	67	0.0E+001	0	-1			; **Withdrawl Bottom** Node in X, Node in Y, From Z1 to
4.25	8.0000	1.0E-0	20	-1					;start t0 days,end t1,dt,kplot(days) time info +1 LOOKS
0.0	0.0	0							; hinc,rinc,iflux
0	0	0	0	0.0	-1				; surface temp patch
97	2	42	42	0.0E+001	0	-1			; **SOURCE** Node in X, Node in Y, From Z1 to z2, rate per

B- Appendix B- Thermal Conductivity Values compiled by Molson and Frind (2006)

Table 1. Summary of thermal conductivities from the literature

Material	Value	Source
Liquid water Quartz particles Clay minerals Organic matter	1.4×10^{-3} cal/cm/s/°C (=0.585 J/m/s/°C) 2.1×10^{-2} (=8.77 J/m/s/°C) 7.0×10^{-3} (=2.92 J/m/s/°C) 6.0×10^{-4} (=0.25 J/m/s/°C)	De Vries (1966) as referenced in: Nobre RCM and Thompson N.R.: The effects of transient temperature gradients on soil moisture dynamics (WRR?)
Water (10 °C) Air Ice	0.574 J/s/m/°C 0.025 J/m/s/°C 2.1 J/m/s/°C	CRC Press 1980 pg. E11 http://www.hukseflux.com/thermal%20conductivity/thermal.htm
Unsaturated sand &gravel Saturated sand/gravel	1.0 $Js^{-1}m^{-1}K^{-1}$ 2.0 $Js^{-1}m^{-1}K^{-1}$	Groundwater modeling study of temperature impacts for a proposed sand and gravel quarry, Township of Brantford, Ontario, 1992 (C.J. Neville, Dames & Moore Canada)
Saturated Borden sand	2.0 J/m/s/°C	3D model: Molson et al., WRR, 28(10), p.2863, 1992.
Rocks: - granite (0°C) - shale (0°C) - quartzite (0°C) - oceanic crust - limestone - sandstone - granite	 0.21 J/m/s/°C (3.0 cal/m/hr/°C) 0.12 J/m/s/°C (1.65 cal/m/hr/°C) 0.34 J/m/s/°C (4.9 cal/m/hr/°C) 2.0 J/m/s/°C 0.58 - 1.3 J/m/s/°C 1.2 – 2.3 J/m/s/°C 1.9 – 4.0 J/m/s/°C	 CRC Press 1980, E16 Yang et al., Geophys. Res. Lett., 23(9), 1996 CRC Press 1980, p.E-5 “ “
Rocks etc.: (room temp.) - granites - basalts - gneiss - quartzites - schists - sandstones - limestone - calcite - dry clay - wet clay - shale - dry sand - wet sand - rock salt	 2.1– 3.8 J/m/s/°C 1.4 – 1.7 1.9 - 4.8 3.6 – 8.0 1.7 – 3.8 1.3 – 4.2 2.0 – 3.3 3.5 – 3.9 0.84 – 2.1 2.5 – 3.3 1.25 – 3.0 0.42 – 0.84 2.5 – 3.3 5.3 – 7.2	Various references as given in Table 1 of Ghislain de Marsily
Sandy gravel - dry - saturated	 0.52 J/m/s/°C 1.57 J/m/s/°C	Mathey, Jour. of Hydrology 34, 315-333, 1977.
Quartz Sand - dry - saturated	3.0 J/m/s/°C 0.35 J/m/s/°C 2.7 J/m/s/°C	http://www.hukseflux.com/thermal%20conductivity/thermal.htm

Table 2. Thermal conductivities from Luckner & Schestakow (1991)

Material	Thermal K (W/m/°C = J/m/s/°C)
Air 0°C	0.024
Air 20°C	0.026
Water 0°C	0.54
Water 12°C	0.58
Water 30°C	0.63
Feldspars	2.5
Quartzite	6.0
Granite	2.2-3.4
Basalt	1.4-2.0
Limestone	2.0-3.0
Marble	2.8-3.2
Sandstone	1.5-5
Clay	0.8-1.2
Coal	5
CaSO4	5.2
NaCl	9.6

Table 3.Thermal Conductivity Parameter Range

	Thermal K (J/m/s/°C)
- Range of all reported values	0.15 – 7.0
- saturated soil	0.6 – 4.0
- dry sand	0.15 – 0.25
- moist sand	0.25 – 2.0
- saturated sand	2 – 4
- dry to moist clay	0.15 – 1.8
- saturated clay	0.6 – 2.5
- soil with organic matter	0.15 – 2
- solid rocks	2-7
- tuff	0.5 – 2.5

Table 4. Specific Heat , Volumetric Heat Capacity, Thermal Diffusivity

Specific Heat (c_w) water (c_w)	1.001 cal/g/°C (=4184 J/kg/°C)	CRC Press (at 10°C)
Specific Heat (c_w) Rocks granite (0°C) shale (0°C) quartzite (100°C)	 0.192 cal/g/°C (=802 J/kg/°C) 0.17 cal/g/°C (=710 J/kg/°C) 0.26 cal/g/°C (=1086 J/kg/°C)	CRC Press 1980, E16
Volumetric Heat Capacity ($Co=\rho\, c_w$) Water (ρ=1000 kg/m^3) Quartz (ρ=2600 kg/m^3) Dry sand (ρ=1600 kg/m^3) Saturated sand (ρ=2100 kg/m^3)	 4.18 x 10^6 J/m^3/C 2.13 x 10^6 J/m^3/C 1.27 x 10^6 J/m^3/C 2.64 x 10^6 J/m^3/C	(1)
Thermal diffusivity $\kappa=\lambda/C_0$ Quartz (ρ=2600 kg/m^3) Dry sand (ρ=1600 kg/m^3) Saturated sand (ρ=2100 kg/m^3)	 141 x 10^{-8} m^2/s 28 x 10^{-8} m^2/s 102 x 10^{-8} m^2/s	(1)
Thermal diffusivity Borden saturated sand	 7.1 x 10^{-7} m^2/s	3D model: Molson et al., WRR, 28(10), p.2863, 1992.

(1) Source: http://www.hukseflux.com/thermal%20conductivity/thermal.htm

Table 5. Thermal conductivity of some common rock-forming minerals
Source: Somerton et al. (1974)

Mineral	Thermal Conductivity	
	($cal \cdot cm^{-1} \cdot s^{-1} \cdot C^{-1}$)	(W/m/°C = J/m/s/°C)
Quartz	0.01837	7.7
Orthoclase	0.00553	2.3
Plagioclase	0.00512	2.1
Calcite	0.00858	3.6
Muscovite	0.00529	2.2
Chlorite	0.00174	0.73
Hornblende	0.00735	3.1
Epidote	0.00627	2.6
Sphene	0.00558	2.3
Biotite	0.00559	2.3

(conversion factor : **1 $cal \cdot cm^{-1} \cdot s^{-1} \cdot C^{-1}$ = 4.18x10^2 W/m/°C**) (CRC 1980, p.E17)

Table 6. Thermal Conductivity of Dolomite

Thermal K (W m^{-1} K^{-1})	Source
1.6 – 6.6 mean: 3.62	Cermak & Rybach (1982)
5.501	Horai, K. (1971),
4.78 ± 0.54 (at 25°C)	Clauser, C. and E. Huenges (1995)
3.75 - 6.30	Blackwell, D. D., and J. L. Steele (1
4.013 - 5.518	Clark, S. P. Jr. (1966),

Appendix C
Time-Elevation Head Sections: Improved Visualization of Multi-level Installation Data

Peeter Pehme[1] and B.L. Parker2.

C1. Overview

As hydrogeologic investigations of fractured rock evolve towards increasing spatial and temporal resolution with deployment of multilevel systems 10 or more intervals in a single borehole with auto-sampling sensors monitoring pressure, temperature or chemistry for weeks or months, large quantities of densely sampled (time and space) data are produced. These data are typically displayed as hydrographs for analysis of site specific controls on groundwater flow. We present a method for presentation of high density pressure head data from multilevel installations referred to as time-elevation head (TEH) sections that improves visualizion of spatial and temporal responses of the hydrogeologc system to external stresses.

Data collected from two multi-level installations, each with 13 functioning pressure transducers monitoring the upper 40m of a dolostone aquifer, over a period of 83 days, prior to, during and after a pumping test are used to present TEH sections and examples of data processing. TEH sections are produced using commercially available software designed for geophysical data collected at closely spaced intervals along sub-parallel lines. These algorithms perform calculations orthogonally either in time ("X" axis) or elevation ("Y" axis) to interpolate a regular grid of head and subsequent filtering enhances characteristics of the data. The base and filtered TEH sections are used to interpret response of the system to transients and infer hydrogeologic characteristics of the site. The utility of process is dependent on the precision and accuracy of the head data as well as an informed user to avoid introducing spurious features into the sections.

C2. Introduction

There is an increasing use of both auto sampling devices such as transducers to measure groundwater pressure (head) and employment of these within multilevel installations in fractured rock investigations (Sorenson and Butcher, 2011). Sampling devices are becoming smaller and more robust, measure more parameters, and have data storage capacity to allow for increasing temporal frequency and sampling

duration. New multilevel monitoring installation technologies such as the FLUTe Water system (Cherry et al 2007) have become available in addition to the established Westbay (Black et al 1986) and the Waterloo (Cherry and Johnson, 1982) systems. Investigations in fractured rock can now involve continuous monitoring of 10-20 or more ports (e.g. Meyer et al. 2008). Although many types of information (water temperature, chemistry etc) can be collected, the most common is the water pressure (head) for analysis of flow as well as monitoring responses to transients to estimate hydraulic parameters and interconnectivity. When multi-levels are instrumented with pressure transducers that are set to automatically record and digitally store data hourly (or more often) for weeks and months, these yield large amounts of data at relatively high spatial and temporal density.

As the volume and spatial density of data increases, it becomes progressively more difficult to present and analyze the results so as to conceptualize the hydrogeologic processes occurring. The conventional approach to presenting head data collected over a period are hydrographs; line plots of pressure (as elevation) against time (e.g. Sittner et. al. 1969). Although hydrographs are extensively used for both surface water and groundwater analysis, the plots become difficult to resolve when data from more than 3-4 monitoring ports are directly compared on the same axis. The purpose of this paper is introduce and demonstrate the use of software designed for interpretation and visual presentation of high-resolution geophysical data sets akin to the high density pressure head data from such high resolution multi-level systems. The data presentations referred to as Time-Elevation-Head (TEH) sections, are intended as a method to improve presentation of spatial and temporal variations in pressure head to natural and induced hydraulic stimuli.

C3. **Site Description**

The data used in this paper is a subset of data from Belan (2010) collected as part of a large-scale multi-well pumping test on municipal water supply wells in the area of a G360 industrial research site in Guelph, Ontario is used. The geology in the general area consists of 4-5m of overburden above approximately 110m of dolostone aquifer (formations of the Silurian, Lockport group) which overlies a regional shale aquitard (the Clinton Group). Beneath much of the research site, approximately 35-40mbgs within the Lockport formation is the Eramosa member, a 5-10m thick laterally discontinuous argillaceous unit described as an aquiclude by Brunton (2008). Further details of the local geology are provided by Pehme et al (2010) and Perrin et al (2011). The dolostone aquifer is regionally extensive and near the research site it had been pumped from two pumping wells referred to herein as PW1 and PW2 (approximately 450m south-southeast and 900m to the northwest of the study area respectively). These two wells had not been pumped since 1994 and in December 2008, a large scale extensively monitored, pumping test was conducted to evaluate the prospects for returning these wells to operation. Water was

extracted (16.4L/s) from below 65mbgs at PW1 for 13 days (starting December 9, 2008), with additional pumping from PW2 (13.3L/s) for the latter 7days. The details of the pump test, monitoring network and results are beyond the scope of this document and are to be presented by Stantec (2009) and Belan (2010).

Herein, the data from two multi-level installations in wells MW-74 and MW-75 (Figure C1) are used as examples of the proposed data form and processing procedures available for enhanced visualization and hydrogeologic interpretation. MW74 and MW75 are 10cm diameter boreholes cored to the anticipated top of the Eramosa unit, at approximately 40mbgs. Each has a FLUTe multilevel monitor system (referred to as an "MLS") (Cherry et. al 2007) installed with 16 measuring ports at depth intervals selected based on borehole specific measurements (see Table C1), with a dedicated pressure transducer (PDX-261, In-Situ, Fort Collins, Colorado, USA) monitor the water pressure in each port. The transducers have a manufacture specified accuracy of ±0.05% of full scale (which should provide resolution of water level elevation to <0.006m if properly deployed), however, three transducers in each installation (italicized and shaded in Table C1) were clearly nonfunctional and are ignored. The transducers were sampled at 1 hr intervals for 55 days prior to pumping, (starting on 15 October, 2008) and 15 days beyond the end of the pumping test (83 days in total).

Figure C2 shows a conventional hydrograph presentation of the head data (as elevation) from the 13 functional transducers in MW74 (Belan, 2010). The hydrographs distinctly show the response to pumping from wells PW1 and PW2. Many of the transducers show minor responses prior to pumping, however a relationship to recharge (precipitation) or more distant hydraulic events are difficult to establish. Although all the temporal data from these MLS is presented in the traditional X-Y (time-head) format using color coding, the interpretation and integration of results between adjacent ports is not self-evident or supported by this traditional data presentation style, limiting the visual presentation of results and making interpretation of system behavior difficult.

C4. **Method**

Presented herein is an alternative method for plotting 3 dimensional data from multi-level installations referred to as a Time-Elevation Head (TEH) section. The processing is an adaption of common geophysical plotting algorithms referred to as line gridding (or BIGRID in the Geosoft – Montage software, www.geosoft.com). Note: any program that deals with data in a similar fashion can be used for the data processing; however the aforementioned software is only such algorithm we are familiar with. Line gridding is designed to present data collected at a relatively high density (often sub-metre) along parallel or sub-parallel lines at a fairly regular, moderate spacing (eg. 1 to 5m) apart. The data are first interpolated along the lines to an evenly spaced (user specified) interval and then orthogonally between

lines to create a dense, regularly spaced grid of values which can be colour shaded and/or contoured. The key characteristics of the process critical in this application are:

i. the data is dealt with orthogonally and therefore:

   a. the interpolation process is not a combination of x and y coordinates, and

   b. sharp changes that occur in one of the dimensions and not the other are better honored than occurs with 2 dimensional interpolation.

ii. the degree to which the data is honored can be controlled with the splining process from completely true (with a linear interpolation) to a much smoother result (based on a cubic relationship). The "akima-spline" is a compromise between these extremes, providing a relatively smooth result while closely honoring the original data (Akima, 1969).

There are many different pressure transducers available in the market place and the details of the systems and data transfer from field detectors will vary between manufacturers and is inconsequential to the methods herein presented. Of critical importance however, is the resolution and relative accuracy of the pressure transducers which can vary considerably (Sorenson and Butcher, 2011), but needs to be optimum to insure relevance of the analysis. We assume all pertinent corrections for atmospheric pressure changes, temperature and salinity (if required), depth as well as quality assurance and quality control have been applied and a single data file of: time, monitoring elevation, and pressure is available as input to the procedures described here.

C5. **Results**

The line gridding process is adapted to multilevel data by using time as the X axis and elevation (or depth) for the Y axis. Figure C3 shows TEH sections for MW-74 and MW-75 for 52 days prior to, during and 15 days after the pumping test, with the Y-axis as elevation and the X-axis time (days). Details of the parameters presented in each figure are summarized in Table C 2. Precipitation (rain and snow) is shown above the sections as histograms. Pressure head is represented using a linear colour distribution with dark blue as low (330.60m) and pale pink for the highest values (338.60m). Resolution is controlled by data and grid density; in this case data are gridded at 0.2 (m,days) using an akima spline.

The background (pre pumping) portion of the plot indicates a distinct layering of the pressure head, with at least three zones of relatively lower pressure. Gamma logs for each well are provide to place the features in a geologic context showing lithologic variability of the dolostone rock subunits. The highest pressures are observed in the upper two monitors at MW-74. These are likely under the influence of the nearby drainage ditch which cuts through the overburden to the bedrock surface immediately to the

northwest of the monitoring well. Note the propagation of precipitation events through the sections as vertically co relatable high pressure pulses prior to pumping. The TEH response to recharge will vary with location, ground conditions and whether the precipitation occurs as rain or snow. The influence of pumping is clearly indicated by a change in the overall colour of the sections to green and then blue as the head in the monitors decrease in Figure C3.

Scaling TEH sections is best implemented by adjusting (multiplying) the X axis (time) by a factor, such that the unit values represent ½ or ¼ days to expand, or weeks to compress. Analysis of the response to pumping is improved by expanding the time scale to ½ days relative to the start of pumping PW1. Figure C4 shows expanded TEH sections for MW-74 and MW-75 starting five days prior to pumping (the vertical reference line). The low pressure zones appear to respond to the pumping immediately, whereas the portions of the rock at higher pressure exhibit a delayed response. In MW75 the zone from 320-323masl and from 329-333masl both have a delayed and muted response to pumping, as does the interval 320-326masl in MW74. At MW74 there is no obvious response to pumping above 332masl, presumably because of recharge from the drainage ditch.

The TEH sections also allow for a similar analysis of recovery after the pumps are turned off. The decrease in pressure persists through the end of the sections although the character of the recovery varies with depth. Overall, both sections indicate lower pressures are measured at depth which is consistent with the most hydraulically conductive zone being at approximately 270 masl and the pumping being primarily constrained to below 283masl, well beyond the bottom of these sections.

The nature of the grid and algorithms provided in the software allow the interpreter several options for filtering and processing the grid. Figure C5 is the TEH section for MW74 with a 10m low pass filter in depth that effectively suppresses the horizontal layering in the grid and enhances time dependent (vertical) changes. The result minimizes the influence of the ditch on the shallow monitors and the effect of the pumping is shown to extend upward to surface. Increasing the overall extraction rate by initiating pumping of PW2 creates a very sharp decrease in pressure (upward bend of contours) at depth, but that influence is shown to decrease towards surface, and may be countered by the coincidence of a rain event. The concurrent cessation of pumping both wells creates a corresponding downward bend in the contours (increase in pressure) which is immediately followed by two large precipitation events. Although the precipitation likely distorts the pattern during recovery, that influence may be minimal as it fell in the form of snow. The influence of recharge from several earlier precipitation events is manifested by downward bending of the head contours and suggests that the pressure pulse from these events also propagates through the entire portion of the rock monitored. The change in the vertical gradient caused by pumping is qualitatively represented by a comparison of the density of the contours, but since the grid has

been filtered, a quantitative estimate of the vertical gradient would be suspect. However, the representation of filtered data remains true in time and therefore a time dependent analysis of such characteristics as the downward propagation rate of the pressure pulse remains valid.

Another useful manipulation of the original gridded data is the calculation of gradients either in time or space. Figure C6 shows the Time-Elevation Vertical Gradient (TEVG) section for MW-74 and MW-75 through the complete time period. The colour scheme is linear and set so the shades of yellow-green-blue represent a downward gradient, and orange-red-pink an upward gradient. Although both locations are predominantly shaded in yellow-blue indicating an overall downward gradient, several thin layers with moderate (red) to high (pink) upward gradients exist. This representation provides additional insights into the behavior of the rock mass under hydraulic stresses. For example above 323masl at MW74 and 325masl at MW75 pumping increases the downward gradient sufficiently that at some depths the vertical gradients are reversed. Below these critical depths pumping has minimal influence on the vertical hydraulic gradient. This is a valuable observation in that this visualization tool facilitates the overall understanding of horizontal versus vertical flow and the distinct behavior of the responses from each layer. Further discussion of the hydraulic phenomena and the implications are beyond the scope of this paper and reserved for a complete analysis of the pumping test data set from this site.

C6. **Discussion**

The environmental geophysical community has numerous data processing techniques for enhancing features, controlling noise, and suppressing undesirable influences on data sets sampled frequently in time or space. The TEH sections, and their derivatives presented here (as well as other yet unexplored options in data processing) depend on densely sampled data, in both time and space. One must be aware that data from conventional multilevel systems using 2 or 3 monitoring ports do not lend themselves to these processes as the gridding will suffer from inadequate vertical density and be aliased. The patterns produced in these sections and the inferences drawn are dependent on both the accuracy and the resolution of the transducer as well as proper correction for atmospheric pressure variations. Poor resolution, as well as overly aggressive data processing of the grid or contouring manifest as irregular colour patterns and contours, conditions readily apparent in the resultant plots. The interpreter must also be conscious of the colour distribution used to present the results. The choice of either linear or equal area colour schemes and various modifications of these can either enhance or suppress variability. Manipulation must be properly tracked during data processing, although the software used herein maintains a log of steps applied.

The example data invites a sub-division into “pressure (head) units”, which could potentially be related to the “hydrogeologic” units presented by Meyer et al (2008). However, even with the large number of ports (vertical data density) possible in modern multi-level installations, the vertical resolution remains coarse relative to geophysical data sets. If the design of multilevel installations is generally skewed towards monitoring ports being located where the probability of groundwater flow is highest, potentially avoiding or missing zones of lower hydraulically conductivity between. This may result in successive “pressure units” being miss-represented as a single interval if the intervening units is not sampled. Alternatively if narrow ports are not properly deployed or if transducers responses drift, two ports within the same pressure unit may appear to respond differently and be inappropriately subdivided. A careful comparison of the dynamic ranges of the data as the transducers respond to hydraulic stresses such as rain events or pumping can provide clues that these situations may exist. Refer to Sorenson and Butcher (2011) for further discussion of transducer accuracy and drift.

The interpreter also needs to clearly understand that the interpolation processes as well as their choices in input parameters and options can create false highs or lows between monitoring intervals. These can be controlled by better honoring the data with akima or linear interpolation (these are our preferred algorithms for gridding), but at the potential expense of an unrealistically “blocky” representation. Similarly, although manipulation of the data beyond the original grid provides the interpreter many options for suppressing or enhancing features of the data and gaining additional insights, a thorough understanding of the processes applied is required. Prudence is warranted if extrapolating conclusions from highly processed images.

The risk of inappropriate application of “black box” algorithms is increased in TEH sections because the process mixes coordinates of different units. It is important to reiterate that the data grid must be produced using an orthogonal (line) gridding process, a 2-dimensional spatial gridding system such as random gridding or krigging cannot be applied. Orthogonality is fundamentally required because it is inappropriate to mix units of time and space. Were that aspect ignored and least square distance type gridding applied, the grid would not properly honor the data resulting in distortion and loss of resolution.

C7. **Conclusion**

As higher spatial and temporal data densities are achieved with deployment of modern equipment for subsurface hydrogeologic characterization, there is an associated increase in need for new and improved methods for presenting, visualizing, interpreting and maximizing the insights obtained from these data sets. Time-Elevation-Head (and Vertical Gradient) sections provide highly visual tools for the interpreter to examine temporal variations in multilevel data with the potential of adding new insights into

hydrogeologic conditions. Although pressure head data is used in these examples the same processes are applicable to other forms of time varying data such as temperature and chemical analyses. Adoption of geophysical processing algorithms allows for effective removal or enhancement of trends in either space, time or both. However, the mechanics of the instrumentation and the numerical processes applied must be controlled and well understood to avoid misrepresentation of the field conditions or over-interpretation of the data, just as is the case for these same tools being applied with geophysical data sets.

C8. **Acknowledgements**

The author gratefully acknowledges the hard work of several research scientists and students in the G360 Center of Applied Groundwater Research at the University of Guelph involved in the design, installation of the multi-levels and data collection processing and validation of the pressure transducer data set (C. Stewart, P. Quinn, J. Kennel and K. Belan). The transducer data collection and validation from the MLS systems was performed by Karl Belan for his MSc. Thesis (2010).

Funding for this work was provided through a National Science and Engineering Research Council of Canada (NCERC) IRC grant No 400125 and associated corporate sponsors to Dr Beth Parker at the University of Guelph.

C9. **References**

Akima, H., 1969, A Method of Smooth Curve Fitting, ESSA Tech. Rep. ERL 101-ITS 73 (Washington, D.C.: U.S. Government Printing Office)

Meyer, J. R. Beth L. Parker and John A. Cherry, 2007 Detailed hydraulic head profiles as essential data for defining hydrogeologic units in layered fractured sedimentary rock, Environmental Geology,

Geosoft, http://www.geosoft.com/.

Belan, K.P. 2010, Characterizing a fractured rock aquifer with hydraulic testing at a contaminated municipal well using flexible liner methods and depth discrete monitoring, Unpublished MSc Thesis University of Guelph, Ontario Canada, 193 p.

Black, W.H., H.R. Smith, and F.D. Patton. 1986. Multiple-level ground-water monitoring with the MP system. In Proceedings of the Conference on Surface and Borehole Geophysical Methods and Ground Water Instrumentation. Dublin, Ohio: National Water Well Association

Brunton, F.R. 2008. Preliminary revisions to the Early Silurian stratigraphy of Niagara Escarpment: integration of sequence stratigraphy, sedimentology and hydrogeology to delineate hydrogeologic units; in Summary of Field Work and Other Activities, 2008, Ontario Geological Survey, Open File Report 6226, p.31-1 to 31-18

Cherry, J.A., and P.E. Johnson. 1982. A multilevel device for monitoring in fractured rock. Ground Water Monitoring Review 2, no. 3: 41–44.

Cherry J.A., B.L. Parker, and C.Keller, 2007. A new depth-discrete multilevel monitoring approach for Fractured rock. Ground Water Monitoring & Remediation 27(2):57–70

Meyer, J.R., B.L. Parker, and J.A. Cherry. 2007. Detailed hydraulic head profiles as essential data for defining hydrogeologic units in layered fractured sedimentary rock. Environmental Geology. DOI10.1007/s00254-007-1137-

Pehme, P.E., Parker B.L, Cherry J.A. and Greenhouse J. P., 2010, Improved Resolution of Ambient Flow through Fractured Rock with Temperature Logs, Ground Water, Vol 28, No 2 pp.191-211.

Perrin, J., B.L. Parker and J. A. Cherry, 2011. Assessing the flow regime in a contaminated fractured and karstic dolostone aquifer supplying municipal water. Journal of Hydrology, 400: 396-410.

Sittner W.T., C.E. Schauss, and J.C. Monro, 1969. Continuous Hydrograph Synthesis with an API-Type Hydrologic Model, Water Resources Research, Vol.5, NO. 5, pg 1007-1022.

Sorenson J.P.R. and Andrew S. Butcher, 2011. Water level monitoring pressure transducers – a need for industry – wide standards. Ground Water Monitoring & Remediation 31(4):56-62.

Stantec. 2009 Smallfield and Sacco production wells well rehabilitation and hydrogeologic assessment progress report for the period December 2008 to March 2009. Prepared for the City of Guelph.

Table C1: Details of Monitoring Ports, *Note: nonoperational transducers are italicized and shaded.*

Monitoring Interval	MW74		MW75	
	Midpoint	Length	Midpoint	Length
ML1	335.78	1.52	336.19	1.52
ML2	333.49	1.83	333.90	1.83
ML3	*331.20*	*0.91*	332.07	0.61
ML4	*329.83*	*1.22*	331.00	0.91
ML5	328.00	1.22	329.48	0.91
ML6	*326.33*	*0.91*	*327.35*	*1.52*
ML7	325.11	0.91	*325.22*	*1.52*
ML8	322.97	0.91	323.84	0.61
ML9	321.14	0.91	322.32	1.22
ML10	319.01	0.91	*320.64*	*0.91*
ML11	317.18	0.91	319.12	0.91
ML12	315.81	0.61	*317.29*	*1.52*
ML13	314.44	0.91	315.00	1.22
ML14	312.31	1.52	313.02	1.52
ML15	310.02	1.22	310.59	1.52
ML16	308.34	1.52	308.60	1.22

Table C 2: Parameter Summary for Figures

Figure	**X axis 1 unit=**	**Y axis 1 unit=**	**Data**	**Comment** (grid all at 0.2data units)
Figure C3	1day	1m	Head (m)	Basic data presentation
C4	½ day	1m	Head (m)	Expanded horizontal scale for detailed analysis of pumping test
C5	1 day	1m	Filtered Head (m)	Data filtered to enhance vertical variations and suppress temporally continuous conditions
C6	1 day	1m	Vertical hydraulic gradient	Section highlights the uniformity of the vertical gradient before pre pumping and response during pump test

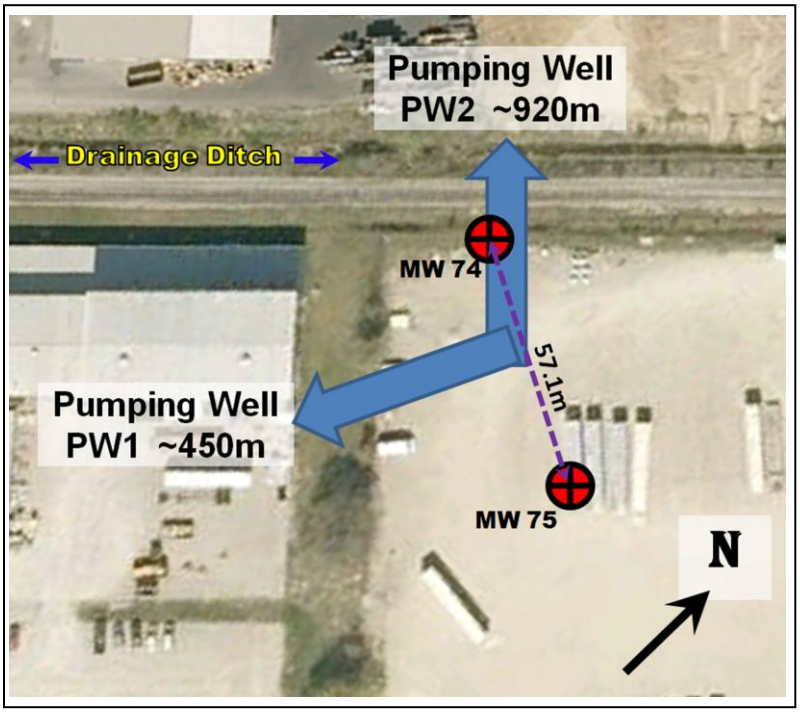

Figure C1: Plan Map of the configuration of monitoring wells

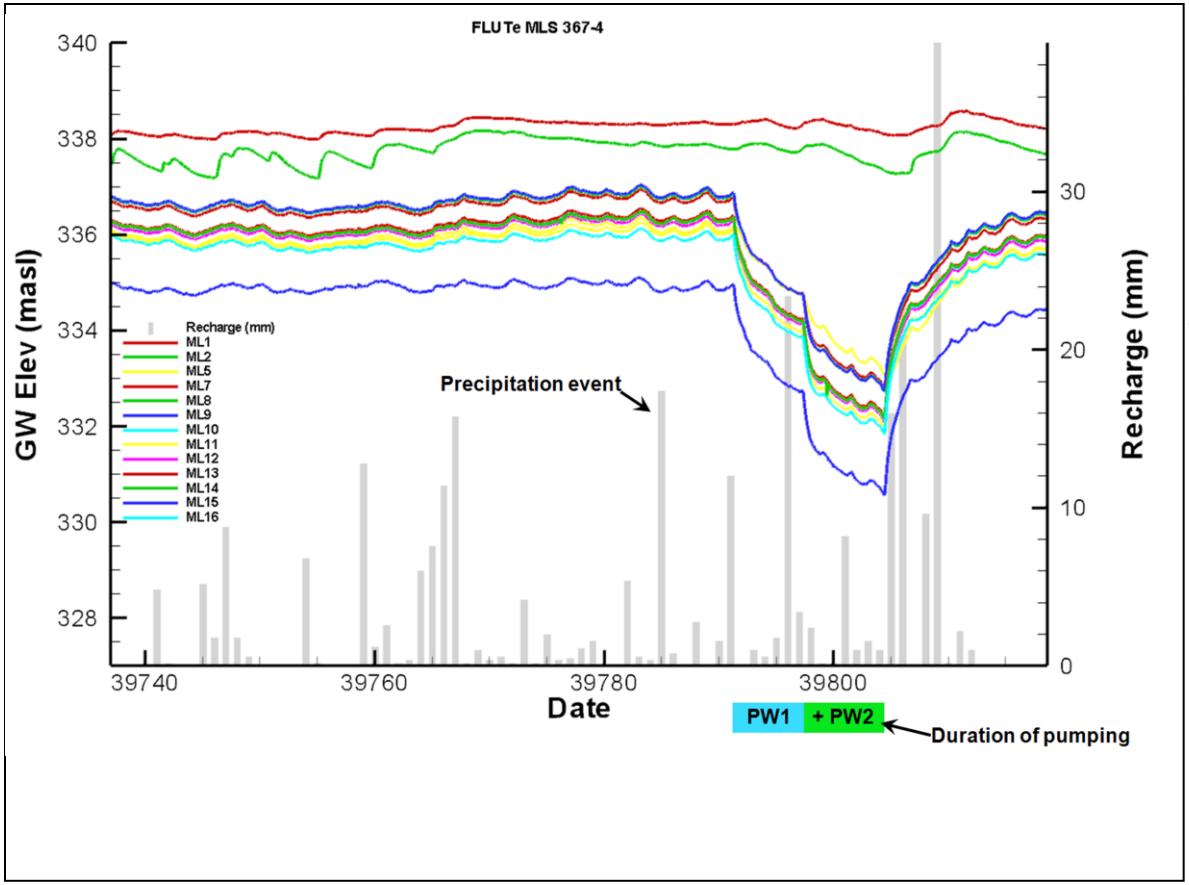

Figure C2: Hydrographs (groundwater elevation (masl) vs time (days)) from the 13 functioning transducers in MW-74. Precipitation (rain or snow) is shown as histograms, extent of pumping of PW1 and PW2 indicated. This is the conventional method for presenting and comparing variations in head over time. Although the responses of individual monitors can be resolved, it is difficult in this representation to compare the variation in head with depth and access the vertical extent of the effects of recharge and pumping. *Note: day 39740 = 19/10/2008.*

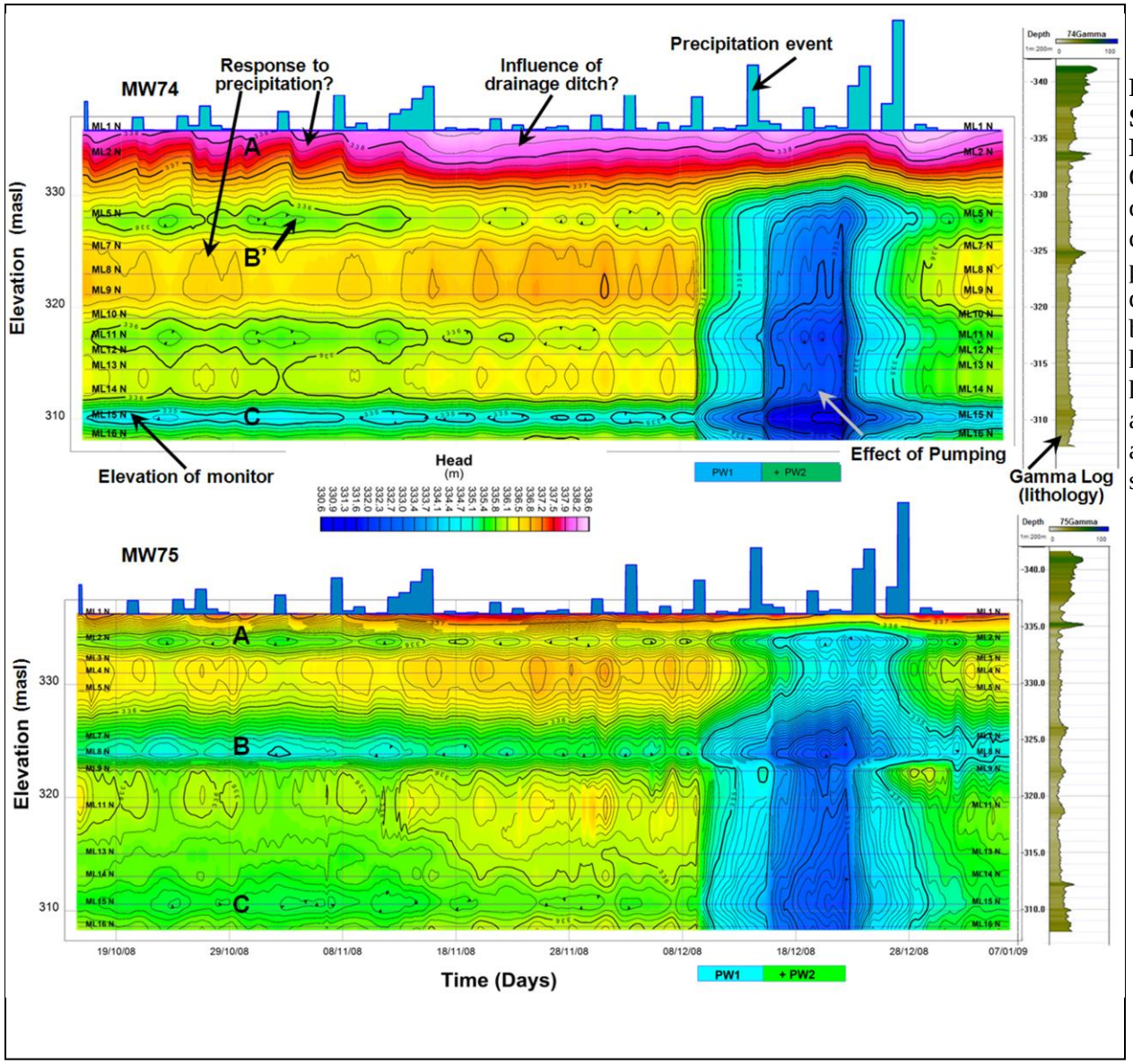

Figure C3: Time-Elevation Head Sections (85 days) for MW74 (top) and MW75 (bottom).
Gamma logs indicate variations in clay content. Note downward inflections in contours and increasing pressure after precipitation events the effect of which decreases with depth and the similarities between the sections in patterns (depth horizons A,B and C) of relatively low and high pressure. Although pumping creates an overall decrease in pressure there appears to have minimal influence near surface in MW74.

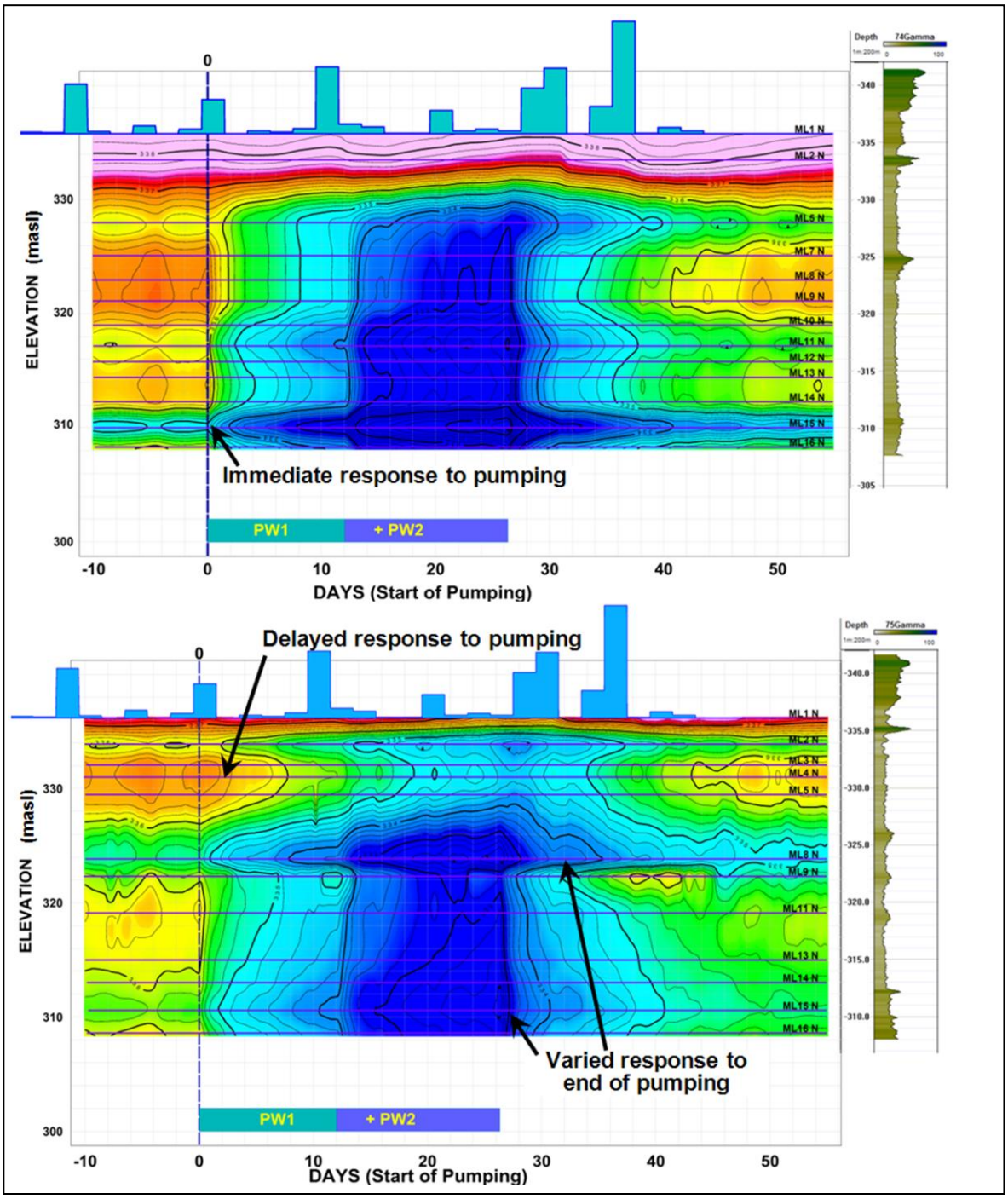

Figure C4: Time-Elevation Head Sections MW74 (top) and MW75(bottom) Expanded to ½ day increments.

Time scale doubled and days are normalized to the start of pumping. Pumping primarily draws from elevations of approximately 270masl, well below the bottom of the TEH sections. Expanded views allow for a detailed assessment of the timing of the response as pumping is initiated and then during hydraulic recovery after pumping stops.

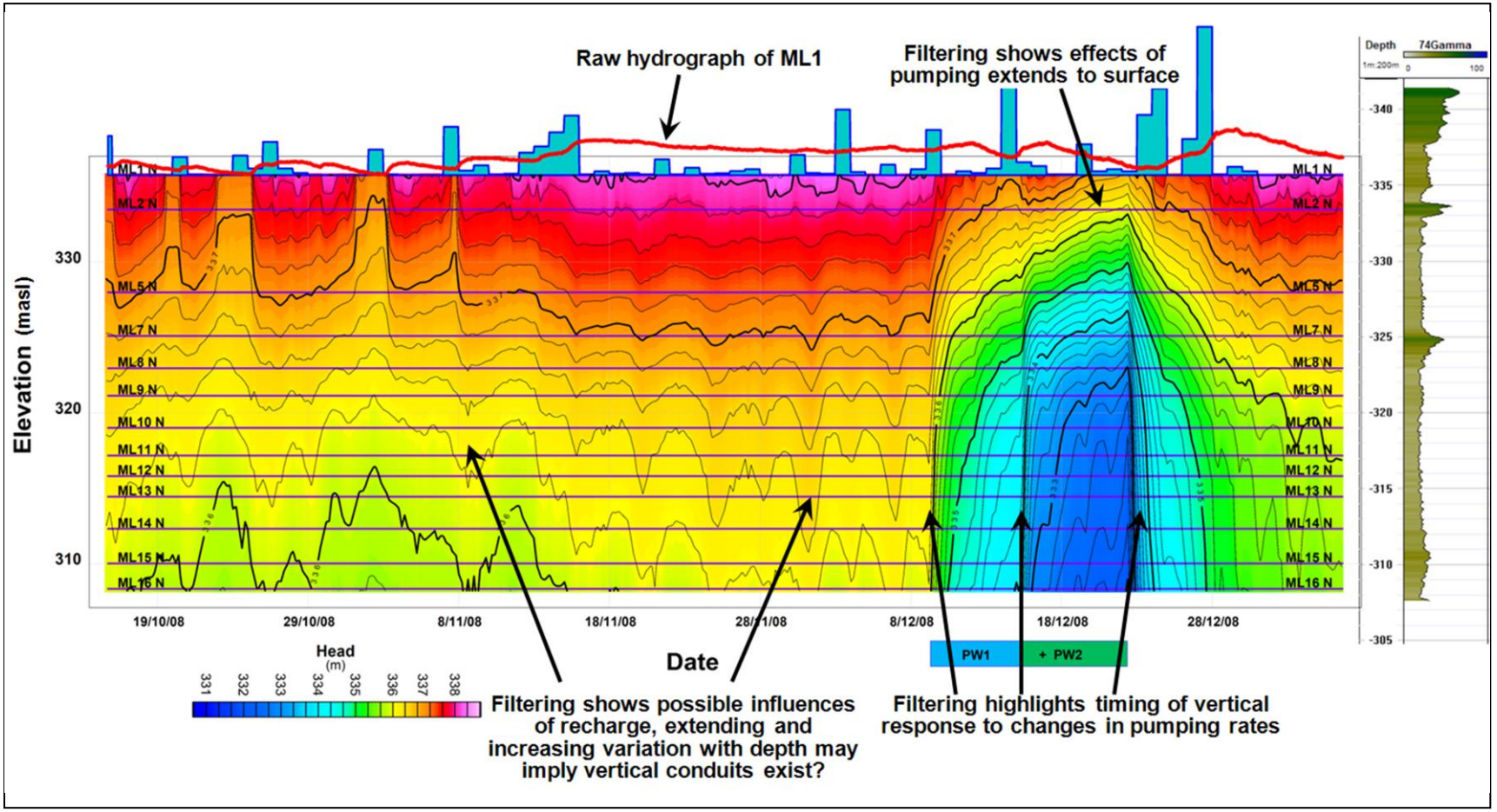

Figure C5: MW74 Time-Elevation Head Section Filtered to Enhance Vertical Connection and Suppress Horizontal Trends.
Note effect of nearby drainage ditch is suppressed allowing the influence of pumping to be recognized to extend to surface.

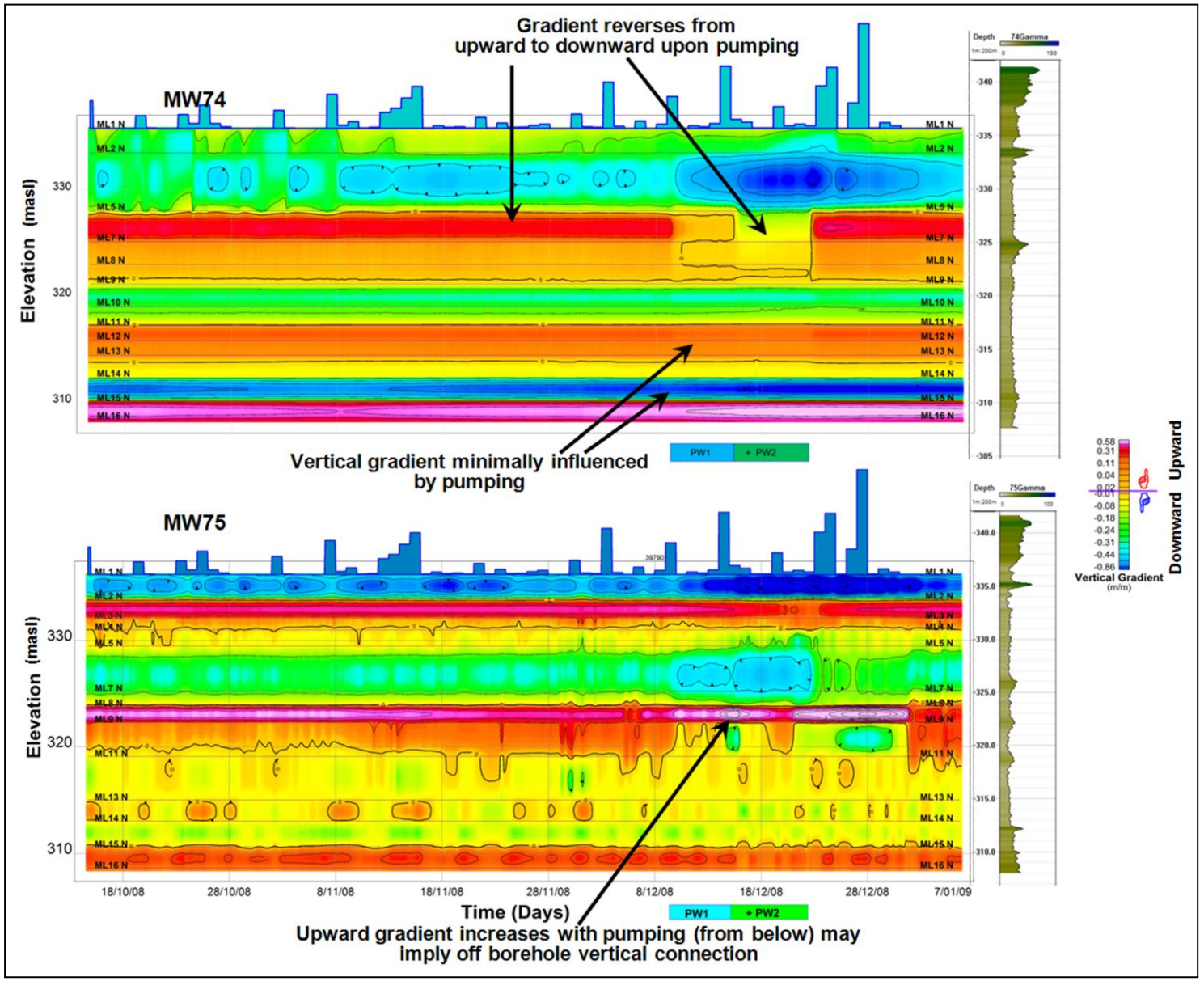

Figure C6: Time-Elevation Vertical Gradient Sections for MW74 (top) and MW75 (bottom). Orange-Red and Pink indicate upward hydraulic gradient, yellow-green-blue indicate downward hydraulic gradient. Note change vertical reverse from upward to downward during pumping in MW74. In MW75 at 323masl the upward gradient increases during pumping in spite of the overall decrease in head observed in Figure 4 implying both lateral and vertical flow is increased because of circuitous flow paths.

Permissions

JOHN WILEY AND SONS LICENSE
TERMS AND CONDITIONS

Aug 10, 2012

This is a License Agreement between Peeter Pehme ("You") and John Wiley and Sons ("John Wiley and Sons") provided by Copyright Clearance Center ("CCC"). The license consists of your order details, the terms and conditions provided by John Wiley and Sons, and the payment terms and conditions.

All payments must be made in full to CCC. For payment instructions, please see information listed at the bottom of this form.

License Number	2965431092202
License date	Aug 10, 2012
Licensed content publisher	John Wiley and Sons
Licensed content publication	Ground Water
Licensed content title	Improved Resolution of Ambient Flow through Fractured Rock with Temperature Logs
Licensed content author	P.E. Pehme,B.L. Parker,J.A. Cherry,J.P. Greenhouse
Licensed content date	Oct 14, 2009
Start page	191
End page	205
Type of use	Dissertation/Thesis
Requestor type	Author of this Wiley article
Format	Print and electronic
Portion	Full article
Will you be translating?	No
Order reference number	
Total	0.00 USD
Terms and Conditions	

TERMS AND CONDITIONS

This copyrighted material is owned by or exclusively licensed to John Wiley & Sons, Inc. or one of its group companies (each a "Wiley Company") or a society for whom a Wiley Company has exclusive publishing rights in relation to a particular journal (collectively WILEY"). By clicking "accept" in connection with completing this licensing transaction, you agree that the following terms and conditions apply to this transaction (along with the billing and payment terms and conditions established by the Copyright Clearance Center Inc., ("CCC's Billing and Payment terms and conditions"), at the time that you opened your Rightslink account (these are available at any time at http://myaccount.copyright.com)

References

Chapters 1 and 6:

Anderson, M.P. 2005. Heat as a ground water tracer. *Ground Water* 43, no. 6: 951-968

Berkowitz, B. 2002. Characterizing flow and transport in fractured geological media: A review. Advances in Water Resources 25, no. 8-12: 861-884.

Berthold, S and F. Börner, 2008, Detection of free vertical convection and double-diffusion in groundwater monitoring wells with geophysical borehole measurements. Environmental Geology 54, 1547-1566.

Bidaux, P., and C. Drogue. 1993. Calculation of low-range flow velocities in fractured carbonate media from borehole hydrochemical logging data comparison with thermometric results. *Ground Water* 31, no.1: 19-26.

Burchfield, J.D. Lord Kelvin and the Age of the Earth, 1975, Sci. Hist. Pub., New York. 260pp.

Cherry, J.A., B.L. Parker, and C. Keller, 2007. A new depth-discrete multilevel monitoring approach for fractured rock. Ground Water Monitoring and Remediation 27, no. 2: 57-70.

Conway, J.G. 1977. Deconvolution of Temperature Gradient Logs, Geophysics, Vol 42, no. 4 pp.823-837

Drogue, C. 1985. Geothermal gradients and groundwater circulations in fissured and karstic rocks: The role played by the structure of the permeable network. J. Geodynamics,no.4, pp.219-231.

Ge, S. 1998, Estimation of groundwater velocity in localized fracture zones from well temperature profiles, Journal of Volocanology and Geothermal Research 84, pg93-101.

Genthon, P., A. Bataille, A. Fromant, D. D'Hulst, and F. Bourges. 2005. Temperature as a marker for karstic waters hydrodynamics. Inferences from 1 year recording at La Peyrére cave (Ariège, France). Journal of Hydrology 311, no. 1-4: 157-171

Greenhouse, John P. and P.E. Pehme, 2002, Monitoring the Temperature in a Sleeved Borehole: Implications for Fracture Detection, Proceedings of the 55th Canadian Geotechnical and 3rd Joint IAH-CNC and CGS Groundwater Specialty

Keys, W.S., and R.F. Brown. 1978. The use of temperature logs to trace the movement of injected water. Ground Water 16, no. 1: 32-48.

Malard F., and R. Chapuis. 1995. Temperature logging to describe the movement of sewage-polluted surface water infiltrating into a fractured rock aquifer. *Journal of Hydrology* 173, no. 1-4: 191-217.

Meyer, J.R., B.L. Parker and J.A. Cherry, 2008. Detailed hydraulic head profiles as essential data for defining hydrogeologic units in layered fractured sedimentary rock. Environmental Geology, 56(1): 27-44, doi 10.1007/s00254-007-1137-4.

Neuman, S.P. 2005. Trends, prospects and challenges in quantifying flow and transport through fractured rocks. Hydrogeologic Journal, doi: 10.1007/s10040-004-0397

Novakowski K.S., Bickerton G., Lapcevic P., Voralek J., Ross N., 2005. Measurements of groundwater velocity in discrete rock fractures. Journal of Contaminant Hydrology 82: 44-60.

Keller, C.E., J.A. Cherry and B.L. Parker. submitted A new method for fracture identification and continuous hydraulic conductivity profiling in fractured rock boreholes. Ground Water.

Paillet F.L. 2000, A Field Technique for Estimating Aquifer Parameters using Flow Log Data. Ground Water Vol. 38, No 4 pages 510-521

Parker, B.L., R.W. Gillham, and J.A. Cherry. 1994. Diffusive disappearance of immiscible phase organic liquids in fractured geologic media. Ground Water 32, no. 5: 805-820.

Parker, B.L., J.A. Cherry and S.W. Chapman. 2011. Advances in the DFN approach for investigating contaminated sites on fractures sedimentary rock. Presented at the 2011 NGWA Focus Conference on Fractured Rock and Eastern Groundwater Regional Issues, Burlington, Vermont, September 26-27.

Pehme, P., J.P. Greenhouse and B.L. Parker, 2007a, The Active Line Source Temperature Logging Technique and its application in fractured rock hydrogeology, Journal of Environmental and Engineering Geophysics, V 12 No 4 pp. 307-322.

Pehme, P.E., B.L Parker, J.A. Cherry and J.P. Greenhouse, 2007b, The Potential for Compromised Interpretations When Based on Open Borehole Geophysical Data in Fractured Rock. 2007 NGWA/U.S. EPA Fractured Rock Conference: State of the Science and Measuring Success in Remediation, Portland, Maine. September 24-26, 2007

Pehme, P.E., Parker B.L, Cherry J.A. and Greenhouse J. P., 2010, Improved Resolution of Ambient Flow through Fractured Rock with Temperature Logs, Ground Water, Vol 28, No 2 pp.191-211.

Price, M. and A. Williams, 1993. The Influence of Unlined Borehole on Groundwater Chemistry: A Comparative Study Using Pore-Water Extraction and Packer Sampling, J.IWEM Water and Environment Journal 7 651-659

Quinn, P.M., B.L. Parker and J.A. Cherry, 2011. Using constant head packer tests to determine apertures in fractured rock. Journal of Contaminant Hydrogeology, 126, (1-2) 85-99.doi: 10.1016/j.jconhyd.2011.07.002.

Robinson R., S. Stilliman, and C. Cady. 1993. Identifying fracture interconnections between boreholes using natural temperature profiling: II. Application to fractured dolomite. Log Analyst 34, no. 1: 69-77.

Sterling, S.N., B.L. Parker, J.A. Cherry, J.H. Williams, J.W. Lane Jr., and F.P. Haeni. 2005. Vertical cross contamination of trichloroethylene in a borehole in fractured sandstone. *Ground Water* 43, no. 4: 557-573.

Trainer, F.W. 1968. Temperature profiles in water wells as indicators of bedrock fractures. Professional Paper 600-B, Washington DC: USGS.

Chapter 2 - References

ALT, 2002. FAC40 Televiewer, Notes on use and operation, Advance Logic Technologies sárl. 31p.

Anderson, M.P. 2005. Heat as a ground water tracer. Ground Water 43, no. 6: 951-968

Bejan, A. 1993. Heat Transfer, New York: John Wiley & Sons.

Berkowitz, B. 2002. Characterizing flow and transport in fractured geological media: A review. Advances in Water Resources 25, no. 8-12: 861-884.

Bidaux, P., and C. Drogue. 1993. Calculation of low-range flow velocities in fractured carbonate media from borehole hydrochemical logging data comparison with thermometric results. Ground Water 31, no.1: 19-26.

Bradbury, K.R., M.B. Gotkowski, D.J. Hart, T.T. Eaton, J.A. Cherry, B.L. Parker, and M.A. Borchardt. 2007. Contaminant transport through aquitards: Technical guidance for aquitard assessment. Report 91133B. Denver, Colorado: American Water Works Foundation.

Burns, L.S. 2005. Fracture network characteristics and velocities of ground water, heat and contaminants in a dolostone aquifer in Cambridge, Ontario. Unpublished MSc thesis, University of Waterloo.

Blohm, D. 2007. President, IFG Corporation Inc. Phone interview, September 12, Brampton, Ontario.

Carter, R.S., W.H. Steibel, P.J. Nalasco, and D.L. Pardieck. 1995. Investigation and remediation of ground water contamination at a pesticide facility – a case study. Water Quality Research Journal of Canada 30, no. 3: 469-491.

Cherry, J.A., B.L. Parker, and C. Keller, 2007. A new depth-discrete multilevel monitoring approach for fractured rock. Ground Water Monitoring and Remediation 27, no. 2: 57-70.

Coniglio, M. 2007. Professor, University of Waterloo. Personal communication, March 22, Waterloo, Ontario.

Davis, S.N. 1999. Humboldt, Aargo, and the temperature of groundwater. Hydrogeology Journal 7, no. 5: 501-503.

Drogue, C. 1985. Geothermal gradients and ground water circulations in fissured and karstic rocks: The role played by the structure of the permeable network. Journal of Geodynamics 4, no. 1-4: 219-231.

Drury, M.J. 1984. Borehole temperature logging for the detection of water flow. Geoexploration 22, no 3-4: 231-243.

Ferguson G., A.D. Woodbury, and G.L.D. Matile. 2003. Estimating deep recharge rates beneath an interlobate moraine using temperature logs. Ground Water 41, no. 5: 640-661.

Genthon, P., A. Bataille, A. Fromant, D. D'Hulst, and F. Bourges. 2005. Temperature as a marker for karstic waters hydrodynamics. Inferences from 1 year recording at La Peyrére cave (Ariège, France). Journal of Hydrology 311, no. 1-4: 157-171

Greenhouse, J.P., and P.E. Pehme. 2002. Monitoring the temperature in a sleeved borehole: Implications for fracture detection. In Proceedings of the 55th Canadian Geotechnical and 3rd Joint IAH-CNC and CGS Ground Water Specialty Conferences, Niagara Falls, Ontario, October 20-23, 2002. Southern Ontario Section of the Canadian Geotechnical Society.

Henninges, J., G. Zimmermann, G. Büttner, J. Schrötter, K. Erbas, and E. Huenges. 2005. Wireline distributed temperature measurements and permanent installations behind casing. In Proceedings World Geothermal Congress Antalya, Turkey, 24-29 April 2005.

IFG. 1993. Temperature Logging, Tech Note Ref: 9303-01-01. Brampton, Ontario: IFG Corporation.

Keys, W.S. 1989. Borehole geophysics applied to ground-water investigations. Techniques of Water-Resources Investigations of the United States Geological Survey. Chapter E2, 109-149.

Keys, W.S., and R.F. Brown. 1978. The use of temperature logs to trace the movement of injected water. Ground Water 16, no. 1: 32-48.

Malard F., and R. Chapuis. 1995. Temperature logging to describe the movement of sewage-polluted surface water infiltrating into a fractured rock aquifer. Journal of Hydrology 173, no. 1-4: 191-217.

Meyer, J.R., B.L. Parker, and J.A. Cherry. 2007. Detailed hydraulic head profiles as essential data for defining hydrogeologic units in layered fractured sedimentary rock. Environmental Geology, doi: 10.1007/s00254-007-1137-4.

Molson J., P. Pehme, J. Cherry, and B. Parker. 2007. Numerical analysis of HEAT transport within fractured sedimentary rock: Implications for temperature probes. In 2007 NGWA/U.S. EPA Fractured Rock Conference: State of the Science and Measuring Success in Remediation, Portland, Maine, 24-26 September 2007.

Neuman, S.P. 2005. Trends, prospects and challenges in quantifying flow and transport through fractured rocks. Hydrogeologic Journal, doi: 10.1007/s10040-004-0397.

National Research Council (NRC). 1996. Rock fractures and fluid flow: Contemporary understanding and applications. Washington, D.C.: National Academy Press.

Parker, B.L., 2007, Investigating Contaminated Sites on Fractured Rock Using the DFN Approach, NGWA/U.S. EPA Fractured Rock Conference: State of the Science and Measuring Success in Remediation, Portland, Maine, September 2007, pp. 150-168,

Parker, B.L., D.B. McWhorter, and J.A. Cherry. 1997. Diffusive loss of nonaqueous phase organic solvents from idealized fracture networks in geologic media. Ground Water 35, no. 6: 1077-1088.

Parker, B.L., R.W. Gillham, and J.A. Cherry. 1994. Diffusive disappearance of immiscible phase organic liquids in fractured geologic media. Ground Water 32, no. 5: 805-820.

Pehme, P., J.P. Greenhouse, and B.L. Parker. 2007a. The Active Line Source temperature logging technique and its application in fractured rock hydrogeology, Journal of Environmental and Engineering Geophysics 12, no. 4: 307-322.

Pehme, P.E., J.P. Greenhouse, and B.L. Parker. 2007b. The Active Line Source (ALS) technique, a method to improve detection of hydraulically active fractures and estimate rock thermal conductivity. In Proceedings of 60th Canadian Geotechnical Conference & 8th Joint IAH-CNC Ground water Conference, Ottawa, Ontario.

Pehme, P.E., B.L Parker, J.A. Cherry, and J.P. Greenhouse. 2007c. The potential for compromised interpretations when based on open borehole geophysical data in fractured rock. In 2007 NGWA/U.S. EPA Fractured Rock Conference: State of the Science and Measuring Success in Remediation, Portland, Maine. 24-26 September 2007.

Perrin, J., B.L. Parker, and J.A. Cherry. 2009. Evidence for a non-Karstic flow system within a confined Karstic and fractured dolostone aquifer. Journal of Hydrology, submitted 2009.

Prensky, S. 1992. Temperature measurements in boreholes: An overview of engineering and scientific applications. The Log Analyst 33, no. 3: 313-333.

Robinson R., S. Stilliman, and C. Cady. 1993. Identifying fracture interconnections between boreholes using natural temperature profiling: II. Application to fractured dolomite. Log Analyst 34, no. 1: 69-77.

Sara, M.N. 2003. Site Assessment and Remediation Handbook, 2nd edition. New York: Lewis Publishers.

Sammel, E.A. 1968. Convective flow and its effects on temperature logging in small diameter wells. Geophysics 33, no. 6: 1004-1012.

Silliman, S., and R. Robinson. 1989. Identifying fracture interconnections between boreholes using natural temperature profiling: I. Conceptual basis. Groundwater 27, no. 3: 393-402.

Sterling, S.N., B.L. Parker, J.A. Cherry, J.H. Williams, J.W. Lane Jr., and F.P. Haeni. 2005. Vertical cross contamination of trichloroethylene in a borehole in fractured sandstone. Ground Water 43, no. 4: 557-573.

Trainer, F.W. 1968. Temperature profiles in water wells as indicators of bedrock fractures. Professional Paper 600-B, Washington DC: USGS.

VanderKwaak, J.E., and E.A. Sudicky, 1996. Dissoloution of non-aqueous-phase liquids and aqueous-phase contaminant transport in discretely-fractured porous media. Journal of Contaminant Hydrogeology 23: 45-68.

Williams, J.H., J.W. Lane Jr., K. Singha, and F.P. Haeni. 2002. Application of advanced geophysical logging methods in the characterization of a fractured sedimentary bedrock aquifer, Ventura County, California. USGS Water-Resources Investigations Report 00-4083. Boulder, Colorado: U.S. Geological Survey.

Wisian, K.W., D.D. Blackwell, S. Bellaniti, J.A. Henfling, R.A. Normann, and P.C. Lynse. 1998. Field comparison of conventional and new technology temperature logging systems. Geothermics 27, No. 2: 131-141.

Chapter 3- References

ALT, 2002. FAC40 Televiewer – Notes on use and operation, Advanced Logic Technologies (ALT), http://www.alt.lu/acoustic_televiewer.htm, Luxembourg. 31p.

Anderson, M.P. 2005. Heat as a Groundwater Tracer, Ground Water, 43 (6): 951-968.

Berkowitz, B. 2002. Characterizing flow and transport in fractured geological media: A review. Advances in Water Resources 25, no. 8-12: 861-884.

Bidaux, P. and C. Drogue, 1993. Calculation of Low-Range Flow Velocities in Fractured Carbonate Media from Borehole Hydrochemical Logging Data Comparison with Thermometric Results, Groundwater, 31, no.1, 19-26.

Burns, L.S., 2005. Fracture network characteristics and velocities of groundwater, heat and contaminant in a dolostone aquifer in Cambridge, Ontario. MSc Thesis, Department of Earth Sciences, University of Waterloo, Waterloo, Ontario , Canada, N2L 3G1, 303pp

Drogue, C. 1885. Geothermal gradients and groundwater circulations in fissured and karstic rocks: The role played by the structure of the permeable network. J. Geodynamics,no.4, pp.219-231.

Freifeld, B. M., S. Finsterle, T.C. Onsott, P. Toole and L.M. Pratt, 2008. Ground surface temperature reconstructions: Using in situ estimates for thermal conductivity acquired with a fiber-optic distributed thermal perturbation sensor, Geophysical Research Letters, 35, L14309, doi:10.1029/2008GL034762.

Greenhouse, John P. and P.E. Pehme, 2002, Monitoring the Temperature in a Sleeved Borehole: Implications for Fracture Detection, Proceedings of the 55th Canadian Geotechnical and 3rd Joint IAH-CNC and CGS Groundwater Specialty Conferences, Niagara Falls, Ontario, October 20-23, 2002,

Keller, C.E., J.A. Cherry and B.L. Parker. Revised and re-submitted Feb, 2012. A new method for continuous hydraulic conductivity profiling in fractured rock. Ground Water.

Keys, W.S. 1989. Borehole geophysics applied to ground-water investigations. Techniques of Water-Resources Investigations of the United States Geological Survey. Chapter E2, 109-149.

Molson J.W. and E.O. Frind 2012, Heatflow/Smoker, Ver 4.0, Density-Dependent Flow and Thermal Energy Transport Model in Three Dimensions, User Guide. Dept. of Geology & Geological Engineering, Université Laval, and Dept. of Earth Sciences, University of Waterloo.

Molson, J., P. Pehme, J.A. Cherry and B.L. Parker, 2007. Numerical analysis of heat transport within fractured sedimentary rock: Implications for temperature probes. Proceedings, NGWA/EPA Fractured Rock Conference: State of the Science/Measuring Success in Remediation, Portland, ME, Sept. 24-26, pp. 489-502.

National Research Council (NRC). 1996. Rock fractures and fluid flow: Contemporary understanding and applications. Washington, D.C.: National Academy Press.

Parker, B.L., 2007. Investigating contaminated sites on fractured rock using the DFN approach. 2007 NGWA/U.S. EPA Fractured Rock Conference: State of the Science and Measuring Success in Remediation, Portland, ME, September 24-27, pp. 150-168.

Parker, B. L., Gillham, R. W., and Cherry, J. A., 1994, Diffusive disappearance of immiscible-phase organic liquids in fractured geologic media: Ground Water, v. 32, p. 805-820.

Parker, B. L., McWhorter, D. B., and Cherry, J. A., 1997, Diffusive loss of non-aqueous phase organic solvents from idealized fracture networks in geologic media: Ground Water, v. 35, p. 1077-1088.

Pehme, P.E., Parker B.L, Cherry J.A. and Greenhouse J. P., 2010, Improved Resolution of Ambient Flow through Fractured Rock with Temperature Logs, Ground Water, Vol 28, No 2 pp.191-211.

Pehme, P., J. Greenhouse and B.L. Parker, 2007. The Active Line Source (ALS) technique, a method to improve detection of hydraulically active fractures and estimate rock thermal conductivity. 60th

Canadian Geotechnical Conf & 8th Joint CGS/IAH-CNC Groundwater Conf, Ottawa, ON, October 21-24. 8 pp.

Perrin, J., B.L. Parker and J. A. Cherry, 2011. Assessing the flow regime in a contaminated fractured and karstic dolostone aquifer supplying municipal water. Journal of Hydrology, 400: 396-410.

Quinn P.M., J.A. Cherry and B.L. Parker. October, (In press) A versatile packer system for high resolution hydraulic testing in fractured rock boreholes. Submitted to Hydrogeological Journal,.

Quinn, P.M., J.A. Cherry and B.L. Parker, 2011. Quantification of non-Darcian flow observed during packer testing in fractured rock. Water Resources Research. 47 (9): W09533 doi:10.1029/2010WR009681

Robinson R., S. Stilliman and C. Cady, 1993, Identifying Fracture Interconnections between Boreholes Using Natural Temperature Profiling: II. Application to fractured Dolomite, Log Analyst 34, no. 1 pp. 69-77

Sara, M.N. 2003. Site Assessment and Remediation Handbook, 2nd edition. New York: Lewis Publishers.

Sterling, S.N., B.L. Parker, J.A. Cherry, J.H. Williams, J.W. Lane Jr., and F.P. Haeni. 2005. Vertical cross contamination of trichloroethylene in a borehole in fractured sandstone. Ground Water 43, no. 4: 557-573.

Sudicky, E.A. and McLaren, R.G., 1992. The Laplace transform Galerkin technique for large-scale simulation of mass transport in discretely fractured porous formations, Water Resour. Res., 28(2), 499-514, doi:10.1029/91WR02560

Taniguchi, M. 1993. Evaluation of vertical groundwater fluxes and thermal properties of aquifers based on transient temperature- depth profiles. Water Resources Research 29, no. 7: 2021–2026.

Therrien, R. and Sudicky, E.A., 1996. Three-dimensional analysis of variably-saturated flow and transport in discretely-fractured porous media: Model development and illustrative examples, Jour. Contam. Hydrol., 23(1-2), 1-44, doi:10.1016/0169-7722(95)00088-7

Trainer, F.W. 1968. Temperature profiles in water wells as indicators of bedrock fractures. Professional Paper 600-B Washington DC: USGS.

Trefry, M.G., and C. Muffels, 2007. FEFLOW: a finite-element ground water flow and transport modeling tool. Ground Water 45(5), 525–528.

Chapter 4- References:

ALT, 2009. QL40-ABI Acoustic Televiewer: Notes on use and operation. Advanced Logic Technology SA, Route de Neiderpallen, Redange-sur-Attert, 8506 Luxembourg. http://www.alt.lu/acoustic_televiewer.htm

ALT, 2012 OBI40-ABI Optical Televiewer: Advanced Logic Technology SA, Route de Neiderpallen, Redange-sur-Attert, 8506 Luxembourg. http://www.alt.lu/optical_televiewer.htm

Berthold, S and F. Börner, 2008, Detection of free vertical convection and double-diffusion in groundwater monitoring wells with geophysical borehole measurements. Environmental Geology 54, 1547-1566.

Blohm, D. 2007. President, IFG Corporation Inc. Phone interview, September 12, Brampton, Ontario.

Cherry, J.A., B.L. Parker, and C. Keller, 2007. A new depth-discrete multilevel monitoring approach for fractured rock. Ground Water Monitoring and Remediation 27, no. 2: 57-70.

Freeze R.A. and J.A. Cherry, 1979.Groundwater. Prentice-Hall, Englewood Cliffs, New Jersey 07632 604p.

Greenhouse, John P. and P.E. Pehme, 2002, Monitoring the Temperature in a Sleeved Borehole: Implications for Fracture Detection, Proceedings of the 55th Canadian Geotechnical and 3rd Joint IAH-CNC and CGS Groundwater Specialty Conferences, Niagara Falls, Ontario, October 20-23, 2002, Southern Ontario Section of the Canadian Geotechnical Society,

Halevy, E. H. Moser, O. Zellhofer, and A. Zuber. 1967. Borehole dilution techniques: a critical review. Isotopes in Hydrogeology. IAEA, Vienna, pp.531-564.

Kerfoot, W.B. 1992, The use of flowmeters and slow release dyes to determine bedrock flow for wellhead protection, in Proceedings, The Sixth National Outdoor Action Conference on Aquifer Restoration, Ground Water Monitoring and Geophysical Methods, National Groundwater Association, May 11-13, 1992, Las Vegas, Nev., 755-763.

Meyer, J.R., B.L. Parker and J.A. Cherry, 2008. Detailed hydraulic head profiles as essential data for defining hydrogeologic units in layered fractured sedimentary rock. Environmental Geology, 56(1): 27-44, doi 10.1007/s00254-007-1137-4.

Mount Sopris, 2012. http://www.mountsopris.com/index.php/products/downhole-probes/item/stand-alone-logging-toolsa/2dva1000

Pehme, P.E., Parker B.L, Cherry J.A. and Greenhouse J. P., 2010, Improved Resolution of Ambient Flow through Fractured Rock with Temperature Logs, Ground Water, Vol 28, No 2 pp.191-211.

Sudicky, E.A. and McLaren, R.G., 1992. The Laplace transform Galerkin technique for large-scale simulation of mass transport in discretely fractured porous formations, Water Resour. Res., 28(2), 499-514, doi:10.1029/91WR02560

Therrien, R. and Sudicky, E.A., 1996. Three-dimensional analysis of variably-saturated flow and transport in discretely-fractured porous media: Model development and illustrative examples, Jour. Contam. Hydrol., 23(1-2), 1-44, doi:10.1016/0169-7722(95)00088-7

Chapter 5 - References

Bataille A., Geebthon P., Rabinowicz M. and Fritz B., 2006. Modeling the coupling between free and forced convection in a vertical permeable slot:Implications for the heat production of an Enhanced Geothermal System. Geothermics 35 p654-682.

Berthold, S and F. Börner, 2008, Detection of free vertical convection and double-diffusion in groundwater monitoring wells with geophysical borehole measurements. Environmental Geology 54, 1547-1566.

Brush D.J and N.R. Thomson, 2003. Fluid flow in synthetic rough-walled fractures: Navier-Stokes, Stokes and local cubic law simulations, Water Resources Research, V. 39, No4, 1085-1100.

Cermak V., L. Bodri and J. Safanda, 2008. Precise temperature monitoring in boreholes: evidence for oscillatory convection? Part II: theory and interpretation Int J Earth Sci (Geol Rundsch) (2008) 97:375–384. OI 10.1007/s00531-007-0250-7

Frick H and R.M. Clever, 1982. The influence of side walls on finite amplitude convection in a layer heated from below. J Fluid Mech 111:467–480

Gershuni G.Z.,and E.M. Zhukhovitskii, 1976, Convective stability of incompressible fluids. Keter Publishing House Jerusalum Ltd. ISBN:0706515625 9780706515626

Gretener, P.E, 1967. On the thermal instability of large diameter well, an observational report. Geophysics, 32, 727-738.

Hales AL 1937. Convection currents in geysers. Mon Not Roy Ast Soc Geophys Suppl 4:122–131

Molson J., P. Pehme, J. Cherry, and B. Parker. 2007. Numerical analysis of Heat transport within fractured sedimentary rock: Implications for temperature probes. In 2007 NGWA/U.S. EPA Fractured Rock Conference: State of the Science and Measuring Success in Remediation, Portland, Maine, 24-26 September 2007.

Molson J.W., E.O. Frind and C.D. Palmer 1992, Thermal Energy Storage in an Unconfined Aquifer 2. Model Development, Validation and Application. Water Resources Research, Vol28, No10, p2857-2867.

Molson J.W. and E.O. Frind 2012, Heatflow/Smoker, Ver 4.0, Density-Dependent Flow and Thermal Energy Transport Model in Three Dimensions, User Guide. Dept. of Geology & Geological Engineering, Université Laval, and Dept. of Earth Sciences, University of Waterloo.

Pehme, P.E., B.L Parker, J.A. Cherry and J.P. Greenhouse, 2007c, The Potential for Compromised Interpretations When Based on Open Borehole Geophysical Data in Fractured Rock. 2007 NGWA/U.S. EPA Fractured Rock Conference: State of the Science and Measuring Success in Remediation, Portland, Maine. September 24-26, 2007

Quinn, P.M., J.A. Cherry and B.L. Parker, 2011. Quantification of non-Darcian flow observed during packer testing in fractured rock. Water Resources Research. 47 (9): W09533 doi:10.1029/2010WR009681

Sammel, E.A. 1968. Convective flow and its effects on temperature logging in small diameter wells. Geophysics. V.33, no.6, pp.1004-1012.

Sterling, S.N. 1999. Comparison of discrete depth sampling using rock core and a removable multilevel system in TCE contaminated fractured sandstone. M.Sc Thesis University of Waterloo Department of Earth Sciences 108p.

Sterling, S.N., B.L. Parker, J.A. Cherry, J.H. Williams, J.W. Lane Jr., and F.P. Haeni. 2005. Vertical cross contamination of trichloroethylene in a borehole in fractured sandstone. Ground Water 43, no. 4: 557-573.

Su G.W., B.M. Friefield,C.M. Oldenburg, P.D. Jordan and P.F. Daley, 2006. Interpreting Velocities from Heat-Based Flow Sensors by Numerical Simulation, Ground Water. V44, No.3. pp 386-393.